

# **The regulation of DNA damage signalling and repair by MOB2**

Ramazan Gundogdu

A thesis submitted to University College London for the degree of  
Doctor of Philosophy in the School of Life and Medical Sciences,  
Faculty of Medical Sciences

**University College London, 2016**

## Declaration of Originality

I, Ramazan Gundogdu, confirm that the work presented in this thesis is my own. Where information has been derived from other sources, I confirm that this has been indicated in the thesis. Some parts of this thesis have been reprinted from Cellular Signalling, 27/2, Gomez, V., Gundogdu, R., Gomez, M., Hoa, L., Panchal, N., O'Driscoll, M. and Hergovich, A., Regulation of DNA damage responses and cell cycle progression by hMOB2, 326–339., Copyright (2015), with permission from Elsevier (for details please see below).

License details provided by Elsevier and Copyright Clearance Center (RightsLink)	
License Number	3923230104627
License Date	Aug 06, 2016
Type of Use	reuse in a thesis/dissertation
Portion and Format	full article, both print and electronic

.....

## **Acknowledgements**

First and foremost I thank Allah for giving me the patience during my studies.

I am enormously grateful to my supervisor Dr. Alexander Hergovich. Alex thank you very much for believing in me, for your guidance, support, and constant encouragement during my Master`s and PhD`s studies in your lab. Thank you also for all your help during my thesis writing. I would also like to thank my second supervisor Prof. John Hartley for all his guidance and support whenever I needed.

This study would not have been possible without support from the Ministry of National Education, The Republic of Turkey. I am very grateful to them on behalf of Turkish nation for funding my studies over the last six years. I also thank Education Counsellor of the Turkish Embassy in London.

I am thankful to Dr. Valenti Gomez for his support, patience and help during my studies. I am also grateful to all the past and present members of the Hergovich laboratory, especially Dr. Marta Gomez, Lily Hoa, and Yavuz Kulaberoglu for their support and friendship. Special thanks to Alexandra Kidane, Lily Hoa and Ahmad Sharif for reading my PhD thesis and providing supportive comments.

I would further like to thank the “drug-DNA interactions” research lab, and of course, a special thank goes to Dr. Victoria Spanswick for her help and support. I also thank all lab members of the “Cell Signalling Research Group” for their kind help and support, great thanks to Sibel Sari for her friendship and support especially during my thesis writing. I am also thankful to all the members of the Bjedov lab, especially Celia Lujan Nunez, Carolina Soto Palma, and Victoria Martinez Miguel for their friendship and support.

I would also like to thank my mentors Prof. Kazim Sahin and Dr. Mehmet Tuzcu for encouraging me right from the beginning of my graduate studies. I am also thankful to Dr. Can Ali Agca, Dr. Hasan Gencoglu and Mahmut Canga for their continuous support and encouragement during my studies.

I would like to express my deepest gratitude to my cousins Ergul, Kemal, Meral, Rohat and Mehmet Akkaya, Filiz Tekin, Nezaket Bingol, and Ahmet Bingol for their support over the last six years in London. Thank you so much Ergul for all your help and support throughout these years. I am also thankful to Ali Riza Gundogdu, Huseyin Yesiltan and Mehmet Yesilta for believing in me and being an official guarantor of my scholarship.

Finally, I would like to thank my parents Husniye and Veli for helping me to get through my PhD, and my sisters Enise and Gulsen and my brother Enes for all their love and support throughout the most puzzling time of my life. Mom and dad, thank you very much for believing in me, without your constant support and pray I would not be able to handle this long journey. Enise and Gulsen, I know you always pray for me, and I believe it helped me a lot during my studies. Having two great angels like you always makes me feel special and lucky, thank you so much. Enes, I am terribly sorry for not being able to be with you in the last six years, and I know that you are looking forward to seeing me back home. Please forgive me and thank you very much for your patience. I am also extremely grateful to the rest of my family, especially my uncles Burhan and Celal Gundogdu, and Celal Yesilta for their constant encouragement during my studies. Last, but not least, my greatest gratitude goes to Resul Celebi who always supports and prays for me. I would never forget your help, thank you very much.

*To my parents,*  
*my grandmother, Aliye Yesilta*  
*and Astsubay Omer Halisdemir*

## ABSTRACT

Human MOB2 (hMOB2) is a member of the highly conserved MOB protein family. MOBs have essential functions as regulators of diverse signalling pathways. In this regard, a recent genome wide screen for novel players in the DNA damage response (DDR) suggested hMOB2 as a potential candidate awaiting validation of its potential role in the DDR. Therefore, as the DDR is critical to maintain genomic integrity and to prevent tumorigenesis, my PhD project focused on understanding the involvement of hMOB2 in the DDR. Significantly, we found that in normal growth conditions hMOB2 is required to prevent the accumulation of unrepaired DNA double-strand breaks (DSBs) in untransformed proliferating human cells. hMOB2 supports cell cycle checkpoint activation, DDR signalling, and cell survival upon exposure to exogenously induced DNA damage. Surprisingly, these novel functions of hMOB2 appear to be linked with the MRE11-RAD50-NBS1 (MRN) complex, since hMOB2 interacts with RAD50 and supports the recruitment of the MRN and activated ATM to damaged chromatin. Equally important, hMOB2-deficient cells display impaired DSB repair by homologous recombination repair (HRR) as judged by GFP-recombination assays and RAD51 foci formation. Remarkably, hMOB2 knockdown compromises PLK1-mediated phosphorylation of RAD51, which is significant for ssDNA-RAD51 nucleofilament stabilisation. Strikingly, our research further revealed that defective HRR due to hMOB2 knockdown may provide a novel translational approach for future clinical studies. Notably, hMOB2 knockdown sensitises human tumour cells to inter-strand crosslinking (ICL) chemotherapeutics and poly (ADP-ribose) polymerase (PARP) inhibitors. Considering further that the human *MOB2* gene appears to display loss of heterozygosity in more than 50% of testicular, bladder, cervical, ovarian and lung carcinomas, our findings cumulatively propose that hMOB2 expression may be considered as a candidate biomarker in the evaluation for targeted therapies of cancer with defective HRR.

## TABLE OF CONTENTS

<b>Chapter 1 Introduction .....</b>	<b>21</b>
1.1 The Hippo signalling pathway .....	21
1.2 The MOB protein family.....	22
1.3 From yeast to mammals: MOB2.....	26
1.4 Genome instability and cancer .....	29
1.5 Cell cycle progression and checkpoint control in mammalian cells ...	32
1.5.1 Cell cycle progression in mammalian cells.....	32
1.5.2 Checkpoint control in mammalian cells.....	35
1.5.2.1 The G1/S cell cycle checkpoint.....	40
1.5.2.2 The intra-S phase cell cycle checkpoint.....	40
1.5.2.3 The G2/M cell cycle checkpoint .....	41
1.6 DNA damage signalling and repair pathways in mammalian cells ....	42
1.6.1 DNA damage response (DDR) signalling.....	43
1.6.2 DNA double-strand break (DSB) repair pathways.....	49
1.6.2.1 Classical non-homologous end-joining (c-NHEJ) repair.....	50
1.6.2.2 Homologous recombination repair (HRR) pathway.....	51
1.6.2.3 Alternative DSB repair pathways (MMEJ and SSA).....	55
1.6.3 DNA interstrand crosslink (ICL) repair.....	56
1.6.4 Other DNA damage repair pathways .....	59
1.6.4.1 Base excision repair (BER).....	59
1.6.4.2 Nucleotide excision repair (NER) .....	60
1.6.4.3 Mismatch Repair (MMR) .....	60
1.7 Cancer treatments with DNA damaging agents .....	61
1.7.1 Radiotherapy.....	63
1.7.2 Chemotherapy .....	63
1.7.2.1 DNA inter-strand crosslink (ICL)-inducing agents .....	64
1.7.2.2 Topoisomerase inhibitors.....	66
1.7.2.3 Other DNA damaging agents.....	68
1.7.3 Personalised therapy: synthetic lethal approaches .....	69
1.7.3.1 ATM inhibitors.....	70
1.7.3.2 DNA-PK inhibitors.....	71

1.7.3.3	PARP inhibitors.....	72
1.8	The scope of this project .....	78
<b>Chapter 2</b>	<b>Materials and Methods .....</b>	<b>79</b>
2.1	Materials.....	79
2.1.1	Bacterial Media .....	79
2.1.2	Buffers and solutions.....	80
2.1.2.1	Buffers used in DNA agarose gel electrophoresis.....	80
2.1.2.2	Buffers used in immunoblotting (IB) experiments.....	80
2.1.2.3	Buffers used in immunoprecipitation (IP) experiments .....	83
2.1.2.4	Buffers used in chromatin isolation experiments.....	83
2.1.2.5	Buffers used in immunofluorescence (IF) experiments .....	84
2.1.2.6	Buffers used for cell cycle analysis by DNA content .....	84
2.1.2.7	Buffers used in alkaline Comet assays .....	85
2.1.2.8	Solutions used in colony survival assays .....	85
2.1.3	Cell culture reagents .....	85
2.1.4	General buffers .....	87
2.1.5	List of antibodies used in this project .....	88
2.1.6	List of plasmids used in this project.....	91
2.1.7	List of siRNAs used in this project.....	92
2.1.8	List of primers used in this project (for qRT-PCR).....	92
2.2	Methods .....	93
2.2.1	DNA protocols – Molecular cloning techniques.....	93
2.2.1.1	Restriction digest and ligation of DNA fragments.....	93
2.2.1.2	PCR mutagenesis .....	93
2.2.1.3	DNA agarose gel electrophoresis .....	95
2.2.1.4	Bacterial techniques.....	96
2.2.2	RNA analysis – Quantitative Real-Time PCR (qRT-PCR).....	98
2.2.2.1	Total RNA extraction .....	98
2.2.2.2	cDNA synthesis.....	99
2.2.2.3	qRT-PCR .....	100
2.2.2.4	qRT-PCR Data Analysis .....	102
2.2.3	Protein analysis.....	103



2.2.3.1	Immunoblotting (IB).....	103
2.2.3.2	Immunoprecipitation (IP).....	106
2.2.3.3	Yeast 2 Hybrid (Y2H) screen .....	108
2.2.3.4	Chromatin isolation .....	108
2.2.3.5	Immunofluorescence (IF) .....	109
2.2.4	Mammalian tissue culture methods.....	110
2.2.4.1	Cell lines and culture conditions.....	110
2.2.4.2	Cell culture maintenance .....	110
2.2.4.3	Cryopreservation and retrieval of cell lines .....	111
2.2.4.4	Cell counting for seeding and proliferation assays.....	112
2.2.4.5	Cell transfections .....	112
2.2.4.6	Drug/inhibitor treatments and irradiation .....	114
2.2.5	Functional assays .....	117
2.2.5.1	Cell proliferation assays.....	117
2.2.5.2	Cell cycle analysis by DNA content (Flow cytometry) .....	117
2.2.5.3	The alkaline Comet assay.....	118
2.2.5.4	Colony survival assays (clonogenic assays) .....	121
2.2.5.5	I-SceI-based GFP recombination (DNA repair) assays.....	124
2.2.6	Statistical analysis.....	126
2.2.7	Supplementary information .....	127

### **Chapter 3 hMOB2 prevents the accumulation of spontaneous DNA damage in untransformed human cells ..... 130**

3.1	Introduction .....	131
3.2	Research aims .....	133
3.3	Results .....	134
3.4	Discussion.....	153
3.5	Supplementary Information .....	158

### **Chapter 4 hMOB2 interacts with RAD50 and supports MRN-mediated ATM signalling and homologous recombination-mediated DSB repair 161**

4.1	Introduction .....	162
-----	--------------------	-----

4.2 Research aims .....	164
4.3 Results .....	165
4.4 Discussion .....	182
4.5 Supplementary information .....	187
<b>Chapter 5 hMOB2 supports cancer cell survival upon ICL-inducing drugs and PARP inhibitors .....</b>	<b>192</b>
5.1 Introduction .....	193
5.2 Research aims .....	195
5.3 Results .....	196
5.4 Discussion .....	216
5.5 Supplementary information .....	223
<b>Chapter 6 Final conclusions .....</b>	<b>226</b>
<b>Chapter 7 Bibliography .....</b>	<b>237</b>

## LIST OF FIGURES

<b>Figure 1.1</b> The general scheme of NDR/LATS kinase signalling in humans. .....	22
<b>Figure 1.2</b> General scheme of the DNA damage response (DDR).....	31
<b>Figure 1.3</b> Molecular regulation of the cell cycle progression.....	34
<b>Figure 1.4</b> Activation of DNA damage signalling pathway: key molecules and cell cycle checkpoints. ....	37
<b>Figure 1.5</b> p53 regulates various biological processes through transcriptional activation of target genes.....	38
<b>Figure 1.6</b> The pRb-E2F pathway controls the G1/S transition. ....	39
<b>Figure 1.7</b> The ATM/ATR-mediated mammalian DDR pathway.....	44
<b>Figure 1.8</b> Representative model of the MRN complex.....	47
<b>Figure 1.9</b> The NHEJ DSB repair mechanism.....	51
<b>Figure 1.10</b> The HRR DSB repair mechanism. ....	52
<b>Figure 1.11</b> The Fanconi anaemia (FA) pathway. ....	58
<b>Figure 1.12</b> DNA damages caused by radiotherapy and chemotherapy agents, and the repair pathways dealing with these lesions. ....	62
<b>Figure 1.13</b> Synthetic lethality mechanism with PARP inhibitor. ....	74
<b>Figure 2.1</b> Design of the HRR and NHEJ assays.....	126
<b>Figure 3.1</b> hMOB2 overexpression neither affected cell cycle markers nor cell proliferation.....	135
<b>Figure 3.2</b> hMOB2 depletion causes a G1/S cell cycle arrest in RPE1 cells. .....	136

<b>Figure 3.3</b> hMOB2-depleted cells displayed a markedly delayed G1/S cell cycle transition. ....	137
<b>Figure 3.4</b> hMOB2 knockdown activates p53/p21 cascade and causes transcriptional activation of p53. ....	139
<b>Figure 3.5</b> The G1/S cell cycle arrest upon hMOB2 depletion is p53-dependent.....	141
<b>Figure 3.6</b> The G1/S cell cycle arrest induced by hMOB2 knockdown is through p21 activation. ....	142
<b>Figure 3.7</b> hMOB2 promotes G1/S cell cycle arrest in response to exogenously induced DNA damage.....	144
<b>Figure 3.8</b> The cell cycle effect of hMOB2 depletion is independent of NDR1/2 kinase signalling.....	146
<b>Figure 3.9</b> In normal growth conditions hMOB2 knockdown triggers ATM-CHK2-p53 signalling. ....	149
<b>Figure 3.10</b> hMOB2 depletion triggers the DNA Damage Response due to the accumulation of DSBs.....	151
<b>Figure 4.1</b> hMOB2 interacts with the MRN component RAD50.....	166
<b>Figure 4.2</b> hMOB2 interacting with the MRN component RAD50 regulates MRN-ATM recruitment to damaged chromatin. ....	168
<b>Figure 4.3</b> hMOB2 supports IR-induced ATM-NBS1-SMC1 signalling.....	170
<b>Figure 4.4</b> hMOB2 promotes the DSB repair pathway HRR. ....	173
<b>Figure 4.5</b> hMOB2 is dispensable for the DSB repair pathway NHEJ. ....	174
<b>Figure 4.6</b> hMOB2-deficient cells have increased RPA formation.....	176
<b>Figure 4.7</b> hMOB2 promotes the damage-induced RAD51 focus formation .....	178

<b>Figure 4.8</b> hMOB2 is needed for efficient phosphorylation of RAD51. ....	180
<b>Figure 5.1</b> hMOB2-depleted cells display significantly increased sensitivity to mitomycin C. ....	197
<b>Figure 5.2</b> hMOB2 deficiency significantly decreases survival of cancer cells upon cisplatin treatment. ....	198
<b>Figure 5.3</b> Increased ICL-sensitivity of hMOB2-knockdown cells is not caused by inconsistent formation of ICL adducts. ....	199
<b>Figure 5.4</b> hMOB2-knockdown cells show augmented sensitivity to ICL-inducing agents independent of the FA pathway. ....	201
<b>Figure 5.5</b> hMOB2-depleted cells display reduced survival upon DNA-PK inhibition. ....	203
<b>Figure 5.6</b> hMOB2 deficiency elevates radiosensitivity of DNA-PK-inhibited cells. ....	204
<b>Figure 5.7</b> ATM inhibition does not alter the survival of hMOB2-knockdown cells. ....	206
<b>Figure 5.8</b> hMOB2-depleted cells show increased sensitivity to PARP inhibition by olaparib. ....	208
<b>Figure 5.9</b> PARP inhibition causes a significant reduction in the survival of the hMOB2-depleted human colorectal and ovarian cancer cells. ....	209
<b>Figure 5.10</b> hMOB2-depleted cells show elevated sensitivities to the PARP inhibitors rucaparib and veliparib. ....	210
<b>Figure 5.11</b> The levels of hMOB2 protein correlate with the survival of ovarian cancer cells upon PARP inhibition. ....	212
<b>Figure 5.12</b> hMOB2 supports cell survival in response to PARP inhibition. ....	214

<b>Figure 5.13</b> hMOB2 knockdown promotes radiosensitivity of PARP-inhibited cells. ....	215
--	-----

<b>Figure 6.1</b> The working model of regulation of DNA damage response and repair by hMOB2.....	229
---	-----

## **LIST OF SUPPLEMENTARY FIGURES**

<b>Figure S2.1</b> The representative image of the performed 2% agarose gel .	127
---	-----

<b>Figure S3.1</b> Gene expression profiling of hMOB2-depleted RPE1 cells....	158
---	-----

<b>Figure S3.2</b> p53 levels increases upon hMOB2 depletion.....	159
---	-----

<b>Figure S3.3</b> Average cell size does not change upon hMOB2 knockdown	160
---	-----

<b>Figure S4.1</b> hMOB2 neither interacts with full-length nor HECT domain only UBR5 .....	187
---	-----

<b>Figure S4.2</b> Neither MRN was decreased, nor p53 levels were increased following 24 h of hMOB2 depletion .....	188
---	-----

<b>Figure S4.3</b> hMOB2 supports mitomycin C-induced ATM signalling .....	189
--	-----

<b>Figure S4.4</b> hMOB2 supports cisplatin-induced ATM signalling.....	190
---	-----

<b>Figure S4.5</b> hMOB2 supports doxorubicin-induced ATM signalling .....	191
--	-----

<b>Figure S5.1</b> hMOB2 promotes cell survival response to IR-induced DNA damage.....	223
--	-----

<b>Figure S5.2</b> hMOB2 deficiency shows different cellular response against DNA-damaging topoisomerase inhibitors.....	224
--	-----

<b>Figure S5.3</b> hMOB2 knockdown does not enhance radiosensitivity of ATM-inhibited cells .....	225
---	-----

## LIST OF TABLES

<b>Table 1-1:</b> Sequence identities of the MOB protein family in yeast, fly and human cells (Hergovich, 2011). .....	23
<b>Table 1-2:</b> PARP1 inhibitors that are currently under clinical investigation for cancer therapy (Wang et al., 2016).....	75
<b>Table 2-1:</b> The reaction mix for PCR mutagenesis.....	94
<b>Table 2-2:</b> The temperature program for PCR mutagenesis. ....	94
<b>Table 2-3:</b> The recommended concentration of UltraPure Agarose required resolving DNA fragments of the approximately indicated range. ....	95
<b>Table 2-4:</b> The reaction mix for cDNA synthesis. ....	100
<b>Table 2-5:</b> The temperature program for cDNA synthesis. ....	100
<b>Table 2-6:</b> The reaction mix for qRT- PCR. ....	101
<b>Table 2-7:</b> The temperature program for qRT-PCR.....	101
<b>Table 2-8:</b> Ct value calculation for qRT-PCR analysis.....	102
<b>Table 2-9:</b> The resolution range of proteins depending on the % of the gel .....	104
<b>Table 2-10:</b> Compounds used in cell cycle checkpoint analysis, colony survival assays and DNA damage repair experiments. ....	115
<b>Table 2-11:</b> Preparation of drug/inhibitor stocks and details of the chemicals. ....	116
<b>Table 2-12:</b> The number of cells seeded for the corresponding dose of indicated treatments in colony survival assays. ....	122
<b>Table 6-1:</b> Copy number variations of the MOB2 locus in human cancers as collated in cBioPortal (Cerami et al., 2012).....	235

## LIST OF SUPPLEMENTARY TABLES

<b>Table S2.1</b> The measurements of total RNA concentration and absorbance determined by a Nanodrop® spectrophotometer .....	128
<b>Table S2.2</b> List of all novel binary binding partners of hMOB2 identified by yeast two-hybrid (Y2H) screens .....	129



## LIST OF ABBREVIATIONS

53BP1	p53-binding protein 1
5FU	5-fluorouracil
A-T	Ataxia-telangeictasia
AAK1	Adaptor-associated kinase 1
alt-NHEJ	Alternative non-homologous end
ANOVA	Analysis of variance
ATLD	Ataxia-telangiectasia-like disorder
ATM	Ataxia telangeictasia mutated
ATR	Ataxia telangiectasia and Rad3-related protein
ATRIP	ATR-interacting protein
APE1	Apurinic/apyrimidinic endonuclease 1
APH	Aphidicolin
APS	Ammonium sulphate
ART	ADP-ribosyltransferases
BAX	BCL2-Associated X Protein
BARD1	BRCA1-associated RING domain protein 1
BER	Base excision repair
BRCA1	Breast cancer type 1 susceptibility
BRCA2	Breast cancer type 2 susceptibility
BRCT	Breast cancer 1 carboxy-terminal
BRIP1	BRCA1-interacting protein C-terminal helicase 1
BTD	Breakthrough therapy designation
c-NHEJ	Classical non-homologous end joining
CDC25	Cell division cycle 25
CDK	cyclin-dependent kinase
CKI	CDK inhibitors
CHK1	Checkpoint kinase 1
CHK2	Checkpoint kinase 2
CPT	Camptothecin
DDR	DNA damage response
DMSO	Dimethyl sulfoxide
DMEM	Dulbecco's Modified Eagle Medium
DNA-PK	DNA-dependent protein kinase
DSB	Double strand break
dsDNA	Double-strand DNA

ECL	Enhanced chemiluminescence
EGF	Epithelial growth factor
EtOH	Ethanol
EMA	European Medicine Agency
ERCC1	Excision repair cross-complementation group 1
EXO1	Exonuclease 1
FA	Fanconi anemia
FACS	Fluorescence activated cell sorting
FANCD2	Fanconi anemia complementation group D2
FBS	Foetal Bovine Serum
FDA	Food and Drug Administration
FHA	Forkhead-associated
GBM	Glioblastoma multiforme
GG-NER	Global genomic NER
HCC	Hepatocellular carcinoma
HCCA2	Hepatocellular carcinoma-associated gene 2
HRR	Homologous recombination repair
ICL	Inter-strand crosslink
IDL	Insertion-deletion loops
IR	Ionising radiation
KAP1	[Kruppel-associated box domain]-associated protein 1
LATS	Large tumour suppressor
LOH	Loss of heterozygosity
MAPK	Mitogen-activated protein kinase
MDC1	Mediator of DNA checkpoint 1
MDM2	Mouse double minute 2
MK2	MAPK-activated kinase 2
MOB	Monopolar spindle-one-binder
MMC	Mitomycin C
MMEJ	Microhomology-mediated end joining
MMR	Mismatch repair
MST	mammalian ste20-like
MSH2	MutS homolog 2
MSH6	MutS homolog 6
MRE11	Meiotic recombination 11
MRN	MRE11-RAD50-NBS1

MYPT1	Myosin phosphatase-targeting subunit 1
NAD	Nicotinamide adenine dinucleotide
NBS	Nijmegen breakage syndrome
NBS1	Nijmegen breakage syndrome 1
NBSLD	NBS-like disorder
NDR	Nuclear Dbf2-related
NEK	NimA related kinase
NER	Nucleotide excision repair
NSCLC	Non-small-cell lung carcinoma
ORF	Open reading frame
PAGE	Polyacrylamide gel electrophoresis
PALB2	Partner and localizer of BRCA2
PAR	Polymers of ADP-ribose
PARP	Poly (ADP Ribose) polymerase
PBS	Phosphate buffered saline
PCR	Polymerase chain reaction
Pen/Strep	Penicillin/Streptomycin
PIKK3	Phosphatidylinositol 3-kinase-related kinase
PLK1	Polo-like kinase 1
PMAIP1	Phorbol-12-myristate-13-acetate-induced protein 1
PMSF	Phenylmethanesulfonylfluoride
pRb	Retinoblastoma protein
PUMA	p53 upregulated modulator of apoptosis
qPCR	quantitative real time PCR
PVDF	Polyvinylidene fluoride
RASFF1A	Ras association domain family member 1
RPA	Replication-protein A
RPM	Revolutions per minute
RIF1	RAP1-interacting factor 1
RNAi	RNA interference
RNF8	Ring finger protein 8
RNF168	Ring finger protein 168
RT-PCR	Reverse transcription polymerase chain reaction
ROS	Reactive oxygen species
SDS	Sodium Dodecyl Sulphate
Ser	Serine

SMC1	Structural maintenance of chromosomes protein 1
SSA	Single strand annealing
SSB	Single strand break
SSBR	Single-strand break repair
ssDNA	Single-strand DNA
TAZ	Transcriptional co-activator with PDZ-binding motif
TBS	Tris-buffered saline
TBS-T	Tris-buffered saline Tween
TCGA	The Cancer Genome Atlas
TC-NER	Transcription coupled-NER
TEMED	Tetramethylethylenediamine
Thr	Threonine
TLS	Translesion DNA synthesis
TNBC	Triple-negative breast cancer
TOPO I	Topoisomerase I
TOPO II	Topoisomerase II
Trc	Tricornered
UTR	Untranslated Region
UV	Ultra-violet
Wip1	Wild-type p53-induced phosphatase 1
XP	Xeroderma pigmentosum
XRCC4	X-Ray repair cross-complementing protein 4
YAP	Yes-associated protein

# Chapter 1 Introduction

## 1.1 The Hippo signalling pathway

The Hippo signalling pathway is a tumour suppressor cascade participating in the coordination of tissue growth and homoeostasis (Yu and Guan, 2013, Yu et al., 2015, Meng et al., 2016). In mammalian cells, the Hippo signalling pathway has multidirectional signal transmission mechanisms governed by a group of proteins forming the kinase core of the signalling pathway. Briefly, as illustrated in Figure 1.1, members of the MST protein kinase family (mammalian Ste20-like serine/threonine) are responsible for the phosphorylation-mediated activation of NDR/LATS (NDR1/2: nuclear Dbf2-related and LATS1/2: large tumour suppressors) protein kinases (Chan et al., 2005, Vichalkovski et al., 2008, Hergovich et al., 2009, Tang et al., 2015). In addition to the MST kinases, members of the Ste20-like MAP4K family have recently been reported to function as upstream kinases of NDR1/2 (Selimoglu, 2014) and LATS1/2 (Meng et al., 2015, Zheng et al., 2015). The NDR/LATS kinases maintain the signalling process by activating downstream signal transduction factors, such as negative regulation of the YAP (Yes-associated protein) proto-oncogene and TAZ protein (transcriptional co-activator with PDZ-binding motif) (Zhao et al., 2007, Dong et al., 2007, Zhang et al., 2015). In addition, protein-protein interactions (PPI) of NDR kinases with members of the MOB (Mps one binder) protein family have been reported to be required for a full activation of NDR/LATS protein kinases (Hergovich, 2011).

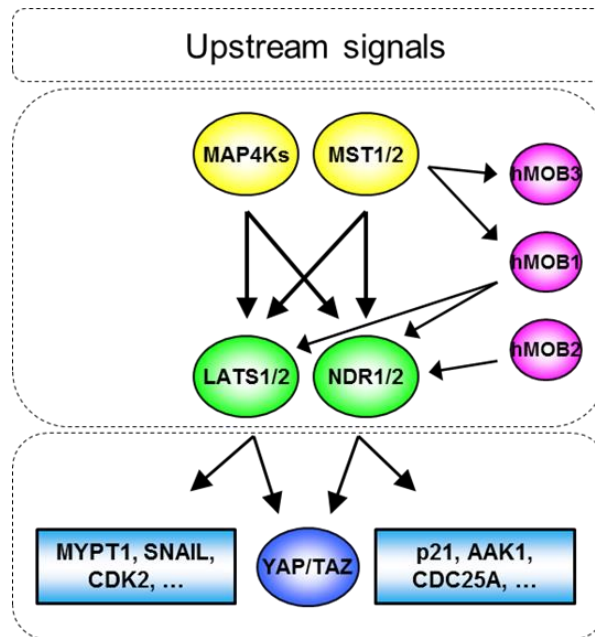


**Figure 1.1**

**The general scheme of NDR/LATS kinase signalling in humans.**

Members of the MST1/2 protein kinase family activate the NDR/LATS protein kinases by phosphorylation. This process is supported by PPIs between NDR/LATS and the hMOB1 protein which is defined as an activator element of NDR/LATS regulation. In contrast to hMOB1, hMOB2 has been defined biochemically as an inhibitory element of the NDR1/2 kinases, without any interaction with the LATS kinases. In addition to MST1/2, the MAP4K kinases can also activate phosphorylation of NDR/LATS signalling. Activated NDR/LATS protein kinases transmit the signal throughout downstream targets including YAP and TAZ (Hergovich, 2012, Meng et al., 2016), MYPT1 (Chiyoda et al., 2012), Snail (Zhang et al., 2012), CDK2 (Pefani et al., 2014), p21/cip1 (Cornils et al., 2011b), AAK1 (Ultanir et al., 2012), CDC25A (Fukasawa et al., 2015). Also, hMOB3 interacts with the MST1 kinase upon cell-cell contact and apoptotic stimuli (Tang et al., 2015). However, it is currently unclear whether hMOB3 participates in the Hippo signalling pathway.

## 1.2 The MOB protein family

The family of MOB proteins is highly conserved from yeast to humans (Hergovich, 2011). The first MOB protein (Mob1p) was described in yeast as a mitotic exit regulator more than a decade ago (Luca and Winey, 1998). Yeast expresses two MOB proteins (Mob1p and Mob2p), the *Drosophila* genome encodes three different MOBs (dMOB1, dMOB2, dMOB3), and human cells encode at least six different MOBs (hMOB1A, hMOB1B,



The Dbf2p/Dbf20p and Cbk1p kinases have been revealed as the counterparts of human NDR/LATS kinases in budding yeast (*Saccharomyces cerevisiae*), whereas the Sid2p and Orb6p kinases have been classified as the NDR/LATS kinases in fission yeast (*Schizosaccharomyces pombe*) (Hergovich, 2011, Hergovich et al., 2006c). In budding and fission yeast, Mob1p interacts with Dbf2p and Sid2p, and Mob2p associates with Cbk1p and Orb6p, respectively. Mob1p is essential for both mitotic exit network (MEN) through regulation of the Dbf2p kinase in *S. cerevisiae*, and septation initiation network (SIN) in collaboration with the Sid2p kinase in *S. pombe*. Collectively, Mob1p bears an essential role in the control of mitotic exit (for a detailed review please see Hergovich and Hemmings (2012)). Mob2p will be defined in detail in section 1.3 below.

The Trc (tricornered) and Warts kinases are the counterparts of the human NDR1/2 and LATS1/2 kinases in *Drosophila melanogaster*, respectively (Hergovich et al., 2006c). In *Drosophila*, dMOB1 (aka Mats: MOB as tumour suppressor) has been demonstrated to be significant for cell proliferation and cell death as a central component of Hippo signalling (Lai et al., 2005). Essentially, Lai et al. (2005) reported that dMOB1 corresponds to hMOB1A since ectopic hMOB1A expression could rescue phenotypes caused by the loss of dMOB1. Altogether, dMOB1 functions as an essential tumour suppressor together with the fly LATS kinase Warts (Harvey et al., 2013). Although the genetic interaction between dMOB3 and Trc has been primarily reported by He et al. (2005), dMOB3's molecular functions remain elusive. dMOB2 will be described in detail in section 1.3 below.

The NDR/LATS protein kinases are conserved from yeast to humans (Hergovich et al., 2006c). Human cells encode four NDR/LATS protein kinases: namely NDR1 (aka serine/threonine kinase 38: STK38), NDR2 (aka STK38L), LATS1 and LATS2. In mammalian cells, the tumour suppressive role of hMOB1 as a regulator of the LATS kinase remains conserved (Harvey et al., 2013, Hergovich, 2013). Considerably, MOB1-deficient mice (Nishio et al., 2012, Nishio et al., 2016) develop a broader range of tumours as reported for loss of LATS kinases (Harvey et al., 2013), highlighting that MOB1 performs significant biological functions independent of LATS



signalling. Although hMOB1A/B are cytoplasmic proteins, they can bind and activate the NDR/LATS protein kinases when targeted to the plasma membrane of cells (Hergovich et al., 2005, Hergovich et al., 2006b). Particularly, hMOB1A/B proteins bind to all four members of the NDR/LATS kinases (NDR1/2 and LATS1/2) via a highly conserved NTR region positioned near to the catalytic domain (Bichsel et al., 2004, Hergovich et al., 2005, Hergovich et al., 2009, Kohler et al., 2010, Hergovich et al., 2006a, Devroe et al., 2004, Bothos et al., 2005, Yabuta et al., 2007, Ponchon et al., 2004, Stavridi et al., 2003, Hoa et al., 2016). Studies have emphasized that the binding of hMOB1 proteins to NDR/LATS is required for complete activation of downstream factors; hence, the hMOB1 proteins have been described as important co-activators of the LATS/NDR protein kinases (Hergovich et al., 2006c, Hergovich, 2011). The biological functions of hMOB1 have been mainly defined in cell proliferation (Praskova et al., 2008), apoptosis (Vichalkovski et al., 2008), and centrosome duplication (Hergovich et al., 2009). Similar to hMOB1, the hMOB3 proteins have also been found to be localized in the cytoplasm (Hergovich et al., 2009). However, it has been observed that these cytoplasmic hMOB3 proteins neither interact with LATS1/2 nor with NDR1/2 kinases (Kohler et al., 2010, Hergovich, 2011). Significantly, a recent work showed that upon apoptotic stimuli and cell-cell contact hMOB3 protein physically interacts with the MST1 kinase, causing negative regulation of apoptotic signalling by MST1 in glioblastoma multiforme (GBM) cells, thereby potentially promoting tumorigenesis (Tang et al., 2014). hMOB2 will be described in detail in section 1.3 below.

### 1.3 From yeast to mammals: MOB2

As indicated earlier, MOB proteins are encoded by two independent genes in budding and fission yeast: Mob1p interacts with Dbf2p and Sid2p, and Mob2p associates with Cbk1p and Orb6p, respectively. Importantly, Mob1p does not associate with Orb6p, and Mob2p does not interact with Sid2p (Hou et al., 2004, Hou et al., 2003), revealing independent and non-interchangeable roles for Mob1p and Mob2p in the regulation of two different biological events. Specifically, research showed that Mob2p participates in the daughter-specific genetic programs through transcriptional activator Ace2p, suggesting a significant role for Mob2p in the control of asymmetry in budding yeast (Colman-Lerner et al., 2001, Weiss et al., 2002). Additionally, research revealed that the yeast Mob2p/Cbk1p complex is involved in the regulation of polarised growth (Jansen et al., 2006, Nelson et al., 2003). Studies in *S. pombe* demonstrated that Mob2p in complex with the yeast NDR/LATS kinase Orb6p regulates a cell morphogenesis network (Hou et al., 2003, Kanai et al., 2005).

In contrast to yeast, individual fly MOB proteins (dMOB1, dMOB2 and dMOB3) associate with both fly NDR/LATS kinases Trc/Warts (He et al., 2005). The biological responsibilities of dMOB2 are less revealed in flies, however, dMOB2 has reported roles in neuromuscular junctions (Campbell and Ganetzky, 2013) and photoreceptors (Liu et al., 2009). Significantly, dMOB2 has been reported to form a protein complex with Trc, suggesting a potential collaboration between the functions of dMOB2 and Trc in flies (He et al., 2005). Fundamentally, the function of dMOB2 appears to be different from that of dMOB1 in flies since mutations in the gene encoding dMOB2 do not specifically correspond to loss or gain of function in Trc kinase in the context of morphological phenotypes. Nonetheless, a truncated form of dMOB2 overexpression has been shown to cause a fly wing phenotype as reported for flies with the mutant Trc expression, suggesting a potential dominant-negative function for dMOB2 in flies (He et al., 2005, Hergovich, 2011). However, more research is required to fully understand the physiologically relevant roles of dMOB2.

As previously mentioned, human cells encode at least six different MOB proteins hMOB1A/B, hMOB2, hMOB3A/B/C. In contrast to the cytoplasmic hMOB1 and hMOB3 proteins, hMOB2 resides mainly in the nucleus (Hergovich et al., 2005). Besides, hMOB2 can also participate in the control of NDR1/2 signalling (Kohler et al., 2010). Interestingly, hMOB2 protein has been demonstrated to interact with only the NDR1 and NDR2 protein kinases, and no interactions with the LATS1/2 proteins have been identified (Bothos et al., 2005, Hergovich et al., 2006b, Kohler et al., 2010). The recent findings by Kohler et al. (2010) showed that hMOB2 efficiently competes with hMOB1A for binding to the same domain of NDR1 kinases (N-terminus), resulting in the inhibition of the NDR kinase activation by hMOB1. In this respect, they revealed that hMOB2 specifically interacts with the unphosphorylated NDR complexes (Kohler et al., 2010). Therefore, hMOB2 has been described as an inhibitor of the NDR kinase activity, whereas hMOB1 proteins are specified as co-activator of the NDR kinase pathway (Kohler et al., 2010, Hergovich, 2011). Nevertheless, this biochemistry focused study by Kohler et al. (2010) did not uncover the biological functions of endogenous hMOB2.

The PPIs of NDR1/2 kinases with hMOB1A/B proteins are essential for apoptotic signalling and centrosome duplication (Zhou et al., 2009, Hergovich et al., 2009). In this context, Kohler et al. (2010) also examined whether NDR kinase inhibition by hMOB2 affects these NDR functions pointed out above. Consequently, they have observed that hMOB2-mediated inhibition of NDR kinases (upregulated hMOB2 expression) interferes with NDR kinase-regulated apoptosis and centrosome duplication, supporting the putative inhibitory role of hMOB2 in two distinct biological contexts (Kohler et al., 2010). However, these observations are solely based on results obtained upon hMOB2 overexpression, leaving the function(s) of endogenous hMOB2 yet to be defined.

In the context of cancer development, the upregulation of hMOB2 (also termed HCCA2: hepatocellular carcinoma-associated gene 2) mRNA levels might be related to malignant hepatoma cellular carcinoma (HCC) progression (Wang et al., 2001). However, the *hMOB2* gene also encodes an

overlapping (but completely distinct) open reading frame (ORF) (Wang et al., 2001). Thus, it is currently not certain whether the upregulation of HCCA2 mRNA or hMOB2 mRNA is stimulating tumour development. Furthermore, when the inhibitory effect of hMOB2 on the pro-apoptotic function of the NDR kinases is elaborated, one can speculate that hMOB2 regulation might be implicated in different tumorigenic transformation (Hergovich, 2011). However, the exact involvement of the hMOB2 protein in mammalian neoplastic development is very poorly understood. Additionally, although the human *hMOB2* gene appears to display loss of heterozygosity (LOH) in more than 50% of testicular, bladder, cervical, and ovarian carcinomas (The Cancer Genome Atlas, TCGA, please see also Table 6.1, page 235) (Cerami et al., 2012), any defined physiological cancer-related functions of mammalian MOB2 have yet to be described. So far, it has only been reported that MOB2 can contribute to morphological changes in murine neurites and rat astrocytes (Fang et al., 2012, Lin et al., 2011).

On the other hand, a recent genome-wide screen for new players in the DNA damage response (DDR) signalling has proposed hMOB2 as one of many candidates awaiting validation of their potential role in the DDR (Cotta-Ramusino et al., 2011). Specifically, this study suggested that hMOB2 might contribute to mitomycin C sensitivity and activation of the IR-induced G2/M cell cycle checkpoint (Cotta-Ramusino et al., 2011), although the successful manipulation of hMOB2 levels by RNA interference (RNAi) was not verified. Therefore, up to recently (Gomez et al., 2015), direct or indirect functions of hMOB2 in the DDR have not been described.

#### 1.4 Genome instability and cancer

Cancer is described as a group of diseases principally characterised by uncontrolled cellular proliferation driving the perpetual transformation of normal cells into malignant counterparts through a complex multi-step process. In addition to previously defined hallmarks of cancer (Hanahan and Weinberg, 2000), the sheer volume of reports suggests additional “enabling and emerging characteristics of cancer” such as genomic instability by virtue of amplified oncogenic mutation incidences (Hanahan and Weinberg, 2011, Klausner, 2002, Negrini et al., 2010). Considerably, mutations can trigger uncontrolled cell proliferation and malignant transformation by causing the loss of essential tumour suppressor genes and the erroneous activation of oncogenes (Hoeijmakers, 2009), hence highlighting the importance of a maintained genomic stability.

Numerous molecular events involved in the cell cycle regulation and DDR have been identified to preserve cell survival and genome integrity (Craig, 2010, Alberts, 2008). Therefore, mammalian cells employ various molecular mechanisms to distinguish DNA replication into the synthesis (S) phase from the equal distribution of identical genetic materials during the mitosis (M) phase. These distinct set of specialised biochemical events are coordinated by the activities of cyclin-dependent kinases (CDKs) and cell cycle phase specific cyclins, two key regulatory molecules of the cell cycle progression (Hochegger et al., 2008, Malumbres et al., 2009).

In addition to deficient genome replication and/or chromosome segregation, the genetic integrity is also being constantly threatened by both spontaneously induced endogenous DNA damage (e.g. replication stress, telomere shortening, lipid peroxidation by-products, oxygen free radicals, and endogenous alkylating agents) or exogenous physical (e.g. ultraviolet [UV] radiation, ionising radiation [IR]), and chemical DNA damaging factors (e.g. chemotherapeutics) (Curtin, 2012, Goldstein and Kastan, 2015). Mammalian cells utilise a complex signalling network to detect, signal and repair DNA damage with the aim to restore genomic stability (Jackson and Bartek, 2009, Ciccia and Elledge, 2010). In case the DNA damage is beyond repair, the damaged cell is removed from the proliferating cell pool through the means

of cell death or cellular senescence. However, if the cells fail to repair DNA and/or promote cell death/senescence, mutations may arise and accumulate within the genome, consequently resulting in the dysregulation of several genes that are responsible for regulating cell growth, proliferation and/or death, which in turn would increase the risk of tumour development and progression as well as development of other diseases (Ciccia and Elledge, 2010, Jackson and Bartek, 2009, Bunting and Nussenzweig, 2013, Goldstein and Kastan, 2015).

The mammalian DDR comprises a DNA repair network that is connected with cell cycle progression, DNA replication, transcription, and chromatin remodelling (Figure 1.2) (Hoeijmakers, 2009, Kastan and Bartek, 2004). Significantly, DDR defects can promote cancer predisposition and many other syndromes such as premature ageing and impaired immune biology due to the gradual accumulation of mutagenic lesions (Jackson and Bartek, 2009). Our current understanding of the mammalian DDR system has been traced back from studying certain human genetic disorders induced by critical deficiencies in both DDR and DNA damage repair signalling pathways (Goldstein and Kastan, 2015). Recent data have emerged that patients diagnosed with these syndromes appears to have a deficiency of specific DDR proteins, leading to an obstruction of accurate detection and/or repair of induced DNA lesions, which would potentially result in tumorigenesis (Goldstein and Kastan, 2015). For instance, hereditary mutations in the *ATM* (ataxia telangiectasia mutated) gene (please see also section 1.6.1, page 48) can cause the cancer-prone phenotype termed A-T (ataxia telangiectasia) syndrome since its product participates in detecting and further signalling DNA DSBs (double-strand breaks), ultimately resulting in lymphoid malignancy predisposition (Lavin and Shiloh, 1997).

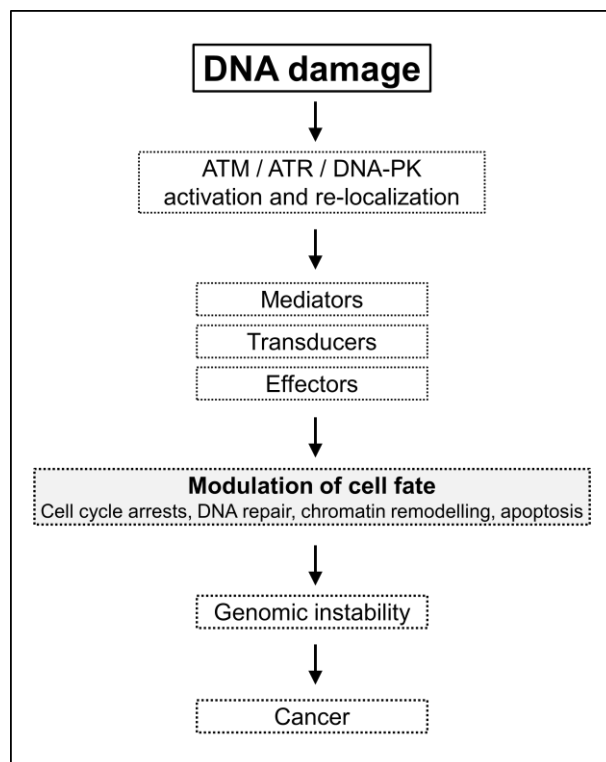


**Figure 1.2**

**General scheme of the DNA damage response (DDR).**

The DDR mechanism is connected with cell cycle progression in combination with other substrates to coordinate the outcome of the cell fate (adapted from Bain et al. (2001) and Kastan and Bartek (2004)).

The entire components of DDR needs to be accurately and orderly organised to protect genome stability, which can also influence the consequence of cancer treatments (Goldstein and Kastan, 2015). Since genome instability is a well-established hallmark of nearly all cancer forms (Hanahan and Weinberg, 2011, Negrini et al., 2010, Stratton et al., 2009) and many cancer treatments aim to triggering cellular death by damaging DNA (Hoeijmakers, 2009), the enhancement of our understanding of the DDR and repair signalling has acquired widespread attention in order to advance DNA-damaging cancer treatments, with the ultimate aims of (i) increasing therapeutic response, and (ii) decreasing the frequency of therapy resistance (Holohan et al., 2013). Remarkably, a potential interest in this field is to define a therapeutic strategy by taking advantage of the compromised genomic maintenance. Considering the intricacy of the DDR and repair

mechanisms, there is a growing interest in the development of novel small molecule inhibitors and prognostic biomarkers by taking advantage of the selective sensitivity of cancer cells arisen from their altered DNA repair capacity and damage tolerance (Hoeijmakers, 2009).

In the following sections, we will first describe the cell cycle progression and checkpoint control mechanisms in mammalian cells. Secondly, we will explain our current understanding of the DDR signalling and DNA damage repair pathways, followed by the elucidation of commonly used cancer treatment strategies.

## **1.5 Cell cycle progression and checkpoint control in mammalian cells**

### **1.5.1 Cell cycle progression in mammalian cells**

Cell cycle regulation is a highly complex challenge for every eukaryotic cell, specifically among multicellular organisms with numerous specialised cell types. Cells need to be able to immediately detect any types of DNA damages and trigger the activation of DDR signalling to establish checkpoints, which are the cell cycle phase specific, allowing tolerable time for different forms of DNA repair (Kastan and Bartek, 2004).

#### ***Definition of cell cycle stages***

The mammalian cell cycle progression has two successive processes: DNA replication in the S phase and cell segregation of duplicated chromosomes in the M phase. Each of these essential cellular processes has a preliminary phase; gap-1 (G1 phase) and gap-2 (G2 phase), which are the critical preparation steps before DNA synthesis (S), and mitosis (M), respectively (G1, S, and G2 stages are together known as interphase) (Vermeulen et al., 2003, Alberts, 2008).

In a nutshell, in the G1 phase, the cell grows and accumulates nutrients, ensuring that adequate building blocks and the proper environmental conditions are accessible for an efficient DNA duplication and cell division. During the S phase, the total amount of double-stranded DNA



molecules in the cell is successfully doubled. The G2 phase is essential for the cell to prepare for the mitotic division and cytokinesis. The M phase is subdivided into six stages: prophase, prometaphase, metaphase, anaphase, telophase and cytokinesis. The cell division occurs by the distribution of the identical chromosomes between daughter cells during the M phase (Vermeulen et al., 2003, Alberts, 2008).

Overall, the cell cycle regulation among mammalian cells assures to replicate its genetic material accurately in the S phase and to segregate chromosomes into daughter cells properly in the M phase. Significantly, the cell has numerous mechanisms for the detection and correction of endogenously or exogenously induced DNA lesions by initially activating the cell cycle checkpoints to halt cell cycle progression at the G1, S or G2 phases (Kastan and Bartek, 2004, Alberts, 2008), as summarised in section 1.5.2, page 35.

### ***Molecular regulation of cell cycle progression***

The cell cycle progression through all four phases is properly regulated based on various protein phosphorylation-dependent events (Kastan and Bartek, 2004, Reinhardt and Yaffe, 2009). The serine/threonine CDKs and cyclins collaborate to constitute catalytically active heterodimer complex molecules during the cell cycle progression. Cyclins bear no catalytic activity and CDKs are only fully activated in the presence of a partner cyclin. Significantly, the maintenance of the timely duplication and segregation of genetic information has long been established to be tightly regulated by the activities of CDKs. Furthermore, the context-specific CDK inhibitors (CKIs) including p21 (CIP1/WAF1) and p27 (KIP1) also control CDK activities by specific activating or inhibiting phosphorylations and interactions (Sherr and Roberts, 1999).

A number of CDKs participate in the regulation of cell cycle progression (Figure 1.3). For example, CDK2, CDK4 and CDK6 have been identified to be active in the G1 phase, CDK2 during the S phase, and CDK1 during the G2 and M phases. Phosphorylation events performed by the

CDK4/6-cyclin D heterodimer present in early G1, and the CDK2-cyclin E heterodimer present in late G1 are responsible for the G1 progression and the transition from G1 to S phases (Kastan and Bartek, 2004, Harris and Levine, 2005). The CDK2-cyclin E and CDK2-cyclin A complex-dependent phosphorylations coordinate progression through the S phase. The CDK1-cyclin A and CDK1-cyclin B complexes are responsible for both the G2/M transition and M phase progression together with other mitotic kinases including Aurora, PLK1 (Polo-like kinase 1), NEK (NimA related kinase) and Greatwall (Ma and Poon, 2011a).

### **Figure 1.3**

#### **Molecular regulation of the cell cycle progression.**

CDKs and cell cycle phase specific cyclins are the two key regulatory molecules of the cell cycle control. CDK2, CDK4 and CDK6 are active in the G1 phase, CDK2 during the S phase, and CDK1 during the G2 and M phases. CDK4/6-cyclin D and CDK2-cyclin E heterodimers controls the G1 progression and the G1/S transition. The CDK2-cyclin E and CDK2-cyclin A complexes regulate progression through the S phase, while the CDK1-cyclin A and CDK1-cyclin B complexes are activated for the G2/M transition and M phase progression, respectively (adapted from Vermeulen et al. (2003)).

During normal cell cycle regulation, the mitotic entry is prompted by swiftly increased activities of the CDK1-cyclin B complexes, which is dependent on the clearance of inhibitory phosphorylations on the CDK1 kinase generated by the Wee1 and Myt1 proteins (Okamoto and Sagata, 2007). The clearance of these inhibitory phosphorylations is performed by

members of the CDC25 (cell division cycle 25) family of phosphatases. Essentially, phosphorylation events responsible for the CDC25 activation are conducted by PLK1, MAPKs (mitogen-activated protein kinases) and CDK1, whereas those responsible for the CDC25 inhibition in response to DNA damage are performed by CHK1 (checkpoint kinase 1), CHK2 and MK2 (MAPK-activated protein kinase 2) (Reinhardt and Yaffe, 2013, Falck et al., 2001).

The activities of CDKs and other cell cycle kinases are essential to prevent an incorrect cell cycle progression, which therefore needs to be firmly regulated by particular interactions with CKIs. In this respect, the cell cycle progression is actively regulated by two principal protein families of CKIs: (i) the INK4 family (containing p15, p16, p18 and p19), which appears to block the CDK4/6 activity by inhibiting the formation of CDK4/6-cyclin D heterodimer, and (ii) the WAF proteins including p21 which function primarily by inhibiting the CDK4-cyclin D and CDK2-cyclin E heterodimer complexes (Reinhardt and Yaffe, 2013).

### **1.5.2 Checkpoint control in mammalian cells**

In response to various types of DNA lesions, mammalian cells can activate the DNA damage cell cycle checkpoints to delay the cell cycle progression and initiate the DNA damage repair mechanisms (Wahl et al., 1997, Deckbar et al., 2011, Bartek and Lukas, 2007). These checkpoints act as cell cycle regulators to guard cells against the accumulation of DNA damage (Kerzendorfer and O'Driscoll, 2009). Since DSBs are the most cytotoxic and complicated DNA lesions (Khanna and Jackson, 2001), we focus on describing DNA damage checkpoints activated in response to DSBs.

There are three distinctive cell cycle checkpoints in DDR: (i) the G1/S, (ii) intra-S phase, and (iii) G2/M checkpoints (Figure 1.4). The signal transduction pathways governed by ATM and ATR (ataxia telangiectasia and Rad3-related) are mainly in charge of DSB recognition and activation of relevant repair pathways in order to control several DNA damage checkpoints, depending on the type of DSB lesions. The ATM/ATR kinase

cascades initiate a series of phosphorylation events to induce cell cycle arrest via the activation of cell cycle checkpoints upon DNA damage. In this regard, the CHK1 and CHK2 kinases serve as essential signal transducers to modulate the checkpoint functions of the activated ATM/ATR kinases. Upon activation, CHK1 and CHK2 phosphorylate and thereby activate or inhibit a number of overlapping pools of downstream substrates including the p53 tumour suppressor protein (Bain et al., 2001). p53 is mostly responsible for the activation of cell cycle checkpoints (Kastan and Bartek, 2004, Bartek et al., 2007, Riley et al., 2008), and has been considered as a central, versatile and multi-functional player during the cellular DNA damage response. Upon cytotoxic stress, p53 is upregulated and stabilised to induce transcriptional programmes that are responsible for promoting transient cell cycle arrest, permanent cell cycle arrest in form of senescence, DNA repair and/or apoptosis (Vousden and Lane, 2007, Speidel, 2015, Vousden, 2006, Vousden and Prives, 2009). Since p53 is a very significant determinant involved in many aspects of DNA damage checkpoints, we will first outline our current knowledge on p53 in the context of DNA damage before describing our current understanding of the cell cycle checkpoints.

**Figure 1.4**

**Activation of DNA damage signalling pathway: key molecules and cell cycle checkpoints.**

DNA damage-activation of the ATM/ATR protein kinases leads to phosphorylation of target proteins including CHK1/2 and p53 to control cell cycle progression. There are three critical cell cycle checkpoints: the G1/S, intra-S and G2/M checkpoints, which are controlled by different regulators. The p53 protein can be targeted and phosphorylated by both the ATM/ATR and CHK2/CHK1 kinases upon DNA damage, which in turn activates the G1/S cell cycle checkpoint via p21-dependent CDK2 inhibition. CDC25A is another CHK1/2 substrate which inhibits the CDK2 activity and causes the G1/S and/or intra-S cell cycle arrest. The CHK1/2-dependent phosphorylation of CDC25C, on the other hand, results in cytoplasmic retention of CDC25C to trigger the G2/M cell cycle arrest due to a reduction in the activity of CDK1 (adapted from Bain et al. (2001)).

***The p53 tumour suppressor protein in DDR signalling***

The p53 protein functions as a tumour suppressor and nearly 50% of all human cancers bear mutations in the *p53* gene (Petitjean et al., 2007). Researchers have shown that p53 is significantly upregulated at the level of protein stabilisation in response to genotoxic stresses such as UV radiation, IR and chemotherapeutic agents (Maltzman and Czyzyk, 1984, Kastan et al., 1991, Fritsche et al., 1993, Lowe et al., 1993). Upon DNA damage, p53 is broadly modified (thereby stabilised) by phosphorylations and other various post-translational modifications (Kruse and Gu, 2009). The DDR kinases ATM, ATR, DNA-PK (DNA-dependent protein kinase), CHK1 and CHK2 are upstream regulators of p53. These modifications can induce p53 dissociation from its negative regulator MDM2 (mouse double minute 2) and lead to the

transcriptional activation of p53 (Kruse and Gu, 2009), which consequently results in the enhanced transcription of p53 targets including the CKI p21 (Figure 1.5) (Bunz et al., 1998, Speidel, 2015).

### **Figure 1.5**

#### **p53 regulates various biological processes through transcriptional activation of target genes.**

Examples of the key p53-activated target genes involved in diverse biological processes including the canonical p53-linked responses: cell cycle arrest, apoptosis and metabolism. Upon cell stress, the activated DDR signalling target p53, leading to p53 stabilisation and disassociation from its negative regulator MDM2, consequently promoting the transcriptional regulation of p53 target genes (adapted from Menendez et al. (2009) and Bieging et al. (2014)).

p53 is a transcription factor which can bind to DNA in a sequence-specific manner (Menendez et al., 2009) in order to activate or repress the transcription of genes involved in the cell cycle arrest, metabolism, apoptosis, DNA repair, autophagy, and others (Figure 1.5) (Vousden and Prives, 2009, Menendez et al., 2009, Bieging et al., 2014). Through transcriptional induction of p21, p53 can indirectly suppress CDK activity, which in turn enables the activation of the retinoblastoma protein (pRb) tumour suppressor pathway (Kastan and Bartek, 2004). Hypo-phosphorylated pRb binds to E2F transcription factors and therefore represses its transcriptional activity and

successively blocks the cell cycle progression (Figure 1.6) (Munro et al., 2012, Dyson, 1998, Mittnacht, 1998). Consequently, cells are provided time to repair induced DNA damage. In case the DNA damage is unrepairable, p53 can initiate programmed cell death, apoptosis (Vousden and Lu, 2002, Fridman and Lowe, 2003).

### **Figure 1.6**

#### **The pRb-E2F pathway controls the G1/S transition.**

Under normal conditions, hypophosphorylated pRB binds to E2F transcription factors and therefore represses its transcriptional activity. However, once phosphorylated by CDKs, pRb cannot bind to E2F complex and thereby allows the G1/S transition. Conversely, in response to DNA damage, p53/p21-dependent CDK inhibition restricts pRb phosphorylation and hence hypophosphorylated pRb inhibits the cell cycle progression by blocking E2F (adapted from Munro et al. (2012)).

Furthermore, high p53 levels can also prompt a transient or permanent cell cycle arrest (Di Leonardo et al., 1994, Agarwal et al., 1998, Stewart et al., 1995, Sugrue et al., 1997, Taylor et al., 1999). Although many factors have been reported to participate in these distinct types of cell cycle arrest (summarised in Speidel (2015)), the parameters describing the choice between apoptosis and a transient cell cycle blockage and a permanent growth arrest (senescence) are not entirely understood yet. In this context, it is worth to note that sustained p53 stabilisation induces a permanent proliferation arrest through senescence, whereas pulses of stabilised p53

cause a transient, reversible cell cycle arrest (Purvis et al., 2012). A misbalance between DNA damage and DNA repair normally results in higher p53 levels through pulses (Loewer et al., 2010), initiating a transient p53-mediated G1/S cell cycle arrest (Purvis et al., 2012). This pulsatile behaviour of p53 can be described at least in part by ATM-elicited activation of p53 that is followed by the transactivation of MDM2 and Wip1 (wild-type p53-induced phosphatase 1), the two known negative regulators of p53. The induction of MDM2 and Wip1 neutralises p53 activity as a negative feedback loop (Batchelor et al., 2009).

#### **1.5.2.1 The G1/S cell cycle checkpoint**

A small degree of DSB induction can be sufficient to activate the G1/S cell cycle checkpoint (see Figure 1.4 above on page 37) (Deckbar et al., 2010). There are two distinct processes controlling the stimulation of the G1/S checkpoint upon DNA lesions (Bartek et al., 2001, Wahl et al., 1997), namely (i) the ATM-p53-p21 (Wahl et al., 1997, Kastan et al., 1992), and (ii) the ATM-CHK2-CDC25A signalling pathways (Bain et al., 2001).

The p53 protein is particularly important in the first G1/S cell cycle arrest pathway. In response to DNA damage, p53 is targeted and phosphorylated by the ATM and/or ATR kinases as well as the CHK2/CHK1 transducers, which thereafter stimulates the stabilisation of p53 and consequent G1/S cell cycle arrest. On the other hand, the second process of G1/S cell cycle checkpoint does not completely block the S phase entry. In this process, the ATM/ATR-dependent activation of CHK2/1 further targets the family of CDC25 tyrosine phosphatases. Specifically, it has been shown that CHK2 phosphorylates CDC25A, which in turn causes its degradation, leading to diminished CDK2 activity and consequently G1/S cell cycle arrest (Deckbar et al., 2010, Bain et al., 2001, Falck et al., 2001).

#### **1.5.2.2 The intra-S phase cell cycle checkpoint**

Replication of the genome occurs during the S phase and monitoring the integrity of DNA before and during replication process is highly critical for



genome stability. The intra-S phase checkpoint is responsible for blocking DNA replication in the case of cytotoxic stress, thus preventing the accumulation of DNA damage in healthy cells (see Figure 1.4 above page 37) (Grallert and Boye, 2008). Similar to the G1/S checkpoint, the intra-S phase checkpoint can be subjected into two different branches, (i) to block ongoing replication fork progression, and (ii) to inhibit the late-firing of DNA replication origins. Significantly, during the S phase, in response to radiation-mediated DNA damage, the DNA synthesis is decelerated by two ATM-dependent signalling cascades: ATM-NBS1-SMC1 and ATM-CHK2-CDC25A branches (Kastan and Bartek, 2004, Falck et al., 2001). Late-firing of new replication origins can also be inhibited by the ATR-CHK1 signalling (Cimprich and Cortez, 2008). Specifically, upregulation of the CHK1 kinase activity causes CDC25A phosphorylation and thereby its proteasomal degradation, which in turn reduces the activity of CDKs to block the cell cycle progression (see Figure 1.4 above page 37) (Donzelli and Draetta, 2003, Sorensen et al., 2003).

#### **1.5.2.3 The G2/M cell cycle checkpoint**

In contrast to the G1/S checkpoint, the G2/M cell cycle checkpoint has higher DNA damage tolerance. For example, at least 10 to 15 DSBs are estimated to be required to induce efficient activation of the G2/M checkpoint (see Figure 1.4 above page 37) (Deckbar et al., 2011, Goodarzi and Jeggo, 2013). Hence, the G2/M checkpoint might be ineffective to preserve genome stability of the cells with a defective G1/S checkpoint (Deckbar et al., 2011). Upon DNA damage induction, the activated G2/M checkpoint thwarts the entry of G2 cells into mitosis, thus inhibiting transmission of the damaged DNA material to the offspring.

In this checkpoint, DNA damage-dependent activation of ATM and ATR kinases further phosphorylate their effectors, CHK2 and CHK1, inducing the activation of the G2/M cell cycle checkpoint. CHK2 and CHK1 kinases inhibit CDC25C activity by enabling it to interact with the 14-3-3 proteins and causing a phosphorylation-dependent nuclear export of CDC25C. As a

result, CDK1 becomes inactivated due to the continuous phosphorylation by Wee1, causing rapid blockage of M-phase entrance (Bartek and Lukas, 2007, Donzelli and Draetta, 2003, Bartek and Lukas, 2003). Initially, ATM stimulates the activation of the G2/M checkpoint; however, a late ATR response leads to a constant G2/M checkpoint response. Particularly, the change from ATM dependency to ATR dependency is determined by the DNA end resection following initial activation of the G2/M checkpoint in response to DNA damage (Lindqvist et al., 2009). Although the induction of the G2/M arrest does not require p53 (Kastan et al., 1991), p53 and its effector p21 seem to be necessary for the maintenance of the G2/M cell cycle checkpoint (Bunz et al., 1998, Taylor and Stark, 2001).

## **1.6 DNA damage signalling and repair pathways in mammalian cells**

The genetic material receives continual threats of damage from intracellular sources including stalled replication forks, telomere shortening and reactive oxygen species (ROS) produced during cellular metabolism and extracellular physical and chemical agents, such as IR and environmental DNA-damaging factors, respectively (Lindahl and Nyberg, 1972, Loeb and Harris, 2008, Lindahl and Barnes, 2000). Accumulation of DNA aberrations by the reason of unrepaired or incorrectly repaired lesions can block genome replication and transcription, resulting in cell death or genomic instability with a range of genetic alterations, such as base oxidation, DNA SSBs (single strand breaks) or DSBs. These critical lesions can cause point mutations, deletions, insertions, and/or chromosomal translocations, which in turn may induce the loss of chromosomal regions encoding tumour suppressors or eliciting oncogenic gene fusions and/or amplifications (Polo and Jackson, 2011, Helleday et al., 2008, Curtin, 2012).

The genome of a healthy cell is protected by an accurate and fully functional DDR system with numerous defence mechanisms that reflect the particular DNA lesion caused by various DNA-damaging agents (Chapman et al., 2012). For nearly every form of DNA damage, the cell has evolved a range of repair pathways, and almost each pathway has many specialised

kinases and other enzymes to promote cell survival and to prevent tumour formation/cell death. Most of the repair pathways utilise an excision mechanism to eliminate the damage from one strand of the DNA double helix by using the other strand as a template (Symington and Gautier, 2011). The DNA repair mechanisms can be classified into at least five key multi-step pathways: BER (base excision repair), NER (nucleotide excision repair), MMR (mismatch repair), NHEJ (non-homologous end joining), and HRR (homologous recombination repair) (Mao et al., 2008, Goldstein and Kastan, 2015, O'Driscoll and Jeggo, 2006, Bartek et al., 2007). In the following parts, the DDR mechanism will be first summarised, and then our current understanding of the DNA repair mechanisms will be discussed in the following sections.

### **1.6.1 DNA damage response (DDR) signalling**

The DDR network detects and signals genotoxic stresses in order to activate cell cycle checkpoints (please see section 1.5.2 above) in parallel with DNA damage repair pathways. Furthermore, the DDR signalling also modulates overall cellular homeostasis and apoptosis depending on the severity of induced damage (Jackson and Bartek, 2009, Curtin, 2012, Goldstein and Kastan, 2015, Bartek et al., 2007). Therefore, the DDR cascade has a number of different components determining, depending on the magnitude of DNA damage and the cell type, the outcome in cells with damaged DNA (Figure 1.7). The DDR constituents are responsible for: (i) rapid damage detection to trigger activation of signalling pathways and induction of cell cycle checkpoints, and (ii) DNA damage repair or (iii) activation of apoptotic pathways to eliminate terminally damaged cells. Thus, it appears to be vital to understand better the DDR coordination, since this would allow us to improve the outcome of cancer treatment in the context of manipulating DDR within the cell cycle checkpoints, specifically the DDR components that cancer cells tend to rely on for their survival.

### Figure 1.7

#### **The ATM/ATR-mediated mammalian DDR pathway.**

An accurately organised DDR signalling protects the genome against any type of DNA damage induction. In this context, the components of the DDR signalling detect and signal DNA-damaging factors to trigger the activation of the cell cycle checkpoints and DNA damage repair pathways. DDR employs a wide variety of enzymes such as kinases, nucleases, and helicases. The initial reaction of DDR is primarily maintained by the ATM and ATR kinases, which in turn activate DNA damage mediators and consequently downstream kinases and effector proteins in order to determine the cellular response to DNA damage (adapted from Sulli et al. (2012).

The DDR signalling is a signal transduction cascade employing a variety of enzymes including kinases, nucleases, helicases, recombinases, glycosylases, ligases, topoisomerases, and phosphatases (Ciccia and Elledge, 2010). The initial DDR response is primarily maintained by the ATM and ATR kinases, which are the components of the PIKKs (phosphatidylinositol 3-kinase related kinases) family of serine/threonine protein kinases (Bakkenist and Kastan, 2004). Another member of the PIKK family is the DNA-PK (DNA-dependent protein kinase) kinase, which participates in DSB repair regulation together with ATM (Lieber et al., 2003). The ATM kinase orchestrates hundreds of substrates that are actively

involved in the HRR pathway, while DNA-PK primarily coordinates a smaller number of proteins that are mostly employed in the NHEJ pathway. Importantly, RPA (replication protein A)-coated ssDNA (single-strand DNA) regions created at stalled replication forks and DSBs recruit ATR, as a complex with ATRIP (ATR-interacting protein), which is thereafter activated to transmit DNA damage signal and control the corresponding DDR pathways (Ciccio and Elledge, 2010).

The DNA damage sensor complex MRN and other factors including Ku70/80 and PARP proteins are reported to be initially activated upon formation of DSBs (Ciccio and Elledge, 2010). Activated MRN is recruited to the vicinity of DNA lesions; promoting activation of the ATM kinase by recruiting ATM at the DSBs site (Lee and Paull, 2004, Lee and Paull, 2005a). The ATM kinase initially activates many mediator proteins (e.g. adaptors, signal modifiers) through phosphorylation to amplify the DDR signal by serving as recruiters of ATM substrates (Ciccio and Elledge, 2010, Jackson and Bartek, 2009, Panier and Durocher, 2009, Thompson, 2012, Reinhardt and Yaffe, 2013, Panier and Durocher, 2013). The MRN complex and ATM kinase will be initially summarised in the following sections before reviewing the DNA damage repair pathways.

### ***The MRN complex***

The MRN multiprotein complex contains the MRE11 (meiotic recombination 11), RAD50 and NBS1 (Nijmegen breakage syndrom 1, aka nibrin) proteins. As a DNA damage sensor, the MRN complex plays a key role in the initial detection of a DSB by regulating the activation of ATM kinase, and thereafter initiates and regulates DSB repair via the HRR and NHEJ repair mechanisms (Hopfner et al., 2001, Moreno-Herrero et al., 2005, Lee and Paull, 2005a, Rupnik et al., 2010, Stracker and Petrini, 2011). MRE11 is the core component of the MRN complex and forms a nuclease homodimer. The RAD50-MRE11 interaction stimulates MRE11's DNA binding activity, ssDNA endonuclease activity and 3'-5' exonuclease activity. By taking advantage of these activities, MRN gains the capability to be able to initiate DNA end

resection to promote further DNA damage repair steps (Williams et al., 2008).

RAD50 is a member of a protein family termed as SMC (structural maintenance of chromosome), that have been identified to play a central role in supporting sister-chromatid cohesion and chromosome condensation in cells (Rupnik et al., 2010). RAD50 has an ATPase domain that comprises of an N-terminal Walker A motif and a C-terminal Walker B motif. These motifs are required for its activities to bind and partially unwind DNA double helix strands once ATP is available ("closed" form as illustrated in Figure 1.8) (Hopfner et al., 2001, Paull and Gellert, 1998). The ATPase domain is formed by bridging the two Walker motifs in close vicinity. A large coiled-coil (cc) domain between the motifs contains a "hinge" region that consists of a zinc-hook, supporting MRE11 complexes in recombination and repair (Hopfner et al., 2002). The fundamental functions of RAD50 are to tether the two ends of the broken DSB in close vicinity, and more significantly to link joints of ssDNA/dsDNA arising from stalled replication forks to avoid replication fork collapse (Costanzo et al., 2001, Trezn et al., 2006).

## Figure 1.8

### **Representative model of the MRN complex.**

MRE11 (dark grey) harbours the nuclease/dimerization and the capping domains, interconnected to the linker which associates with the coiled-coil (cc) domain of RAD50. RAD50 (light grey) has an ATPase domain formed by an N-terminal Walker A motif and a C-terminal Walker B motif, required for its activities of binding and partial unwinding DNA double helix strands when ATP is available ("closed"). The intramolecular and antiparallel cc domains bind to each other via the zinc hook (Zn hook) motifs. The closed form of the complex bears a higher binding affinity for DNA ends to tethering (adapted from Paull (2016)).

The third module of the MRN complex is NBS1 that contains a number of domains displaying PPI activities and supports MRE11 nuclease activity. The "Forkhead-associated" (FHA) domain accommodated at the N-terminus of the polypeptide shows a phosphorylation-dependent protein binding activity (Williams et al., 2009), which is essential for the phosphorylation-regulated protein interactions. To exemplify, following DSB-induction H2AX protein is phosphorylated (which is then termed  $\gamma$ H2AX), generating a binding site for NBS1 via the FHA domain, which further assists the MRN complex to be localised close to the vicinity of the DNA lesion (Kobayashi et al., 2002). Next to the FHA region, there are two motifs called BRCT (breast cancer 1 carboxy-terminal) (Becker et al., 2006) and a MRE11 binding domain positioned at the C-terminus (Williams et al., 2009). Additionally, the ATM binding domain is another key carboxyterminal motif, since studies suggest that this domain is also required for the ATM localisation to damaged chromatin (Falck et al., 2005).

Null mutations of the MRN components have been revealed to be embryonically lethal, highlighting the significance of the MRN complex for

survival. Patients diagnosed with the *NBS1* gene mutations have been observed to suffer from an autosomal recessive disorder known as NBS (Nijmegen breakage syndrome). These patients are likely to pose other risk factors including chromosomal instability, immunodeficiency and cancer predisposition (Varon et al., 1998). Likewise, ATLD (ataxia-telangiectasia-like disorder) is another example of a genomic instability syndrome induced by mutations in the *MRE11* gene, displaying the same defect as observed in patients with an ATM deficiency (Stewart et al., 1999). Furthermore, inherited mutations in the *RAD50* gene causes NBSLD (NBS-like disorder) (Stracker and Petrini, 2011). On the cellular level, cells with MRN deficiency show aberrant cell proliferation, amplified sensitivity to DNA damaging agents, dysfunctional cell cycle checkpoints, and suboptimal ATM activation (Rupnik et al., 2010, Stracker and Petrini, 2011, Williams et al., 2010).

### ***The ATM protein kinase***

As a member of the PIKKs-family, ATM is a central transducing kinase that is activated and recruited upon DSBs induction (Shiloh, 2003, Kastan and Lim, 2000). As stated earlier, patients bearing a mutation in the *ATM* gene display the rare autosomal recessive disorder called A-T (Savitsky et al., 1995). A-T patients have a broad spectrum of symptoms, such as radiation hypersensitivity, cancer predisposition and neurodegeneration (Savitsky et al., 1995, Meyn, 1995), underscoring the significance of the ATM kinase as an important protector of genome stability.

In the absence of any DNA lesion, ATM exists as a catalytically inactive homodimer which predominantly localises within the nucleus. In response to DNA lesion, ATM is recruited to damaged chromatin by the C-terminus of NBS1, leading to ATM autophosphorylation at Ser1981, thereby stimulating dimer dissociation into catalytically active monomers (Bakkenist and Kastan, 2003, Lee and Paull, 2004, Lee and Paull, 2005b). Afterwards, more than 700 identified downstream targets that participate in the cell cycle regulation and DNA damage repair mechanisms are possibly phosphorylated by the active ATM kinase (Matsuoka et al., 2007). Among many others,



H2AX is immediately phosphorylated by ATM at Ser139 site ( $\gamma$ H2AX) in response to DNA damage. Once phosphorylated,  $\gamma$ H2AX interacts with MDC1 (mediator of DNA checkpoint protein 1), which serves as a scaffold protein to recruit RNF8 (ring finger protein 8) and RNF168 E3 ubiquitin (Ub)-protein ligases. By ubiquitylating H2A, these two factors would establish docking spots for Ub-binding proteins including Rap80/Abraxas that mediates the recruitment of 53BP1 (p53-binding protein 1) and BRCA1 (breast cancer type 1 susceptibility). As explained in the following sections, 53BP1 and BRCA1 stimulate DSB repair through the NHEJ and HRR pathways, respectively (Ciccio and Elledge, 2010, Jackson and Bartek, 2009, Panier and Durocher, 2009, Thompson, 2012, Reinhardt and Yaffe, 2013, Panier and Durocher, 2013).

Moreover, as elucidated in detail in section 1.5.2.1 (starting from page 37), p53 is another essential target of ATM phosphorylation in response to DNA-damaging factors (Kastan and Bartek, 2004, Deckbar et al., 2010). Likewise, the ATM signalling cascade can induce the intra-S phase cell cycle checkpoint activation as already summarised in section 1.5.2.2, page 41 (Kastan and Bartek, 2004). Importantly, the G2/M cell cycle checkpoint can also be activated by the ATM signalling cascade as already outlined in section 1.5.2.3, page 41 (Kastan and Bartek, 2004, Bartek and Lukas, 2003, Donzelli and Draetta, 2003).

### **1.6.2 DNA double-strand break (DSB) repair pathways**

Among various DNA lesions, DSBs are extremely complicated to repair and can arise directly via physiological DNA metabolism (e.g. topoisomerase I/II) (Lindahl and Barnes, 2000, Khanna and Jackson, 2001) or after a continues exposure to exogenous factors (e.g. IR) (Curtin, 2012, Helleday et al., 2008). Alternatively, upon exposure to these factors, a DSB can also be indirectly formed when two SSBs occur in close vicinity, or when the DNA replication machinery penetrates into a SSB or other types of DNA lesions (Jackson and Bartek, 2009). This kind of DSBs that is produced indirectly by replication

fork collapse is called replication-associated DSBs (Shrivastav et al., 2008, Ciccia and Elledge, 2010, Helleday, 2010, Chapman et al., 2012).

Although DSBs can cause numerous chromosomal alterations that can then induce malignant transformation through the loss of genome stability, DSB-inducing agents (e.g. IR, topoisomerase inhibitors) are commonly employed in cancer treatment to target and eliminate cancer cells. There are two well-identified DSB repair mechanisms: the NHEJ and HRR pathways. NHEJ is defined as an error-prone repair mechanism, that can be actively employed throughout the entire cell cycle phases, whereas HRR is described as an error-free mechanism which can cope with DSBs only in the late S and G2 stages of the cell cycle since it requires a homologous sequence that is positioned on the sister chromatid. Replication-associated DSBs have been reported to be significantly critical for cancer treatment as their repair processes mainly depends on the HRR pathway (Goldstein and Kastan, 2015). There are also alternative DSB repair mechanisms, which will be outlined in section 1.6.2.3, page 55.

#### **1.6.2.1 Classical non-homologous end-joining (c-NHEJ) repair**

In mammalian cells, the NHEJ repair mechanism is active throughout the entire cell cycle phases, with NHEJ having been highlighted as the predominant DSB repair pathway (Goodarzi and Jeggo, 2013). Following the recognition of a DSB, the first reaction in NHEJ is the recruitment of Ku70/Ku80 protein complex to the vicinity of DSB and after that, the catalytic subunit DNA-PKcs are activated and recruited towards the damaged DNA site (Figure 1.9). Active DNA-PK molecules phosphorylate and activate different downstream targets comprising of ligase IV, XRCC4 and XLF proteins. Consequently, the religation of two suitable DNA ends is performed by the XRCC4-ligase IV enzyme complex (Goldstein and Kastan, 2015).

## **Figure 1.9**

### **The NHEJ DSB repair mechanism.**

A DSB is detected and bound by the Ku complex (Ku70–Ku80 heterodimer), which in turn induces DNA-PKcs activation and recruitment towards the breakage. Active DNA-PKcs molecules phosphorylate and activate various downstream targets including the ligase IV, XRCC4, and XLF proteins. The religation of two suitable DNA ends is ultimately catalysed by the XRCC4-ligase IV enzyme complex. After the ligation of DSB ends by DNA ligase IV, the DNA-repair components are removed (adapted from Lopez-Contreras (2012)).

### **1.6.2.2 Homologous recombination repair (HRR) pathway**

In mammalian cells, the HRR mechanism becomes active when an undamaged DNA template is available, which is used for restoring sequence information precisely. Therefore, the HRR mechanism becomes functional only in late S and G2 phases when a sister chromatid is accessible (Goodarzi and Jeggo, 2013, Ciccia and Elledge, 2010, Chapman et al., 2012, Jasin and Rothstein, 2013, Krejci et al., 2012). Most of the reports separate HRR into six different stages (Goodarzi and Jeggo, 2013) as follows: (i) 3' ssDNA generation by the 5'-3' end resection, (ii) recruitment of RPA on resected 3' ssDNA overhangs, (iii) displacement of RPA by RAD51 assisted by BRCA2 (breast cancer type 2 susceptibility) to form RAD51 nucleoprotein filaments, (iv) strand invasion, formation of displacement loop (D-loop) and

Holliday junction formation, (v) branch migration, and (vi) resolution of the Holliday junctions (Figure 1.10).

### **Figure 1.10**

#### **The HRR DSB repair mechanism.**

Once a DSB is recognised by MRN, RAD50 keeps the broken DNA ends together, the MRE11 endonuclease together with CtIP nicks the 5' strand at a distance from the DSB to trigger DSB resection. Consequently, specific sections of DNA at the 5' ends of the break are nucleolytically resected by nucleases creating an 3' ssDNA overhangs, which in turn promotes binding of RPA to the ssDNA tails. The RPA molecules are displaced by RAD51 to form nucleoprotein filaments, which is mediated by the BRCA1-PALB2-BRCA2 complex. The ssDNA-RAD51 nucleofilament invades into a homologous DNA sequence and the D-loop formed after strand invasion step is extended by DNA synthesis. Once strand exchange takes place, the resulting Holliday junction formation is resolved (adapted from Buisson et al. (2010)).

Following DSB recognition by the MRN complex, RAD50 keeps the broken DNA ends together, while the MRE11 endonuclease along with the CtIP nuclease nicks the 5' strand at a distance from the DSB to trigger initial DSB end resection. Next, specific sections of DNA at the 5' ends of the break are further resected by nucleases including EXO1 (Exonuclease 1) and DNA2 to generate 3' ssDNA tails, which are then coated by the RPA

complex (consisting of RPA70, RPA32, and RPA14). The trimeric RPA complex harbours high binding affinity for 3' ssDNA overhangs, causing inhibition of RAD51 loading and the HRR progression (Ciccio and Elledge, 2010, Jasin and Rothstein, 2013, Krejci et al., 2012). However, the BRCA1-PALB2-BRCA2 and BRCA1-BARD1 (BRCA1-associated RING domain protein 1) complexes have been demonstrated to assist RAD51 loading to the 3' ssDNA tails (Buisson et al., 2010, Deans and West, 2011, Densham et al., 2016).

The two different domains of BRCA2 has been shown to interact with RAD51: BRC repeats and the carboxy-terminal domain. The interaction between BRC repeats and RAD51 monomers has been indicated to be essential for the subsequent RAD51-ssDNA nucleofilament formation. However, RAD51 polymers interact with the BRCA2 C-terminus, which assists to protect RAD51-ssDNA nucleofilament formation from disassembly by BRC repeats (Esashi et al., 2007, Davies and Pellegrini, 2007, Schlacher et al., 2011). It has been reported that the C-terminal region of BRCA2 that interacts with RAD51 is phosphorylated by CDKs at Ser3291 site, which abolishes RAD51-ssDNA nucleofilament formation (Esashi et al., 2005). As mentioned earlier, upon DNA damage the CDK kinase activity is inhibited throughout different DDR pathways such as the ATM/p53/p21 and ATM/CHK2/CDC25 cascades (Kastan and Bartek, 2004). Significantly, in response to DNA damage or during the cell cycle, reduced CDK-dependent Ser3291 phosphorylation of BRCA2 has been reported to promote interactions between the BRCA2 C-terminus and RAD51, which consequently stimulate and stabilise RAD51 nucleofilament formation on ssDNA (Esashi et al., 2005, Esashi et al., 2007, Schlacher et al., 2011). Of note, numerous novel mechanisms have been recently described to involve in the CDK-mediated Ser3291 phosphorylation of BRCA2 and RAD51 nucleoprotein stability including RASSF1A-LATS1 (Pefani et al., 2014) and cyclin D1 (Chalermrujanant et al., 2016).

Besides CDKs, PLK1 has also been established to be a cell cycle regulator (Ma and Poon, 2011b). Strikingly, the cell cycle- and DNA damage-dependent RAD51 phosphorylations initially by PLK1 at Ser14 and

subsequently by CK2 (casein kinase 2) at Thr13 have been suggested to promote RAD51 recruitment onto ssDNA through NBS1 binding (Yata et al., 2012). In this context, reports have lately revealed that the PLK1-based phosphorylation of RAD51 at Ser14 residue is facilitated by BRCA2 (Yata et al., 2014) and also by TOPBP1 (topoisomerase II-binding protein 1) (Moudry et al., 2016), which in turn is likely to stabilise RAD51-dependent genome maintenance.

Additionally, through the binding to BRCA2, the PALB2 protein (partner and localizer of BRCA2) controls its localisation and stability, specifically during the recruitment of RAD51 to the RPA-coated ssDNA (Xia et al., 2006). Moreover, RAD52 is also considered to promote the accurate localisation of RAD51 by forming a complex with RAD51 to suppress the inhibitory effect of RPA (San Filippo et al., 2008).

Consequently, the RAD51-coated 3' ssDNA overhangs invade the intact homologous DNA strands, a process called "the strand invasion step". The RAD51-coated 3' strand is employed as a primer for DNA synthesis, yielding a repaired chromosome (Downs et al., 2007, Chapman et al., 2012, Krejci et al., 2012). The D-loop generated after strand invasion step is extended by DNA synthesis until it can join to the second end over the complementary sequence. Once strand exchange occurs, the resulting Holliday junction formation is resolved (Chapman et al., 2012). In this respect, BRIP1 (BRCA1-interacting protein C-terminal helicase 1) has been revealed to finalise the HRR by inhibiting premature recombination activities by virtue of its helicase activity. Furthermore, a RAD51 paralog, RAD51C has been also shown to be employed in the later phase of HRR for the resolution of Holliday junctions (Kim and D'Andrea, 2012).

In contrast to NHEJ, the HRR process is slower and restricted to the late S and G2 phases of the cell cycle due to the employment of sister chromatids as templates, providing error-free repair (Chapman et al., 2012). In the G1 cells, when HRR is not functional, DNA end resection and formation of RPA coated ssDNA tails events are prevented by 53BP1-RIF1 (Rap1-interacting factor 1) complexes, causing NHEJ to be active (Daley and Sung, 2013). Conversely, CDK-phosphorylated CtIP drives DSB end

resection in the S/G2 cells. This event is mediated by the BRCA1-dependent clearance of 53BP1-RIF1 complexes from the DSB sites, which in turn stimulates recruitment of the MRN complex to damaged chromatin and consequently promotes DNA repair by the BRCA1/2-mediated HRR pathway (Sartori et al., 2007, Daley and Sung, 2013, Chapman et al., 2012). In other words, 53BP1 protein prevents CtIP in G1 to inactivate resection, whereas the BRCA1 protein stimulates abstraction of 53BP1 in the S phase to allow CtIP-assisted resection. The fundamental point in the choice of which repair pathway should be activated is the competition between protection and resection of DSB ends (Symington and Gautier, 2011, Chapman et al., 2012, Daley and Sung, 2013).

Notably, loss of HRR functionality induces increased genome instability, which at the same time, render cancer cells sensitive to DNA crosslinking agents (please see section 1.7.2.1, page 64) and PARP inhibitors where HRR is exclusively required (Lord and Ashworth, 2016). This is further explained in section 1.7.3.3, page 72.

### **1.6.2.3 Alternative DSB repair pathways (MMEJ and SSA)**

In addition to previously explained DSB repair pathways, there are two other DSB repair mechanisms namely MMEJ (microhomology-mediated end joining) and SSA (single strand annealing). MMEJ mechanism can be supported by c-NHEJ and alt-NHEJ (alternative-NHEJ) repair pathways, and it employs short homologous sequence fragments (microhomologies) to affiliate DSB ends before ligation step. Although alt-NHEJ and MMEJ pathways are mostly pointed as synonyms, alt-NHEJ process serves possibly as only a type of the MMEJ sub-pathways (Goodarzi and Jeggo, 2013). Given that alt-NHEJ does not possibly become active unless c-NHEJ is dysfunctional, alt-NHEJ can be considered as backup process for c-NHEJ (Iyama and Wilson, 2013). Notably, c-NHEJ factors including Ku70/Ku80 and Ligase IV are not utilised in the alt-NHEJ pathway, whereas alt-NHEJ contains PARP1, XRCC1, Ligase I/III, and the MRN complex (Goodarzi and Jeggo, 2013).

The biology of the induced DSB is an essential determinant of which repair pathway to be used to correct the nucleotide fragments. In this regard, the SSA mechanism can be utilised when the induced DSB is bordered by repetitive homologous sequences on both sides of the breakage (Iyama and Wilson, 2013). This mechanism enables the DSB ends to anneal with each other following resection without strand invasion that appears in the HRR pathway. Therefore, RPA and other HRR factors are required but not RAD51 during SSA, since the SSA mechanism does not require sister chromatid exchange to repair DSBs (Iyama and Wilson, 2013). Remarkably, the SSA mechanism can induce a deletion while dealing with DSBs, hence SSA has the potential to be error-prone in comparison to HRR.

### **1.6.3 DNA interstrand crosslink (ICL) repair**

DNA inter-strand crosslink (ICL)-forming agents (e.g. mitomycin C) generate covalent links between two strands of the same DNA helix, causing a fatal cytotoxicity by effectively blocking both DNA transcription and DNA replication. The initial recognition and repair of ICL formations, which can be induced either before or during DNA replication, require a specialised DNA repair pathway. The Fanconi anaemia (FA) pathway is crucial for the repair of ICL lesions induced during DNA replication (Deans and West, 2011, Williams et al., 2013).

As a genome instability disorder causing cancer predisposition, FA is prompted by a germline defect in genes contributing to ICL resolution. The FA pathway consisting of at least 15 proteins can be divided into three subgroups: the multiprotein FA core complex (an ubiquitin E3 ligase complex; FANC-A/B/C/E/F/G/L/M), the FANCD2–FANCI complex, and downstream FA proteins (FANCD1/BRCA2, FANCI/BRIP1 and FANCD1/PALB2). The FA core complex stimulates the FANCD2–FANCI monoubiquitination in response to DNA damage. Significantly, the FANCD2 mono-ubiquitination coordinates several DNA repair pathways including NER, TLS (translesion DNA synthesis) and HRR, which are essential for the



resolution of ICL lesions (Deans and West, 2011, Williams et al., 2013, Andreassen and Ren, 2009).

During DNA replication, ICL lesion stalls the replication fork by inhibiting helicase progression, which in turn deploys “replication-dependent ICL repair” requiring HRR (as demonstrated in Figure 1.11) (Williams et al., 2013). Initially, the FANCM/FAAP24 DNA damage sensor assists recognition of the ICL lesion and subsequently initiates the repair pathway. Notably, the FANCM/FAAP24 complex immediately activates cell cycle checkpoints through the ATR-CHK1 signalling (Collis et al., 2008), particularly upon ICL-forming agents which robustly distort the double helix (e.g. cisplatin). Specifically, the resulting ssDNA formation is rapidly coated by the RPA complex, which subsequently interacts with ATRIP, and afterward induces ATR-mediated checkpoint activation (Zou and Elledge, 2003). Several DNA endonucleases such as MUS81-EME1 and XPF-ERCC1 can promote the removal of ICL from both strands of DNA; a process termed “unhooking”. As a result of the unhooking process, a stalled replication fork is converted into a DSB, which is then repaired by the HRR pathway (Williams et al., 2013, Andreassen and Ren, 2009). Importantly, cells with HRR deficiency are hypersensitive to ICL-forming agents, highlighting the significance of HRR for the precise resolution of ICLs (Wang and Gautier, 2010, Deans and West, 2011, Kim and D'Andrea, 2012, Williams et al., 2013).

### **Figure 1.11**

#### **The Fanconi anaemia (FA) pathway.**

An ICL is recognised by FANCM, leading to the localisation of the FA core complex and FANCD2-FANCI mono-ubiquitylation, which then recruits nucleases and polymerases for the ICL repair. HRR is involved in ICL repair, which is regulated by the recruitment of BRCA1, FANCN (aka PALB2) and BRCA2 complexes in order to stabilise the stalled replication fork (adapted from Deans and West (2011)).

The accurate localisation of RAD51 onto resected 3' ssDNA tails and the following strand invasion stages are recognised as critical steps in the HRR pathway as already explained in section 1.6.2.2, page 51 (Goodarzi and Jeggo, 2013, Ciccia and Elledge, 2010, Jasin and Rothstein, 2013). Intriguingly, multiple downstream constituents of the FA pathway, such as FANCD1 (aka BRCA2), FANCN (aka PALB2), FANCI (aka BRIP1), and FANCD2 (aka RAD51C) have been indicated to be able to directly participate in these processes (Kim and D'Andrea, 2012). Significantly, to finalise the ICL repair, the FA pathway promotes HRR while silencing NHEJ pathway, which suggests that the FA pathway renders ICL-induced DSBs to be

accurately repaired by HRR (Adamo et al., 2010), highlighting why HRR deficiency can sensitise cells to ICL-inducing agents.

#### **1.6.4 Other DNA damage repair pathways**

##### **1.6.4.1 Base excision repair (BER)**

The BER pathway is responsible for coping with damaged bases in DNA, such as N-alkylated purines and 8-oxo-7,8-dihydroguanine (8-OxoG), abasic sites and SSBs throughout all phases of the cell cycle (Iyama and Wilson, 2013). The BER pathway is predominantly responsible for the removal of non-bulky small nucleobase modifications, cleaving and replacing faulty base (e.g. uracil) or damaged (e.g. 3-methyladenine, 8-oxoG) bases generated by deamination, oxidation or alkylation. Briefly, an incorrect base or damaged substrate is detected and excised by specific DNA glycosylases, revealing an AP (apurinic or apyrimidinic) site intermediate, followed by an incision of the AP site by an AP endonuclease or AP lyase. After detachment of the protruding sugar fragment by a phosphodiesterase enzyme, a displacement reaction of either a single nucleotide (called short-patch BER) or up to 13 nucleotides (called long-patch BER) arises at the cleaved DNA site. Following DNA synthesis by a DNA polymerase, the nick is sealed by a DNA ligase enzyme. DNA ligase III, XRCC1, and PARP1 enzymes participate in the process of short-patch BER, on the other hand, DNA ligase I and PCNA (proliferating cell nuclear antigen) are employed in the long-patch BER pathway (Christmann et al., 2003, Kim and Wilson, 2012). SSBs are initially recognised by PARP1 (poly [ADP-ribose] polymerase 1) enzyme, catalysing the formation of PAR (poly-ADP-ribose) chains on itself and other proteins (termed PARylation) to stimulate the recruitment of dedicated BER and DNA repair components such as XRCC1, Ligases I and III (Iyama and Wilson, 2013, Goldstein and Kastan, 2015). Importantly, PARP (BER) inhibitors have recently gained much attention due to their very promising effects in cancer treatments (Lord and Ashworth, 2016, Wang et al., 2016) as elaborated in more detail in section 1.7.3.3, page 72.

#### **1.6.4.2 Nucleotide excision repair (NER)**

The NER pathway serves to fix “bulky” DNA adducts including UV-induced lesions, intra-strand crosslink formations generated by genotoxic agents such as cisplatin, ROS-induced base modifications, and others (Iyama and Wilson, 2013). Additionally, NER participates in the initial steps of ICL repair before the resulting DSB substrate is completely corrected by the HRR pathway. NER has two distinct sub-pathways referred as transcription-coupled NER (TC-NER) that fixes DNA adducts blocking RNA polymerase movement on the DNA strand, and global genomic NER (GG-NER) that functions independent from transcription. The GG-NER and TC-NER sub-pathways drive different recognition steps of DNA lesions, and share the remaining DNA repair machinery. In the NER pathway, the XP (Xeroderma pigmentosum) protein family is responsible for the instant detection of the DNA lesion to initiate DNA unwinding and then specific cleavage of the lesion by XPG and ERCC1-XPF proteins. After the removal of the damaged DNA fragment, the gap is filled by DNA polymerases and subsequently DNA ligation is carried out by ligase I enzyme (Christmann et al., 2003, Goldstein and Kastan, 2015, Iyama and Wilson, 2013).

#### **1.6.4.3 Mismatch Repair (MMR)**

The MMR pathway deals with the recognition and removal of base mismatches and IDL (insertion-deletion loops) which are induced spontaneously by replication errors and homologous recombination mistakes. MMR is highly significant to maintain faithful genomic transmission across generations by selectively detecting and repairing mismatch errors on the newly synthesised DNA strand. The mismatch error is first recognised by the MutS $\alpha$  protein complex, containing MSH2 and MSH6 proteins. The MutS $\alpha$  complex is specifically loaded to the lesion site in complex with the MutL $\alpha$  complex consisting of MLH1/3 and PMS1/2 proteins. After the endonucleases PMS2 and MLH3 introduce an incision at the location of the DNA lesion, a multi-nucleotide gap is formed by the exonuclease EXO1 (Exonuclease 1), and the gap is then filled and ligated by DNA polymerase  $\delta$

and Ligase I, respectively (Iyama and Wilson, 2013, Jiricny, 2006, Goldstein and Kastan, 2015).

### **1.7 Cancer treatments with DNA damaging agents**

The main goal of cytotoxic radiotherapy and chemotherapy is to eradicate tumour cells without harming normal tissue cells. A large number of cancer therapy agents including IR and chemotherapeutics target DNA to introduce unendurable cytotoxic lesions which can activate cell cycle checkpoints, further leading to the cell cycle arrest and ultimately apoptosis. IR, DNA cross-linking agents, topoisomerase inhibitors and DNA methylating agents are commonly utilised in cancer treatments, each promoting different types of DNA damages that is repaired by specialised DNA repair mechanisms (Figure 1.12). These agents can cause cell death by either directly or following DNA replication. Thus, DNA-damaging cancer therapy is more cytotoxic to replicating cells compared to non-replicating cells, underlying the success of DNA-targeting cancer treatment since tumour cells proliferate rapidly in most cases (Helleday et al., 2008, Veuger and Curtin, 2014). DNA lesions introduced during DNA replication cause lethal mutations or cell death by blocking, or even collapsing, DNA replication fork (Veuger and Curtin, 2014).

**Figure 1.12**

**DNA damages caused by radiotherapy and chemotherapy agents, and the repair pathways dealing with these lesions.**

Each colour signifies a specific repair mechanism repairing a particular DNA lesion. IR induces various types of DNA damages including DSBs, SSBs and 8-OxoG adducts. In addition, camptothecin induces both DSBs and SSBs, and etoposide introduces DSBs due to the inhibition of topoisomerase I and II, respectively. DSBs are repaired by the DNA-PK-mediated NHEJ and/or ATM-mediated HRR mechanisms. SSBs and chemical adducts are corrected by the PARP1/APE1-dependent BER pathway. Significantly, cisplatin and other DNA crosslinking agents cause intra- and inter-strand crosslinks (ICL). Intra-strand crosslinks are fixed by NER, whereas ICL formations are repaired by a specialised ICL repair system that contains FA, NER, TLS and HRR pathways (modified from Goldstein and Kastan (2015)).

Healthy cells have a well-coordinated DDR and several DNA repair mechanisms (Lindahl, 1993, Lindahl and Wood, 1999), which, at the same time, may offer therapy resistance to tumour cells by reducing the toxicity of DNA-targeting agents. Indeed, tumour cells can gain therapeutic resistance by increasing the activities of compensatory DDR and repair pathways (Curtin, 2012). Hence, the DDR and repair mechanisms have become promising therapeutic targets for novel personalised cancer therapy strategies, which are summarised in section 1.7.3, page 69.

### **1.7.1 Radiotherapy**

Radiation therapy is a main cancer treatment modality, which is commonly used to treat cancer patients, particularly with solid tumours (e.g. breast, uterine, lung, pancreatic, prostate and testicular cancer). Ionising radiation (IR) induces DNA damage by numerous mechanisms (e.g. base damage, crosslinking, SSBs and DSBs), which are introduced either directly via damaging DNA molecules or indirectly by generating free radicals. Importantly, it is estimated that 1 Gy radiation results in around 1,000 SSBs and 35 direct DSBs per cell (Veuger and Curtin, 2014, Goldstein and Kastan, 2015). Intriguingly, IR-induced base modifications and SSBs can also indirectly cause cytotoxic replication-associated DSBs by obstructing the replication fork progression (Goldstein and Kastan, 2015). Significantly, the NHEJ is the principal mechanism in repairing direct DSBs, whereas the HRR pathway is actively employed to deal with replication-associated DSBs in collaboration with other repair pathways (Figure 1.12) (Helleday et al., 2008), highlighting the importance of efficient HRR for the outcome of radiation treatment. However, since IR introduces a variety of DNA damage forms, different DNA repair mechanisms are employed alone or (mostly) in collaboration to deal with the damage, with HRR being the only one of them (Santivasi and Xia, 2014).

### **1.7.2 Chemotherapy**

#### ***Background***

In addition to radiation therapy, chemotherapy is another major treatment option, which is extensively used alone or in combination with radiotherapy and/or personalised therapeutics. Chemotherapy agents can be categorised depending on numerous aspects including their mechanism of actions and chemical compositions (Figure 1.12). The common mechanistic action of therapeutics that target replication fork progression is to introduce chemical adducts to DNA bases so that they can directly damage DNA to inhibit cell division. These are termed as alkylating agents, which are electrophilic

compounds bearing a covalent binding affinity for electron-rich atoms (oxygen and nitrogen) in DNA bases (Helleday et al., 2008). Bifunctional alkylating (crosslinking) agents possess two reactive sites to induce crosslinks between DNA and proteins or between DNA bases. There are two types of crosslinking agents: (i) intra-strand crosslinking agents that covalently bind to two bases within the same DNA strand, (ii) inter-strand crosslink (ICL)-inducing agents that covalently link two bases located on opposite DNA strands, frequently causing replication-associated DSBs owing to replication fork collapse. DNA damages induced by intra-strand crosslinking agents are less cytotoxic compared to those induced by ICL-inducing agents since during DNA replication some polymerases can bypass such intra-strand lesions (Helleday et al., 2008, Deans and West, 2011, Goldstein and Kastan, 2015).

In addition to crosslinking drugs, topoisomerase inhibitors are also among the commonly used anticancer agents in the clinic (Helleday et al., 2008, Deans and West, 2011, Goldstein and Kastan, 2015). In the next sections, we will first describe ICL-inducing agents and review topoisomerase inhibitors, followed by summarising examples of other DNA-damaging agents.

#### **1.7.2.1 DNA inter-strand crosslink (ICL)-inducing agents**

The two strands of DNA double helix are separated during cellular processes including transcription and replication. ICL-forming agents including nitrogen mustards, mitomycin C (MMC) and cisplatin are among the most cytotoxic drugs since they obstruct strand separation (Curtin, 2012, Deans and West, 2011, Goldstein and Kastan, 2015). They can cause irreversible covalent linkage via several chemical interactions with two bases on opposing DNA strands. All ICL-forming agents used in the clinic have broadly similar mechanism of action. However, since each ICL-inducing drug displays distinctive base specificity, the produced structural modifications in the DNA bases can trigger different cellular responses (Williams et al., 2013, Deans and West, 2011, Goldstein and Kastan, 2015). ICL-inducing compounds are



particularly deleterious since ICL repair requires specialised repair of the lesion induced on both DNA strands (Noll et al., 2006, Deans and West, 2011). The specialised ICL repair process involves the FA (please see section 1.6.3, page 56), NER (please see section 1.6.4.2, page 60) and HRR (please see section 1.6.2.2, page 51) pathways.

Mitomycin C is classified as a bifunctional alkylating compound and is used to treat cancer patients with different tumours including cervical, pancreatic, stomach, breast and lung cancer (Noll et al., 2006, Bradner, 2001). In contrast to the nitrogen mustards that form crosslinks throughout the major groove of DNA, mitomycin C interact with the minor groove of DNA to interfere with transcription and replication of DNA. Significantly, this may suggest that the mitomycin C-mediated ICL formations located on the minor groove lead to minimal disturbance to the overall DNA structure, which could be a critical determining factor for the initial detection of ICLs in cellular DNA (Noll et al., 2006, Bradner, 2001).

Platinum agents including cisplatin, carboplatin and oxaliplatin are also extensively used in the clinic. Of those, cisplatin is a bifunctional platinum-containing anticancer agent that is particularly used to treat patients with testicular, bladder, cervical, non-small cell lung, ovarian, and breast cancer along with other tumours. Cisplatin molecules react primarily with guanine by forming covalent adducts with the N7-nitrogen of purine bases (Noll et al., 2006, Huang and Li, 2013).

Although there are several other DNA crosslinking agents such as nitrogen mustards and psoralens, mitomycin C and cisplatin are effectively used in a broad range of cancer treatments. Cancer cells require a collaboration of various functional DNA repair mechanisms to cope with the damage induced by mitomycin C and cisplatin (Noll et al., 2006, Williams et al., 2013, Deans and West, 2011). Therefore, their effect most likely offers more specific and selective targeting since some of the repair pathways may be impaired in cancer cells during cellular transformation. Thus, mitomycin C and cisplatin are also widely utilised in pre-clinical studies to assess the damage repair capacity of cancer cells with different settings.

### **1.7.2.2 Topoisomerase inhibitors**

DNA topoisomerase enzymes are in charge of resolving torsional strains by cutting the phosphate backbone of the ssDNA or dsDNA to untangle supercoiled DNA, which is produced during transcription, replication or chromatin remodelling (Champoux, 2001, Pommier et al., 2010). The deliberately broken DNA backbone needs to be resealed again at the end of these processes; however, topoisomerase inhibitors can inhibit resealing activity by trapping the enzymes in complex with modified DNA strand. Topoisomerase enzymes are divided into two groups: type I and type II, hence, the type of induced damage depends on which enzyme is inhibited. Topoisomerase I enzymes transiently break DNA strands one at a time (Pommier, 2006); whereas topoisomerase II enzymes break both strands of the DNA double helix at the same time (Nitiss, 2009). Therefore, while topoisomerase I inhibitors (e.g. camptothecin) most likely induce SSBs and replication-associated DSBs, topoisomerase II inhibitors (e.g. doxorubicin) typically induce direct DSBs. Repair of topoisomerase inhibitor-mediated DNA damage contains several key steps: (i) recognition of drug-protein-DNA complex as DNA damage, (ii) exclusion of the protein that is linked to DNA, (iii) subsequent repair of the strand breaks. Thus, a number of DNA repair pathways have been demonstrated to deal with the damages caused by topoisomerase inhibition. In case cells fail to repair these lesions, apoptotic pathways are triggered to eliminate damaged cells (Wang, 2002, Helleday et al., 2008, Veuger and Curtin, 2014, Pommier et al., 2010).

As a topoisomerase I inhibitor, camptothecin (CPT) stabilises the DNA-topoisomerase I covalent complex by binding to both DNA and the enzyme via hydrogen bonds. Generation of this ternary complex prohibits DNA relegation, thereby inducing DNA damage (e.g. SSBs and replication-associated DSBs) (Adams et al., 2006, Ulukan and Swaan, 2002). Significantly, topoisomerase I inhibitors cannot directly introduce DNA damage and topoisomerase I enzyme is the only cellular target of camptothecin (Pommier, 2006). Therefore, the repair of camptothecin-induced DNA damage is very likely to be less complicated compared to the other anticancer agents (e.g. doxorubicin) that target various factors to

induce damage. The BER pathway (please see section 1.6.4.1, page 59) plays a significant role in the initial repair of camptothecin-induced lesions, which explains why cells with PARP1-deficiency are hypersensitive to topoisomerase I inhibitors (Benafif and Hall, 2015). However, the most cytotoxic mechanism of camptothecin is replication fork collapse, inducing replication-associated DSBs, therefore its toxicity is considered to be cell cycle specific (Pommier, 2006). In this case, the HRR pathway (please see section 1.6.2.2, page 51) is required for an efficient and accurate DNA repair (Pommier, 2006, Deans and West, 2011). Colorectal, lung, and ovarian cancer patients are among those who are commonly treated with camptothecin and its pharmaceutical derivatives (e.g. topotecan and irinotecan) (Takimoto et al., 1998, Pommier, 2006).

The topoisomerase II enzyme has also been pharmaceutically targeted in cancer treatment by using topoisomerase II inhibitors, notably doxorubicin and etoposide. In contrast to topoisomerase I inhibitors, the presence of active DNA replication is not compulsory to generate DSBs in the cells exposed to topoisomerase II inhibitors (Pommier, 2006, Nitiss, 2009).

Doxorubicin, an anthracycline antitumor antibiotic, is an extensively used anticancer agent in various clinical settings to treat cancer patients including those with bladder, lung, and ovarian cancer (Nitiss, 2009, Tacar et al., 2013). Doxorubicin damages cells through various cytotoxic and antimitotic activities. Doxorubicin can block the topoisomerase II activity by stabilising the enzyme-DNA complex. The topoisomerase enzyme-DNA complex impairment ceases the religation of deliberately broken DNA strands that is initially catalysed by the topoisomerase enzymes, thereby ultimately causing DSBs (Nitiss, 2009, Tacar et al., 2013). Further, doxorubicin intercalation inhibits the activities of topoisomerases as well as DNA and RNA polymerases (therefore doxorubicin is also named as topoisomerase poison), ultimately interfering with DNA replication and RNA transcription and causing cellular death (Tacar et al., 2013).

As a cytotoxic anticancer drug and topoisomerase II inhibitor, etoposide prohibits DNA synthesis by generating a ternary complex between

DNA and the topoisomerase II enzyme. This hampers religation of the broken DNA strands; inducing DSBs. Accumulation of DSBs prevents mitotic entry, consequently leading to cell death. In the clinic, especially patients with small cell lung and testicular cancer are commonly treated with etoposide (Pommier et al., 2010).

It has been suggested that etoposide-induced DSBs are less complicated compared to those induced by doxorubicin. Specifically, doxorubicin does not only block the topoisomerase II enzyme but also induces other lesions through DNA intercalation and the generation of ROS, which effects the damage repair kinetics and possibly repair pathway choice. For instance, following removal of doxorubicin, a second DNA damaging effect is sustained by the presence of doxorubicin molecules intercalated directly at the vicinity of DSBs (which keeps distorting DNA), in contrast to etoposide molecules being directly bound to the topoisomerase II enzyme (Capranico et al., 1990, Pommier et al., 1991).

#### **1.7.2.3 Other DNA damaging agents**

There are many other chemotherapeutics commonly used as anticancer agents. Considerably, DNA replication inhibitors target and block DNA synthesis in various ways. For instance, ribonucleotide reductase, required for the dNTP-production used in DNA synthesis, is inhibited by hydroxyurea (HU), while aphidicolin (APH) is employed to directly block DNA polymerase enzymes. They both interfere with replication fork stability and consequently cause numerous DNA lesions, such as DSBs (Helleday et al., 2008, Petermann et al., 2010). Antimetabolites (e.g. 5-fluorouracil, 5FU) inhibit nucleotide metabolism by depleting dNTP pool, threatening fork stability and thereby inducing cell death. Furthermore, radiomimetic drugs (e.g. bleomycin) introduce direct DSBs (DNA replication-independent DSBs), and therefore, these drugs are considered to be more efficient to eradicate non-dividing cells (Helleday et al., 2008).

### **1.7.3 Personalised therapy: synthetic lethal approaches**

Although conventional chemotherapy drugs have been widely used in the treatment of cancer patients for decades, there are a number of major problems with these therapeutics. For instance, chemotherapy drugs do not specifically and selectively kill tumour cells, since they can also potentially target normal cells, especially rapidly dividing healthy cells such as those present in the bone marrow and hair follicles (Helleday et al., 2008). Moreover, the cancer cells forming the tumour mass are generally in different cell cycle stages and often have different transcriptional profiles of genes involved in significant biological processes. These intra-tumour heterogeneities, although mostly ignored by conventional cancer treatments, can affect the outcome of the cellular response to radio- and chemotherapeutics (Shepherd, 2003, Curtin, 2012). Therefore, further understanding of the molecular and biochemical mechanisms driving the treatment response has become crucial in the management of cancer treatment (Helleday et al., 2008, Curtin, 2012, Jackson and Helleday, 2016).

Synthetic lethality in the context of DDR therapeutics is defined as a circumstance where a combination of two DDR deficiencies leads to endogenous DNA damage accumulation resulting in cell death, while only one of these deficiencies does not elicit cell death (Curtin, 2012, Helleday et al., 2008). For cancer research, this approach can be utilised therapeutically to target tumour cells where one of the DDR pathways is impaired, and its corresponding compensatory pathway is blocked via a targeted small molecule drug (Helleday et al., 2008). Notably, the therapeutic compounds which target APE1 and PARP (blocking the BER pathway), ERCC1-XPF (NER), MLH1 (MMR), DNA-PKs (NHEJ), MRE11, RAD51 and BRCA1 (HRR), and ATM, ATR, and CHK1/2 are currently under pre-clinical and clinical investigation in the context of synthetic lethality (Curtin, 2012, Veuger and Curtin, 2014, Kelley et al., 2014, Rabenau and Hofstatter, 2016). Principally, this approach should selectively eradicate tumour cells without harming normal tissue cells, since healthy cells have all DDR pathways functional to protect their DNA from endogenous damage accumulation (Veuger and Curtin, 2014, Dietlein et al., 2014, Lord et al., 2015). In the

following parts, we will outline our current knowledge in regards to DDR inhibitors with specific emphasis on inhibitors of ATM, DNA-PK and PARP, which are being widely investigated in various preclinical and clinical settings (Veuger and Curtin, 2014).

### **1.7.3.1 ATM inhibitors**

The components contributing to cell cycle checkpoint activation and DSB repair can serve optimum pharmaceutical targets in the context of synthetic lethality (Curtin, 2012, Evers et al., 2010). In this regard, the central DDR kinase ATM has been studied pre-clinically as a promising anticancer target for potential clinical applications. Among others, Wortmannin and LY294002 were initially used to block ATM activity (Veuger and Curtin, 2014). However, they are not specific to ATM inhibition, since they also inhibit other phosphoinositide 3-kinases, such as DNA-PK (Veuger and Curtin, 2014). Therefore, KU-55933 has been developed as an effective and specific ATM kinase inhibitor, which inhibits IR-induced activation of ATM signalling cascade and sensitises cells to radiotherapy (e.g. IR) and chemotherapy agents (e.g. topoisomerase inhibitors) (Veuger and Curtin, 2014). Indeed, studies with distinct human cancer cell lines revealed that KU-55933 has a potential radiosensitization activity when combined with IR treatment (Helleday et al., 2008, Veuger and Curtin, 2014, Dietlein et al., 2014, Weber and Ryan, 2015). The KU-60019 and CP466722 compounds have been subsequently developed from KU-55933 as more efficient radiosensitizers with improved potency and selectivity. Although any clinical development has not been conducted for any ATM inhibitors yet, the preclinical studies performed to date undoubtedly display that pharmaceutical inhibition of ATM is very promising for cancer therapy when combined with radiotherapy or certain chemotherapy agents (Weber and Ryan, 2015).

Moreover, apart from being a potent radio- and chemosensitizer, recent findings have shown that ATM inhibitors possess single agent activity due to the synthetic lethal interactions between the ATM-regulated and other DDR pathways. Significantly, for instance, FA-deficient cells have been

reported to be sensitive to ATM inhibition (Kennedy and D'Andrea, 2006, Kennedy et al., 2007). In addition, cells with ATM-deficiency (or inhibition) have also been demonstrated to have decreased survival when treated with PARP1 (Hoglund et al., 2011) or APE1 inhibitors (Sultana et al., 2012). To sum up, ATM inhibition offers a promising cancer strategy either as a single agent through synthetic lethality, as a potential radio- and chemosensitizer or as a predictive biomarker for the benefit of other cancer treatments.

#### **1.7.3.2 DNA-PK inhibitors**

Therapeutic inhibition of NHEJ to impair alternative repair pathway dependencies of tumour cells offers promises for cancer therapy since the efficient repair of DSBs by NHEJ, as the main DSB repair pathway (Iliakis et al., 1991, Goodarzi and Jeggo, 2013), has a vital significance regarding genome stability (Veuger and Curtin, 2014). In this respect, NU7026 and NU7441 have been developed from LY294002 as highly potent and selective DNA-PK inhibitors (Davidson et al., 2013). Upon IR or etoposide treatment, the cells treated with NU7441 showed impaired DSB repair capacity and augmented G2/M accumulation (Zhao et al., 2006), suggesting NU7441 can function as a potent radio- and chemo-sensitizer (Curtin, 2012, Veuger and Curtin, 2014, Dietlein et al., 2014). Currently, NU7026 and NU7441 have not been evaluated in any clinical development yet owing to their metabolic clearance from the blood circulation and limited bioavailability (Davidson et al., 2013). However, preclinical studies are still being carried out to increase potency, bioavailability and target specificity of the compounds (Shaheen et al., 2011).

In the context of synthetic lethality, cancer cells with ATM-deficiency (or inhibition) have been shown to have reduced survival upon DNA-PK inhibition (Gurley and Kemp, 2001, Jiang et al., 2009), suggesting that these cells are most likely addicted to the DNA-PK-mediated NHEJ mechanism as compensatory pathway for their survival. Furthermore, the cancer therapy drug NK314 has recently been demonstrated to inhibit both the topoisomerase II enzyme and DNA-PK kinase with potential activity against

tumour cells (Hisatomi et al., 2011). This may be because DSBs induced by topoisomerase II inhibitors (e.g. etoposide) are predominantly repaired by DNA-PK-mediated NHEJ pathway, which also explains why NU7441 potentiates cytotoxicity of etoposide treatment (Zhao et al., 2006). Considerably, NK314 is currently being tested in clinical trials (Davidson et al., 2013), highlighting further the significance of DNA-PK inhibitors for cancer therapy.

### 1.7.3.3 PARP inhibitors

PARP is an enzyme contributing to a variety of essential cellular processes including the repair of SSBs through the BER pathway (Sonnenblick et al., 2015). The PARP protein family consists of 17 enzymes that are classified under the group of the ARTs (ADP-ribosyltransferases). The ART enzymes are capable of transferring ADP-ribose molecules from NAD<sup>+</sup> (nicotinamide adenine dinucleotide) in order to constitute PAR units (polymers of ADP-ribose, a process termed PARylation), which are covalently attached to acceptor proteins (through specific amino acid sites). For instance, PARP detects and signals induced SSBs by catalysing PAR chains onto following protein substrates. Hence, PARP recruits effector proteins involved in DNA repair (e.g. XRCC1) to damaged chromatin. PARP is eventually released from the site of DNA damage by PARylating itself (termed as autoPARylation) (Lord et al., 2015).

HRR-deficient cells display a hypersensitivity to PARP inhibition (Bryant et al., 2005, Farmer et al., 2005, Lord and Ashworth, 2016). For example, cancer cells with homozygous *BRCA1* or *BRCA2* mutations showed HRR deficiency and a significant hypersensitivity to PARP inhibition compared to those with the heterozygous or wild-type *BRCA1/2* alleles (Farmer et al., 2005, Bryant et al., 2005). Furthermore, human breast cancer cell lines in which *BRCA2* protein was depleted by RNAi also showed hypersensitivity to PARP inhibitors (Bryant et al., 2005), further supporting the potency of PARP inhibition in HRR-deficient human cancers.



One of the mechanisms explaining why PARP inhibition is highly toxic to HRR-deficient cells but not to HRR-proficient cells is the accumulation of DSBs due to unrepaired or inefficiently repaired SSBs (Benafif and Hall, 2015, Lord and Ashworth, 2016). Mechanistically, in HRR-proficient healthy cells naturally occurring SSBs can be efficiently and effectively corrected by the PARP-dependent BER DNA repair pathways (Krokan and Bjoras, 2013). In the case of PARP inhibition, SSBs persist (are left unrepaired) and cause replication-associated DSBs during DNA replication in the S phase, which are subsequently repaired by the BRCA1/2-mediated HRR pathway in normal healthy cells. However, since *BRCA* mutant cancer cells have defective HRR, these HRR-deficient cancer cells presumably cannot efficiently repair replication-associated DSBs that are produced as a result of PARP inhibition, ultimately leading to cell death (as illustrated in Figure 1.13) (Helleday, 2010, Goulouze et al., 2016, Lord and Ashworth, 2016).

Given that pharmacological PARP inhibition (e.g. by olaparib) has been shown to be more cytotoxic compared to genetic ablation of PARP1 (Murai et al., 2012), there should be more than one mechanistic action of PARP inhibitors. In this regard, PARP inhibitors are thought to trap the PARP enzyme onto DNA strand by preventing auto-PARylation when a SSB occurs (referred as PARP-trapping). As a result, the trapping PARP-DNA complex causes DSBs and consequently cell death by blocking transcription and DNA replication (Drew, 2015, Goulouze et al., 2016). Interestingly, different PARP inhibitors possess variable degrees of PARP-trapping activity (Benafif and Hall, 2015). For instance, niraparib (Tesarco) is more potent than olaparib (AstraZeneca). Importantly, veliparib (AbbVie) induces less PARP-trapping compared to other inhibitors, which presumably makes it more tolerable when combined with radio- or chemotherapy (Walsh and Hodeib, 2016, Benafif and Hall, 2015).

**Figure 1.13**

**Synthetic lethality mechanism with PARP inhibitor.**

(A) Normal cells are able to repair spontaneous SSBs through the PARP-dependent BER pathway. Once PARP is blocked, SSBs accumulation induces replication-associated DSBs during the S phase, which are then subjected to be repaired by the BRCA1/2-mediated HRR pathway. (B) In contrast, since *BRCA* mutant cancer cells have the dysfunctional HRR mechanism, these cells most likely fail to cope with replication-associated DSBs generated as a result of PARP inhibition, ultimately leading to cell death (adapted from Goulooze et al. (2016)).

Currently, a number of PARP inhibitors are being clinically evaluated as monotherapy or in combination with radiotherapy and/or chemotherapy agents (please see Table 1.1 below) (Wang et al., 2016). Olaparib (Lynparza, AstraZeneca) is the first PARP inhibitor which has been granted the approval by the EMA (European Medicines Agency) and FDA (the U.S. Food and Drug Administration) for patients with advanced ovarian cancer classified as *BRCA1* or *BRCA2* mutant (Walsh and Hodeib, 2016, Wang et al., 2016, Deeks, 2015). Importantly, rucaparib (AG014699, Clovic Oncology) has been recently granted breakthrough therapy designation (BTD) status by the FDA for advanced ovarian cancer patients with germline or somatic *BRCA1/2* mutation (Brown et al., 2016).

**Table 1-2: PARP1 inhibitors that are currently under clinical investigation for cancer therapy (Wang et al., 2016).**

Drugs	Company	Stage	Identifiers ( <a href="https://clinicaltrials.gov">clinicaltrials.gov</a> )	Patients
Olaparib (AZD2281)	AstraZenaca	Phase III	NCT02000622	Breast cancer
			NCT02032823	Breast cancer
			NCT01874353	Ovarian cancer
			NCT01844986	Ovarian cancer
			NCT02282020	Ovarian cancer
			NCT02184195	Pancreatic cancer
			NCT01924533	Gastric cancer
Rucaparib (AG014699)	Clovis Oncology	Phase III	NCT01968213	Ovarian cancer
Niraparib (MK4827)	Tesaro	Phase III	NCT01847274	Ovarian cancer
			NCT01905592	Breast cancer
Veliparib (ABT-888)	AbbVie	Phase III	NCT02163694	Breast cancer
			NCT02032277	TNBC
			NCT02106546	NSCLC
			NCT02152982	Glioblastoma
Talazoparib (BMN673)	BioMarin	Phase III	NCT01945775	Breast cancer
E7449	Eisai	Phase Ib/II	NCT01618136	Solid tumours or B-cell lymphoma
GPI21016 (E7016)	Eisai	Phase II	NCT01605162	Melanoma
BGB-290	BeiGene	Phase I-a	NCT02361723	Solid tumours
		Phase I-b	NCT02660034	Solid tumours
ABT-767	AbbVie	Phase I	NCT01339650	Solid tumours
The highest stage of clinical studies is listed for each inhibitor. TNBC: <u>t</u> riple- <u>n</u> egative <u>b</u> reast <u>c</u> ancer, NSCLC: <u>n</u> on- <u>s</u> mall <u>c</u> ell <u>l</u> ung <u>c</u> ancer				

An increasing number of preclinical studies have evidenced that PARP inhibitors can serve as potential radiosensitizers (Benafif and Hall, 2015). Therefore, radiotherapy is commonly used in combination with PARP inhibitors since IR induces a significant amount of SSBs that are main targets of the PARP-mediated BER pathway (Drew, 2015). Two clinical studies (Phase I; NCT01460888, NCT01908478) are currently being conducted to assess the efficacy of radiotherapy alone or in combination with PARP inhibitors in patients with advanced pancreatic cancer (Benafif and Hall, 2015). Furthermore, preclinical findings have revealed that PARP inhibition enhances the cytotoxic potency of anticancer agents inducing SSBs. In line with this, alkylating agents (e.g. temozolomide) and topoisomerase inhibitors (e.g. camptothecin, etoposide) have been extensively employed to test the combinational effect of chemotherapy compounds with PARP inhibition (Benafif and Hall, 2015). Several trials are currently being performed to investigate the clinical benefits of PARP inhibitor and chemotherapy combinations (Wang et al., 2016).

The phenotype referred as “BRCAness” according to Lord and Ashworth (2016) indicates the cells which have wild-type *BRCA1/2* genes but show deficient HRR and enhanced sensitivity to PARP inhibitors. In this regard, genes that are central to the HRR pathway (e.g. ATM, CHK2, MRE11, RAD50, NBS1, PALB2) are specifically being investigated in the context of PARP inhibition, since they may offer novel means for a better therapeutic outcome for cancer patients with wild-type *BRCA1/2* alleles (Walsh and Hodeib, 2016). For instance, insufficiency of the MRN complex can display a BRCAness phenotype by rendering breast cancer cells sensitive to PARP inhibition (Oplustilova et al., 2012). Vilar et al. (2011) also reported that MRE11-deficient colorectal cancer cells showed increased sensitivity to PARP inhibition (Vilar et al., 2011). Additionally, a recent study revealed that loss of RAD50 (either via RNAi or copy number deletion) sensitised ovarian cancer cells with wild-type *BRCA1/2* to PARP inhibition (Zhang et al., 2016), signifying RAD50 as a prognostic molecular biomarker for a BRCAness phenotype and PARP inhibitor treatment. Furthermore, the breast cancer cells with ATM deletions have been found to be highly

sensitive to olaparib (Gilardini Montani et al., 2013). In addition to preclinical studies, a recent phase II trial demonstrated that a significant proportion of prostate cancer patients with ATM impairment displayed anti-tumour responses to olaparib (Mateo et al., 2015). Significantly, the FDA has recently granted BTD status to olaparib for prostate cancer-bearing ATM abnormalities (Wang et al., 2016).

Taken together, many studies have significantly highlighted that BRCA status cannot be judged as the only predictive biomarker for PARP inhibitor sensitivity. Hence, non-BRCA biomarkers (Wang et al., 2016) are very likely to offer great promises for the prediction of the therapeutic responses of PARP inhibitors in different clinical settings.

## 1.8 The scope of this project

In general, MOBs are essential scaffold proteins without any known enzymatic activities and human cells encodes at least six different MOB proteins including human MOB2 (hMOB2) (Hergovich, 2011). Up to recently (Gomez et al., 2015), the NDR kinases were the only reported binding partners of hMOB2 (Hergovich, 2011) and hMOB2 binding to NDR can block the NDR activation (Kohler et al., 2010). A recent genome wide screen for novel players in the DDR proposed hMOB2 as one of many candidates with a potential role in the DDR (Cotta-Ramusino et al., 2011). Therefore, considering that the DDR is critical to maintain genomic integrity and to prevent ageing and tumorigenesis (Jackson and Bartek, 2009), we decided to investigate on the cellular and molecular level whether hMOB2 is involved in DDR and is significant in the cellular responses to anticancer treatments. We hypothesised that hMOB2 is a novel DDR protein and hMOB2 expression levels may be considered as a candidate biomarker in the evaluation for targeted therapies of cancer with defective HRR.

**First**, since hMOB2 can function as NDR inhibitor (Kohler et al., 2010), we investigated whether hMOB2 protein levels contribute to the NDR-regulated cell cycle progression (Cornils et al., 2011b, Hergovich, 2013). Additionally, Cotta-Ramusino et al. (2011) suggested that hMOB2-defective cells might have a deficient IR-induced G2/M checkpoint activation; therefore, we also analysed whether other checkpoints were functional in hMOB2-knockdown cells. These results are presented in chapter-3.

**Second**, we aimed to identify novel binding partners of hMOB2. We also sought whether hMOB2 supports DDR upon exposure to exogenously induced DNA damage. Significantly, we also tested whether hMOB2 is involved in DSB repair pathways. These results are shown in chapter-4.

**Third**, since hMOB2 might represent a novel DDR protein that supports survival upon mitomycin C treatment (Cotta-Ramusino et al., 2011), we tested whether hMOB2 is required for cell survival after exposure to DNA-damaging treatments that are currently employed in the clinic to treat cancer patients. This final set of data is presented in chapter-5.

## Chapter 2      Materials and Methods

### 2.1 Materials

#### 2.1.1 Bacterial Media

Bacterial plates		
2.5% w/v	LB Base	(Sigma-Aldrich, L3022)
1.5% w/v	Agar	(Sigma-Aldrich, L2897)
10 mM	MgSO <sub>4</sub>	(Sigma-Aldrich, M7506)
Dissolved in ddH <sub>2</sub> O and the pH was adjusted to 7.2 by adding 10 N NaOH. The resulting solution was autoclaved and cooled down about 45-50°C before the corresponding antibiotic was added. The media was then carefully poured into 10-cm plates which were stored at 4°C. Antibiotic-free plates were prepared for XL1-blue cell preparation (see section 2.2.1.4, page 96).		

Lysogeny broth (LB medium)		
1% w/v	Tryptone	(Sigma-Aldrich, 70172)
0.5% w/v	Yeast Extract	(Sigma-Aldrich, 70161)
1% w/v	NaCl	(Sigma-Aldrich, S9888)
Dissolved in ddH <sub>2</sub> O and the pH was adjusted to 7.2 by adding 10 N NaOH. The resulting solution was autoclaved and cooled down to room temperature, which was then stored at 4°C.		

2x Yeast extract and Tryptone buffer (YT broth)		
1.6% w/v	Tryptone	(Sigma-Aldrich, 70172)
1% w/v	Yeast Extract	(Sigma-Aldrich, 70161)
0.5% w/v	NaCl	(Sigma-Aldrich, S9888)
Dissolved in ddH <sub>2</sub> O and the pH was adjusted to 7.0 by adding 10 N NaOH. The resulting solution was autoclaved and cooled down to room temperature, which was then stored at 4°C.		

IGB buffer		
10% w/v	PEG4000	(Sigma-Aldrich, 95904)
50 mM	MgSO <sub>4</sub>	(Sigma-Aldrich, M7506)
50 mM	MgCl <sub>2</sub>	(Sigma-Aldrich, 84097)
5% v/v	DMSO	(Sigma-Aldrich, D8418)

PEG4000, MgSO<sub>4</sub>, MgCl<sub>2</sub> were first dissolved in LB medium, and DMSO was included. The pH was adjusted to 6.5 by adding 10 N NaOH. The resulting solution was sterile filtered and stored at 4°C.

DMSO: dimethyl sulfoxide

## 2.1.2 Buffers and solutions

### 2.1.2.1 Buffers used in DNA agarose gel electrophoresis

DNA loading buffer (6x)		
40% w/v	Sucrose	(Sigma-Aldrich, 84097)
10% w/v	Bromophenol Blue	(Sigma-Aldrich, B0126)
TBE (Tris-Borate-EDTA)		
89 mM	Tris base	(Sigma-Aldrich, T1503)
89 mM	Boric acid	(Sigma-Aldrich, B6768)
2 mM	0.5 M EDTA, pH 8.0*	(Sigma-Aldrich, 31064)
(*) from general stock, see section 2.1.4, page 87.		
EDTA: <u>e</u> thylene <u>d</u> iamine <u>t</u> riacetic <u>a</u> cid		

### 2.1.2.2 Buffers used in immunoblotting (IB) experiments

Standard protein lysis buffer for IB (150 mM)		
20 mM	1 M Tris-HCl, pH 8.0*	(Sigma-Aldrich, T1503)
150 mM	NaCl	(Sigma-Aldrich, S9888)
10%	Glycerol	(Sigma-Aldrich, G5516)
1%	NP-40	(Sigma-Aldrich, 74385)
5 mM	0.5 M EDTA, pH 8.0*	(Sigma-Aldrich, 31064)
0.5 mM	0.5 M EGTA, pH 8.0*	(Sigma-Aldrich, E3889)
50 mM	0.5 M NaF*	(Sigma-Aldrich, S7920)
20 mM	beta-glycerophosphate	(Sigma-Aldrich, G9422)
1 mM	Na <sub>3</sub> VO <sub>4</sub>	(Sigma-Aldrich, S6508)
Dissolved in autoclaved ddH <sub>2</sub> O, which was sterile filtered and then stored at 4°C.		
(*) from general stock, see section 2.1.4, page 87.		
NP-40: <u>n</u> onidet- <u>P</u> 40, EGTA: <u>e</u> thylene glycol <u>t</u> etraacetic <u>a</u> cid		
EDTA and EGTA (metalloproteases), NaF (serine/threonine and acidic), beta-glycerophosphate (serine/threonine), and Na <sub>3</sub> VO <sub>4</sub> (tyrosine) served as phosphatase inhibitors.		



Protease inhibitors freshly added into protein lysis buffers prior its use		
1 mM	DTT	(Enzo, ALX-280-001-G005)
1 mM	Benzamidine	(Sigma-Aldrich, 12072)
0.5 mM	PMSF	(Sigma-Aldrich, P7626)
1 mM	Leupeptin	(Enzo, ALX-260-009-M025)
All from 1000X stocks stored at -20°C. DTT: <u>d</u> ithio <u>t</u> hreit <u>o</u> l, PMSF: <u>p</u> henyl <u>m</u> ethyl <u>s</u> ulfonyl <u>f</u> luoride DTT, benzamidine (serine), PMSF (serine), and leupeptin (serine and cysteine) served as protease inhibitors.		
Laemmli SDS sample buffer		
1 M	Tris-HCl, pH 6.8	(Sigma-Aldrich, T1503)
0.05% w/v	SDS	(Fisher UK, 10552785)
5%	beta-mercaptoethanol	(Sigma-Aldrich, M3148)
10% w/v	Bromophenol Blue	(Sigma-Aldrich, B0126)

Preparation of separating gel and stacking gel for SDS-PAGE			
Separating gel (10 ml per gel)			
8%	12%		
4.6 ml	3.3 ml	autoclaved ddH <sub>2</sub> O	
2.7 ml	4.0 ml	30% Acrylamide	(Fisher UK, 12381469)
2.5 ml	2.5 ml	1.5 M Tris-HCl, pH 8.8*	(Sigma-Aldrich, T1503)
0.1 ml	0.1 ml	10% SDS	(Fisher UK, 10552785)
0.1 ml	0.1 ml	10% APS*	(Sigma-Aldrich, A3678)
0.006 ml	0.004 ml	TEMED	(Fisher UK, 12331519)
Stacking gel (3%, 3 ml per gel)			
2.1 ml		autoclaved ddH <sub>2</sub> O	
0.5 ml		30% Acrylamide	(Fisher UK, 12381469)
0.38 ml		1.5 M Tris-HCl, pH 6.8*	(Sigma-Aldrich, T1503)
0.03 ml		10% SDS	(Fisher UK, 10552785)
0.03 ml		10% APS*	(Sigma-Aldrich, A3678)
0.003 ml		TEMED	(Fisher UK, 12331519)
First, acrylamide was mixed with ddH <sub>2</sub> O, which was next mixed consecutively with Tris-HCl and SDS. Finally, APS and TEMED were added, and the resulting solution immediately and carefully poured between glass plates, and finally a multi-well comb was placed (for details see section 2.2.3.1, page 103). SDS: <u>s</u> odium <u>d</u> odecyl <u>s</u> ulfate, APS: <u>a</u> mmonium <u>p</u> ersulfate (dissolved in autoclaved ddH <sub>2</sub> O), TEMED: <u>t</u> etramethylethylenediamine.			
(*) from general stocks, see section 2.1.4, page 87.			

<b>SDS running buffer</b>		
190 mM	Glycine	(Sigma-Aldrich, G7126)
25 mM	Tris base	(Sigma-Aldrich, T1503)
1% w/v	SDS (20%)	(Fisher UK, 10552785)
<b>Transfer buffer</b>		
190 mM	Glycine	(Sigma-Aldrich, G7126)
25 mM	Tris base	(Sigma-Aldrich, T1503)
20%	methanol (freshly added)	(Fisher UK, M/4056/17)
<b>Immunoblotting stripping solution</b> (the pH adjusted to 2.5 with 37% HCl)		
25mM	Glycine	(Sigma-Aldrich, G7126)
1% w/v	SDS	(Fisher UK, 10552785)
<b>TBS buffer</b> (Tris-buffered saline, the pH adjusted to 7.4 with 37% HCl and autoclaved)		
0.3 M	NaCl	(Sigma-Aldrich, S9888)
0.1 M	Tris base	(Sigma-Aldrich, T1503)
<b>TBS-T buffer</b> (dissolved in TBS buffer, used for immunoblotting washing)		
0.5%	Tween	(Sigma-Aldrich, P7949)
<b>Membrane blocking buffers</b> (dissolved in TBS-T, stored at 4°C)		
5%	Skim milk powder	(Sigma-Aldrich, 70166)
5%	BSA (bovine serum albumin)	(Roche, 10735108001)
<b>Enhanced chemiluminescent (ECL) substrates</b>		
<b>ECL stock solutions</b> (prepared in DMSO, stored at -20°C)		
250 mM	Luminol	(Sigma-Aldrich, 123072)
90 mM	pCoumaric acid	(Sigma-Aldrich, C9008)
30%	H <sub>2</sub> O <sub>2</sub>	(VWR, 23622.260)
<b>ECL solution-1</b>		
2.5 mM	Luminol (from stock)	(Sigma-Aldrich, 123072)
39.6 mM	pCoumeric acid (from stock)	(Sigma-Aldrich, C9008)
100 mM	1 M Tris-HCl, pH 8.5*	(Sigma-Aldrich, T1503)
<b>ECL solution-2</b>		
0.062%	H <sub>2</sub> O <sub>2</sub> (from stock)	(VWR, 23622.260)
100 mM	1 M Tris-HCl, pH 8.5*	(Sigma-Aldrich, T1503)
Solutions 1 and 2 are mixed (1:1) only prior its application through the membrane. (*) from general stock, see section 2.1.4, page 87.		

### 2.1.2.3 Buffers used in immunoprecipitation (IP) experiments

<b>MILB</b> (low stringency <u>M</u> ST <u>I</u> nteraction <u>L</u> ysis <u>B</u> uffer) (stored at 4°C)		
30 mM	HEPES pH 7.4	(Sigma-Aldrich, T1503)
20 mM	beta-glycerophosphate	(Sigma-Aldrich, G9422)
20 mM	KCl	(Sigma-Aldrich, P9541)
1 mM	0.5 M EGTA, pH 8.0*	(Sigma-Aldrich, E3889)
2 mM	NaF*	(Sigma-Aldrich, S7920)
1 mM	Na <sub>3</sub> VO <sub>4</sub>	(Sigma-Aldrich, S6508)
1%	Triton X-100	(Sigma-Aldrich, T9284)
<p>Additionally, 1000x protease inhibitors stored at -20°C were freshly added to the lysis buffer prior its use (as indicated in standard protein lysis buffer preparation, see 2.1.2.2, page 80).</p> <p>HEPES: N-2-hydroxyethylpiperazine-N'-2-ethanesulfonic acid</p> <p>(*) from general stock, see section 2.1.4, page 87.</p>		

### 2.1.2.4 Buffers used in chromatin isolation experiments

<b>Buffers for chromatin-cytosol isolation</b>		
<b>Buffer A</b>		
10 mM	Pipes	(Sigma-Aldrich, 80635)
100 mM	NaCl	(Sigma-Aldrich, S9888)
300 mM	Sucrose	(Sigma-Aldrich, 84097)
3 mM	MgCl <sub>2</sub>	(Sigma-Aldrich, 84097)
5 mM	0.5 M EDTA, pH 8.0*	(Sigma-Aldrich, 31064)
1 mM	0.5 M EGTA, pH 8.0*	(Sigma-Aldrich, E3889)
50 mM	0.5 M NaF*	(Sigma-Aldrich, S7920)
0.1 mM	Na <sub>3</sub> VO <sub>4</sub>	(Sigma-Aldrich, S6508)
0.1%	Triton X-100	(Sigma-Aldrich, T9284)
1 mM	Benzamidine	(Sigma-Aldrich, 12072)
4 µM	Leupeptin	(Enzo, ALX-260-009-M025)
0.5 mM	PMSF	(Sigma-Aldrich, P7626)
1 mM	DTT	(Enzo, ALX-280-001-G005)
<p>The pH was adjusted to 6.8 with 10 N NaOH.</p> <p>(*) from general stock, see section 2.1.4, page 87.</p>		

Buffer B		
3 mM	0.5 M EDTA, pH 8.0*	(Sigma-Aldrich, 31064)
0.2 mM	0.5 M EGTA, pH 8.0*	(Sigma-Aldrich, E3889)
1 mM	Benzamidine	(Sigma-Aldrich, 12072)
4 $\mu$ M	Leupeptin	(Enzo, ALX-260-009-M025)
0.5 mM	PMSF	(Sigma-Aldrich, P7626)
1 mM	DTT	(Enzo, ALX-280-001-G005)
The pH was adjusted to 8.0 with 10 N NaOH. (*) from general stock, see section 2.1.4, page 87.		

#### 2.1.2.5 Buffers used in immunofluorescence (IF) experiments

Fixation solution (PFA)		
3%	PFA ( <u>p</u> ara <u>f</u> ormal <u>a</u> ldehyde)	(Sigma-Aldrich, P6148)
2%	Sucrose	(Sigma-Aldrich, 84097)
10%	PBS (w/o Ca <sup>++</sup> /Mg <sup>++</sup> )	see section 2.1.4, page 87.
Paraformaldehyde was dissolved in ddH <sub>2</sub> O by heating at 60°C for 15-20 minutes and by slowly adding 10 N NaOH. Next, PBS ( <u>p</u> hosphate <u>b</u> uffered <u>s</u> aline, w/o Ca <sup>++</sup> /Mg <sup>++</sup> ) was included, and sucrose was dissolved. Finally, the pH was adjusted to 7.4 with 37% HCl and stored -20°C.		
Permeabilization solution (freshly prepared from 10X stock dissolved in PBS)		
0.5%	Triton X-100	(Sigma-Aldrich, T9284)
Blocking buffer (freshly prepared in PBS containing 0.05% Triton X-100)		
10%	Goat serum	(Sigma-Aldrich, G6767)

#### 2.1.2.6 Buffers used for cell cycle analysis by DNA content

Propidium iodide staining buffer		
38 mM	Na Citrate pH 7.5	(Sigma-Aldrich, S1804)
69 $\mu$ M	Propidium iodide	(Sigma-Aldrich, 81845)
10 $\mu$ g/ml	RNAse A	(Fisher/MN, NZ740505)

### 2.1.2.7 Buffers used in alkaline Comet assays

<b>Lysis buffer</b> (dissolved in ddH <sub>2</sub> O, stored at 4°)		
100 mM	disodium EDTA	(Sigma-Aldrich, ED2SS)
2.5 M	NaCl	(Sigma-Aldrich, S9888)
10 mM	Tris base	(Sigma-Aldrich, T1503)
The pH was adjusted to 10.5 with 10 N NaOH.		
1%	TritonX-100*	(Sigma-Aldrich, T9284)
*added immediately before its use		
<b>Alkaline buffer</b> (dissolved in ddH <sub>2</sub> O, stored at 4°)		
50 mM	NaOH (pellets)	(Sigma-Aldrich, S5881)
1 mM	disodium EDTA	(Sigma-Aldrich, ed2ss)
The pH was further adjusted to 12.5 with 10 N NaOH.		
<b>Neutralisation buffer</b> (dissolved in ddH <sub>2</sub> O, pH 7.5, stored at 4°)		
0.5 M	Tris base	(Sigma-Aldrich, T1503)
<b>Propidium iodide</b> (stored at 4°)		
2.5 µg/ml	Propidium iodide solution	(Sigma-Aldrich, P4864)

### 2.1.2.8 Solutions used in colony survival assays

<b>Fixation solution</b> (stored at room temperature)		
3x	Methanol	(Sigma-Aldrich, 322415)
1x	Acetic Acid (80% pure)	(Sigma-Aldrich, 27218)
<b>Staining solution</b> (dissolved in methanol, stored at room temperature)		
0.5%	Crystal violet	(Sigma-Aldrich, C3886)

### 2.1.3 Cell culture reagents

<b>Pen/Strep stock cocktail for cell culture medium</b> (1%, stored at -20°C)		
8 mg/ml	Penicillin G (64 µg/ml final conc)	(VWR, A1837.0010)
12.5 mg/ml	Streptomycin (100 µg/ml final conc)	(VWR, A1852.0025)
Dissolved in ddH <sub>2</sub> O, sterile filtered and then stored at -20°C.		

<b>Standard basal medium</b> (stored at 4°C)		
	DMEM ( <u>D</u> ulbecco's <u>M</u> odified <u>E</u> agle <u>m</u> edium)	(Sigma-Aldrich, D6429)
10%	FCS ( <u>f</u> oetal <u>c</u> alf <u>s</u> erum)	(Sigma-Aldrich, F7524)

1%	Pen/Strep cocktail	
----	--------------------	--

**Medium for MCF10A cell line (stored at 4°C)**

	DMEM/F12 medium	(Invitrogen, 31330038)
5%	Horse serum	(Invitrogen, 16050122)
1%	Pen/Strep cocktail	
20 ng/ml	Epidermal growth factor (EGF)	(Peprotech, AF-100-15-1000)
0.5 µg/ml	Hydrocortisone	(Sigma-Aldrich, H0888)
100 ng/ml	Cholera toxin	(Sigma-Aldrich, C8052)
10 µg/ml	Insulin	(Sigma-Aldrich, I1882)

Stocks were prepared for the ingredients as follows: EGF (100 µg/ml stock) was dissolved in autoclaved ddH<sub>2</sub>O. Hydrocortisone (1 mg/ml stock) was resuspended in ethanol (100%). Cholera toxin (1 mg/ml stock) was dissolved in autoclaved ddH<sub>2</sub>O, mixed well, and allowed 10-15 minutes to reconstitute. Insulin (10 mg/ml stock) was dissolved in autoclaved ddH<sub>2</sub>O comprising 1% acetic acid, mixed well, and allowed 10-15 minutes to reconstitute. All were aliquoted in 1.5 ml Eppendorf tubes and stored at -20°C (Debnath et al., 2003).

**Medium for Bj-hTert cell line (stored at 4°C)**

	DMEM: Media199	(Sigma-Aldrich, M4530)
10%	FCS	(Sigma-Aldrich, F7524)
50 µg/ml	Gentamicin	(Invitrogen, 15710049)

**Medium for U2OS cell line integrated with GFP reporter (stored at 4°C)**

	DMEM without sodium pyruvate	(Sigma-Aldrich, D5796)
10%	FCS	(Sigma-Aldrich, F7524)
1%	Pen/Strep cocktail	

**PBS (for general tissue culture use, stored at 4°C)**

	D-PBS w/o Ca <sup>++</sup> /Mg <sup>++</sup>	(Invitrogen, 14190169)
--	--	------------------------

**Trypsin (for general use, stored at 4°C, the stock is at -20°C)**

0.25%	Trypsin	(Invitrogen, 25050-014)
0.5 mM	EDTA	(Sigma-Aldrich, 31064)

**Standard freezing medium (sterile filtered and stored at -20°C)**

10%	DMSO	(Sigma-Aldrich, D8418)
90%	FCS	(Sigma-Aldrich, F7524)

<b>Trypsin</b> (for MCF10A cell line, stored at 4°C, the stock is at -20°C)		
0.05%	Trypsin plus 0.53 mM EDTA	(Invitrogen, 25300096)

<b>Freezing medium</b> (for MCF10A cell line, sterile filtered and stored at -20°C)		
70%	DMEM/F12 medium	(Invitrogen, 31330038)
20%	Horse serum	(Invitrogen, 16050122)
10%	DMSO	(Sigma-Aldrich, D8418)

<b>Tetracycline</b> (dissolved in EtOH, 1000x stock stored at -20°C)		
2 mg/ml	Tetracycline hydrochloride (2 µg/ml final conc)	(Sigma-Aldrich, 87128)

<b>Polybrene</b> (dissolved in ddH <sub>2</sub> O, 1000x stock stored at -20°C)		
0.8 mg/ml	Polybrene (0.8 µg /ml final conc)	(Sigma-Aldrich, H9268)

<b>Antibiotics stock solutions used in tissue culture</b> (stored at -20°C)		
100 mg/ml	G418 (Geneticin)	(Invivogen, ant-gn-5)
10 mg/ml	Puromycin	(Invivogen, ant-pr-1)
10 mg/ml	Blasticidin S	(Invivogen, ant-bl-1)
100 mg/ml	Zeocin	(Invivogen, ant-zn-5)

<b>Mycoplasma and bacterial contamination removal reagents used in tissue culture</b> (stocks stored at -20°C)		
50 mg/ml	Plasmocin	(Invivogen, ant-mpt)
100 mg/ml	Normocure	(Invivogen, ant-noc)

<b>Transfection reagents used in tissue culture</b> (stored at 4°C)		
	Fugene 6	(Promega, E2692)
	Lipofectamine 2000	(Invitrogen, 11668019)
	Lipofectamine RNAiMAX	(Invitrogen, 13778150)

<b>Optimem</b> (stored at 4°C)		
	Optimem	(Invitrogen, 31985-047)

#### 2.1.4 General buffers

<b>PBS, w/o Ca<sup>++</sup>/Mg<sup>++</sup> pH 7.4</b>		
137 mM	NaCl	(Sigma-Aldrich, S9888)

8 mM	Na <sub>2</sub> HPO <sub>4</sub>	(Sigma-Aldrich, S3264)
2.7 mM	KCl	(Sigma-Aldrich, P9541)
1.4 mM	KH <sub>2</sub> PO <sub>4</sub>	(Sigma-Aldrich, P9791)
The pH was adjusted to 7.4 by adding 37% HCl.		

Other stock solutions		
0.5 M	EDTA	(Sigma-Aldrich, 31064)
The pH was adjusted to 8.0 by adding 10 N NaOH.		
0.5 M	EGTA	(Sigma-Aldrich, E3889)
The pH was adjusted to 8.0 by adding 10 N NaOH.		
1 M	Tris-HCl, pH 6.8	(Sigma-Aldrich, T1503)
The pH was adjusted to 6.8 by adding 37% HCl.		
1 M	Tris-HCl, pH 8.5	(Sigma-Aldrich, T1503)
The pH was adjusted to 8.5 by adding 37% HCl.		
1.5 M	Tris-HCl, pH 6.8	(Sigma-Aldrich, T1503)
The pH was adjusted to 6.8 by adding 37% HCl.		
1.5 M	Tris-HCl, pH 8.8	(Sigma-Aldrich, T1503)
The pH was adjusted to 8.8 by adding 37% HCl.		
0.5 M	NaF	(Sigma-Aldrich, S7920)
10% w/v	APS (stored at 4°C)	(Sigma-Aldrich, A3678)

### 2.1.5 List of antibodies used in this project

Primary antibodies for immunoblotting experiments				
Antibody	Source	Company	Cat No	Dilution
hMOB2*	rat	homemade		1/250
hMOB2*	rabbit	homemade		1/250
hMOB2**	rabbit	homemade		1/100
(*) polyclonal, produced in collaboration with Eurogentec (Kohler et al., 2010).				
(**) monoclonal, produced in collaboration with Epitomics (unpublished).				
HA	rabbit	Cell Signaling	3724	1/1000
MYC	rabbit	Cell Signaling	2278	1/1000
FLAG	mouse	Sigma	F3165	1/1000
Cyclin D1	mouse	Cell Signaling	2926	1/1000
Cyclin E	mouse	Santa Cruz	sc-247	1/1000
Cyclin A	rabbit	Santa Cruz	sc-751	1/1000



Cyclin B1	mouse	BD Biosciences	554176	1/1000
Actin	goat	Santa Cruz	sc-1616	1/1000
Tubulin (YL1/2)	rat	homemade		1/1000
CDK2	mouse	Santa Cruz	sc-6248	1/1000
CDK4	mouse	Santa Cruz	sc-53636	1/1000
p53	mouse	Santa Cruz	sc-126	1/1000
p21	rabbit	Cell Signaling	2947	1/1000
MDM2	mouse	Santa Cruz	sc-965	1/200
p-pRb (S807/811)	rabbit	Cell Signaling	9308	1/500
p57	rabbit	Santa Cruz	sc-1040	1/200
p27	rabbit	Santa Cruz	sc-528	1/200
p15	rabbit	Santa Cruz	sc-612	1/200
p16	rabbit	Santa Cruz	sc-759	1/200
p18	mouse	Santa Cruz	sc-56332	1/200
p19	rabbit	Santa Cruz	sc-1063	1/200
p14ARF	goat	Santa Cruz	sc-8613	1/200
p-ATM (S1981)	mouse	Santa Cruz	sc-47739	1/200
ATM	rabbit	Millipore	07-1286	1/1000
p-SMC1 (S957)	mouse	Cell Signaling	4805	1/200
p-SMC1 (S957)	rabbit	Novus Biologicals	NB100-205	1/200
SMC1	rabbit	Cell Signaling	4802	1/1000
p-NBS1 (S343)	rabbit	Cell Signaling	3001	1/500
NBS1	mouse	BD Biosciences	611870	1/1000
NBS1	rabbit	Novus Biologicals	NB100-143	1/1000
RAD50	mouse	BD Biosciences	611010	1/1000
RAD50	mouse	Santa Cruz	sc-56209	1/1000
RAD50	rabbit	Novus Biologicals	NB100-154	1/500
MRE11	mouse	BD Biosciences	611366	1/1000
MRE11	rabbit	Novus Biologicals	NB100-152	1/1000
p-KAP1 (S824)	rabbit	Bethyl	A300-767A	1/1000
KAP1	goat	Abcam	ab3831	1/1000
p-p53 (S15)	rabbit	Cell Signaling	9284	1/500
p-p53 (S20)	rabbit	Cell Signaling	9287	1/500
p-p53 (S37)	rabbit	Cell Signaling	9289	1/500

p-CHK2 (Thr 68)	rabbit	Cell Signaling	2661	1/500
CHK2	rabbit	Cell Signaling	2662	1/500
p-CHK1 (S317)	rabbit	Cell Signaling	2349	1/500
CHK1	mouse	Insight / Santa Cruz	sc-8408	1/500
PCNA	mouse	Dako	M 0879	1/25000
H3	rabbit	Abcam	ab1791	1/25000
NDR1/STK38	mouse	Caltag-MedSystems/Abnova	H00011329-M11	1/1000
NDR2/STK38L	rabbit	homemade (Vichalkovski et al., 2008)		1/500
p-BRCA2 (S3291)	rabbit	provided by Dr. Fumiko Esashi (Esashi et al., 2007)		1/1000
BRCA2	mouse	Millipore / Calbiochem	OP95	1/500
p-RAD51 (S14)	rabbit	provided by Dr. Fumiko Esashi (Yata et al., 2012)		1/1000
RAD51	rabbit	Insight / Santa Cruz	sc-8349	1/500
p-RPA32 (S4-S8)	rabbit	Bethyl labs / Cambridge B	A300-245A	1/1000
RPA32	mouse	Merck Chemicals	NA18	1/1000
<b>Primary antibodies for immunofluorescence experiments</b>				
<b>Antibody</b>	<b>Source</b>	<b>Company</b>	<b>Cat No</b>	<b>Dilution</b>
$\gamma$ H2AX (S139)	rabbit	Cell Signaling	9718	1/400
53BP1	mouse	Millipore	MAB3802	1/200
RAD51	rabbit	Insight / Santa Cruz	sc-8349	1/50
Mitotin / CENPF	mouse	BD Biosciences	610768	1/200
RPA70	mouse	Calbiochem / Millipore	NA13	1/100
Mitotin / CENPF	rabbit	Abcam	Ab5	1/200
<b>Secondary antibodies for immunoblotting experiments</b>				
<b>Antibody</b>	<b>Source</b>	<b>Company</b>	<b>Cat No</b>	<b>Dilution</b>
Rabbit	donkey	GE Healthcare	10794347	1/5000
Mouse	sheep	GE Healthcare	10196124	1/5000
Rat	goat	GE Healthcare	GZNA935	1/5000
Goat	donkey	SC / Insight Biotech	SC-2056	1/5000

Secondary antibodies for immunofluorescence experiments				
Antibody	Source	Company	Cat No	Dilution
FITC (fluorescein isothiocyanate)	rabbit	Stratech – Jackson, UK	711-095-152	1/100
	mouse	Stratech – Jackson, UK	715-095-151	1/100
Texas red	mouse	Stratech – Jackson, UK	715-075-151	1/100
	rabbit	Stratech – Jackson, UK	711-075-152	1/100

### 2.1.6 List of plasmids used in this project

Gene	Vector backbone	Reference
shMOB2#4	pSuper.retro.puro	(based on Qiagen siMOB2#4)
shMOB2#5	pSuper.retro.puro	(Kohler et al., 2010)
shMOB2#6	pSuper.retro.puro	(based on Qiagen siMOB2#6)
shp53#2	pSuper.retro.puro	(Brummelkamp et al., 2002)
shp53#2/shMOB2#4	pSuper.retro.puro	
shNDR1#4	pSuper.retro.puro	(Hergovich et al., 2007)
shp53#2	pMKO.1	(Addgene, 10672)
HA_MOB2	pLXSN	
HA_MOB2 (K131R)	pLXSN	
HA_MOB2	pcDNA3_neo	
myc_MOB2	pcDNA3_neo	
HA_NDR1-PIF	pT-Rex-DEST30	
HA_RAD50	pcDNA3_neo	
FLAG_UBR5	pCMV_neo	(Ling and Lin, 2011)
HA_HECT	pcDNA3_neo	
Empty vector (EV)	pCAGGS	(Tichy et al., 2010)
pCBAScel	pCAGGS	(Tichy et al., 2010)
GFP	pEGFP-C1	

MOB2 and NDR1/2 cDNA and shRNA plasmids were described in Hergovich et al. (2005), Hergovich et al. (2007), and Kohler et al. (2010). The RAD50 cDNA was kindly provided by C. Wyman, Erasmus University Medical Center, Rotterdam, The Netherlands. NDR1-PIF was described in Cook et al. (2014). pCMV-FLAG-UBR5 full-length was kindly provided by R. Sutherland (Garvan Institute of Medical Research, Sydney, Australia), and used as a template to amplify the HECT domain (residues 2501 to 2799). pCAGGS and pCBAScel were kindly provided by E. D. Tichy (University of Cincinnati, Cincinnati, USA). When necessary, subcloning experiments were carried out as described in section 2.2.1.1, page 93. Most of the constructs were prepared by Dr. Valenti Gomez.

### 2.1.7 List of siRNAs used in this project

siRNA	Target sequence
siLUC	5`- aacgtacgcggaataacttcga -3`
siMOB2#4	5`- caggagagacgtgtcagacga -3`
siMOB2#5	5`- ccgcgagattgaccttaacga -3`
siMOB2#6	5`- atgcgtgccgtttgtagagaa -3`
siP21#2	5`- ctggcattagaattattttaa -3`
siFANCD2#6	5`- ctccgtatttccggttactga -3`
siNDR2#5	5`- aggagatgtactgtattata -3`
All siRNAs were purchased from Qiagen. The resuspension of siRNAs was carried out according to the manufacturer's instructions. The siRNA pellet was resuspended in RNase-free ddH <sub>2</sub> O provided by the company to get 10 µM final stock concentrations, which was then aliquoted into smaller volumes and stored at -20°C.	

### 2.1.8 List of primers used in this project (for qRT-PCR)

Gene symbol	Target	Cat No
MOB2	MOB2	QT00056399
RRN18S	18S rRNA	QT00199367
CDKN1A	p21	QT00062090
GADD45A	GADD45A	QT00014084
MDM2	MDM2	QT00056378
PPARGC1A	PRGC1	QT00095578
BAX	BAX	QT00031192
PMAIP2	NOXA	QT01674771
BBC3	PUMA	QT00082859
C12orf5	TIGAR	QT00071225
SCO2	SCO2	QT00239162
SESN2	SESN2	QT00071729
All primers were purchased from Qiagen. The reconstitution of lyophilized forward and reverse (mix) primers was carried out according to the manufacturer's instructions. The primer pellet was resuspended in RNase-free ddH <sub>2</sub> O provided by the company to get 10x final stock concentrations, which was then aliquoted into smaller volumes and stored at -20°C.		

## **2.2 Methods**

### **2.2.1 DNA protocols – Molecular cloning techniques**

#### **2.2.1.1 Restriction digest and ligation of DNA fragments**

All restriction enzymes utilized in this project were bought from New England Biolabs (NEB) and the corresponding experiments were performed according to the manufacturer's instructions. Briefly, to obtain the relevant DNA fragment (vector and insert), 5-10 µg plasmid DNA were digested with the corresponding enzymes (10-20 U) in a total volume of appropriate buffer (e.g. 50 µl) mixture overnight. The next day, the resulting product was run on DNA agarose gel electrophoresis (see section 2.2.1.3, page 95) for 2-6 hours. The determined fragments were cut out and eluted with QIAquick Gel Extraction kit (Qiagen, 28706) as described by the manufacturer. For ligation of the vector and insert fragments, 1 µl of vector DNA (approx. 50-100 ng/µl) was mixed with 8 µl insert DNA, 10 µl of 2x rapid ligation buffer (Promega, C6711) and 1 µl T4 DNA ligase enzyme (400 U/µl, NEB, M0202S). After the incubation at room temperature for 15-30 minutes, the final ligation mixture was transformed into bacteria to amplify the yield (see section 2.2.1.4, page 96).

#### **2.2.1.2 PCR mutagenesis**

All PCR mutagenesis reactions (see Table 2.1 below) were performed using a thermal cycler (Bio-Rad, S1000 Thermal Cycler) with the temperature program indicated in Table 2.2 below.

**Table 2-1: The reaction mix for PCR mutagenesis.**

Nuclease-free ddH <sub>2</sub> O	36 µl
10x buffer	5 µl
dNTPs (from 2.5mM stock)	5 µl
Plasmid DNA template (at 100 ng/µl)	1 µl
Forward primer (100 µM)*	1 µL
Reverse primer (100 µM)*	1 µl
<i>Pfu</i> DNA polymerase (2.5U/µl; MBL, RK-02-031-5)	1 µl
All primers were purchased from Sigma-Aldrich. The resuspension of primers was carried out according to the manufacturer's instructions. The primer pellet was resuspended in RNase-free ddH <sub>2</sub> O to get 100 µM final stock concentrations as described in the relevant datasheet, which was then incubated for 10-15 minutes at 65°C while shaking at a thermomixer (300 rpm). After a short spin down, final stocks were stored at -20°C.	

**Table 2-2: The temperature program for PCR mutagenesis.**

	Temperature	Time	Step
1.	98°C	5 min	Initial denaturation
20 cycles	94-98°C	1 min	DNA denaturation step
	55°C	1 min	primer annealing step
	72°C	2 min per kb of template	polymerase extension step
3.	72°C	20 min	Final extension
4.	4°C	forever	

The resulting product was treated with *DpnI* restriction enzyme (NEB, R0176S) to specifically digest the plasmid template. The bacterial plasmid is methylated, and the PCR product is not methylated, and the *DpnI* enzyme can cut only when its cleavage spot is dam (deoxyadenosine methylated) methylated, allowing us to have an only PCR product. Briefly, 1 µl of *DpnI* restriction enzyme was added into per PCR reaction and mixed by pipetting up and down before the mixture was incubated at 37°C for 2 hours. The final product was transformed into *Escherichia coli* and plasmid DNA was recovered from the bacteria by performing Mini-Prep (see section 2.2.1.4, page 96). Next, DNA agarose gel electrophoresis (see the section below)

was conducted to show the existence of the corresponding cDNA insert (DNA digestion screen). Finally, the presence of the desired mutation was confirmed using multiple sequence alignment software (Clustal Omega, EMBL-EBI) following DNA sequencing (Cambridge Bioscience Limited, UK).

### 2.2.1.3 DNA agarose gel electrophoresis

To separate and analyse DNA fragments, we used horizontal agarose gel system (Bio-Rad, Sub-Cell GT electrophoresis system, 1640302). Depending on the size of the digested DNA fragments, the percentage of agarose in a gel was approx. 0.5 – 2.0% (see Table 2.3). The agarose (UltraPure-Invitrogen, 16500500) was dissolved in TBE (1X) buffer and boiled using the microwave. Once the solution was cooled down to around 50°C, GelRed nucleic acid stain (VWR, 730-2958; 1/10,000) was added in the solution for visualization of the DNA in the gel. Samples were mixed with DNA loading buffer (6X) and carefully loaded into the wells of the gel along with GeneRuler DNA ladder (Fisher UK, FQ-SM0311). Gels were run at 80V for 2-6 hours depending on the size of analysed DNA fragments. DNA products were then visualised using the G:BOX gel documentation system (Syngene, LCI-700-090R). For the composition of all buffers see section 2.1.2.1, page 80.

**Table 2-3: The recommended concentration of UltraPure Agarose required resolving DNA fragments of the approximately indicated range.**

Agarose Concentration	Resolution range
0.8%	500 bp – 12 kb
1.0%	400 bp – 10 kb
1.5%	200 bp – 4 kb
2.0%	100 bp – 2 kb

#### **2.2.1.4 Bacterial techniques**

##### ***Preparation of XL1-blue competent cells***

XL1-blue competent cells (*E. coli*) were used in our project for the purpose of transforming competent cells with plasmid DNA. XL1-blue cells were plated out on antibiotic-free LB agar plates, which were then incubated at 37°C overnight. The following day single colonies were picked and grown overnight in 5 ml LB in a shaking incubator (220 rpm at 37°C). The next day, the overnight cultures were diluted 1:100 in 2X YT (500 ml) and incubated in a shaking incubator (220 rpm, 37°C) until the culture OD<sub>600</sub> (optical density at 600 nm) increased up to 0.3-0.4 nm (took about 1-2 hours). The cultures were next pelleted by centrifugation at 1,300 × *g* for 10 minutes at 4°C. Following aspiration of the supernatant, the pellet was resuspended in 1/10 volume ice cold IGB buffer. Finally, cells were promptly aliquoted into pre-chilled 1.5 ml Eppendorf tubes in the cold room, snap frozen in dry ice and stored at -80°C. For the composition of all buffers, see section 2.1.1, page 79.

##### ***Bacterial transformation***

The competent cells stored at -80°C were thawed on ice, gently mixed, and then 100 µl of cells were aliquoted into a pre-chilled 1.5 ml Eppendorf tube. After adding the experimental plasmid DNA (1 µl, approx. 20-50 ng) or ligation product (e.g. 20 µl) into the aliquot of cells and swirling the tube gently, cells were incubated on ice for 15-30 minutes. Next, cells were heat-pulsed in a 42°C heat block for 45-60 seconds and incubated on ice for 2-3 minutes. Next, 1 ml of preheated antibiotic-free LB medium was added, and the tube was incubated at 37°C heat block for 30-60 minutes with shaking at 400-500 rpm. Approx. 100-150 µl of the resulting transformation reaction (or all the product in case of the ligation) were plated onto pre-warmed 10-cm LB-agar plates (see section 2.1.1, page 79) containing the corresponding antibiotic using a glass Pasteur pipette which had been sterilized using a



Bunsen burner (JFA limited, D2-BS-0167). The plate was incubated overnight at 37°C (at least 16-17 hours for bacterial colony formation).

### ***Bacterial inoculation***

The following morning of transformation, the plate with colonies was placed into 4°C until inoculation. Shortly, 3 ml pre-heated liquid LB with the relevant antibiotic was added into a sterile 15 ml tube for the small-scale preparation of DNA constructs (or 100 ml liquid LB was added to a 500 ml Erlenmeyer flask for the large-scale preparation of DNA constructs). Next, a single colony from the LB-agar plate was cautiously selected using a sterile pipette tip which was then dropped into LB liquid medium. The bacterial culture was swirled gently and incubated overnight in a shaking incubator (220 rpm, 37°C) for 12-18 hours.

### ***Small scale (mini-prep) and large scale (midi-prep) preparation of DNA constructs***

Plasmid DNA was isolated from the bacterial culture using the NucleoSpin Plasmid Mini-Prep Kit (Fisher UK, 12353358) or PureYield Plasmid Midi-Prep System Kit (Promega, A2495), according to manufacturers' instructions. The culture volumes were 3 ml in a 15 ml tube for mini-preps or 100 ml in 500 ml Erlenmeyer flask for midi-preps.

The quality and quantity of the ultimate product of purified plasmid DNA were assessed by measuring the absorbance at 260 nm and 280 nm using a Nanodrop® spectrophotometer (NanoDrop Technologies). The resulting pure plasmid DNA was screened by restriction digest and DNA agarose gel electrophoresis to confirm the identity of the acquired plasmid (as described in section 2.2.1.3, page 95). In case sequence verification of the ligated PCR product was required (e.g. in the case of PCR mutagenesis), the presence of the desired mutation was confirmed using multiple sequence alignment software (Clustal Omega, EMBL-EBI) following DNA sequencing (Cambridge Bioscience Limited, UK).

## **2.2.2 RNA analysis – Quantitative Real-Time PCR (qRT-PCR)**

### **2.2.2.1 Total RNA extraction**

Purification of total RNA was performed at room temperature as instructed by the manufacturer. Aseptic good laboratory practices were applied during the whole procedure of RNA work.

#### ***Homogenizing samples***

Homogenization for total RNA purification from cells was performed using TRIzol® Reagent (Invitrogen, 15596-018). First, the medium on each 6-cm plates was aspirated, and cells were washed twice with cold PBS (w/o  $\text{Ca}^{++}/\text{Mg}^{++}$ ). After that, 1 ml of the TRIzol (for 6-cm plates) was applied to cells, which were collected by using a policeman scraper, and transferred into 2.0 ml Eppendorf tubes. The procedure was carried out carefully under a safety fume hood at room temperature.

#### ***Phase separation***

To separate RNA from other cellular contents, such as DNA and proteins, 200  $\mu\text{l}$  of chloroform (Sigma-Aldrich, C2432) was added to collected samples, and the tubes were shaken vigorously by hand for about 10 seconds. After the resulting mixture had been centrifuged at  $12,000 \times g$  for 15 minutes at  $4^{\circ}\text{C}$ , three separate phases were observed: a lower red phenol-chloroform phase, an interphase, and an upper aqueous phase. Finally, the upper aqueous phase (colourless) containing total RNA was collected carefully and transferred into fresh 1.5 ml Eppendorf tubes.

#### ***RNA Precipitation***

To precipitate RNA, 500  $\mu\text{l}$  of 100% isopropanol (Sigma-Aldrich, I9516) was added to the tubes containing the aqueous phase. The samples were incubated for 10 minutes at room temperature and then centrifuged at  $12,000 \times g$  for 10 minutes at  $4^{\circ}\text{C}$ . Consequently, the pellets were washed with 500  $\mu\text{l}$

75% ethanol at room temperature and centrifuged again at  $10,000 \times g$  for 5 minutes at 4°C.

### ***RNA resuspension***

Lastly, the RNA pellet was dissolved in 30  $\mu$ l of nuclease-free water (Sigma-Aldrich, 7732-18-5) by passing the solution up and down several times, and incubated in a heat block at 55-60°C for 10-15 minutes.

Purified total RNA was loaded onto 2% agarose gel (as described in section 2.2.1.3, page 95) to examine the quality of the total RNA samples. When the agarose gel is exposed to ultraviolet light (UV), binding of the fluorescent nucleic acid gel stain to the RNA allows visualization of 28S/18S ribosomal RNAs, which enabled us to confirm the integrity of isolated total RNAs (for a representative image of the performed agarose gel, please see Figure S2.1 in the Supplementary section, page 127). Furthermore, purified total RNA concentration was determined by measuring the absorbance at 260 nm and 280 nm using a Nanodrop® spectrophotometer (NanoDrop Technologies), which enabled us to determine the quantity and quality of our RNA extractions (suggested absorbance ratio for RNA by the manufacturer is A<sub>260</sub>/A<sub>280</sub> of >1.8, and measured ratios were >1.8 for most of the samples, for example please see Table S2.1 in the Supplementary section, page 127). Next, the equivalent amount of total RNA were subjected to cDNA synthesis as explained in the next section.

#### **2.2.2.2 cDNA synthesis**

Complementary DNA (cDNA) synthesis was performed from ~ 1  $\mu$ g of total RNA extracted from each sample using cDNA Synthesis Kit, which includes 5x reverse-transcription reaction mix, iScript reverse transcriptase, nuclease-free water (iScript One-Step RT-PCR Kit from Bio-Rad, 170-8891). As instructed by the manufacturer, first, 20  $\mu$ l of reaction mix containing 5x cDNA reaction mix (Oligo[dT] primers, random hexamers, buffer, MgCl<sub>2</sub>, dNTPs, DTT, RNase inhibitor), reverse transcriptase enzyme, nuclease-free water, and total RNA were resuspended as indicated in Table 2.4 below.

**Table 2-4: The reaction mix for cDNA synthesis.**

Components	Volume per Reaction	
5x iScript reaction mix	4 $\mu$ l	Total: 20 $\mu$ l
Reverse transcriptase	1 $\mu$ l	
RNA template	1 $\mu$ g of total RNA	
Nuclease-free water	(variable)	

Second, cDNA was reverse transcribed using a thermal cycler (Bio-Rad, S1000). The PCR reaction was carried out as indicated in Table 2.5 below and the produced cDNA samples were stored at -20°C until qRT-PCR analysis was performed.

**Table 2-5: The temperature program for cDNA synthesis.**

Cycling Step	Hold Time	Temperature	# of Cycles
Initial activation*	5 min	25°C	1
Extension	30 min	42°C	1
Termination	5 min	85°C	1
<i>*due to the use of a mix of random hexamers and oligo dT primers</i>			

### 2.2.2.3 qRT-PCR

Relative quantification of the expression levels of selected target genes was monitored by using SYBR green detection kit (iQTM SYBR® Green Supermix from Bio-Rad, 170-8884) on a qRT-PCR detection system (Mastercycler® ep realplex, Eppendorf). Primer sets were purchased from QIAGEN Sciences, Inc (see section 2.1.8, page 92). According to manufacturer's instructions (Bio-Rad), the first master mixture was prepared with SYBR green supermix and nuclease-free water. The second master mixture was set up by mixing both the first mixture and a gene-specific

primer. Finally, ~ 1 µg of cDNA (~1 µl) template was added into separate 1.5 ml Eppendorf tubes containing the second mixture with different primers. After that, the final mixture was pipetted carefully into a 96-well PCR reaction plate (Bio-Rad, HSP9655). For the detailed reaction mix and the temperature program, see Table 2.6 and Table 2.7, respectively. To inspect the amplification efficacy and the reliability of the obtained data, the presence of non-specific products or primer-dimers was monitored by melt-curve analysis. Results were obtained from three independent experiments performed in duplicate.

**Table 2-6: The reaction mix for qRT- PCR.**

Mastermix-1	iQ SYBR Green Supermix	25 µl	Total 50 µl
	Nuclease-free water	19 µl	
Mastermix-2	Mastermix-1	44 µl	
	Specific primer	5 µl	
Final-mix	Mastermix-2	49 µl	
	cDNA sample	~1 µg (1 µl)	

**Table 2-7: The temperature program for qRT-PCR.**

Cycling Step	Hold Time	Temperature	# of Cycles
Initial denaturation and enzyme activation	2 min	95°C	1
Denaturing	10 sec	95°C	40
Annealing	15 sec	55°C	
Final Extension	20 sec	68°C	
Melting curve	10-30 sec	55 -95°C*	1
*in 2°C increments			

#### 2.2.2.4 qRT-PCR Data Analysis

For relative quantification, the determined Ct (Cycle at threshold) values were normalized to 18S rRNA as the housekeeping gene (internal control) and related to the –Tet/48h group as the untreated control (reference, calibrator). The relative amounts of the selected p53 target genes were demonstrated as the fold change in the expression of these genes using the  $2^{-\Delta\Delta Ct}$  equation (Livak and Schmittgen, 2001) where:

$$\Delta\Delta Ct = (Ct_{Gol} - Ct_{HKG})_{Sol} - (Ct_{Gol} - Ct_{HKG})_{REFERENCE} \text{ (see Table 2.8).}$$

Each sample was loaded in triplicate, the Ct values for each sample was calculated separately for each well and then averaged.

**Table 2-8: Ct value calculation for qRT-PCR analysis.**

Sol -target-		Reference (-48h/-Tet)	
Gol	HKG	Gol	HKG
Ct <sub>1</sub> (Gol;Sol)	Ct <sub>1</sub> (HKG;Sol)	Ct <sub>1</sub> (Gol;ref)	Ct <sub>1</sub> (HKG;ref)
Ct <sub>2</sub> (Gol;Sol)	Ct <sub>2</sub> (HKG;Sol)	Ct <sub>2</sub> (Gol;ref)	Ct <sub>2</sub> (HKG;ref)
Ct <sub>3</sub> (Gol;Sol)	Ct <sub>3</sub> (HKG;Sol)	Ct <sub>3</sub> (Gol;ref)	Ct <sub>3</sub> (HKG;ref)
Amount of target: $2^{-\Delta\Delta Ct}$ $\Delta\Delta Ct = (Ct_{Gol} - Ct_{HKG})_{Sol} - (Ct_{Gol} - Ct_{HKG})_{REFERENCE}$			
<i>Sol: Sample of Interest; Gol: Gen of Interest; HKG: House-keeping gen. In our settings, HKG was 18S ribosomal RNA, and reference-calibrator group was -48h/-Tet group (untreated).</i>			

## 2.2.3 Protein analysis

### 2.2.3.1 Immunoblotting (IB)

#### ***Sample preparation; cell lysis and total protein extraction***

To prepare cell lysates, cells were washed with PBS (w/o  $\text{Ca}^{++}/\text{Mg}^{++}$ ), incubated with trypsin for 3-5 minutes at  $37^{\circ}\text{C}$  and finally pelleted by centrifugation at  $300 \times g$  for 4 minutes at room temperature. The cell pellets were then resuspended in 1 ml ice-cold PBS buffer, transferred into pre-chilled 1.5 ml Eppendorf tubes and centrifuged for 10 minutes at  $4,500 \times g$  at  $4^{\circ}\text{C}$ . After that, the cell pellets were snap frozen in dry ice for 30 minutes before storage at  $-80^{\circ}\text{C}$  until the next process.

The cell pellets stored at  $-80^{\circ}\text{C}$  were resuspended in an appropriate amount of standard lysis buffer (25-200  $\mu\text{l}$ ) (for the buffer composition, see section 2.1.2.2, page 80), vortexed and/or fragmented using a 26G Microlance G needle (BD, 10703815) and incubated on ice for 30-60 minutes. Next, the lysates were centrifuged at  $20,000 \times g$  for 10 minutes at  $4^{\circ}\text{C}$  to separate soluble proteins from insoluble proteins. The supernatant parts (soluble protein fractions) were transferred into new pre-chilled 1.5 ml Eppendorf tubes, and protein concentrations were measured by Bradford Protein Assay Reagent (5x, Bio-Rad, 5000006) using a spectrophotometer at 595 nm (Jenway Spectrophotometer 6305) for an equivalent amount of loading in the next step. The obtained measurements were correlated to the one with the lowest concentration for equal loading (relative quantification). Lastly, 5x Laemmli SDS sample buffer (for buffer composition see section 2.1.2.2, page 80) was added to the total cell lysates, and the mixtures were vortexed well and shortly centrifuged before being heated at  $95^{\circ}\text{C}$  for 5 minutes to denature proteins. Lysates were stored at  $-20^{\circ}\text{C}$ .

### ***Protein Detection***

According to the length of the polypeptide, the denatured proteins were separated by the optimum percentage of acrylamide (see Table 2.9) sodium dodecyl sulfate-polyacrylamide (see section 2.1.2.2, page 80) gel electrophoresis (SDS-PAGE/immunoblotting system, Bio-Rad) and transferred onto polyvinylidene difluoride membranes (PVDF from Millipore, IPVH00010), as explained in the following sections.

**Table 2-9: The resolution range of proteins depending on the % of the gel.**

Polyacrylamide concentration	Size separation range
8.0%	60 kDa – 200 kDa
10.0%	25 kDa – 200 kDa
12.0%	20 kDa – 100 kDa

### ***SDS-PAGE (sodium dodecyl sulfate-polyacrylamide gel electrophoresis)***

Gels were prepared as outlined in section 2.1.2.2, page 80. Firstly, 10 µl of pre-stained protein marker (New England Biolabs, P7708S and P7706S) or 6 µl of dual colour protein marker (Bio-Rad, 161-0374) were loaded in the first lane of the wells. After that, equalised amounts of sampled proteins were loaded onto the remaining wells of polyacrylamide gel, and electrophoresis was carried out at 80V for the first 30 minutes then 120V for the remainder in SDS running buffer (for the buffer composition see section 2.1.2.2, page 80). Proteins bigger than 150 kDa were separated on 8% gel at 120V for at least 3-5 hours until 100 kDa mark ran out.

### ***Transfer of proteins to PVDF membrane***

Secondly, proteins in polyacrylamide gel were transferred onto methanol activated PVDF membrane at 400 mA (per 2 gels) for about 75 min (an ice block was used to keep the temperature of transfer buffer closer to room temperature) in transfer buffer (for the buffer composition see section 2.1.2.2,



page 80). The transfer of large proteins (>150 kDa) was performed for 3 hours in transfer buffer containing 10% methanol and 0.05% SDS.

### ***Immunoblotting analysis***

Following the transfer, the membrane was washed with distilled water and rinsed with Ponceau S staining solution (Sigma, P7170-1L) to check protein transfer, and then washed with distilled water and TBS-T (Tris-buffered saline and Tween), respectively. Next, non-specific binding on membranes was blocked with the blocking buffer (for the buffer composition see section 2.1.2.2, page 80) for at least 30 minutes at room temperature. Finally, the membrane was incubated with the corresponding primary antibody diluted in the blocking buffer overnight at 4°C. The following day, unbound antibody was washed away with TBS-T (3 x 10 minutes at room temperature), and samples were incubated with the appropriate horseradish peroxidase-linked secondary antibodies for detection of bounded antibodies for 2 hours at room temperature (primary and secondary antibodies are listed in section 2.1.5, page 88).

Lastly, the membrane was washed with TBS-T buffer (3 x 10 minutes) and subjected to enhanced chemiluminescent (ECL) substrates for detection of horseradish peroxidase (HRP) activity from antibodies (1 ml of each substrate was mixed and used per membrane, for the composition, see section 2.1.2.2, page 80). After one-minute-incubation with the substrates at room temperature, the membrane covered with cling film was placed into an X-ray film cassette (18x24cm, SLS, MOL7336). Under red light (in the dark room), the membrane was exposed to a blue sensitive X-ray film (SLS, MOL7016) (for 3 seconds up to 30 minutes), which was then processed using a film processor (Konica Minolta, SRX-101A) to detect certain protein levels. Films were scanned to store digital images, and where adequate results were normalised to actin,  $\alpha$ -tubulin or GAPDH levels as detailed in section below.

### ***Densitometric analysis***

The ImageJ image processing and analysis software (National Institutes of Health, USA) was employed to compare the intensity of protein bands procured by immunoblotting analysis. Concisely, after X-ray films comprising the relevant protein bands were scanned and bands of interests were selected, the software calculated the intensity of the plotting area of each band. Background intensity and control intensity were detracted to determine the fold differences.

#### **2.2.3.2 Immunoprecipitation (IP)**

Immunoprecipitation experiments were carried out as described in Hergovich et al. (2005) and Hergovich et al. (2007). Cells were gently washed twice with ice-cold PBS (w/  $\text{Ca}^{++}/\text{Mg}^{++}$ ) and 1 ml of MILB lysis buffer (for the buffer composition see section 2.1.2.3, page 83) was added into per 10-cm plate. The cells in buffer were harvested by using a policeman scraper, transferred into pre-chilled 1.5 ml Eppendorf tube and incubated for 30 minutes on ice. Next, samples were centrifuged at  $20,000 \times g$  for 10 minutes at  $4^{\circ}\text{C}$  and supernatants were transferred into new pre-chilled 1.5 ml Eppendorf tubes. Importantly, 5-10% of the total cell lysate of each sample was aliquoted as input lysate control; mixed with Laemmli buffer, boiled for 5 minutes at  $95^{\circ}\text{C}$  and stored at  $-20^{\circ}\text{C}$ . The remaining lysate was subjected to pre-clearing to eliminate unspecific binding to the sepharose beads. In the pre-clearing step, the protein lysate was incubated with Protein A-Sepharose for 1 hour at  $4^{\circ}\text{C}$  (for the preparation of Protein A-Sepharose, please see the section below). After the incubation, the protein extract-Protein A-Sepharose mixture was spin down. Next, the supernatants were transferred into the pre-chilled tubes containing anti-HA 12CA5 (for Anti-HA antibody coupling with Protein A-Sepharose, please see the section below) and incubated overnight in a roller at  $4^{\circ}\text{C}$ . The following day, the mixture of the protein extract-anti-HA 12CA5 was centrifuged at  $20,000 \times g$  for 30 seconds, and the supernatant was carefully removed without disturbing the beads. The beads were then

washed 3 times with MILB lysis buffer before being boiled at 95°C in an appropriate amount (e.g. 20 µl) of Laemmli buffer.

### ***Preparation of Protein A-Sepharose***

1.5 g of Protein A-Sepharose CL-4B (Fisher UK, 17-0780-01) was incubated overnight in 50 ml autoclaved ddH<sub>2</sub>O at 4°C on a roller shaker. The next day, the beads were centrifuged at 300 × *g* for 4 minutes, and residual ddH<sub>2</sub>O was cautiously aspirated without disturbing the beads. In this way, the beads were washed twice with ddH<sub>2</sub>O and with PBS (w/o Ca<sup>++</sup>/Mg<sup>++</sup>), respectively. Subsequently, the beads were transferred into 15 ml falcon tubes, washed once with PBS (w/o Ca<sup>++</sup>/Mg<sup>++</sup>) and then centrifuged at 300 × *g* for 2 minutes at 4°C before PBS (w/o Ca<sup>++</sup>/Mg<sup>++</sup>) was carefully aspirated. Finally, 3 ml PBS (w/o Ca<sup>++</sup>/Mg<sup>++</sup>), 2 ml 100% ethanol and 100 µl 10% Na-Azide were added into 5 ml swollen beads. Beads in 50% slurry with 20% ethanol in PBS and 0.1% Na-Azide were stored at 4°C.

### ***Anti-HA (12CA5) antibody coupling with Protein A-sepharose***

Anti-HA (12CA5) hybridoma supernatant (provided by the Hergovich Laboratory) was incubated with Protein A-Sepharose at 4°C in 1% NP-40 solution to have anti-HA 12CA5 antibody bound to protein A-sepharose. 10 ml of anti-HA (12CA5) supernatant was incubated overnight with 1 ml 10% NP-40 solution and 1.5 ml protein A-sepharose (50% slurry) on roller shaker at 4°C. The following day, the beads were washed two times with PBS (w/o Ca<sup>++</sup>/Mg<sup>++</sup>) and three times with 0.2 M Na-Borate (pH 9.0). 51.8 mg of DMP (dimethyl pimelimidate) (Fisher UK, 21667) dissolved in 5 ml 0.2 M Na-Borate (pH 9.0) was then added to 5 ml beads slurry, which was then incubated for at least 1 hour at room temperature. Next, the beads were washed twice with 0.2 M ethanolamine (pH 8.0) and incubated for 3-4 hours at room temperature with 0.2 M ethanolamine (pH 8.0). Following the incubation, the beads were washed twice with PBS (w/o Ca<sup>++</sup>/Mg<sup>++</sup>) and dissolved in 1.5 ml PBS (w/o Ca<sup>++</sup>/Mg<sup>++</sup>) containing 0.2% Na-Azide, and finally stored at 4°C.

### 2.2.3.3 Yeast 2 Hybrid (Y2H) screen

To identify novel direct hMOB2 binding partners, a normalised universal human tissue cDNA library was screened using pLexA-NhMOB2 (full-length) as bait. The complexity of the pGADT7-recAB based cDNA library was  $2.8 \times 10^6$  with an average insert size of 1.58 kb. Screening of  $1 \times 10^6$  transformants yielded 59 bait dependent hits, resulting in the identification of total 28 putative interactors. Only four novel binding partners of hMOB2 were identified at least twice (RAD50, UBR5, KPNB1, and KIAA0226L). All nine hits for UBR5 were out of the frame and identified the HECT domain of UBR5 as potential interaction site while all four hits for RAD50 were in the frame (see Table S2.2 in the Supplementary section, page 128). The Y2H screen was performed by Dual systems Biotech AG (Zurich, Switzerland).

### 2.2.3.4 Chromatin isolation

Chromatin isolation experiments were conducted as described in Herold et al. (2008). For chromatin–cytosol separations, cells were trypsinized and harvested in ice-cold PBS, centrifuged at  $1,000 \times g$  for 2 minutes at  $4^\circ\text{C}$ , and resuspended in buffer A (for the buffer composition see section 2.1.2.4, page 83). The lysates were incubated for 10 minutes and then centrifuged at  $1,500 \times g$  for 5 minutes at  $4^\circ\text{C}$ . Next, the supernatants were collected as a cytosolic fraction (CF) in fresh pre-chilled 1.5 ml Eppendorf tube. The pellets were washed once with buffer A, lysed for 10 minutes at  $4^\circ\text{C}$  in buffer B (for the composition see section 2.1.2.4, page 83), followed by centrifugation at  $1,700 \times g$  for 5 minutes at  $4^\circ\text{C}$ . Next, the supernatants (soluble nuclear fraction, SNF) were collected in fresh pre-chilled 1.5 ml Eppendorf tube. Pellets (insoluble chromatin fraction, ISCF) were washed once with buffer B and centrifuged at  $9,000 \times g$  for 2 minutes at  $4^\circ\text{C}$ , resuspended in Laemmli buffer and finally fragmented using a 26G Microlance G needle (BD, 613-3917). Cytosolic fraction (CF) and soluble nuclear fraction (SNF) were pooled to one soluble fraction. Equal volumes of fractions (ISCF and CF + SNF) were analysed by immunoblotting as described in section 2.2.3.1, page 103.

### **2.2.3.5 Immunofluorescence (IF)**

Immunofluorescence analysis was performed as described in Hergovich et al. (2005). Exponentially growing  $7 \times 10^4$  cells were plated per well (6-well format) on coverslips covered with 0.1% gelatine (Fisher UK, G/0150/53) then shook up/down and left/right for the equal distribution of individual cells and left to adhere in a 37°C incubator set at 5% CO<sub>2</sub> until analysis. In the following step, the cells were prepared for the analysis as follows. The medium was aspirated and the cells were washed once with PBS (w/o Ca<sup>++</sup>/Mg<sup>++</sup> used all the time) and then fixed in PFA fixation solution (for the composition see section 2.1.2.5, page 84) for 15 minutes at room temperature. After fixation, cells were washed once with PBS and permeabilized in 2 ml 0.5% Triton X-100 in PBS for 2 minutes at room temperature. The coverslips comprising cells were carefully transferred from wells to the washing stands and washed with PBS in a washing basin (5 times, 1 minute each). Next, cells were incubated with IF blocking buffer (for the buffer composition see section 2.1.2.5, page 84) for 30 minutes at room temperature (incubated upside-down on a piece of parafilm with 50 µl blocking buffer in IF chambers). Afterward, cells were washed with PBS and incubated overnight with the corresponding primary antibodies (see section 2.1.5, page 88) diluted in 1% goat serum in PBS at 4°C. The following morning, cells were first washed with PBS, and then incubated with the corresponding secondary antibodies (see section 2.1.5, page 88) diluted in 1% goat serum in PBS at room temperature in the dark. DNA was counterstained with 1 µg/ml 1,4,6-diamidino-2-phenylindole (DAPI, Sigma, 32670-5MG-F). After 2 hours incubation, the cells were washed with PBS and each coverslip was dipped in ddH<sub>2</sub>O for 5 seconds before being inverted into 8 µl Vectashield mounting medium (Vector Lab. Burlingame, CA, H-1000) in a microscope slide. Finally, the corners of the cover slides were sealed with nail polish and slides were stored at 4°C in the dark until being analysed under the microscope. Images were acquired with an ApoTome fluorescence microscope (Zeiss) and processed with AxioVision AxioVS40 V4.8.1.0 (Zeiss) and Photoshop CS5 (Adobe Systems Inc.).

## **2.2.4 Mammalian tissue culture methods**

### **2.2.4.1 Cell lines and culture conditions**

(for details of media, see section 2.1.3, page 85)

Standard cell culture techniques were applied during the experiments. RPE-1, U2OS, COS7, HCT116, HOC 7, OVCA 429, HEY, SKOV 3, OVCAR 3, OVCAR 8, IGROV 1, OVCA 433 and PT67 cell lines were maintained in standard basal medium Dulbecco modified Eagle medium (DMEM), all supplemented with 10% fetal bovine serum at 37°C and 5% CO<sub>2</sub>. MCF10A cells were cultivated in DMEM: Nutrient Mixture F-12 containing horse serum, epidermal growth factor (EGF), hydrocortisone, cholera toxin and insulin at 37°C in 5% CO<sub>2</sub>. BJ-hTert fibroblasts were grown in DMEM:Medium199 comprising 10% FCS and gentamicin. U2OS cells containing GFP-based reporters were grown in DMEM w/o pyruvate. Media were also supplemented with Penicillin and Streptomycin antibiotic cocktail as well as specific selection antibiotics where needed. HOC 7, OVCA 429, HEY, SKOV 3, OVCAR 3, OVCAR 8, IGROV 1, OVCA 433 cells were kindly provided by Dr. Christina Gewinner. U2OS cells containing GFP-based reporters were generously provided by Prof Jeremy M. Stark (Beckman Research Institute of the City of Hope, USA).

### **2.2.4.2 Cell culture maintenance**

All cell lines used in this project were first grown in a T75 flask (75-cm, Greiner, 658175), in humidity-saturated (95%) cell culture incubators (RSBiotech, Galaxy R+), at 37°C and 5% CO<sub>2</sub>. All experimental procedures were performed in Class II Biosafety Cabinet (Esco) using aseptic good laboratory practices. The confluent cells (80-90%) were routinely passaged according to the growth rate of cells. Briefly, the culture medium in the T75 flask was first aspirated, and the residual medium was removed by carefully washing the surface of the flask with 5 ml dPBS (w/o Ca<sup>++</sup>/Mg<sup>++</sup>). Afterward, cells were detached using 3 ml 0.25% Trypsin/EDTA solution at 37°C for 3-5 minutes (MCF10A cells were incubated with 3 ml 0.05% Trypsin solution for

20-25 minutes). Further to the neutralization of trypsin by adding 6 ml of complete growth medium, the cell pellet was obtained by centrifugation at  $300 \times g$  for 4 minutes at room temperature. After discarding the supernatant, cells pellets were resuspended in complete growth medium to seed into new flasks at a ratio of 1/3 to 1/8 depending on the cell line. All cell lines were kept in cell culture at a maximum of 2 months, after which point fresh stocks were taken from liquid nitrogen. Media were stored at 4 °C for a maximum of 3 months.

#### **2.2.4.3 Cryopreservation and retrieval of cell lines**

Cells grown in either 10-cm plates (Fisher UK –Corning, TKV-160-049F) or T175 flasks (175-cm, Greiner, 660175) to 70-80% confluence were trypsinized and centrifuged as described in the section above. The pellet was resuspended in the freezing medium (see section 2.1.3, page 85). The final cell suspension was aliquoted as 1 ml per 2.0 ml cryotubes (Sarstedt, 72.379.992) (not more than  $2 \times 10^6$  cells per ml per vial), and was directly placed into a Mr. Frosty container (VWR – Nalgene, 479-3200) comprising 2-propanol (Fisher UK, A426-4). The cells were initially stored at -80°C for at least 24 hours (cooled 1°C per minute in Mr. Frosty) before being transferred to a liquid nitrogen tank (Lab mode, LS6000) for long term storage.

To bring frozen cells into the culture, cells were retrieved from liquid nitrogen by placing the cryotubes in a sterile 37°C water bath (Jencons – VWR, STUASWB2) for about 45-60 seconds for thawing. Next, cells were immediately resuspended in 5 ml complete growth medium in a 15 ml Falcon and centrifuged at  $300 \times g$  for 4 minutes at room temperature to eliminate possible toxic effects of DMSO which the freezing medium contained. Following the aspiration of the supernatant using a vacuum pump, cell pellets were resuspended in complete growth medium and seeded into a T75 flask, which were then incubated at 37°C and 5% CO<sub>2</sub>.

#### **2.2.4.4 Cell counting for seeding and proliferation assays**

Harvested cells, by centrifugation at  $300 \times g$  for 4 minutes at room temperature, were resuspended in complete growth medium, and 1 ml cell suspension was counted using Vi-Cell® automated cell counter (Cell Viability Analyser, Beckman Coulter), which determines cell concentration and viability based on the trypan blue dye exclusion method.

#### **2.2.4.5 Cell transfections**

##### ***Transient siRNA reverse transfection (RNA interference)***

According to the manufacturer's instructions, Lipofectamine® RNAiMAX transfection reagent (Invitrogen, 13778150) was used in our RNA interference (RNAi) experiments to knockdown mRNA levels of our genes of interest using various concentrations of siRNA oligos purchased from Qiagen (see section 2.1.7, page 92). Briefly, a pre-determined amount of siRNA duplex (depending on the efficacy of siRNA used, the surface area of cell culture vessel used, and the number of cells transfected) and twice the volume of transfection reagent were diluted in separate 1.5 ml Eppendorf tubes containing an appropriate volume of OPTIMEM medium. Following to 5-minute incubation of the transfection reagent in the medium, both solutions were mixed, and the tubes were inverted continuously for 30 seconds. The mixed solution was left for 10 minutes at room temperature to have the final RNA-lipid complexes. Meanwhile, the target cells were harvested and pelleted as previously described, and the pre-determined number of cells (depending on the experiment performed) was resuspended in an appropriate volume of OPTIMEM medium. After RNA-lipid complexes had been mixed with cell suspension for 10 minutes at room temperature, the resulting suspension was diluted accordingly and seeded in the relevant plates. After 24 hours of transfection, the medium was refreshed to avoid any toxicity effect of the reagent. The final concentrations of siRNA oligos varied from 1 – 15 nM. siLuc (see section 2.1.7, page 92) was employed as a negative control. Cells were grown at 37°C and 5% CO<sub>2</sub>, and analysed in the



following 2-12 days depending on the experiment conducted. The successful manipulation in all transfections was confirmed by immunoblotting.

### ***Transient plasmid DNA forward transfection***

Fugene 6 transfection reagent (Promega, E2692) was employed to perform the transient expression of desired plasmid DNA in our target cells as described by the manufacturer. 24 hours before the transfection, exponentially growing cells were plated at a consistent confluence in 10-cm plates. The following day, the transfection was carried out with the ratio of DNA (1 µg): Fugene (3 µl). Briefly, 15 µl of the Fugene reagent was diluted in a total volume of 500 µl OPTIMEM medium in a 1.5 ml Eppendorf tube and incubated for 5 minutes at room temperature. Meantime, 5 µg of pure plasmid DNA was diluted in a total volume of 500 µl OPTIMEM medium in a separate 1.5 ml Eppendorf tube, and finally, the contents of both tubes were mixed well and incubated for 30 minutes after inverting the tube continuously for 30 seconds. During the incubation time, the target cells were washed once with dPBS (w/o Ca<sup>++</sup>/Mg<sup>++</sup>) and supplemented with 5 ml of antibiotic-free medium. Consequently, the mixture was added to the cells dropwise while gently shaking the plates to ensure the even distribution. The cells were incubated at 37°C and 5% CO<sub>2</sub>, and analysed in the following 3-7 days. The successful manipulation in all transfections was confirmed by immunoblotting.

### ***Generation of inducible (Tet-on) and stable cell lines (retroviral infection)***

Tetracycline-inducible (Tet-on) cell lines used in this project were generated by Lily Hoa and Dr. Alexander Hergovich and maintained as described in Gomez-Martinez et al. (2013).

Retroviral pools using pMKO.1 puro, pSuper.retro.puro, or pLXSN plasmids were generated as reported in Hergovich et al. (2007). Briefly, for stable transfection of cells, PT67 cells, a retrovirus packaging cell line, were plated at a consistent confluence (2 x 10<sup>6</sup> cells/10-cm dish). The next day,

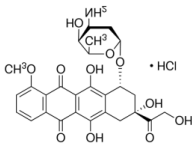
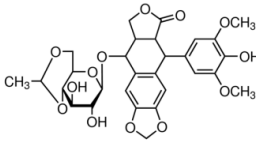
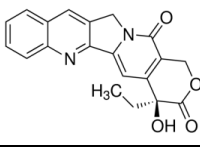
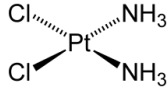
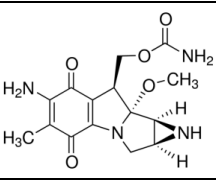
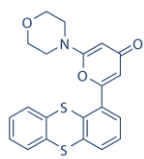
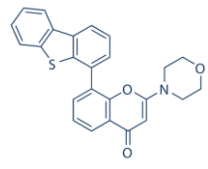
target cells were seeded ( $3-5 \times 10^5$  cell/10-cm dish), and PT67 cells were transfected using Lipofectamine 2000 (Invitrogen, 11668027) as described by the manufacturer. Concisely, 30  $\mu$ l of the transfection reagent was added directly to 720  $\mu$ l OPTIMEM medium in a 2.0 ml Eppendorf tube and mixed by inverting the tube repeatedly for about 30 seconds before the incubation for 5 minutes at room temperature. In the meantime, 12  $\mu$ g of pure plasmid DNA was diluted in a total volume of 750  $\mu$ l OPTIMEM medium and mixed well by inverting the tube repeatedly for about 30 seconds. After a short spin, the contents of both tubes were mixed well and incubated for 20-30 minutes at room temperature. During the incubation time, the PT67 cells were washed once with dPBS (w/o  $\text{Ca}^{++}/\text{Mg}^{++}$ ) and supplemented with 5 ml of antibiotic-free medium. Finally, the DNA/Lipofectamine/OPTIMEM mixture was added to cells dropwise while gently shaking the plates to ensure equal distribution. Cells were incubated for 4 to 6 hours at  $37^\circ\text{C}$  and 5%  $\text{CO}_2$  before the medium were replaced by the fresh antibiotic-free medium to minimize the toxic effect of the reagents. During the following two days, the supernatant of PT67 cells was collected by a syringe, filtered (Filtropur S 0.45  $\mu\text{m}$  filters, Sarstedt, 83.1826), mixed with 0.8  $\mu\text{g}/\text{ml}$  polybrene (see section 2.1.3, page 85), and finally transferred into corresponding target cells which were required to be stably infected. Next, infected target cells were selected for 7-14 days using pre-determined concentration of the corresponding antibiotics, which were determined according to previously performed antibiotic kill curve analysis. The manipulation in all transfections was confirmed by immunoblotting. Before performing the end point analysis, exponentially growing cell pools were stocked in a liquid nitrogen tank (as described in section 2.2.4.3, page 111).

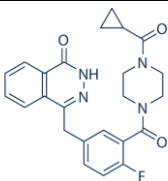
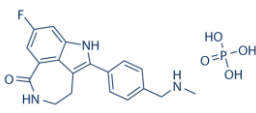
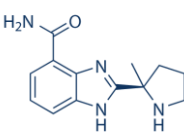
#### **2.2.4.6 Drug/inhibitor treatments and irradiation**

Drugs and inhibitors (please see Table 2.10 for the types of drugs and their chemical structures) used in this project were prepared as specified in Table 2.11 below. The effect of X-rays was chosen to be evaluated in this project, referred as ionising radiation (IR) and measured in Gray (Gy). For IR

treatments, cells were plated at fixed densities, followed by irradiation with indicated doses at a rate of 5 Gy/min (215 kV, 12.0 mA, 1.0 mm Al filter) using an AGO HS 320/250 X-ray machine (AGO X-ray Ltd.), which was equipped with a NDI-321 stationary anode X-ray tube (Varian). The cells were then processed for immunoblotting, clonogenic, or comet assays as described in the corresponding result sections and figure legends.

**Table 2-10: Compounds used in cell cycle checkpoint analysis, colony survival assays and DNA damage repair experiments.**

Compounds	Type of drug	Structure
Doxorubicin hydrochloride	DNA intercalator topoisomerase II inhibitor (poison)	
Etoposide	topoisomerase II inhibitor	
Camptothecin	topoisomerase I inhibitor	
Cisplatin	DNA crosslinking agent	
Mitomycin C	DNA crosslinking agent	
KU55933	ATM inhibitor	
NU7441	DNA-PK inhibitor	

AZD2281	PARP inhibitor (olaparib)	
AG-014699	PARP inhibitor (rucaparib)	
ABT-888	PARP inhibitor (veliparib)	

**Table 2-11: Preparation of drug/inhibitor stocks and details of the chemicals.**

Stock	Drugs	Solvent	Storage	Company, Cat #
5 mM	Doxorubicin (DOX)	ddH <sub>2</sub> O	-20°C	(Sigma-Aldrich, D1515)
5 mM	Etoposide (ETO)	DMSO	-20°C	(Sigma-Aldrich, P1383)
5 mM	Camptothecin (CPT)	DMSO	-20°C	(Cambridge Biosciences, C0150)
3.3 mM	Cisplatin (CDDP)		RT	provided by Dr. Victoria Spanswick
1 mM	Mitomycin C (MMC)	DMSO	-20°C	(Sigma-Aldrich, M4287)
10 mM	ATM inhibitor (KU-55933)	DMSO	-80°C	(Calbiochem/Merck, 118500)
5 mM	DNA-PK inhibitor (NU7441)	DMSO	-80°C	(Selleck, S2638)
10 mM	PARP inhibitor Olaparib (AZD-2281)	DMSO	-80°C	(Enzo/Axxora, LKT-O4402)
10 mM	PARP inhibitor Rucaparib (AG-014699)	DMSO	-80°C	(Selleck/Stratech, S1098)
10 mM	PARP inhibitor Veliparib (ABT-888)	DMSO	-80°C	(Selleck/Stratech, S1004)

## **2.2.5 Functional assays**

### **2.2.5.1 Cell proliferation assays**

A pre-determined number of exponentially growing cells were seeded in 10-cm dishes for proliferation assays. The number of viable cells harvested by trypsinization was then determined with cell counter during the time course of the experiment. Three independent experiments were performed for cell proliferation assays. Alternatively, cell proliferation assays were also performed using kinetic live cell imaging system (The INCUCYTE™ Kinetic Imaging System, Essen BioScience). Concisely, depending on the seeding format, a fixed number of cells (determined based on the preliminary experiments) were seeded in multi-well plates as replicates, which were then placed into the IncuCyte (located on the 4th floor of CI, UCL). The confluency of cells was automatically measured every two hours following two/three weeks. The final analysis was carried out by the IncuCyte software (INCUCYTE™, 2011 Essen BioScience Inc., 2011A Rev2).

### **2.2.5.2 Cell cycle analysis by DNA content (Flow cytometry)**

#### ***Fixation of cells***

DNA content analysis was carried out by propidium iodide (PI) staining to compare cell cycle distribution between control and treatment groups. Cells were first fixed before flow cytometry analysis was employed to study cell cycle profiles. Briefly, exponentially growing cells seeded at a consistent confluence in 10-cm plates were trypsinized and collected by centrifugation at  $300 \times g$  for 4 minutes at 4°C in 15 ml falcon tubes. The cell pellets were then resuspended in 300 µl ice-cold PBS (w/o  $\text{Ca}^{++}/\text{Mg}^{++}$ ). At the same time, 700 µl ice-cold 70% ethanol (stored at -20°C) were added to new pre-chilled 15 ml falcon tubes. The cells resuspended in PBS were added dropwise to pre-chilled 15 ml falcon tubes containing ethanol while vortexing and fixed cells were stored at -20°C until flow cytometry analysis.

### ***Flow cytometry analysis***

To prepare fixed cells for flow cytometry analysis, the cells were centrifuged at  $3,200 \times g$  at  $4^{\circ}\text{C}$  for 4 minutes, and supernatants were removed. After that, the cell pellets were washed with cold PBS (w/o  $\text{Ca}^{++}/\text{Mg}^{++}$ ) by pipetting up and down and centrifuged at  $3,200 \times g$  for 4 minutes at  $4^{\circ}\text{C}$  (twice). In the next step, supernatants were removed, samples were treated with  $10 \mu\text{g}/\text{ml}$  RNase A in 1 ml PI solution (for the buffer composition, see section 2.1.2.6, page 84) and incubated for half an hour at  $37^{\circ}\text{C}$  in the dark. Lastly, cell cycle analysis was carried out using a flow cytometer (CyAn™ ADP Analyzer, Beckman Coulter). The obtained results were evaluated with the Summit v4.3.02 software (Beckman Coulter, Inc.).

### **2.2.5.3 The alkaline Comet assay**

We utilised the alkaline Comet assay (single-cell gel electrophoresis) as a sensitive technique for the detection of DNA damage level (SSBs and DSBs) in the individual eukaryotic cell. The Comet assays were performed as described in Hartley et al. (1999).

### ***Preparation of pre-coated slides and cell lines before setting up the comet assay***

Before starting the assay, slides were pre-coated with 1% type 1-A agarose (Sigma-Aldrich, A-0169; dissolved in ddH<sub>2</sub>O, boiled and cooled to  $40^{\circ}\text{C}$ ) by pipetting 1 ml of molten agarose onto the centre of single-frosted glass microscope slides (VWR, 631-0111). The slides were allowed to set and dry overnight at room temperature. Cells were harvested and subsequently stored in the freezing medium at  $-80^{\circ}\text{C}$  until being analysed by electrophoresis.

### ***Preparation of slides with cells embedded in LGT agarose***

Firstly, frozen cells were thawed and diluted in 4 ml complete medium to have a cell suspension of  $25 \times 10^3$  cells/ml, which was always kept on ice. Each sample including positive control was separated into 2 appropriately labelled 15 ml falcon tubes, and duplicate agarose pre-coated slides were labelled accordingly and placed in a tray on ice. 24-well multi-plate was utilised to mix cell suspension and agarose. In a well of 24-well multi-plate, 0.5 ml of the appropriate cell suspension was mixed with 1 ml of molten 1% LGT-agarose (Sigma-Aldrich, A-4018; dissolved in ddH<sub>2</sub>O, boiled and cooled down to 40°C). 1 ml of the mixture from each well was pipetted onto the centre of the corresponding slides, and a coverslip (VWR, 631-0145) was placed on top of each one (for equal dispersion of the agarose across the slide) before the slides were placed on ice. Once the gels had set, the coverslips were removed, and the slides were placed back in the tray, on ice.

### ***Incubation of cells with lysis and alkaline buffers followed by electrophoresis***

All gels were prepared as above, and samples were incubated with ice-cold lysis buffer on ice in the dark for 1 hour (for the buffer composition, see section 2.1.2.6, page 84, 1% Triton X-100 freshly added). Next, the lysis buffer was carefully removed using the water vacuum pump without disturbing the gels, followed by washing with ice-cold double-distilled water four times (15 minutes each) in the dark. Next, the slides were transferred into the flatbed electrophoresis tank (Flowgen UK, C25599) so that all the slides were laid lengthways in the same direction. Afterward, 3 L of ice-cold alkaline buffer (for the buffer composition, see section 2.1.2.6, page 84) was poured into the tank (completely immersed the slides), and then the samples were incubated in the dark for 45 minutes. After that, electrophoresis was carried out for 25 minutes at 18V (0.6V/cm) and 250mA in the dark.

Following the electrophoresis, the slides were carefully removed from the tank and placed on a horizontal slide rack. Each slide was flooded with 1 ml of neutralisation buffer and left for 10 minutes before rinsing them twice

with 1 ml PBS. After 10 minutes, excess liquid was drained off, and the slides were allowed to dry at room temperature overnight.

### ***Staining of nucleic acids by PI and visualization of the comets***

The following day, the slides were rehydrated by flooding with ddH<sub>2</sub>O and left for 30 minutes. Afterwards, each slide was washed twice with 1 ml of 2.5 µg/ml propidium iodide (PI) solution and incubated for 15-20 minutes at room temperature in the dark. After rinsing off the propidium iodide with ddH<sub>2</sub>O, the slides were left for 20-30 minutes. Finally, following to drying the slides in the oven at 37°C for 2-3 hours, the slides were stored in a slide box until image analysis. Individual cells were visualised, and pictures of comets were taken at x20 magnification using an imaging system attached to a NIKON inverted microscope (with high mercury-arc lamp; 510-560 nm excitation and 590 nm barrier filters). Per sample/time point/experiment at least 100 cells were randomly selected from duplicate slides and individual DNA damage levels in the captured images were analysed using the Komet Analysis software 4.02 (Andor Technology, U.K.). Tail moment of each cell calculated by the software was determined as the difference between the head and tail distributions of damaged DNA. 15-Gy-irradiated samples served as positive controls. At least three independent experiments were conducted for analysis of DNA damage levels.

### ***Measurement of ICL levels using the Comet assay***

A modified Comet assay analysis was also carried out to measure DNA ICL formations in individual cells as described in Spanswick et al. (2010). The experimental methodology was the same with the alkaline Comet assay protocol explained above with minor modifications. After treatment with the indicated ICL-inducing agent, cells were harvested and frozen at indicated time points. Prior to analysis, cells were thawed and subsequently resuspended in ice cold media to a concentration of  $25 \times 10^3$  cells/ml, which was always stored on ice. These cell suspensions were irradiated (17.5Gy) using the AGO HS 320/250 X-ray machine (AGO X-ray Ltd.) (see section



2.2.4.6, page 114) in order to introduce a fixed number of spontaneous DNA strand breaks (procedure performed on ice), immediately prior to analysis.

Significantly, results were stated as percentage decrease in tail moment compared to untreated irradiated controls that is calculated as follows (tail moments were calculated from the same software as previously outlined):

$$\% \text{ decrease in tail moment} = \left[ 1 - \frac{TM_{di} - TM_{cu}}{TM_{ci} - TM_{cu}} \right] \times 100$$

where:  $TM_{di}$  = tail moment of drug-treated irradiated sample  
 $TM_{cu}$  = tail moment of control, unirradiated, untreated  
 $TM_{ci}$  = tail moment of control, irradiated, untreated.

#### 2.2.5.4 Colony survival assays (clonogenic assays)

Clonogenic assays were carried out as defined in Franken et al. (2006) and Roossink et al. (2012). Depending on the dose of the treatments, pre-determined numbers (see Table 2.12 below) of transiently (reverse) transfected cells (with indicated siRNAs, as described in section 2.2.4.5, page 112) were seeded in 6-well plates (Fisher UK –Corning, TKT-520-010C) (shook up/down and left/right every 10 minutes, 3 times for the equal distribution of individual cells) and left to adhere in a 37°C incubator set at 5% CO<sub>2</sub> for 24 hours, before being treated with indicated doses. For every experiment performed, the transfection efficacy was confirmed by immunoblotting. After treatment with the corresponding drug or irradiation and three media washes, cells were replenished with fresh complete medium every three days until colony size reached more than 50 cells per colony. Before colonies started to overlap, cells were first washed with PBS (w/o Ca<sup>++</sup>/Mg<sup>++</sup>), and fixed with MeOH/acidic acid (3:1) solution for 5 minutes, followed by staining with 0.5% crystal violet for 15 minutes at room temperature. The stained plates were rinsed carefully with tap water using an Erlenmeyer to prevent the stained colonies from loosening and washing off.

After letting the plates air-dry overnight at room temperature, the number of colonies having more than 50 cells was counted per well.

**Table 2-12: The number of cells seeded for the corresponding dose of indicated treatments in colony survival assays.**

	Conc	no:cell		Conc	no:cell		Conc	no:cell
<b>Doxorubicin</b>	0 nM	200	<b>X-ray</b>	0 Gy	200	<b>Etoposide</b>	0 $\mu$ M	200
	50 nM	200		1 Gy	200		1 $\mu$ M	200
	100 nM	500		2 Gy	500		2.5 $\mu$ M	200
	250 nM	500		3 Gy	500		5 $\mu$ M	500
	500 nM	1000						
<b>Camptothecin</b>	0 nM	200	<b>Mitomycin C</b>	0 $\mu$ M	200	<b>Cisplatin</b>	0 $\mu$ M	200
	20 nM	500		1 $\mu$ M	500		5 $\mu$ M	200
	200 nM	1000		2 $\mu$ M	1000		10 $\mu$ M	500
				3 $\mu$ M	2000		15 $\mu$ M	500
							20 $\mu$ M	1000
<b>ATM, DNA-PK, PARP inhibitors</b>	0 $\mu$ M	200						
	1 $\mu$ M	200						
	10 $\mu$ M	200						

The surviving fraction was calculated using the plating efficiencies (PE) of the corresponding non-treated controls as a reference. To calculate the PE, the three colony counts for each dose of the relevant treatment were averaged, and the mean was divided by the number of cells plated. This gave the PE as follows:

$$PE = \frac{\text{number of colonies counted}}{\text{number of cells seeded}} \times 100$$

Following the calculation of the PE, the survival fraction (SF) of colonies surviving in each dose of the corresponding treatment was determined. First, all the plating efficiencies of the treated samples were normalised to that of the untreated control samples, consequently considering that to be 100%. The SF was calculated by dividing the PE of the treated cells by the PE of the controls, and then multiplying by 100. This gave the SF as follows:

$$SF = \frac{\text{PE of treated samples}}{\text{PE of controls}} \times 100$$

Results shown are averages of at least three independent experiments performed in triplicate. All buffers/solutions were always prepared fresh as listed in section 2.1.2.8, page 85.

### **2.2.5.5 I-SceI-based GFP recombination (DNA repair) assays**

#### ***Background***

To examine the functionality of DNA double-strand break (DSB) repair pathways, I-SceI-based GFP reporter assays were employed for the HRR and NHEJ repair pathways. The experiments were carried out as described in Gunn and Stark (2012). In principle, DSBs are induced by transient expression of I-SceI enzyme in the corresponding cells. The induced DSBs are then repaired by the relevant repair pathway, which generates a functional full-length GFP gene (Figure 2.1). The produced GFP expression levels are considered as a precise readout for the efficiency of repair pathway tested (Pierce et al., 1999).

#### ***Cell seeding and I-SceI transfection***

24 hours before I-SceI transfection exponentially growing U2OS cells (DFGRP or EJ5GFP) were transiently (reverse) transfected with the corresponding siRNAs as described in section 2.2.4.5, page 112. Next,  $1 \times 10^5$  cells were seeded in duplicate per well (12-well format) (shook up/down and left/right every 10 minutes, 3 times for the equal distribution of individual cells) and left to adhere in a 37°C incubator set at 5% CO<sub>2</sub>. The remaining transfected cells were plated in 6-cm plates and harvested 24 hours later for immunoblotting (to confirm siRNA transfection). The next day, the cells were transfected with either pCAGGS (empty vector) or pCBASceI (I-SceI) (see section 2.1.6, page 91) plasmids using Eugene 6 (Promega, E2692) forward transfection reagent as described in section 2.2.4.5, page 112 with minor modifications as follows: 3.6 µl of the reagent diluted in 100 µl OPTIMEM medium was mixed with 100 µl OPTIMEM medium containing 1.2 µg of the relevant plasmid DNA for 20 minutes, and the resulting mixture was added dropwise to the corresponding cells. The following morning, cell culture medium was refreshed, and the cells were incubated at 37°C and 5% CO<sub>2</sub> and analysed after 72 hours following I-SceI transfection. Cells which were untransfected or transfected with pEGFP (GFP) served as experimental

negative and positive controls, respectively. Cells transfected with pCBASceI (I-SceI) and treated with either 10  $\mu$ M ATM inhibitor for 60 hours or 10  $\mu$ M DNA-PK inhibitor for 60 hours were used as assay controls for DRGFP (HRR) or EJ5GFP (NHEJ), respectively. Since the I-SceI protein contains a hemagglutinin (HA) tag, the expression HA-tagged I-SceI was monitored by immunoblotting using an anti-HA antibody.

### ***Cell fixation and Flow cytometry analysis***

Three days (approx. 72 hours) after I-SceI transfection, cells were analysed by flow cytometry (BD LSRFortessa™ X-20 cell analyser). After washing with PBS (w/o  $\text{Ca}^{++}/\text{Mg}^{++}$ ), cells were incubated with 200  $\mu$ l trypsin for 3-5 minutes at 37°C. Meanwhile, 4% methanol-free formaldehyde was prepared from a 16% stock solution (Fisher UK, 11586711) in PBS (w/o  $\text{Ca}^{++}/\text{Mg}^{++}$ ) and 200  $\mu$ l of it were added to 5 ml sterile polyethylene flow cytometry tubes (Fisher UK, 14-959-2A) labelled appropriately. Following the trypsinization, 400  $\mu$ l complete growth medium was added to cells to inactivate trypsin, and duplicates were pooled (total 1.2 ml cell suspension for each group). 600  $\mu$ l of the whole trypsinized sample were dispersed by pipetting and placed into a pre-labelled 1.5 ml Eppendorf tube (for immunoblotting analysis of HA). The remaining 600  $\mu$ l mixture was added dropwise to the 5 ml flow cytometry tubes containing 200  $\mu$ l 4% formaldehyde while vortexing (hence the final concentration of formaldehyde was 1%). The GFP signal was evaluated in all samples. A plot of forward scatter (FSC) versus side scatter (SSC) was generated by gating for events that were consistent with individual cells before all cells were analysed in a plot monitoring green fluorescence. The obtained results were evaluated with the Summit v4.3.02 software (Beckman Coulter, Inc.).

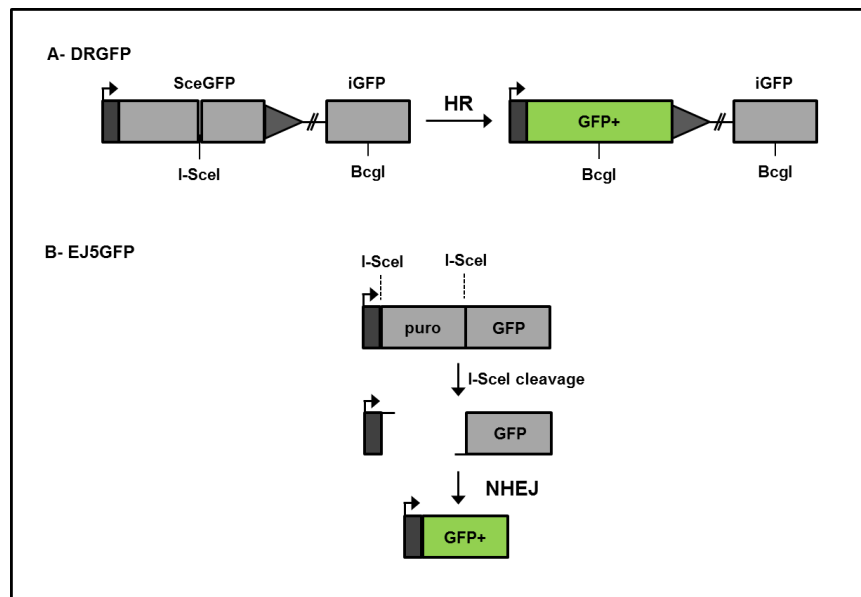


**Figure 2.1**

### Design of the HRR and NHEJ assays.

(A) DR-GFP reporter construct measures the efficacy HRR. This construct bears two defective GFP genes; the first one has an *I-SceI* endonuclease site and the second one is a truncated form of GFP sequence. Transient *I-SceI* expression induces DSB induction, which can be repaired by HRR, resulting in GFP+ cells measured by a flow cytometer. (B) EJ5-GFP reporter construct measures the efficacy of NHEJ. This reporter has one GFP sequence interrupted by a puromycin cassette along with two *I-SceI* sites. Transient *I-SceI* expression results in DSB induction and the broken ends can be ligated by NHEJ, resulting in GFP+ cells measured by a flow cytometer.

### 2.2.6 Statistical analysis

Graphics and statistical analyses were carried out using the GraphPad Prism 6 and the Microsoft Excel 2010 software. All results are presented as mean of replicates and error bars as mean  $\pm$  standard error of mean (SEM), unless stated otherwise. The significance of differences between the means or the population distributions was determined using the two-way ANOVA test (for proliferation analysis), or one-tailed unpaired Student's t-test (for qRT-PCR,  $\gamma$ H2AX/53BP1 and RPA foci, comet experiments, clonogenic survival assays, cell cycle checkpoint experiments, and GFP-reporter assays), unless stated otherwise. For all tests, differences were considered statistically significant when *p*-values were below 0.05 (\*), 0.01 (\*\*), or 0.001 (\*\*\*), respectively. *p*-values are indicated in the corresponding figures and their legends.

### 2.2.7 Supplementary information

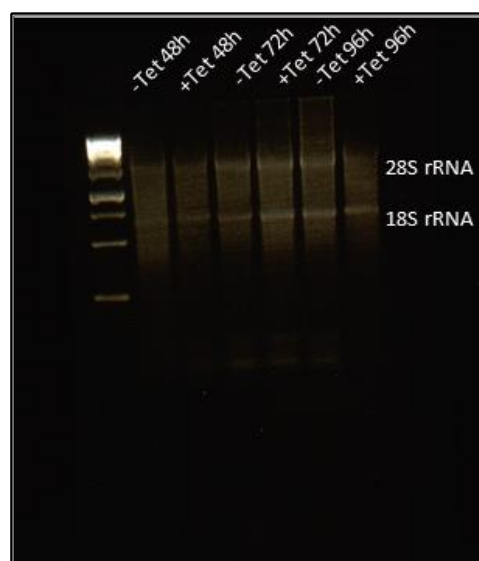


**Figure S2.1**

The representative image of the performed 2% agarose gel, suggesting total RNAs extracted from samples were of high quality for cDNA synthesis. The gel allows visualization of two central bands indicating 28S and 18S ribosomal RNAs, respectively (please see section 2.2.2.1, page 98).

Group	Concentration	Absorbance (A260/280)
-tet 48h	600 ng/μl	1.90
+tet 48h	1.355 ng/μl	1.86
-tet 72h	915 ng/μl	1.88
+tet 72h	1.140 ng/μl	1.95
-tet 96h	1.070 ng/μl	1.96
+tet 96h	1.660 ng/μl	1.88

**Table S2.1**

The measurements of total RNA concentration and absorbance determined by a Nanodrop® spectrophotometer, to determine the quantity and quality of our RNA extractions before the equivalent amount of total RNA were subjected to cDNA synthesis (please see section 2.2.2.1, page 98).



Group	Class	Prey-ID	Frame	uniprot ID	protein name (description)	Harvester link
1	B	hMOB2_pre_40	2	B7ZBN5	Chromosome 13 open reading frame 18 OS=Homo sapiens GN=C13orf18 PE=4 SV=1	B7ZBN5
		hMOB2_pre_48	2	B7ZBN5	Chromosome 13 open reading frame 18 OS=Homo sapiens GN=C13orf18 PE=4 SV=1	B7ZBN5
2	A	hMOB2_pre_02	1	O95071	E3 ubiquitin-protein ligase UBR5 OS=Homo sapiens GN=UBR5 PE=1 SV=2	O95071
		hMOB2_pre_05	1	O95071	E3 ubiquitin-protein ligase UBR5 OS=Homo sapiens GN=UBR5 PE=1 SV=2	O95071
		hMOB2_pre_06	1	O95071	E3 ubiquitin-protein ligase UBR5 OS=Homo sapiens GN=UBR5 PE=1 SV=2	O95071
		hMOB2_pre_07	1	O95071	E3 ubiquitin-protein ligase UBR5 OS=Homo sapiens GN=UBR5 PE=1 SV=2	O95071
		hMOB2_pre_11	1	O95071	E3 ubiquitin-protein ligase UBR5 OS=Homo sapiens GN=UBR5 PE=1 SV=2	O95071
		hMOB2_pre_18	1	O95071	E3 ubiquitin-protein ligase UBR5 OS=Homo sapiens GN=UBR5 PE=1 SV=2	O95071
		hMOB2_pre_41	2	O82878	Isoform 2 of DNA repair protein RAD50 OS=Homo sapiens GN=RAD50	O82878
3	A	hMOB2_pre_35	2	O82878	Isoform 3 of DNA repair protein RAD50 OS=Homo sapiens GN=RAD50	O82878
		hMOB2_pre_42	2	O82878	Isoform 3 of DNA repair protein RAD50 OS=Homo sapiens GN=RAD50	O82878
		hMOB2_pre_49	2	O82878	Isoform 3 of DNA repair protein RAD50 OS=Homo sapiens GN=RAD50	O82878
		hMOB2_pre_55	2	F5H4R7	Uncharacterized protein OS=Homo sapiens GN=KPNB1 PE=4 SV=1	F5H4R7
4	B	hMOB2_pre_57	2	F5H4R7	Uncharacterized protein OS=Homo sapiens GN=KPNB1 PE=4 SV=1	F5H4R7
		hMOB2_pre_01	1	E7ET84	Uncharacterized protein OS=Homo sapiens GN=UBR5 PE=4 SV=1	E7ET84
5	A	hMOB2_pre_08	1	E7ET84	Uncharacterized protein OS=Homo sapiens GN=UBR5 PE=4 SV=1	E7ET84
		hMOB2_pre_15	1	E7ET84	Uncharacterized protein OS=Homo sapiens GN=UBR5 PE=4 SV=1	E7ET84
-	C	hMOB2_pre_46	2	P17028	Zinc finger protein 24 OS=Homo sapiens GN=ZNF24 PE=1 SV=4	P17028
-	C	hMOB2_pre_43	3	P42330	Aldo-keto reductase family 1 member C3 OS=Homo sapiens GN=AKR1C3 PE=1 SV=4	P42330
-	C	hMOB2_pre_38	3	Q8N9D7	cDNA FLJ37680 fis, clone BRHIP2012923, highly similar to FOCAL ADHESION KINASE 1 (EC 2.7.1.112) OS=Homo sapiens PE=2 SV=1	Q8N9D7
-	C	hMOB2_pre_14	1	B4E164	cDNA FLJ56613, highly similar to Serine/threonine-protein kinase TBK1 (EC 2.7.11.1) OS=Homo sapiens PE=2 SV=1	B4E164
-	C	hMOB2_pre_12	1	Q59FH0	H2A histone family, member Y isoform 2 variant (Fragment) OS=Homo sapiens PE=2 SV=1	Q59FH0
-	C	hMOB2_pre_36	3	P98164	Low-density lipoprotein receptor-related protein 2 OS=Homo sapiens GN=LRP2 PE=1 SV=3	P98164
-	C	hMOB2_pre_39	2	P15088	Mast cell carboxypeptidase A OS=Homo sapiens GN=CPA3 PE=1 SV=2	P15088
-	C	hMOB2_pre_28	1	Q5VUU6	Myeloid cell nuclear differentiation antigen OS=Homo sapiens GN=MNDA PE=2 SV=1	Q5VUU6
-	C	hMOB2_pre_29	2	P13056	Nuclear receptor subfamily 2 group C member 1 OS=Homo sapiens GN=NR2C1 PE=1 SV=2	P13056
-	C	hMOB2_pre_34	2	Q9NRE3	OVN6-2 (Fragment) OS=Homo sapiens PE=2 SV=1	Q9NRE3
-	C	hMOB2_pre_03	2	P54277	PMS1 protein homolog 1 OS=Homo sapiens GN=PMS1 PE=1 SV=1	P54277
-	C	hMOB2_pre_50	1	O94988	Protein FAM13A OS=Homo sapiens GN=FAM13A PE=1 SV=2	O94988
-	C	hMOB2_pre_19	1	O00372	Putative p150 OS=Homo sapiens PE=4 SV=1	O00372
-	C	hMOB2_pre_44	2	O43533	RIG-like 5-6 OS=Homo sapiens PE=4 SV=1	O43533
-	C	hMOB2_pre_47	2	Q9NSD5	Sodium- and chloride-dependent GABA transporter 2 OS=Homo sapiens GN=SLC6A13 PE=1 SV=3	Q9NSD5
-	C	hMOB2_pre_21	3	Q8NC60	Uncharacterized protein C4orf14 OS=Homo sapiens GN=C4orf14 PE=1 SV=2	Q8NC60
-	C	hMOB2_pre_37	1	A40263	Uncharacterized protein C7orf72 OS=Homo sapiens GN=C7orf72 PE=4 SV=2	A40263
-	N	hMOB2_pre_33	2	Q8I5G7	Conserved Plasmodium protein OS=Plasmodium falciparum (isolate 3D7) GN=PFL1205c PE=4 SV=2	
-	N	hMOB2_pre_13	1	Q6GYP7	Isoform 15 of Ral GTPase-activating protein subunit alpha-1 OS=Mus musculus GN=Ralgapa1	
-	N	hMOB2_pre_16	3	Q711G1	Glucose-6-phosphate isomerase OS=Agaricus bisporus GN=gpi1 PE=3 SV=1	
-	N	hMOB2_pre_32	1	Q711G1	Glucose-6-phosphate isomerase OS=Agaricus bisporus GN=gpi1 PE=3 SV=1	
-	N	hMOB2_pre_56	3	Q95EC9	Maturase K OS=Mammillaria haageana GN=matK PE=3 SV=1	
-	N	hMOB2_pre_45	1	Q9KZH7	Micronemal protein 4 OS=Toxoplasma gondii GN=MIC4 PE=1 SV=1	
-	N	hMOB2_pre_04	1	C5XQ6	Putative uncharacterized protein Sb02g025860 OS=Sorghum bicolor GN=Sb02g025860 PE=4 SV=1	
Class A Interactors: Interactors which have been rescued more than three times. They represent highly likely interactors of your bait.						
Class B Interactors: Interactors which have been identified two times. They represent highly likely interactors of your bait.						
Class C Interactors: Interactors which found only once in the screen ("singletons"). Although some of those may indeed represent true interactors of your protein of interest, others represent common false positives						
Class F are considered false positives, based on comparison with our in-house false positives database						
Class N are considered to be non-relevant alignments (Expectation E score above 0.01)						
Frame 2 is in frame with the Gal4 activation domain						

**Table S2.2**

List of all novel binary binding partners of hMOB2 identified by yeast two-hybrid (Y2H) screens (please see section 2.2.3.3, page 108). Please see also Gomez et al. (2015)

### Chapter 3      hMOB2 prevents the accumulation of spontaneous DNA damage in untransformed human cells

The entire work presented in this chapter has been reprinted from Cellular Signalling, 27/2, Gomez, V., **Gundogdu, R.**, Gomez, M., Hoa, L., Panchal, N., O'Driscoll, M. and Hergovich, A., Regulation of DNA damage responses and cell cycle progression by hMOB2, 326–339., Copyright (2015), with permission from Elsevier (for details please see below).

License details provided by Elsevier and Copyright Clearance Center (RightsLink)	
License Number	3923230104627
License Date	Aug 06, 2016
Type of Use	reuse in a thesis/dissertation
Portion and Format	full article, both print and electronic

### 3.1 Introduction

MOB1-deficient mice develop a wide range of tumours (Nishio et al., 2012, Nishio et al., 2016) as reported for loss of LATS kinases (Harvey et al., 2013), suggesting that hMOB1 plays essential roles in various biological functions independent of the LATS signalling. Perhaps this involves the interaction of hMOB1 with the NDR kinases since hMOB1 can interact with NDR via a domain conserved between the LATS and NDR kinases (Hergovich et al., 2006c, Hergovich, 2013).

In contrast, although hMOB2 binds to this same conserved domain of NDR kinases, hMOB2 can only associate with NDR, but not with the LATS kinases (Bothos et al., 2005, Hergovich et al., 2006c, Kohler et al., 2010). Biochemical experiments suggest that the co-activator hMOB1 competes with the inhibitor hMOB2 for NDR binding; hence hMOB2 binding blocks the NDR activity (Kohler et al., 2010). Nonetheless, despite these opposing forces of hMOB1 and hMOB2, hMOB1 is already defined as cell cycle regulator (Hergovich, 2011), while any biological function of hMOB2 remains to be uncovered. Furthermore, hMOB3 neither interacts with NDR nor LATS (Kohler et al., 2010), but rather associates with the pro-apoptotic MST1 kinase, thereby negatively regulating apoptotic signalling in glioblastoma multiforme (Tang et al., 2014). Therefore, mammalian hMOB1 and hMOB3 have been attributed tumour suppressive or oncogenic roles, respectively. Albeit the human *MOB2* gene appears to show LOH in more than 50% of testicular, ovarian, cervical, and bladder carcinomas (The Cancer Genome Atlas, TCGA, please see also Table 6.1, page 235) (Cerami et al., 2012), any defined physiological cancer-related functions of mammalian MOB2 have yet to be described. So far, it has only been reported that MOB2 can contribute to morphological changes in murine neurites and rat astrocytes (Fang et al., 2012, Lin et al., 2011), hence the definition of the functions of hMOB2 are yet to be defined. Significantly, a genome-wide screen for novel DDR players proposed hMOB2 as one of the many potential candidates, suggesting that hMOB2-deficient cells may have compromised activation of the IR-induced G2/M cell cycle checkpoint (Cotta-Ramusino et al., 2011).

The DDR signalling activates cell cycle checkpoints to halt cell cycle progression and triggers DNA repair mechanisms in response to endogenous or exogenous DNA damage, and the p53 tumour suppressor protein is mainly responsible for the activation of checkpoints (Wahl et al., 1997, Deckbar et al., 2011, Bartek and Lukas, 2007). Following recognition of DNA damage, p53 is extensively modified by its upstream regulators including ATM, ATR, DNA-PK, CHK1, and CHK2 through phosphorylations and other post-translational modifications. p53 indirectly suppresses CDK activity to arrest cell cycle progression via transcriptional induction of p21, (Kruse and Gu, 2009). To optimise physiological responses against cellular stresses, p53 can activate or repress the transcription of genes involved in cell cycle, DNA repair, apoptosis, metabolism, and others (Vousden and Prives, 2009, Menendez et al., 2009).

### **3.2 Research aims**

hMOB2 binding blocks NDR kinase activity (Kohler et al., 2010) and NDR kinases can regulate diverse significant biological settings, such as the cell cycle progression mediated by the p21/Cip1 protein (Cornils et al., 2011a, Cornils et al., 2011b). Importantly, Cotta-Ramusino et al. (2011) has recently proposed in their DDR screen that cells with hMOB2 deficiency may have impaired activation of the IR-induced G2/M cell cycle checkpoint. On the bases of these observations, our initial aim was to investigate whether:

- hMOB2 overexpression blocks hMOB1/NDR-mediated cell cycle progression,
- hMOB2 knockdown interferes with hMOB1/NDR-mediated cell cycle progression,
- the p53-regulated G1/S checkpoint is also supported by hMOB2.

### 3.3 Results

**hMOB2 knockdown leads to a G1/S cell cycle arrest.** The hTERT-RPE1 (hTERT: human telomerase reverse transcriptase, RPE1: retinal pigment epithelium) cell line was primarily used in this chapter. The hTERT-RPE1 cell line (hereinafter referred to as RPE1 cells) is considered to be ideal for the investigation of the long-term biochemical characteristics of cell growth since it preserves the diploid status, normal growth characteristics (e.g. functional cell cycle checkpoints), and standard gene expression pattern as normal epithelial cells (Bodnar et al., 1998). Our laboratory engineered untransformed RPE1 cells either expressing a cDNA or an shRNA against a target mRNA under the regulator of tetracycline inducible promoter (Gomez-Martinez et al., 2013). These Tet-inducible (hereinafter referred to as Tet-on) RPE1 cells allowed us to analyse cell cycle progression in consistent overexpression or knockdown conditions. To study cell cycle progression, we applied three independent approaches in a time-dependent manner. First, the protein levels of essential cell cycle markers were biochemically tested by immunoblotting experiments. Second, cell proliferation assays were conducted to monitor proliferation progression. Third, cell cycle profiles of individual cells were analysed by performing propidium-iodide based DNA content analysis using a flow cytometry.

Considering that the NDR kinases can regulate the cell cycle progression through the p21/Cip1 protein (Cornils et al., 2011a, Cornils et al., 2011b), we initially analysed cells with Tet-on inducible overexpression of hMOB2 to seek whether hMOB2 functions as an inhibitor of the NDR kinase (Kohler et al., 2010) in the context of its role in the cell cycle progression (Cornils et al., 2011a, Cornils et al., 2011b). Our results showed that hMOB2 overexpression neither affected cell cycle markers nor cell proliferation (Figure 3.1). In contrast, Tet-on inducible knockdown of hMOB2 augmented the levels of the G1/S cell cycle markers cyclin D1 and E, whereas reducing the S/G2/M markers cyclin A and B1 (Figure 3.2A), suggesting that the cell cycle regulation was impaired upon hMOB2 silencing. These alterations in cyclin expression were accompanied by compromised cell proliferation upon hMOB2 depletion (Figure 3.2B). Analysis of the cell cycle status revealed

that hMOB2-knockdown cells showed a G1/S cell cycle arrest (Figure 3.2C). Taken together, our findings illustrated that hMOB2 knockdown induces a G1/S cell cycle arrest in untransformed human RPE1 cells.

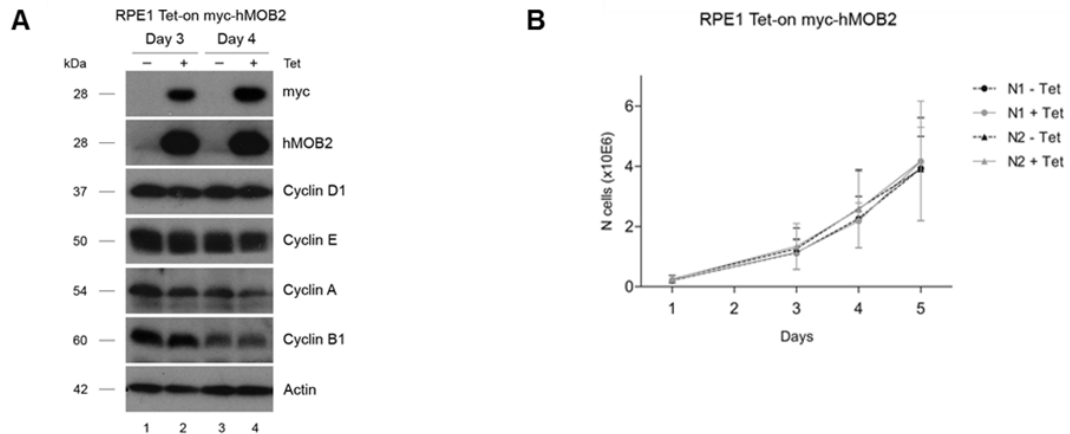


**Figure 3.1**

**hMOB2 overexpression neither affected cell cycle markers nor cell proliferation.**

(A) RPE1 cells bearing inducible Tet-on myc-tagged hMOB2 gene (clone N1) were processed for immunoblotting after 3 or 4 days with (+) or without (-) tetracycline treatment (2  $\mu$ g/ml) as indicated. Expression of hMOB2 was assessed with both anti-myc and anti-hMOB2 antibodies while cell cycle status was analysed using a panel of anti-cyclin D1, E, A and B1 antibodies. Blots represent three individual experiments. (B) Cell proliferation analysis of RPE1 Tet-on myc-hMOB2 cells. Proliferation rates of two independent clones (N1 and N2) are shown after tetracycline (2  $\mu$ g/ml) (solid pattern lines) or control (dashed pattern lines) treatment (n=3). Results are presented as mean of replicates and error bars as mean  $\pm$  standard error of mean (SEM), statistical significance was calculated using the two-way ANOVA test. The experiment was performed by Dr Valenti Gomez.

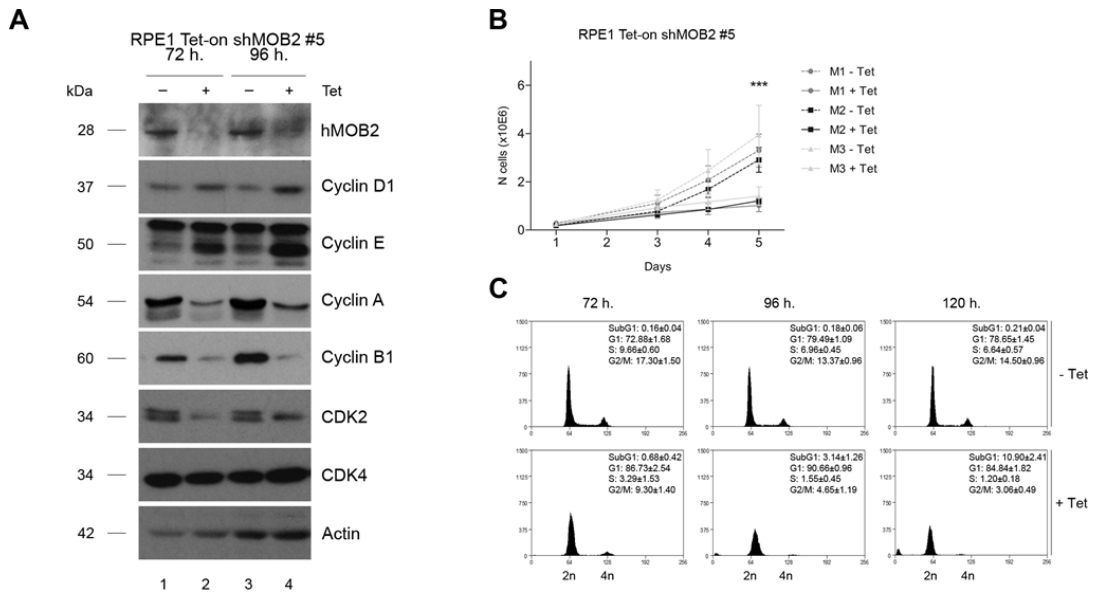


**Figure 3.2**

**hMOB2 depletion causes a G1/S cell cycle arrest in RPE1 cells.**

(A) Immunoblotting with indicated antibodies of RPE1 Tet-on shMOB2 cell lysates after incubation of cells with (+Tet) or without (–Tet) tetracycline (2 µg/ml) as indicated. Blots represent three individual experiments. (B) Proliferation rates of three independent RPE1 Tet-on shMOB2 clones (n = 3; *p*-value = 1.2E-03). Results are presented as mean of replicates and error bars as mean ± standard error of mean (SEM), statistical significance was calculated using the two-way ANOVA test. (C) Cell cycle analyses of RPE1 Tet-on shMOB2 cells at indicated time points with (+Tet) or without (–Tet) of tetracycline (2 µg/ml). Percentages of cells in each cell cycle phase are presented (n = 3). The experiment was performed by Dr Valenti Gomez.

Next, the dynamics of cell cycle transition in normal and hMOB2-depleted cells were compared by performing a time-course DNA content analysis using flow cytometry. Importantly, the stable Tet-on system allowed us to reduce hMOB2 levels in serum-starved cells, before addition of serum to synchronously release cells from G0/G1 into S-phase. Notably, this approach revealed that synchronised hMOB2-knockdown cells displayed a markedly delayed G1/S cell cycle transition (Figure 3.3A-B), which was supported by an immunoblotting analysis with indicated cell cycle markers that shows a delayed accumulation of cyclin A and B1 in synchronised cultures of hMOB2-depleted cells (Figure 3.3C). Taken together, these



results (Figures 3.1, 3.2, and 3.3) indicate that endogenous hMOB2 is required for normal cell cycle progression of untransformed human cells.

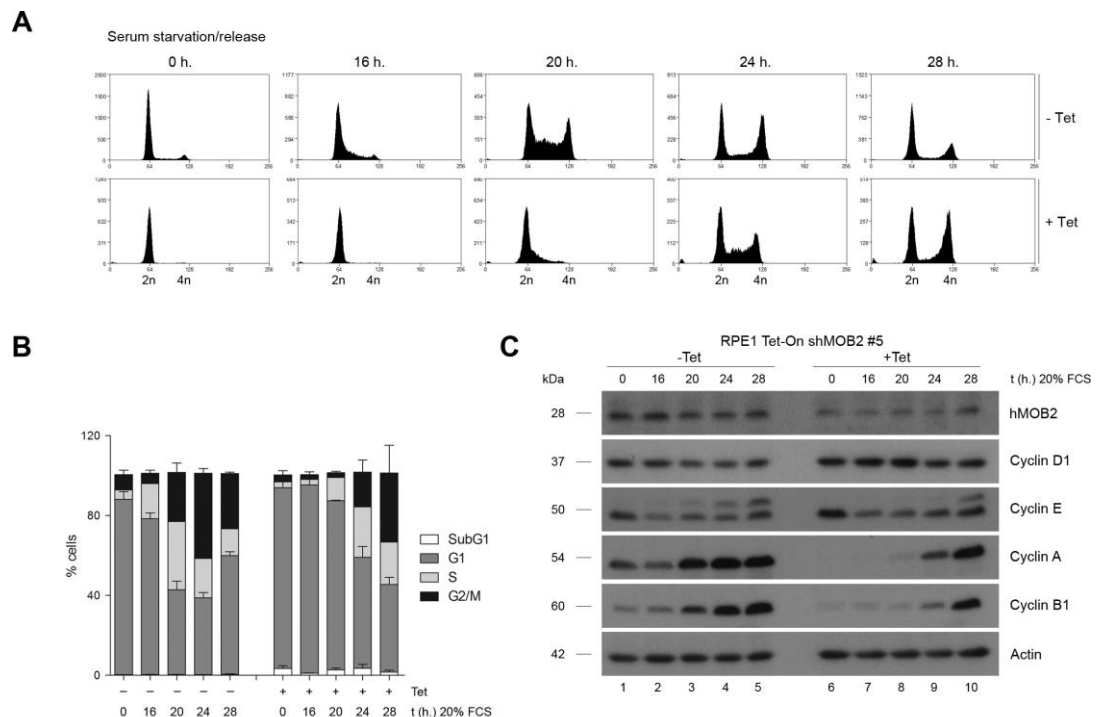


**Figure 3.3**

**hMOB2-depleted cells displayed a markedly delayed G1/S cell cycle transition.**

(A) RPE1 Tet-on shMOB2 cells with (+Tet) or without (-Tet) tetracycline (2 µg/ml) were serum starved for 72 h, washed twice, released in medium containing 20% FCS, and processed for cell cycle analysis at indicated time points. (B) Histograms showing the percentage of synchronised cells in each cell cycle phase (n=3). Results are presented as mean of replicates and error bars as mean ± standard error of mean (SEM), statistical significance was calculated using the one-tailed unpaired Student's *t*-test. (C) Immunoblotting with indicated antibodies of cell lysates obtained from synchronised cell cultures described in A. The experiment was performed by Dr Valenti Gomez with my intellectual contribution. Blots represent three individual experiments.

**hMOB2 depletion activates the p53/p21 cascade and causes transcriptional activation of p53 target genes.** To define the underlying molecular basis of the G1/S cell cycle arrest upon hMOB2 depletion, we expanded our analysis by studying a panel of cell cycle regulators using immunoblotting. Significantly, we observed activation of the p53-pRb axis (Kastan and Bartek, 2004) through p53 stabilisation and decreased pRb

phosphorylation (Mitnacht, 1998) following Tet-on hMOB2 knockdown in RPE1 cells (Figure 3.4A). Furthermore, p21/Cip1 and MDM2, two established p53 target genes (Kruse and Gu, 2009), were elevated at the protein level (Figure 3.4A). These changes may help us to explain the underlying molecular mechanism of the G1/S cell cycle arrest in hMOB2-knockdown cells.

Further, a collection of p53 target genes was analysed to examine whether the observed p53 upregulation in hMOB2-depleted cells (Figure 3.4A) represented an activation of a p53-dependent transcriptional programme. For this aim, we designed a time-course experiment using previously defined Tet-on shMOB2 RPE1 cells to analyse a panel of p53 target genes by quantitative real-time PCR. We first confirmed approximately 50% decrease in the mRNA levels of hMOB2 induced by Tet-on-mediated shMOB2 induction (see Figure S3.1 in the Supplementary section, page 156). Importantly, there was no difference observed in p53 mRNA levels (see Figure S3.1 in the Supplementary section, page 156), suggesting that hMOB2 depletion induced only post-transcriptional activation and/or stabilisation of p53. However, consistent with the immunoblotting results (Figure 3.4A), we detected a statistically significant upregulation of p21 and MDM2 mRNA levels (Figure 3.4B), signifying that increased p21 protein levels are through transcriptional upregulation of p21 mRNA expression upon hMOB2 silencing. In addition, other established p53 target genes (Menendez et al., 2009) were upregulated upon hMOB2 knockdown. More specifically, elevated GADD45A (growth arrest and DNA damage-inducible 45 alpha), BAX (Bcl-2-associated X) and PUMA (p53 upregulated modulator of apoptosis), and TIGAR (TP53-inducible glycolysis and apoptosis regulator) mRNA expressions were also detected (Figure 3.4B), suggesting that DNA repair, apoptosis and metabolism mechanisms could be transcriptionally regulated by stabilised p53 upon hMOB2 depletion. Expression of other p53 target genes including pro-apoptotic NOXA protein (aka PMAIP1: phorbol-12-myristate-13-acetate-induced protein 1), and metabolic SCO2 (cytochrome oxidase deficient homolog 2) and SESN2 (sestrin 2) proteins was also significantly altered (see Figure S3.1 in the Supplementary section, page

158). Collectively, these findings indicate that transcriptionally active p53 is stabilised upon hMOB2 silencing.

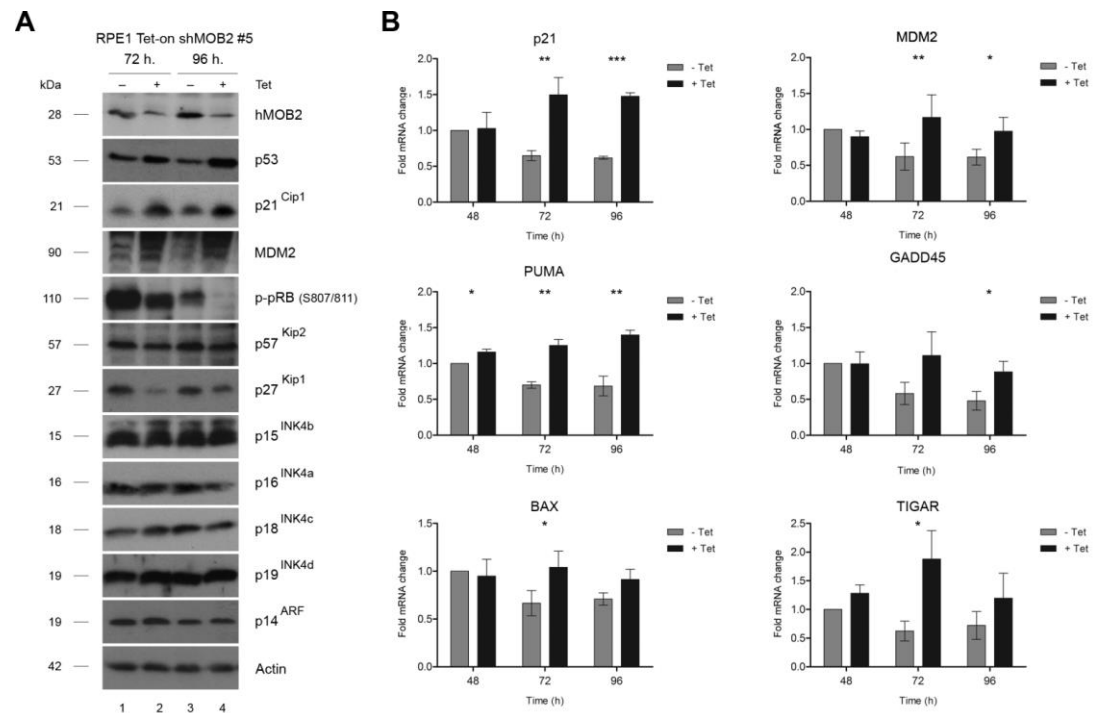


**Figure 3.4**

### **hMOB2 knockdown activates p53/p21 cascade and causes transcriptional activation of p53.**

(A) Immunoblotting with indicated antibodies of RPE1 Tet-on shMOB2 cell lysates from cells incubated with (+Tet) or without (–Tet) tetracycline (2 µg/ml) as indicated. The experiment was performed by Dr Valenti Gomez with my intellectual contribution. Blots represent three individual experiments. (B) Quantitative real-time PCR analysis of indicated p53 target genes in RPE1 Tet-on shMOB2 cells at indicated time points in the presence (black bars) or absence (gray bars) of tetracycline (2 µg/ml) (n=3). *p*-values are: p21, 72 h=5.5E–03, 96 h=5.2E–05; MDM2, 72 h=1.3E–03, 96 h=0.018; PUMA, 48 h=0.033, 72 h=1.7E–03, 96 h=4.4E–03; GADD45, 96 h=0.026; BAX, 72 h=0.047; TIGAR, 72 h=0.025. Results are presented as mean of replicates and error bars as mean ± standard error of mean (SEM), statistical significance was calculated using the one-tailed unpaired Student's *t*-test.

Next, three different untransformed human cell lines (RPE1, human BJ fibroblast and human MCF10A mammary epithelial cells) were employed to confirm increased p53 levels upon hMOB2 knockdown. In contrast to the previous experimental setting (Tet-on inducible expression of shMOB2#5),

cells were transiently transfected with three independent siRNAs (siMOB2#4, #5, #6; please see section 2.1.7, page 91) directed against hMOB2. As a result, these experiments approved consistently elevated p53 levels upon hMOB2 reduction (see Figure S3.2 in the Supplementary section, page 159). Moreover, to ensure that p53 activation was due to loss of hMOB2, we conducted a phenotype RNAi rescue experiment. To do so, RPE1 cells stably expressing wild-type HA-hMOB2 were generated. Subsequently, an siRNA targeting the 3' UTR region of the hMOB2 gene (siMOB2#6) allowed us to knockdown only endogenous hMOB2 in RPE1 cells with stable expression of exogenous HA-hMOB2 being unaffected. This approach confirmed that expression of hMOB2 interfered with p53 induction upon hMOB2 depletion (Figure 3.5A), hence rescuing the phenotype caused by RNAi-mediated silencing of hMOB2. Consequently, these approaches highlight that the stabilisation of active p53 upon hMOB2 depletion is very unlikely a consequence of RNAi off-target effects.

#### **The G1/S cell cycle arrest upon hMOB2 depletion is p53/p21-dependent.**

To investigate whether hMOB2 silencing indeed induced a transient p53/p21-dependent G1/S cell cycle arrest, we co-depleted hMOB2 together with either p53 or p21 in Tet-on shMOB2 RPE1 cells. More specifically, given that p53 can indirectly block CDK activity to arrest cell cycle progression via upregulation of p21, (Kruse and Gu, 2009), we sought whether the G1/S cell cycle arrest observed upon hMOB2 depletion was mediated by p53 through p21.

An shRNA targeting the p53 mRNA (shp53#2, see section 2.1.6, page 90) or an siRNA against the p21 mRNA (sip21#2, see section 2.1.7, page 91) were used for genetic ablation of the indicated genes. For the co-depletion of hMOB2 and p53 protein, RPE1 cells expressing Tet-on shMOB2 were stably infected with shp53, whereas the Tet-on shMOB2 RPE1 cells were transiently transfected with sip21. Following the confirmation of successful co-depletions, we studied cell cycle regulators and cell cycle progression. Our results revealed that hMOB2 silencing triggers a transient p53-dependent arrest since co-depletion of hMOB2 together with p53 restored

normal cell proliferation, abolishing the G1/S cell cycle arrest (Figure 3.5B-D). Likewise, co-depletion of hMOB2 and p21 resulted in a similar restoration of cell cycle progression despite increased p53 levels (Figure 3.6A-C). Therefore, p53-mediated upregulation of p21 likely underlies the G1/S cell cycle arrest observed upon hMOB2 reduction under normal growth conditions.

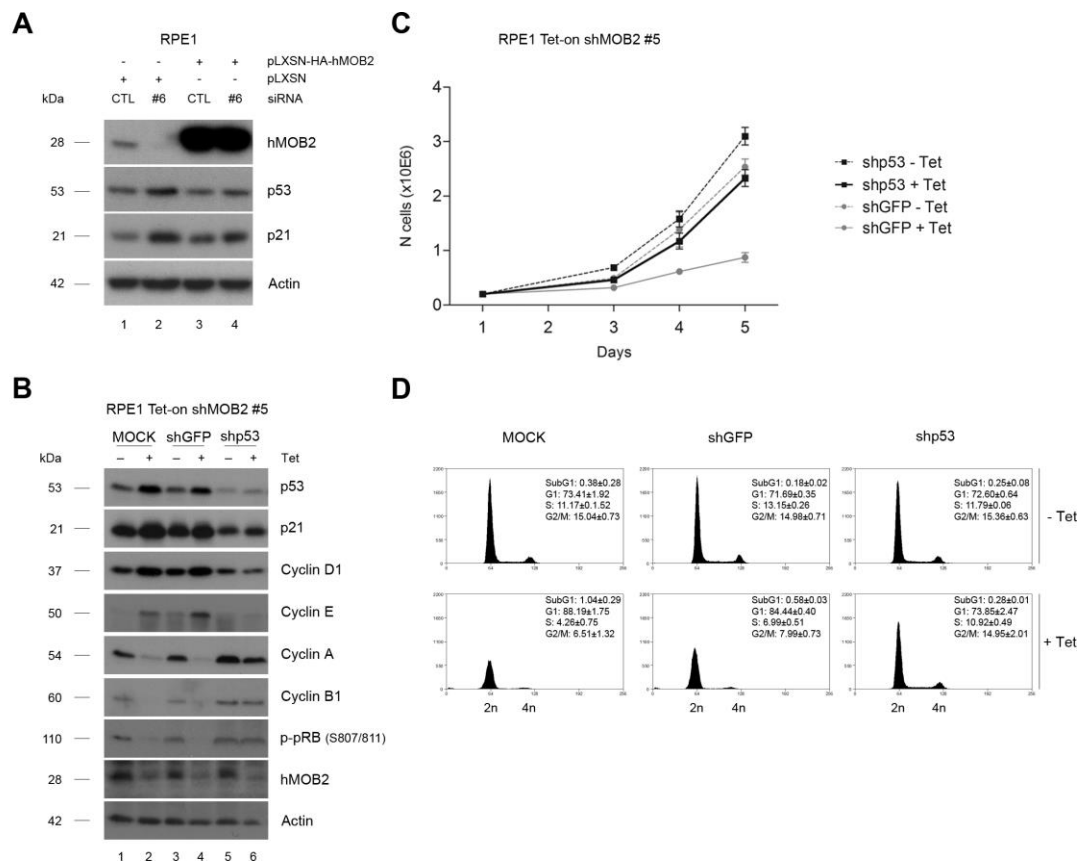


**Figure 3.5**

**The G1/S cell cycle arrest upon hMOB2 depletion is p53-dependent.**

(A) Immunoblotting of RPE1 cell lysates from cells stably expressing empty vector (pLXSN) or siRNA-resistant hMOB2 (pLXSN-HA-hMOB2) transfected with indicated siRNAs (CTL, control; #6, siRNA targeting the 3' UTR of hMOB2). (B) Immunoblotting of RPE1 Tet-on shMOB2 cell lysates from cells infected with indicated plasmids. Cell pools were analysed after 4 days with (+Tet) or without (-Tet) tetracycline (2 µg/ml). Each blot represents three individual experiments. (C) Cell proliferation rates of cell pools described in B were analysed in the presence (+Tet) or absence (-Tet) of tetracycline (2 µg/ml) (n=3). Results are presented as mean of replicates and error bars as mean ± standard error of mean (SEM), statistical significance was calculated using the one-tailed unpaired Student's *t*-test. (D) Cell cycle analyses of cell pools after 4 days in the presence (+Tet) or absence

(–Tet) of tetracycline (2 µg/ml). Percentages of cells in each cell cycle phase are shown (n= 3). The experiment was performed by Dr Valenti Gomez with my intellectual contribution.

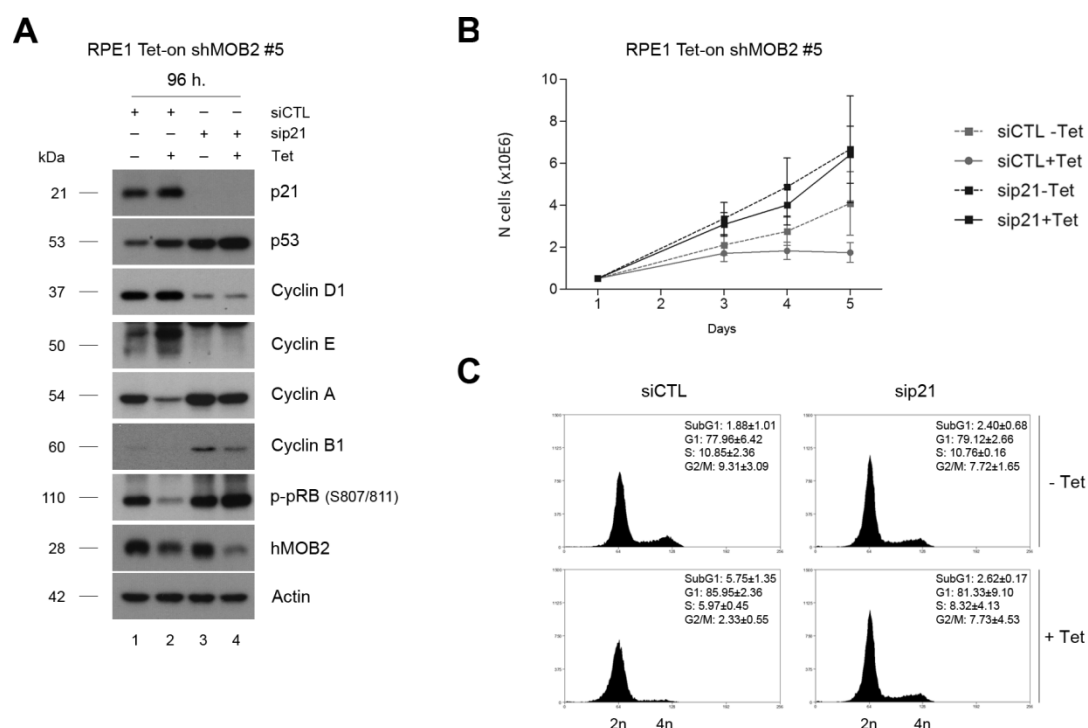


**Figure 3.6**

**The G1/S cell cycle arrest induced by hMOB2 knockdown is through p21 activation.**

(A) Immunoblotting of RPE1 Tet-on shMOB2 cell lysates from cells transfected with indicated siRNAs. Cell pools were analysed after 4 days with (+Tet) or without (–Tet) tetracycline (2 µg/ml) (n=3). (B) Cell proliferation rates of cell pools described in B were analysed in the presence (+Tet, 2 µg/ml) or absence (–Tet) of tetracycline. Blots represent three individual experiments. Results are presented as mean of replicates and error bars as mean ± standard error of mean (SEM), statistical significance was calculated using the one-tailed unpaired Student's *t*-test. (C) Cell cycle analyses of cell pools after 4 days in the presence (+Tet, 2 µg/ml) or absence (–Tet) of tetracycline. Percentages of cells in each cell cycle phase are shown (n= 3). The experiment was performed by Neelam Panchal and Dr Valenti Gomez with my intellectual contribution.

**hMOB2 supports a G1/S cell cycle arrest upon exogenously induced DNA damage.** Cotta-Ramusino et al. (2011) showed in their DDR screen that hMOB2-knockdown cells may have impaired activation of the IR-induced G2/M cell cycle checkpoint. We, therefore, asked whether other DDR cell cycle checkpoints are also supported by hMOB2. To address the p53-

regulated G1/S checkpoint we chose to employ a previously reported approach using untransformed human MCF10A cell line (Colaluca et al., 2008), which is a commonly used *in vitro* model for human mammary epithelial cells (Qu et al., 2015). By stable transfection of shMOB2 or/and shp53 constructs, MCF10A cells were chronically depleted of hMOB2, p53 or both together (Figure 3.7A). To induce exogenous DNA damage, we employed the topoisomerase II inhibitor doxorubicin, which is a widely used anticancer agent in the clinic (Nitiss, 2009). By intercalation and inhibition of topoisomerase II enzyme, doxorubicin induces a variety of DNA damage (e.g. DSBs) thereby triggering cell cycle checkpoint activation, consequently inducing cell death in case the DNA lesions cannot be repaired (Nitiss, 2009). DDR-mediated cell cycle perturbations were assessed at selected time points after treatment and washout of indicated doxorubicin doses (Figure 3.7B-C). As expected (Kastan and Bartek, 2004), control cells arrested predominantly at the G1/S and G2/M cell cycle phases, while p53-knockdown cells arrested mostly at the G2/M checkpoint compared to control cells. hMOB2-depleted cells initially blocked at G1/S similar to controls. Upon washout of 100 nM doxorubicin, controls and hMOB2-depleted cells rapidly resumed cell cycle progression. However, upon washout of 500 nM doxorubicin, hMOB2-depleted cells quickly resumed G1/S cell cycle progression in contrast to controls (Figure 3.7C, bottom panel), indicating a defective DNA damage tolerance of G1/S checkpoint in hMOB2-depleted cells upon exposure to high DNA damage levels. Collectively, these findings together with the data by Cotta-Ramusino et al. (2011) suggest that upon exogenously induced DNA damage hMOB2 functions in promoting cell cycle checkpoint activation in response to DNA damage, a significant hallmark of the DDR signalling.

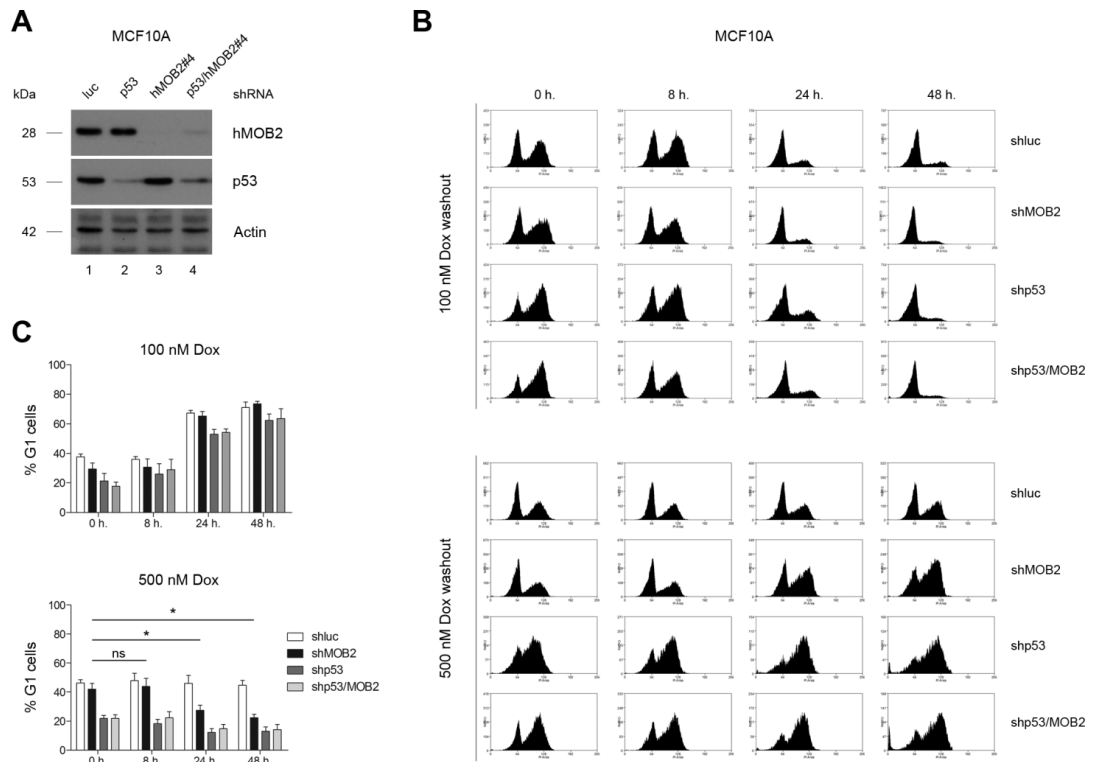


**Figure 3.7**

**hMOB2 promotes G1/S cell cycle arrest in response to exogenously induced DNA damage.**

(A) Immunoblotting with indicated antibodies of MCF10A cell lysates from pSuper.retro.puro infected cells expressing indicated shRNAs. (B) Cell cycle analysis of MCF10A cell pools treated with indicated doxorubicin doses, before releasing in drug-free medium for indicated time points. Representative time courses are shown. (C) Histograms showing percentages of MCF10A cells in the G1 cell cycle phase (n=3). Control (shLuc), hMOB2-depleted (shMOB2), p53-depleted (shp53), and hMOB2/p53 co-depleted (shp53/MOB2) cells were compared. *p*-values are: 8 h = 0.397 (ns, not significant), 24 h = 0.027, and 48 h = 0.011. Results are presented as mean of replicates and error bars as mean  $\pm$  standard error of mean (SEM), statistical significance was calculated using the one-tailed unpaired Student's *t*-test. The stable cell line clones were generated by me and the experiment was performed by me and Dr Valenti Gomez.

**The G1/S cell cycle arrest upon hMOB2 reduction is not caused by altered NDR kinase signalling.** It is well established that p53 stabilisation/activation can be triggered by a variety of distinct mechanisms (Kruse and Gu, 2009). Considering that NDR is the only reported binding partner of hMOB2 (Hergovich, 2011), we interrogated the NDR signalling as a possible mechanism underlying the p53/p21-dependent cell cycle arrest in



response to hMOB2 silencing. More specifically, we speculated that hMOB2 depletion might cause hypo- or hyperactivation of the NDR signalling which potentially could help us to understand how hMOB2 depletion triggers a p53-dependent G1/S cell cycle arrest. To study the importance of NDR signalling in our settings, we pursued three different avenues and analysed cell cycle markers, cell proliferation and cell cycle dynamics in each strategy as conducted earlier. First, we employed RPE1 cells with Tet-on inducible overexpression of constitutively hyperactive NDR1-PIF generated by our laboratory (Cook et al., 2014) to mimic possible hyperactivation of NDR upon hMOB2 depletion. However, unexpectedly, overexpression of hyperactive NDR1 did not negatively affect cell proliferation (Figure 3.8A-C).

Next, RPE1 cells with Tet-on inducible expression of shRNA targeting NDR1 (shNDR1#4) were produced by our laboratory and used to mimic possible hypo-activation of NDR1 signalling in our settings. Also, RPE1 cells were transiently transfected with an siRNA against NDR2 (siNDR2#5) to phenocopy possible hypo-activation of the NDR2 signalling in our settings. However, neither NDR1 nor NDR2 depletions had any effect on cell proliferation (Figure 3.8D-I), overall suggesting that hMOB2 knockdown may impair cell cycle progression independently of NDR1/2 kinase signalling.

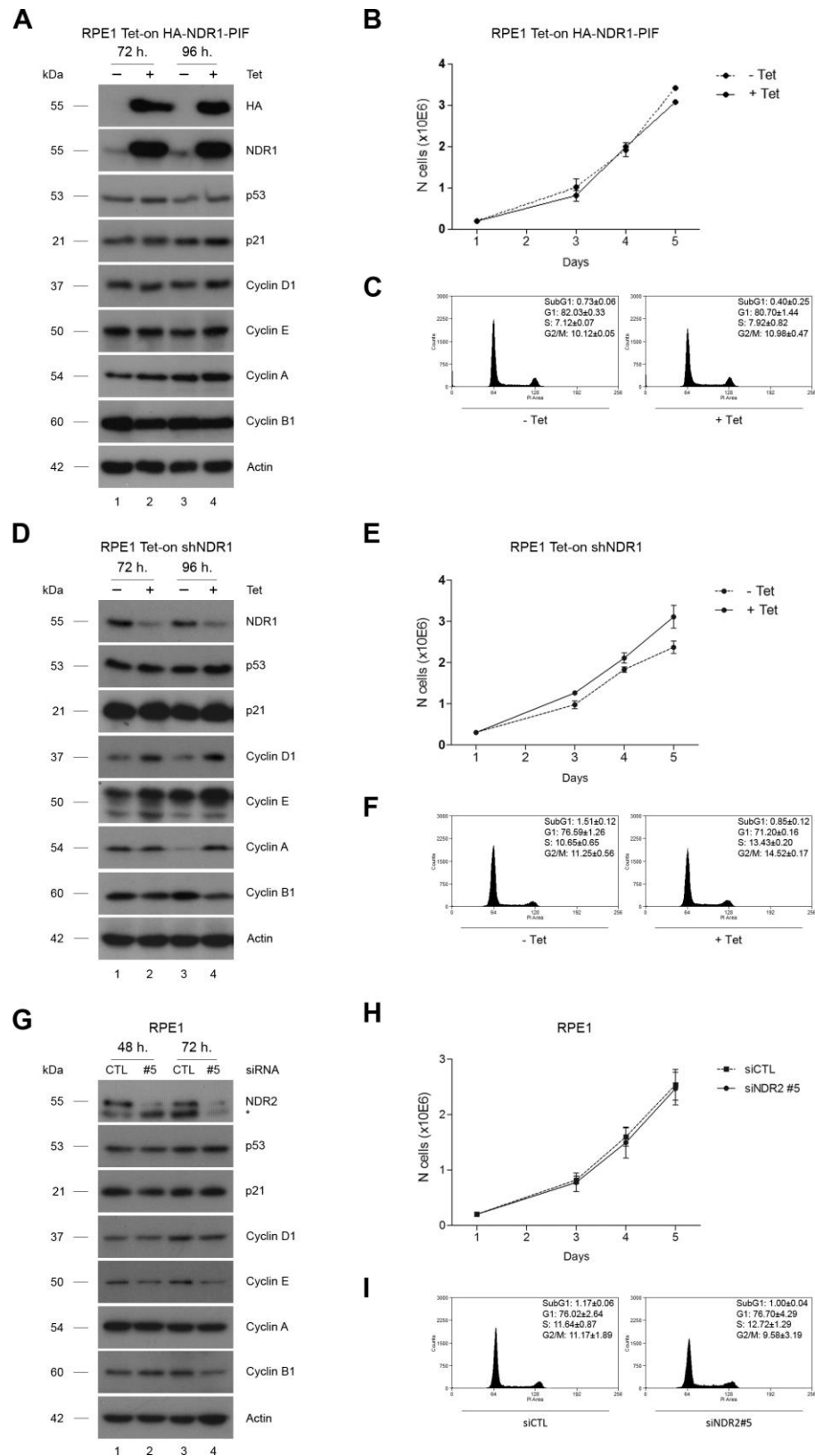


**Figure 3.8**

**The cell cycle effect of hMOB2 depletion is independent of NDR1/2 kinase signalling.**

(A) Immunoblotting of RPE1 Tet-on HA-NDR1-PIF cell lysates from cells incubated with (+Tet, 2 µg/ml) or without (–Tet) tetracycline for indicated times. (B) Proliferation rates of RPE1 Tet-on HA-NDR1-PIF cells (n=3). (C) Cell cycle analyses of RPE1 Tet-on HA-NDR1-PIF cells after 96 h in the presence (+Tet, (2 µg/ml) or absence (–Tet) of tetracycline (n=3). (D) Immunoblotting of RPE1 Tet-on shNDR1#4 cell lysates as described in A (E) Proliferation rates of RPE1 Tet-on shNDR1#4 cells (n=3). (F) Cell cycle analyses of RPE1 Tet-on shNDR1#4 cells after 96 h in the presence (+Tet, 2 µg/ml) or absence (–Tet) of tetracycline (n=3). (G) Immunoblotting of RPE1 cell lysates from cells transfected with indicated siRNAs (CTL, control; #5, siNDR2). An asterisk (\*) in NDR2 blot marks an unspecific band. (H) Proliferation rates of indicated cell lines (n=3). (I) Cell cycle analyses of RPE1 cells 96 h after indicated siRNA transfections (n= 3). All results are presented as mean of replicates and error bars as mean ± standard error of mean (SEM), statistical significance was calculated using the one-tailed unpaired Student's *t*-test. Each blot represents three individual experiments.

### **hMOB2 depletion triggers a DNA damage-ATM-CHK2-p53-p21 cascade.**

Following our observation that the G1/S cell cycle arrest induced by hMOB2 silencing was p53/p21-dependent (Figures 3.5 and 3.6), we further investigated the potential mechanism of p53 stabilisation/activation upon hMOB2 knockdown. Importantly, sustained p53 stabilisation results in a permanent proliferation arrest through senescence, while pulses of stabilised p53 yield a transient arrest (Purvis et al., 2012). Using increased cell size as an established senescence marker for RPE1 cells (Kim et al., 2007), we found that hMOB2 depletion does not result in senescence (see Figure S3.3 in the Supplementary section, page 158). Our data rather suggest that hMOB2 knockdown triggers a transient p53/p21-dependent G1/S cell cycle arrest since co-depletion of hMOB2 together with p53 or p21 abolished the arrest (Figures 3.5 and 3.6). Since a misbalance between DNA damage and repair results in higher p53 levels through pulses (Loewer et al., 2010) which can cause a transient p53-dependent cell cycle arrest (Purvis et al., 2012), we speculated that compromised DNA damage sensing/repair was causing the p53-mediated arrest in hMOB2-depleted cells. Considering further that the p53/p21 pathway is a master regulator of the G1/S cell cycle transition in the DDR (Kruse and Gu, 2009, Vogelstein et al., 2000, El-Deiry et al., 1993, el-Deiry et al., 1994, Harris and Levine, 2005, Kastan and Bartek, 2004, Speidel, 2015), we were prompted to examine p53 in the context of DDR signalling in hMOB2-depleted cells under normal growth conditions. We

hypothesised that a DDR defect due to hMOB2 knockdown could explain why hMOB2-depleted cells displayed a p53-dependent G1/S cell cycle arrest. Possibly hMOB2-depleted cells accumulate unrepaired DNA damage, which can trigger p53 activation.

Therefore, we studied how p53 signalling is triggered in hMOB2-depleted cells (Figure 3.9). Since increased p53 protein levels did not correlate with elevated levels of p53 mRNA (Figure 3.4A and see Figure S3.1 in the Supplementary section, page 158), we examined p53 phosphorylation as possible stabilisation mechanism (Kruse and Gu, 2009). By conducting immunoblotting experiments, we biochemically analysed the phosphorylation status of p53 along with other significant DDR regulators. For this aim, a time-course experiment was designed with Tet-on shMOB2 RPE1 cells. Interestingly, we found that Ser15 phosphorylation of p53 was increased upon hMOB2 depletion in RPE1 cells (Figure 3.9A). In parallel, we examined ATM/ATR kinases, which phosphorylate Ser15 upon genotoxic stress (Wahl and Carr, 2001), in our experimental settings. ATM activity judged by CHK2 phosphorylation was elevated, while ATR activation monitored by CHK1 phosphorylation decreased upon hMOB2 depletion (Figure 3.9B). Moreover, aside from testing DDR activation in Tet-on RPE1 cell system, we conducted an experiment where we confirmed phosphorylation-dependent p53 stabilisation in different cells with an independent siRNA. Specifically, we showed that untransformed human MCF10A and BJ cells transiently transfected with an siRNA targeting hMOB2 (siMOB2#4) also displayed activated DDR signalling as judged by elevated CHK2 and p53 phosphorylation (Figure 3.9C). Taken together, these findings suggest that DDR signalling is elevated in hMOB2-depleted cells, most likely triggered by the elevated levels of endogenous DNA damage.

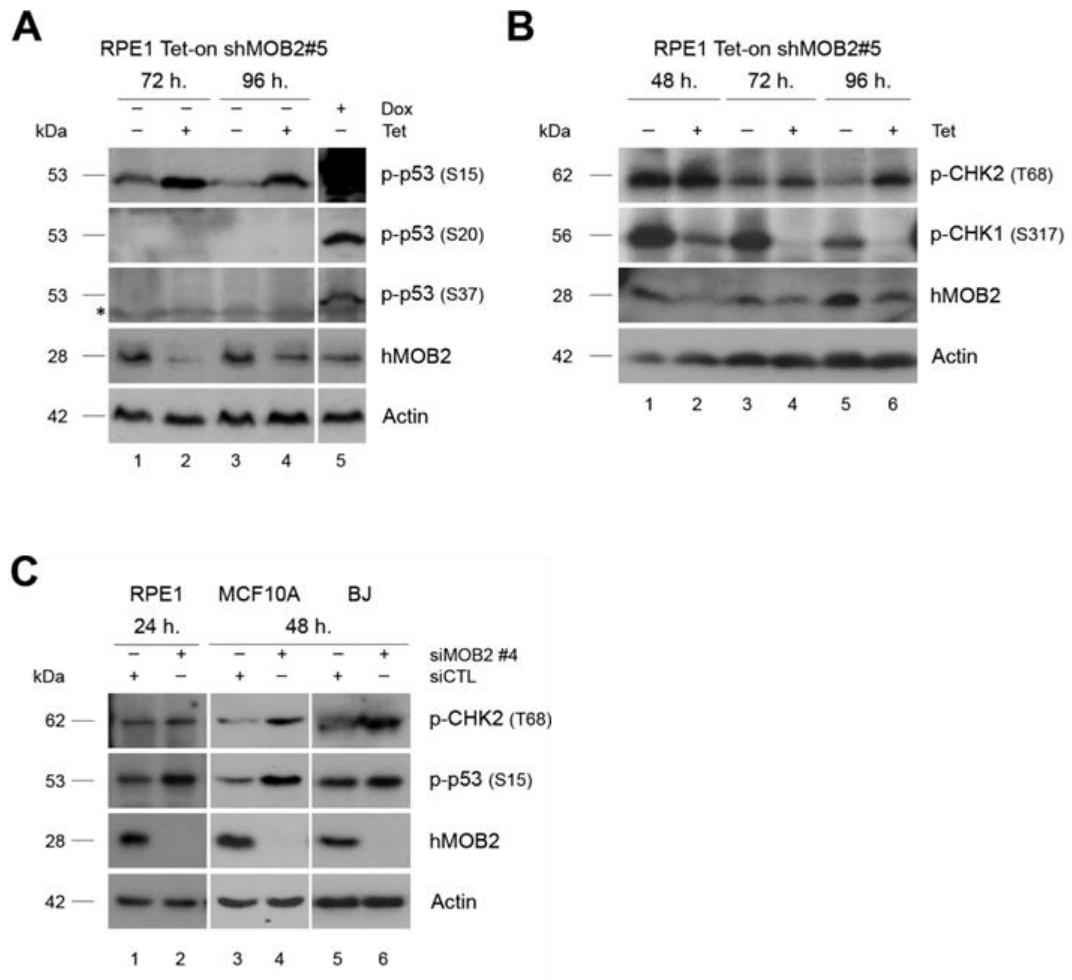


**Figure 3.9**

**In normal growth conditions hMOB2 knockdown triggers ATM-Chk2-p53 signalling.**

(A, B) Immunoblotting of RPE1 Tet-on shMOB2 cell lysates from cells incubated with (+Tet, 2 µg/ml) or without (-Tet) tetracycline for indicated times. Controls were incubated with doxorubicin (+Dox). (C) Immunoblotting of RPE1, MCF10A, and BJ cell lysates from cells transiently transfected with indicated siRNAs. The experiments were performed by Dr Valenti Gomez with my intellectual contribution. Each blot represents more than one individual experiment.

Next, to probe whether DDR signalling was increased as a consequence of elevated DNA damage levels, we performed immunofluorescence experiment (Figure 3.10A). In this regard, we examined DSB formation by co-labelling for the DNA repair mediators  $\gamma$ H2AX and 53BP1, two key players in the DDR mechanism (Kleiner et al., 2015). Our immunofluorescence study revealed that the number of cells with more than five DSBs per cell augmented three-fold upon hMOB2 knockdown in the

absence of exogenous DNA damage (Figure 3.10B). Next, we asked whether the observed spontaneous DSB accumulation was dependent on the cell cycle progression by performing a serum starvation experiment. Significantly, hMOB2 depletion in non-cycling (serum-starved) cells had no effect (Figure 3.10C-D). In line with this, we also checked whether the activation of DDR signalling upon hMOB2 silencing was proliferation-dependent. This extended analysis showed that proliferating hMOB2-depleted cells displayed activation of ATM-CHK2-p53-p21 signalling, whereas controls and serum-starved cells did not (Figure 3.10E). To complement these molecular and cell biological approaches, we next conducted alkaline Comet assays in Tet-on RPE1 cells to measure DNA breakage directly at the single-cell level. Our analysis revealed that upon hMOB2 depletion cells rapidly accumulate DNA breaks (Figure 3.10F-G). Collectively, these observations suggest that hMOB2 depletion causes spontaneous accumulation of unrepaired DSBs, thereby triggering DDR-mediated p53 stabilisation, which consequently elevates p21 expression to arrest damaged cells in the G1/S cell cycle checkpoint.

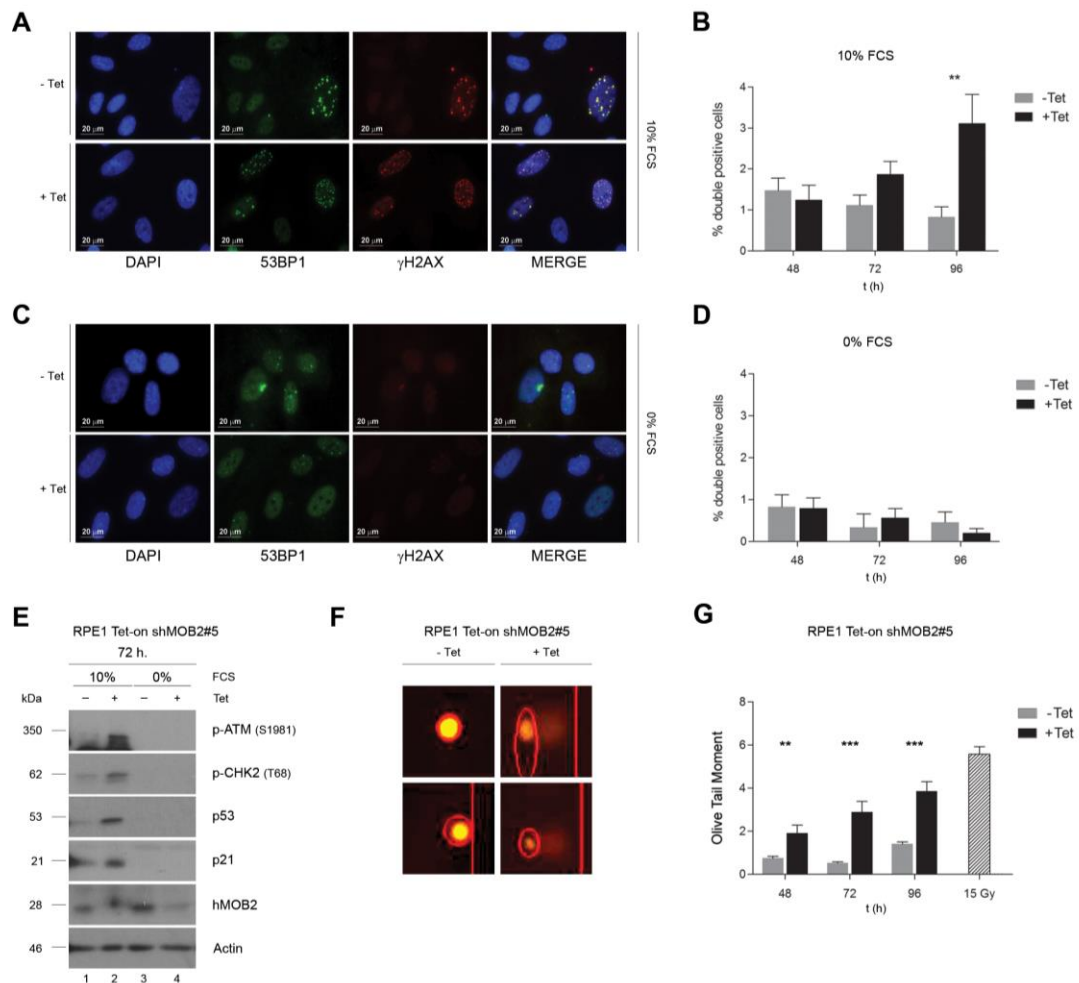


**Figure 3.10**

**hMOB2 depletion triggers the DNA Damage Response due to the accumulation of DSBs.**

(A) Immunodetection of 53BP1 (green) and  $\gamma$ H2AX (red) in RPE1 Tet-on shMOB2 cells grown in the presence (+Tet, 2  $\mu$ g/ml) or absence (-Tet) of tetracycline for 96 h. DNA is stained blue. (B) Histograms showing percentages of cells with DSBs in the presence of serum. Only cells displaying at least ( $\geq$ ) 5 double positive 53BP1/ $\gamma$ H2AX DSB foci per nuclei were counted as DSB positive (1000 cells per time point in control (grey) or hMOB2-depleted (black) cells ( $p$ -value = 0.006). (C) Immunodetection of 53BP1 (green) and  $\gamma$ H2AX (red) in RPE1 Tet-on shMOB2 cells cultured in the presence (+Tet, 2  $\mu$ g/ml) or absence (-Tet) of tetracycline without serum (0% FCS) for 96 h. (D) Histograms showing percentages of cells with DSBs in the absence of serum. Cells were scored as described in B. (E) Immunoblotting of RPE1 Tet-on shMOB2 cell lysates from cells serum-starved for 72 h with (+Tet, 2  $\mu$ g/ml) or without (-Tet) tetracycline, before addition of medium without (0% FBS) or with serum (10% FBS) for another 72 h. Blots represent three individual experiments. (F) Measurement of DNA breaks by alkaline Comet assays in RPE1 Tet-on shMOB2 cells treated with (+Tet, 2  $\mu$ g/ml) or without (-Tet) tetracycline for 96 h. (G) Quantification of DNA damage by alkaline Comet assay in RPE1 Tet-on

shMOB2 cells at indicated time points (n= 3). *p*-values are: 48 h = 2.67E-03; 72 h = 1.69E-05; 96 h = 2.23E-20. IR at 15Gy served as positive control. The experiments were performed by me and Dr Valenti Gomez. All results are presented as mean of replicates and error bars as mean  $\pm$  standard error of mean (SEM), statistical significance was calculated using the one-tailed unpaired Student's *t*-test.



### 3.4 Discussion

Our data presented in this chapter suggest that loss of hMOB2 induces the accumulation of unrepaired DSBs, which in turn triggers the DDR-mediated p53 stabilisation and consequently promotes p21 upregulation to ultimately arrest damaged cells at the G1/S cell cycle checkpoint.

The serine/threonine CDKs and cyclins collaborate to constitute catalytically active heterodimer complex molecules during the cell cycle progression (Vermeulen et al., 2003, Sherr and Roberts, 1999). For example, CDK2, CDK4 and CDK6 are active in the G1 phase, CDK2 during the S phase, and CDK1 during the G2 and M phases. Phosphorylation events achieved by the CDK4/6-cyclin D complexes and the CDK2-cyclin E complexes are responsible for the transition from G1 to S (Kastan and Bartek, 2004). Our findings in Figure 3.2 show that hMOB2 reduction in untransformed human cells prompted a G1/S cell cycle arrest, whereas hMOB2 overexpression neither affected cell cycle markers nor cell proliferation (Figure 3.1). Considering that synchronised hMOB2-knockdown cells elicited a markedly delayed G1/S cell cycle transition (Figure 3.3), these findings indicate that endogenous hMOB2 is required for normal cell cycle progression.

The p53 tumour suppressor protein is a key effector of the DDR kinase signalling (Harris and Levine, 2005). In response to cellular stress conditions, levels of the p53 protein increase dramatically to mediate a G1/S cell cycle arrest that is mainly through the transcriptional upregulation of p21 (El-Deiry et al., 1993, el-Deiry et al., 1994, Kastan and Bartek, 2004, Vogelstein et al., 2000). Under these circumstances, the p53 stabilisation occurs via post-translational modifications, without any significant elevation of p53 mRNA levels (Kastan et al., 1991). The p53-mediated p21 upregulation, in turn, inhibits CDK2-cyclin E complex and activates pRb signalling to block the cell cycle regulation at the G1/S phase following the recognition of intra- and extracellular stresses (Vogelstein et al., 2000, Kruse and Gu, 2009).

Therefore, transcripts and protein levels of various cell cycle regulators were tested to understand how hMOB2-depleted cells arrested at

the G1/S cell cycle checkpoint. We observed that p53 protein levels (but not mRNA levels) were increased, while pRb phosphorylation was decreased in hMOB2-depleted RPE1 cells (Figure 3.4), indicating activation of the well-established p53-p21-pRb tumour suppressor axis (Kastan and Bartek, 2004). Equally important, p21/Cip1 and MDM2, two recognised p53 targets (Kruse and Gu, 2009), were elevated on protein and mRNA levels (Figure 3.4A-B), suggesting that p53 was stabilised to trigger cell cycle inhibition upon hMOB2 silencing.

mRNA levels of other p53 target genes were also significantly altered upon hMOB2 reduction (Figure 3.4B and see Figure S3.1 in the Supplementary section, page 156), suggesting that transcriptionally active p53 was stabilised to trigger a specific expression programme upon hMOB2 knockdown. Elevated GADD45A mRNA expression (Figure 3.4B) suggests that GADD45A-mediated DNA repair mechanism(s) (Hollander and Fornace, 2002) could be activated upon hMOB2 depletion. Additionally, hMOB2 deficient cells displayed significantly elevated mRNA levels of *BAX* and *PUMA* genes, two main pro-apoptotic regulators (Yu and Zhang, 2009, Czabotar et al., 2014) (Figure 3.4B). Interestingly, the mRNA levels of the pro-apoptotic regulator, NOXA (Oda et al., 2000), showed a significant decrease in response to hMOB2 knockdown (see Figure S3.1 in the Supplementary section, page 158). In this context, it is worth noting that the violent apoptotic effect of the upregulation of BAX and PUMA proteins could be compensated by the downregulation of NOXA, thereby preventing massive induction of apoptosis in hMOB2-depleted cells to allow DNA repair upon cell cycle checkpoint activation. This speculative model is supported by the observations that in hMOB2-deficient cells p21 mRNA and protein levels are increased (Figure 3.4) to trigger a transient p53-p21 dependent cell cycle arrest (Figure 3.2). Additionally, activation GADD45 mRNA expression could allow cells to arrest and repair their DNA damage instead of driving cells to death by apoptosis as reported in other settings (Shibue et al., 2006, Ploner et al., 2008). Furthermore, our experiments suggest that in hMOB2-depleted cells the metabolic pathways seem to be adapted to stress conditions by p53 upregulation, since mRNA expression levels of TIGAR (a glycolysis

regulator) (Green and Chipuk, 2006) and SCO2 (an OXPHOS regulator) (Matoba et al., 2006) were dramatically elevated (Figure 3.4). Collectively, these changes in the p53-driven transcriptional programmes strongly suggest that p53 is stabilised and becomes transcriptionally active, which is essential for the adaptation of diverse physiological settings to stress conditions triggered upon hMOB2 knockdown.

This notion was further supported by demonstrating that p53-mediated p21 upregulation, as cyclin/CDK inhibitor (Kastan and Bartek, 2004), was directly responsible for the observed G1/S cell cycle arrest (Figures 3.5 and 3.6). Moreover, we showed that expression of siRNA-resistant hMOB2 interfered with p53 induction upon hMOB2 depletion (Figure 3.5A). Also, transfection of three different untransformed human cell lines with three independent siRNAs targeting hMOB2 fully confirmed that transient hMOB2 depletion consistently elevated p53 and p21 levels (see Figure S3.2 in the Supplementary section, page 159).

hMOB2 is further required to support activation of the G1/S and G2/M cell cycle checkpoints in RPE1 cells treated with high levels of exogenously induced DNA damage. We report here a defective G1/S checkpoint in hMOB2-depleted cells upon exposure to high DNA damage levels (Figure 3.7), and Cotta-Ramusino et al. (2011) showed that hMOB2-depleted cells may have a compromised activation of the IR-mediated G2/M cell cycle checkpoint (Cotta-Ramusino et al., 2011).

Based on the reported link between hMOB2 and NDR1/2 kinases (Kohler et al., 2010), we asked whether the p53/p21-dependent cell cycle arrest upon hMOB2 depletion was through the NDR1/2 kinase signalling. Our data demonstrated that overexpression of constitutively hyperactive NDR (Cook et al., 2014) or NDR (NDR1 or NDR2) depletion had no effect on cell proliferation (Figure 3.8), suggesting that the NDR signalling is unlikely to play a role in these settings. However, further investigations are required to completely validate that the NDR1/2 signalling is not linked to cell cycle process through hMOB2, since various studies have recently suggested possible compensatory mechanisms that may arise upon selective NDR1 or NDR2 manipulations (Schmitz-Rohmer et al., 2015).

Furthermore, considering that the p53/p21-dependent G1/S cell cycle arrest is a hallmark of the DDR (Kruse and Gu, 2009), we examined p53 in the context of DDR signalling in hMOB2-knockdown cells under normal growth conditions. Our biochemical experiments conducted in three different untransformed cell line displayed that upon hMOB2 reduction ATM-CHK2-p53 cascade became post-translationally activated (through phosphorylation) (Figure 3.9), revealing a possible stabilisation mechanism of p53 via elevated ATM activity (Kruse and Gu, 2009). Furthermore, we revealed that the number of cells with more than five DSBs per cell increased three-fold upon hMOB2 silencing by co-labelling for the DNA repair mediators  $\gamma$ H2AX and 53BP1 (Figure 3.10A-B), which was proliferation dependent since hMOB2 depletion in non-cycling cells had no effect (Figure 3.10C-D). In line with this, proliferating hMOB2-knockdown cells displayed activation of ATM-CHK2-p53-p21 signalling, while controls and serum-starved cells did not (Figure 3.10E). Consequently, our findings further support the notion of the activation of a DNA damage-DDR-p53-p21 cascade by hMOB2 depletion. Moreover, our single cell Comet analysis also showed that cells rapidly accumulate endogenous DNA breaks upon hMOB2 depletion (Figure 3.10F-G). Significantly, we further found that in hMOB2-depleted cells, general DNA breakage was elevated before DSBs were detectable by immunofluorescence (compare Figures 3.10B and 3.10G). Since  $\gamma$ H2AX/53BP1 accumulate at DSBs only after DDR activation (Polo and Jackson, 2011), these results suggest that DNA lesions precede DDR activation in hMOB2-knockdown cells.

To sum up, under normal growth conditions, proliferating hMOB2-depleted cells accumulate unrepaired DSBs, which activate the DDR signalling and trigger the p53/p21-dependent G1/S cell cycle arrest. Based on the data presented in this section and reported in Cotta-Ramusino et al. (2011), one can speculate that impaired detection/repair of endogenous DNA damage (as normally induced by cellular mechanisms (Lindahl and Barnes, 2000)) may be the initial trigger of the DDR activation in hMOB2-depleted cells. Therefore, we were interested in deciphering how hMOB2 may play a role as a DDR protein on a molecular level as presented in the next chapters.

## **Acknowledgements**

Before I started the project described in this chapter, Dr. Valenti Gomez had already performed initial experiments to understand the involvement of hMOB2 in the cell cycle progression as outlined in the relevant figure legends. I would like to thank him for his help, contribution and collaboration in this chapter. I would also like to thank Lily Hoa and Dr. Alexander Hergovich for the generation of Tet-on RPE1 cells, and Neelam Panchal for her contribution to Figure 3.6. I further thank Dr. Victoria Spanswick for kindly assisting me to establish alkaline Comet assays.

### 3.5 Supplementary Information

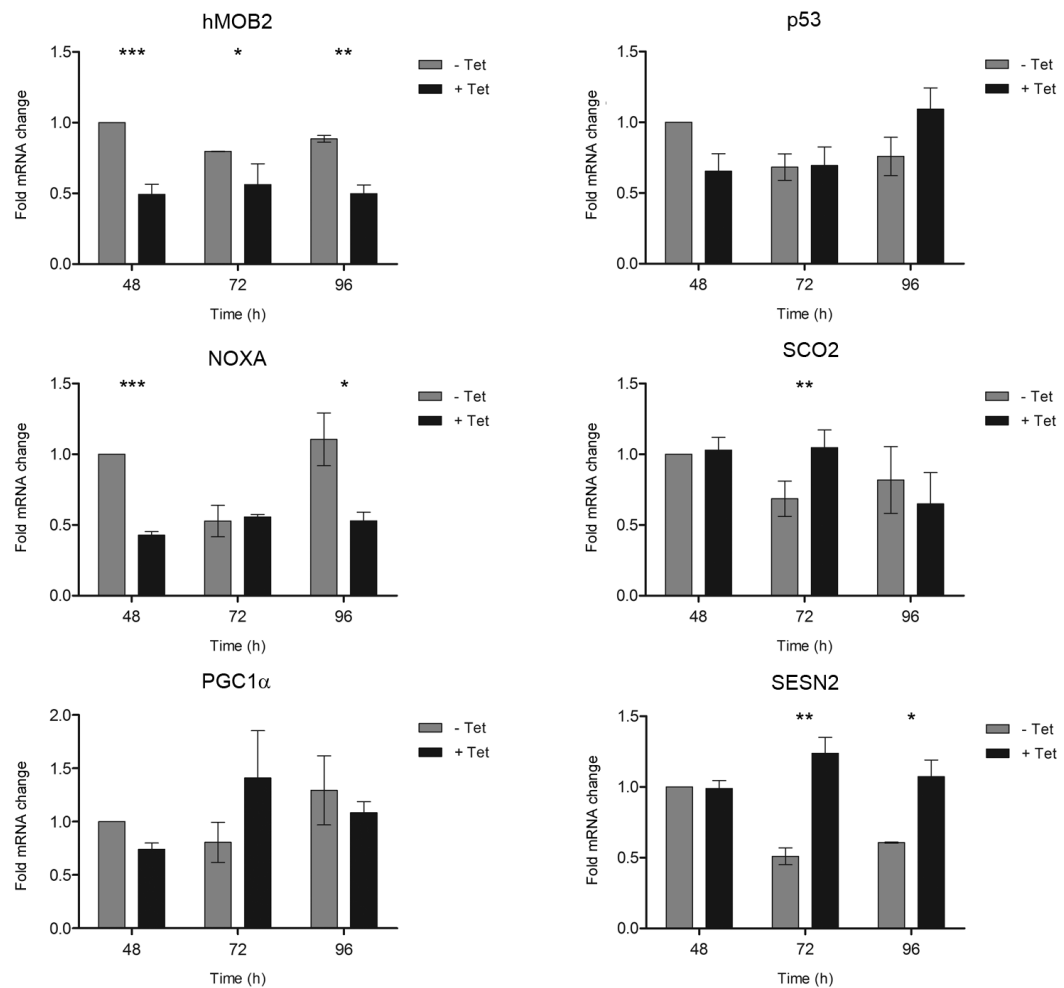


**Figure S3.1**

**Gene expression profiling of hMOB2-depleted RPE1 cells (in support of Figure 3.4).**

mRNA levels of indicated genes were analysed in RPE1-hTert Tet-On shMOB2#5 cells treated with (black bars) or without (grey bars) tetracycline for 24, 48 and 72 hours. Results were normalized to the untreated condition at 48 h. and shown as average  $\pm$ S.E.M. of four independent experiments (*p*-values: hMOB2, 48h = 6.4E-04, 72h = 0.038, 96h = 9.2E-03; Noxa, 48h = 1.8E-04, 96h = 0.021; Sco2, 72h = 7.0E-03; Sesn2, 72h = 1.8E-03, 96h = 0.035).

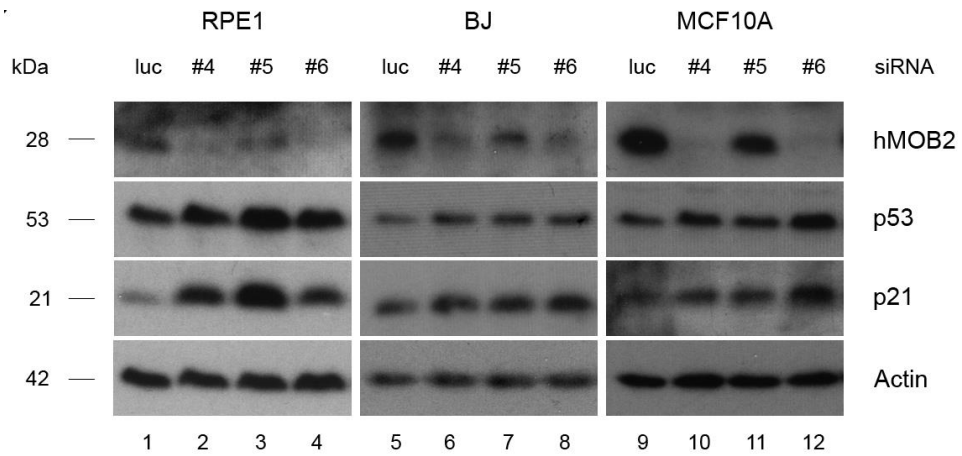


**Figure S3.2**

**p53 levels increases upon hMOB2 depletion (in support of Figure 3.4).** RPE1, BJ and MCF10A cells transiently transfected with 3 different siRNAs directed against hMOB2 (#4, #5, #6) were processed for immunoblotting 48 hours after transfection and expression levels of hMOB2, p53 and p21 were assessed. Blots represent more than one individual experiment.

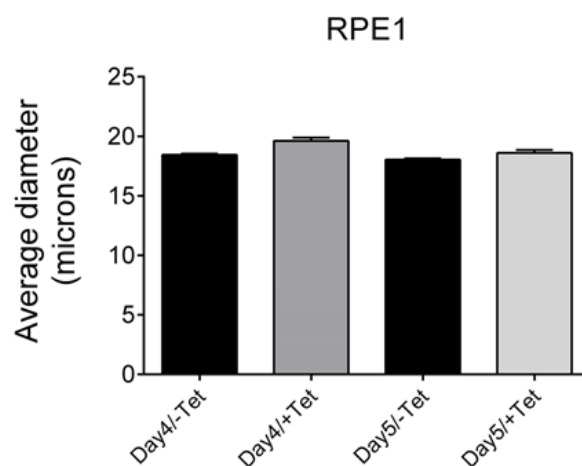


**Figure S3.3**

**Average cell size does not change upon hMOB2 knockdown.**

Cell size analyses of RPE1 Tet-on shMOB2 cells at indicated time points with (+Tet) or without (-Tet) of tetracycline (2  $\mu$ g/ml) using a cell counter (Beckman Coulter, Inc. Vi-CELL XR 2.03). Bars show average cell size of >1.000 cells scored in 50 images per group.



## Chapter 4      hMOB2 interacts with RAD50 and supports MRN-mediated ATM signalling and homologous recombination-mediated DSB repair

Figures 4.1, 4.2, 4.3, and Supplementary Figures 4.1 and 4.2 have been reprinted from Cellular Signalling, 27/2, Gomez, V., **Gundogdu, R.**, Gomez, M., Hoa, L., Panchal, N., O'Driscoll, M. and Hergovich, A., Regulation of DNA damage responses and cell cycle progression by hMOB2, 326–339., Copyright (2015), with permission from Elsevier (for details please see below).

License details provided by Elsevier and Copyright Clearance Center (RightsLink)	
License Number	3923230104627
License Date	Aug 06, 2016
Type of Use	reuse in a thesis/dissertation
Portion and Format	full article, both print and electronic

## 4.1 Introduction

In the previous chapter, we found that upon hMOB2 depletion under normal conditions (without exogenous stress induction) unrepaired spontaneous DNA damage accumulates, initiating DNA damage-p53 signalling, which promotes p21 expression to activate the G1/S cell cycle checkpoint. Based on these observations, we hypothesised that hMOB2 promotes DDR signalling by supporting DNA damage detection/repair and cell cycle checkpoints.

The genome is constantly subjected to endogenous and exogenous DNA damaging factors, which induces a variety of DNA lesions including double strand breaks (DSBs) (Lindahl and Barnes, 2000). The immediate detection of these lesions and subsequent damage sensing/repair signalling is mediated by the DDR pathway (Symington and Gautier, 2011, Chapman et al., 2012). Apart from PARP and Ku70/80 (Polo and Jackson, 2011), DSBs are avidly detected by the MRN (MRE11-RAD50-NBS1) complex, which is then employed to tether broken DNA ends prior to repair by the NHEJ pathway or to facilitate end resection prior to repair by the HRR pathway (Lee and Paull, 2004, Lee and Paull, 2005a). Damage-induced structural change on chromatin promotes initial intermolecular autophosphorylation of ATM, inducing homodimer disassociation (Kastan and Bartek, 2004). Once activated, ATM monomers are recruited to the vicinity of DSBs by NBS1 (Rupnik et al., 2010, Stracker and Petrini, 2011, Williams et al., 2010), which further supports catalytically active ATM monomers by its autophosphorylation at Ser1981 residue (Bakkenist and Kastan, 2003). The ATM kinase, in turn, phosphorylates a broad spectrum of substrates (e.g. p53, CHK2 and H2AX) that controls diverse aspects of cellular processes including cell cycle regulation, chromatin remodelling and DNA damage repair mechanisms (Matsuoka et al., 2007, Shiloh and Ziv, 2013). DSBs can be induced directly by physiological DNA metabolism (e.g. through topoisomerase enzymes) or during exposure to external DNA-damaging factors (e.g. IR), and DSBs are deleterious lesions that are extremely complex to repair (Lindahl and Barnes, 2000).

The homologous recombination repair (HRR) and non-homologous end-joining (NHEJ) mechanisms are the two most important DNA damage repair pathways dealing with DSBs (Goodarzi and Jeggo, 2013, Khanna and Jackson, 2001, Chapman et al., 2012, Jasin and Rothstein, 2013). NHEJ is an error-prone repair mechanism that is active throughout the entire cell cycle. In contrast, HRR is an error-free mechanism that deals with DSBs only in the late S and G2 phase when a homologous DNA sequence is available (Goldstein and Kastan, 2015). Following the initial detection of DSBs, the HRR pathway is considered to be divided into six steps as follows: (i) overhanging 3' ssDNA formation, (ii) recruitment of the RPA complex on resected chromatin, (iii) replacement of RPA by RAD51 nucleofilament, (iv) homology search, strand invasion, generation of D-loop and Holliday junctions, (v) branch migration, and finally (vi) resolution of the Holliday junction (Goldstein and Kastan, 2015). Among other steps, the stabilisation of the nucleoprotein filament formed by RAD51-ssDNA is essential for the subsequent HRR stages (Prakash et al., 2015).

The initial interaction of RAD51 monomers with BRCA2 has been reported to be significant for RAD51-ssDNA nucleoprotein filament formation (Esashi et al., 2007, Davies and Pellegrini, 2007, Schlacher et al., 2011). Subsequently, polymerised RAD51 interacts with the C-terminal region of BRCA2, which further assists stabilisation of RAD51 nucleofilament formation (Esashi et al., 2007, Davies and Pellegrini, 2007, Schlacher et al., 2011). CDK-mediated phosphorylation of BRCA2 at Ser3291 blocks the interaction between RAD51 polymers and BRCA2, which disrupts RAD51-ssDNA formation (Esashi et al., 2005). Upon DNA damage, phosphorylation of BRCA2 at Ser3291 diminishes in order to promote stabilisation of RAD51 nucleoprotein formation, consequently facilitating fork protection and HRR (Esashi et al., 2005, Schlacher et al., 2011). Furthermore, RAD51 can be phosphorylated at Ser14 by the PLK1 kinase and subsequently by CK2 at Thr13 (Yata et al., 2012). These phosphorylation events occur within the BRCA2 complex and in a CDK-dependent manner (Yata et al., 2014), and hence are of significance for RAD51 recruitment onto ssDNA, followed by DSB repair through accurate HRR (Yata et al., 2012).

## **4.2 Research aims**

We revealed that hMOB2 is required to prevent spontaneous DSB accumulation under normal circumstances and supports cell cycle checkpoint activation upon high levels of exogenous DNA damage. However, the absence of any mechanistic link that explains how hMOB2 contributes to the DDR signalling pathway and DSB sensing/repair inspired us to investigate:

- (i) whether hMOB2 has novel binding partners that are related to DDR signalling,
- (ii) whether hMOB2 promotes ATM-mediated DDR signalling,
- (iii) whether hMOB2 supports DSB repair pathways.

### 4.3 Results

**hMOB2 interacts with the MRN component RAD50.** To explore how hMOB2 can function as a DDR protein, a yeast-two-hybrid (Y2H) assay was performed with full-length hMOB2 as a bait. Our goal was to define novel direct (binary) binding partners of hMOB2, which contribute to DDR signalling (see Table S2.2 in the Supplementary section, page 128). Significantly, two well-known DDR proteins, UBR5 and RAD50 were discovered as top candidates by this screen (Figure 4.1A). The most frequently isolated prey was the HECT domain E3 ligase UBR5 (also termed EDD1) (Figure 4.1A, and see Table S2.2 in the Supplementary section, page 128). However, all hits for UBR5 were not in frame with the GAL4 activation domain (see Table S2.2 in the Supplementary section, page 128), and the interaction between hMOB2 and UBR5 was not detectable by co-immunoprecipitation experiments upon overexpression in mammalian cells (see Figure S4.1 in the Supplementary section, page 187). This implies that the detected Y2H interaction between hMOB2 and UBR5 is very likely a Y2H artefact. Therefore, we aimed to understand the interaction between hMOB2 and RAD50, which was repeatedly detected by Y2H (Figure 4.1A).

As a key component of the MRN complex, RAD50 is required for DNA damage detection to triggering DDR signalling, subsequently activating cell cycle checkpoints and DNA repair pathways (Rupnik et al., 2010, Stracker and Petrini, 2011, Williams et al., 2010). Hence, the identification of novel MRN regulators is essential for our understanding of the DDR in human cell biology (Jackson and Bartek, 2009). Furthermore, a mechanistic link between hMOB2 and MRN function could explain why hMOB2-knockdown cells show impaired cell cycle checkpoints, accumulation of unrepaired spontaneous DSBs, and a cell cycle progression defect.

We first aimed to ratify the interaction of hMOB2 with RAD50 in mammalian cells. In contrast to our results concerning UBR5 (see Figure S4.1 in the Supplementary section, page 187), co-immunoprecipitation experiments using mammalian cell lysates readily detected the formation of hMOB2/RAD50 complexes on endogenous and exogenous levels (Figure 4.1B-C). Moreover, Y2H mapping displayed the region surrounding the zinc

hook domain and a C-terminal stretch encompassing part of the ABC domain of RAD50 as binary binding sites for hMOB2 (Figure 4.1D). Consequently, hMOB2 interacts with the MRN component RAD50, which in turn may promote MRN functionality in context of the DDR.

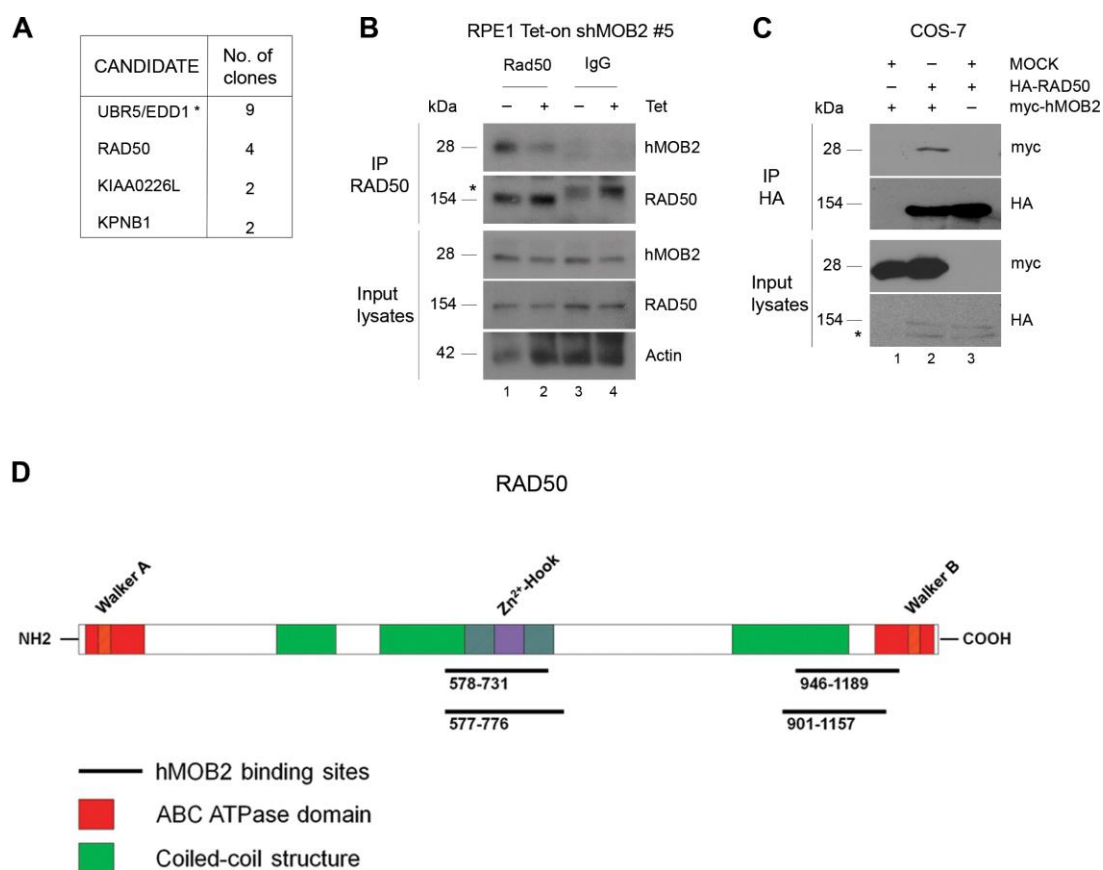


**Figure 4.1**

**hMOB2 interacts with the MRN component RAD50.**

(A) List of novel hMOB2 binding partners identified at least twice by yeast two-hybrid (Y2H) screens. The number of independent hits is indicated. The Y2H screen was performed by Dual systems Biotech AG (Zurich, Switzerland). (B) RPE1 Tet-on shMOB2 cells incubated with (+Tet, 2  $\mu$ g/ml) or without (–Tet) tetracycline for 96 h were subjected to immunoprecipitation (IP) using anti-RAD50 (RAD50) or control (IgG) antibodies before inputs and immunoprecipitates were analysed by immunoblotting. Asterisk (\*) marks an unspecific band in the RAD50 blot. Blots represent three individual experiments. (C) COS-7 lysates transiently expressing indicated combinations of HA-tagged RAD50 and myc-tagged hMOB2 were subjected to immunoprecipitation using an anti-HA 12CA5 antibody, before immunoblotting of immuno-complexes and input lysates. Blots represent three individual experiments. (D) Primary structure of RAD50 indicating direct hMOB2 binding sites defined by Y2H mapping. Known functional domains of RAD50 are

highlighted. The experiment was performed by Dr Valenti Gomez with my intellectual contribution.

**The interaction of hMOB2 with RAD50 may regulate MRN-ATM recruitment to damaged chromatin.** Considering the link between hMOB2 and MRN through the hMOB2/RAD50 interaction, we wondered whether hMOB2 contributes to DNA damage-induced chromatin binding of MRN and subsequent ATM recruitment, which is crucial for efficient MRN-mediated ATM signalling (Rupnik et al., 2010, Stracker and Petrini, 2011, Williams et al., 2010). It is worth to note that MRN protein levels are cell cycle regulated (Stumpf et al., 2013). Therefore, in order to avoid indirect cell cycle effects in our analysis of MRN functionality, we analysed cells 24 h after siRNA transfection, since at this time point neither MRN nor p53 levels were affected despite efficient hMOB2 depletion (see Figure S4.2 in the Supplementary section, page 188). To induce exogenous DNA damage, cells were treated with doxorubicin, before cells were subjected to chromatin-cytosol fractionations, followed by immunoblotting of MRN to detect DNA damage-induced enrichment at chromatin. Notably, this analysis revealed that hMOB2 is required for normal MRN recruitment to DNA damaged chromatin, since DNA damage-induced enrichment of MRN at chromatin was severely compromised upon hMOB2 knockdown (Figure 4.2). In addition, enrichment of activated ATM at DNA damaged chromatin was also dependent on normal hMOB2 levels (Figure 4.2, top panel). Collectively, these experiments (Figures 4.1 and 4.2) unveiled hMOB2 as an MRN regulator, indicating that the DNA damage binding/sensing function of MRN is dependent on normal hMOB2 levels. Therefore, this explains how in hMOB2-depleted cells compromised DNA damage sensing can result in the accumulation of unrepaired DSBs, triggering a DNA damage-p53-p21 cascade to halt cell cycle progression.

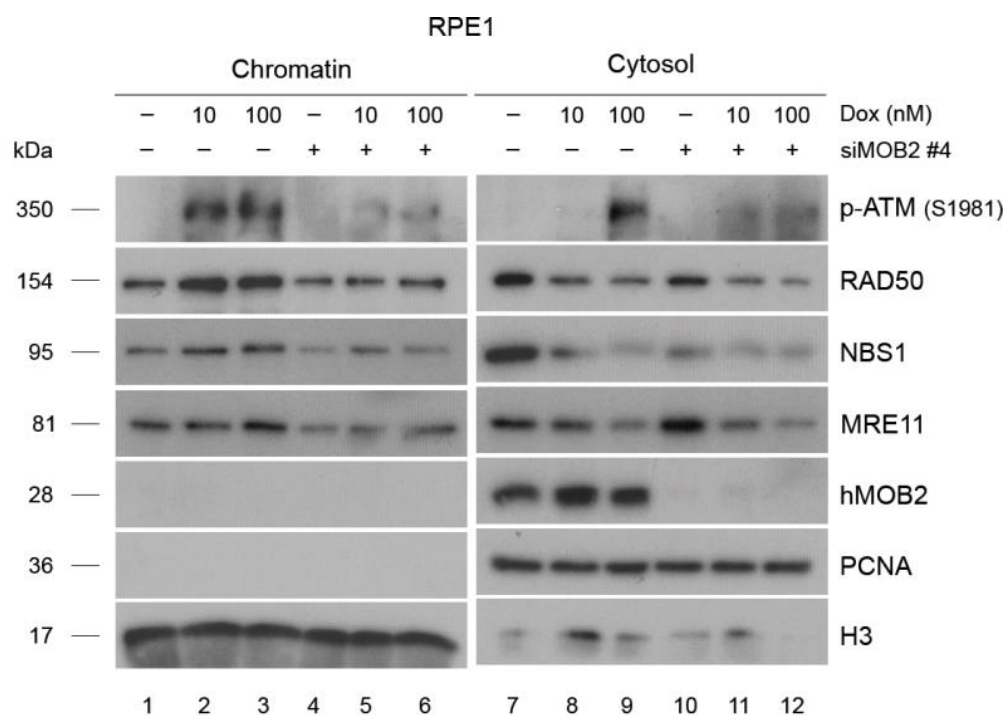


**Figure 4.2**

**hMOB2 interacting with the MRN component RAD50 regulates MRN-ATM recruitment to damaged chromatin.**

RPE1 cells transiently transfected for 24 h with indicated siRNAs (-, siCTL;+, siMOB2) were treated with indicated doxorubicin doses, before separation into chromatin and cytosolic fractions, and subsequent immunoblotting with indicated antibodies. The experiment was performed by Dr Valenti Gomez with my intellectual contribution. Blots represent three individual experiments.

**hMOB2 is required for normal ATM-mediated DDR signalling in response to exogenous DNA damage.**

Having established an essential role for hMOB2 in MRN-ATM recruitment to damaged chromatin sites prompted us to investigate the effect of hMOB2 depletion on the cellular response of ATM signalling upon exogenously induced DNA damage in untransformed cells. Following DNA damage induction, the MRN complex binds avidly to damaged chromatin to activate a finely co-ordinated panel of activities (Polo and Jackson, 2011), which involves MRN-mediated recruitment of the ATM kinase to DSBs (Rupnik et al., 2010, Stracker and Petrini, 2011, Williams et al., 2010). Once activated, the central DDR protein kinase ATM phosphorylates many substrates involved in DDR signalling, such as p53, CHK2, and KAP1, as well as the MRN component NBS1 to



create a positive feedback loop maintaining ATM activity (Shiloh and Ziv, 2013). In addition, ATM further phosphorylates SMC1, which has been reported to be required for cell survival in response to DNA damage (Kim et al., 2002, Kitagawa et al., 2004, Yazdi et al., 2002). Thus, to examine these multiple branches of DDR signalling, IR-induced phosphorylation of ATM and a panel of ATM substrates was compared between controls and hMOB2-depleted cells 24 h post-siRNA transfections (Figure 4.3). Interestingly, this analysis showed that the IR-induced phosphorylation levels of ATM, SMC1 and NBS1 were significantly compromised in hMOB2-knockdown cells, whereas p53, CHK2, and KAP1 phosphorylation was unaffected when compared to controls (Figure 4.3). This indicates that hMOB2 is dispensable for some ATM activities while being required for optimal ATM activation and ATM-mediated phosphorylation of NBS1 and SMC1. Additionally, we expanded our analysis by testing cells treated with the ICL-inducing agents mitomycin C or cisplatin as well as the topoisomerase II inhibitor doxorubicin (see Figures S4.3, S4.4, and S4.5 in the Supplementary section, pages 189-191). Taken together, these findings demonstrated that selective branches of ATM-mediated DDR signalling were severely impaired in hMOB2-depleted cells, which could very likely be the reason of the observed defective cell cycle checkpoint activation upon hMOB2 knockdown.

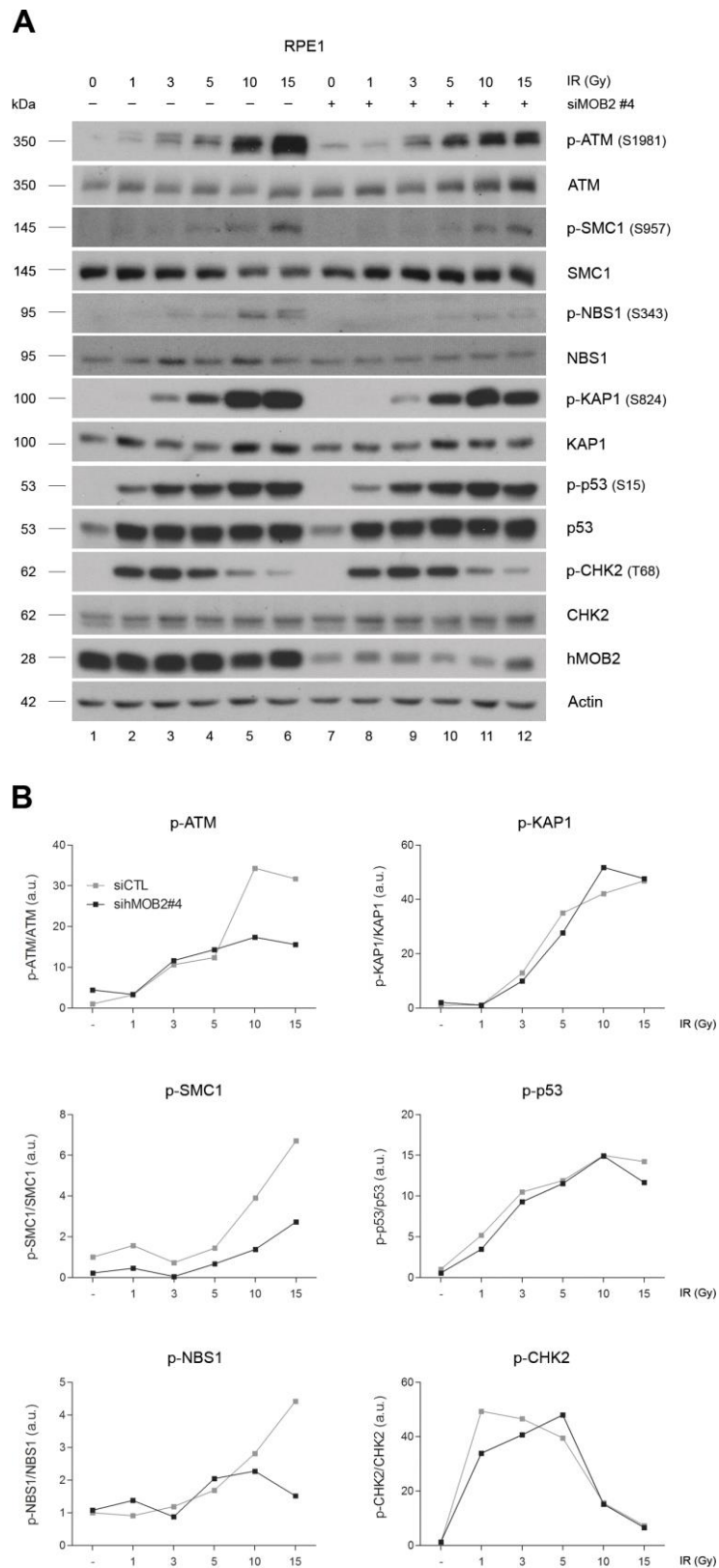


**Figure 4.3**

**hMOB2 supports IR-induced ATM-NBS1-SMC1 signalling.**

(A) Phosphorylation of ATM and ATM substrates analysed by immunoblotting with

indicated antibodies of RPE1 cell lysates from cells transiently transfected for 24 h with indicated siRNAs (–, siCTL; +, siMOB2). Cells were treated with indicated ionising radiation (IR) doses, before processing for immunoblotting. Blots represent three individual experiments. (B) Graphs showing the kinetics of ATM activation as judged by Ser1981 auto-phosphorylation and substrate phosphorylations by ATM obtained by densitometry quantification of Western blots shown in A (phosphorylated/total proteins).

### **hMOB2 is required for the efficient DSB repair by the HRR pathway.**

Next, we hypothesised that inefficient MRN functionality in hMOB2-depleted cells might impair the integrity of DSB repair pathways, which could be the mechanistic reason of the spontaneous DSB accumulation upon hMOB2 knockdown. To investigate the involvement of hMOB2 in DSB repair, the GFP reporter assays DR-GFP and EJ5-GFP were utilised to assess the efficiency of the HRR and NHEJ pathways, respectively (Gunn and Stark, 2012).

On the one hand, the U2OS DR-GFP cells are stably modified to carry two *GFP* gene repeats; the upstream one is flanked by an I-Sce1 (a rare cutting endonuclease) recognition site, and the downstream one represents a truncated non-functional form of the gene. Exogenous expression of the I-Sce1 endonuclease induces a site-specific (experimental) DSB within the upstream GFP, which is restored by the HRR pathway employing the downstream GFP sequence as a template (Figure 4.4A). The resulting GFP signal scored by flow cytometry is considered to be an appropriate readout for the efficiency of HRR (Figure 4.4D) (Pierce et al., 1999). On the other hand, U2OS EJ5-GFP cells are stably modified with an inactive GFP-expressing sequence that is separated from its promoter by a *puromycin* gene flanked by two I-Sce1 recognition sequence. Exogenous expression of the I-Sce1 enzyme produces two DSBs followed by the excision of the *puromycin* gene by NHEJ. The NHEJ pathway subsequently ligates the promoter with the GFP-expressing gene (Figure 4.5A), producing a GFP signal that is scored to assess the efficiency of NHEJ (Figure 4.5D) (Gunn and Stark, 2012).

U2OS DR-GFP and EJ5-GFP cells with or without transient hMOB2 knockdown (Figures 4.4B and 4.5B) were transfected with empty vector or

pCBASce1 plasmid that expresses HA-tagged I-Sce1 in order to introduce experimental DSBs (Figures 4.4C and 4.5C). The cells were processed for flow cytometry to monitor GFP<sup>+</sup> cells 72 h after transfection. Strikingly, this experiment showed that hMOB2 depletion attenuated HRR by nearly 50% (Figure 4.4E), suggesting that hMOB2 knockdown impaired the efficiency of HRR. We monitored the integrity of the assay by employing the ATM inhibitor KU-55933 (Figure 4.4E), which has been previously reported to inhibit HRR in this DR-GFP system (Gunn et al., 2011).

Equally important, we found that hMOB2-depleted cells displayed a significantly increased fraction of GFP<sup>+</sup> signals (Figure 4.5E), suggesting that upon hMOB2 depletion NHEJ activity is elevated. Importantly, this assay specifically monitored NHEJ activity, since the GFP signals were severely reduced upon DNA-PK inhibition as already reported in Gunn et al. (2011) (Figure 4.5E). Thus, our findings highlight that hMOB2 is not essential for NHEJ. As an additional control, we confirmed by immunoblotting that the reduced HRR and increased NHEJ activities as observed in hMOB2-depleted cells were not a consequence by unequal expression of the HA-tagged I-Sce1 enzyme (Figures 4.4C and 4.5C, respectively).

Collectively, we show so far in this chapter that hMOB2 is required for (i) the recruitment of the MRN complex and activated ATM to chromatin with DNA damage, (ii) selective aspects of ATM-mediated DDR signalling, and (iii) efficient HRR-mediated DNA repair in response to DNA damage.

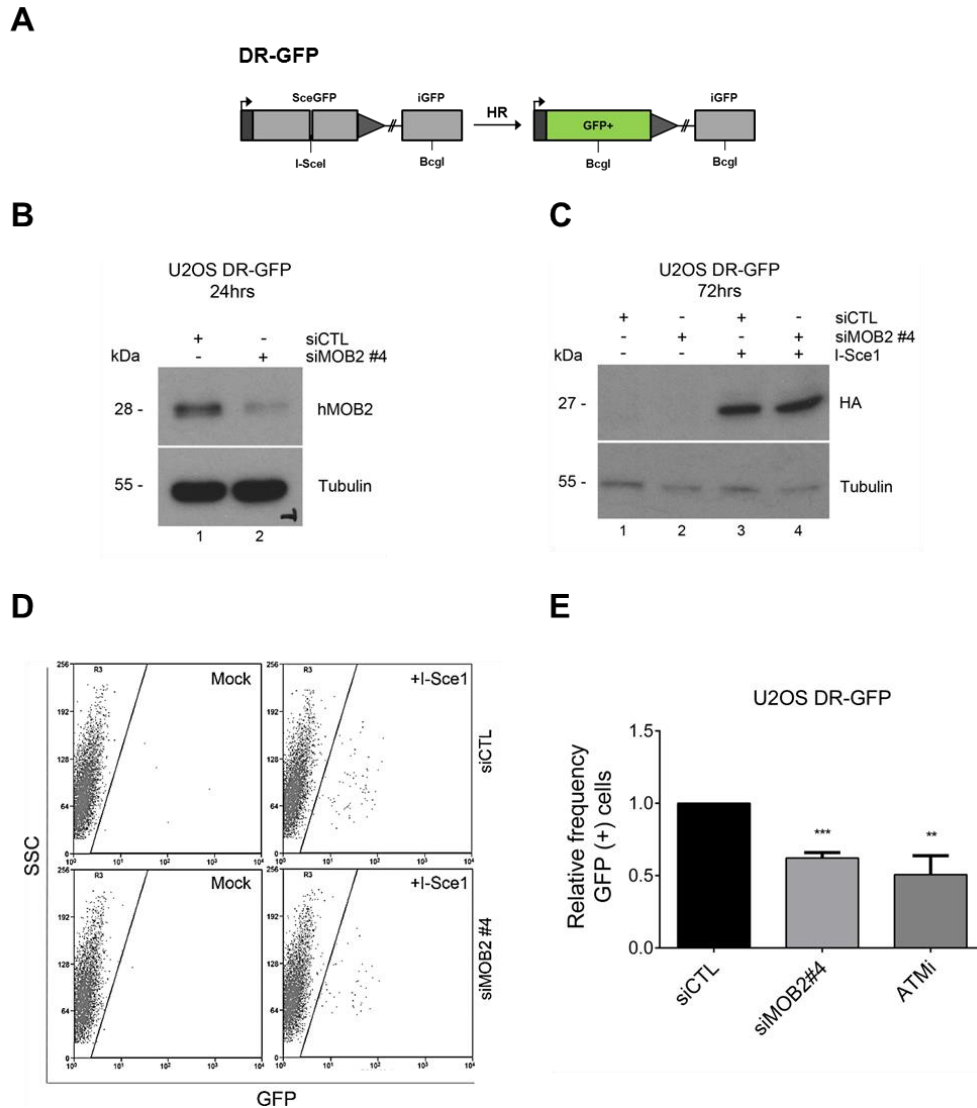


**Figure 4.4**

**hMOB2 promotes the DSB repair pathway HRR.**

(A) A schematic diagram of the HRR (DR-GFP) reporter assay. Adapted from Gunn and Stark (2012). iGFP: internal GFP (B) Immunoblotting with indicated antibodies of U2OS DR-GFP cell lysates from cells transiently transfected for 24 h with indicated siRNAs. (C) The cells prepared as in B were transiently transfected for 72 h with or without pCBASce1 (I-Sce1) and harvested for immunoblotting with indicated antibodies. (D) Representative FACS plots of the cells with GFP+ signals following 72 h of I-Sce1 transfection as outlined in C. (E) The cells prepared as in C were analysed after 72 h following I-Sce1 transfection. Cells which were untransfected or transfected with pEGFP (GFP) served as experimental negative and positive controls, respectively (data not shown). Cells transfected with pCBASce1 (I-Sce1) and treated with 10  $\mu$ M ATM inhibitor (KU-55933) for 60 hours were used as an assay control. The bar graph displays the relative frequency of GFP+ cells normalised to control cells, calculated according to raw GFP% (n=4, *p*-values are: siMOB2=2.9E-04, ATMi=9.7E-03 compared to siRNA control). Results

are presented as mean of replicates and error bars as mean  $\pm$  standard error of mean (SEM), statistical significance was calculated using the one-tailed unpaired Student's *t*-test.

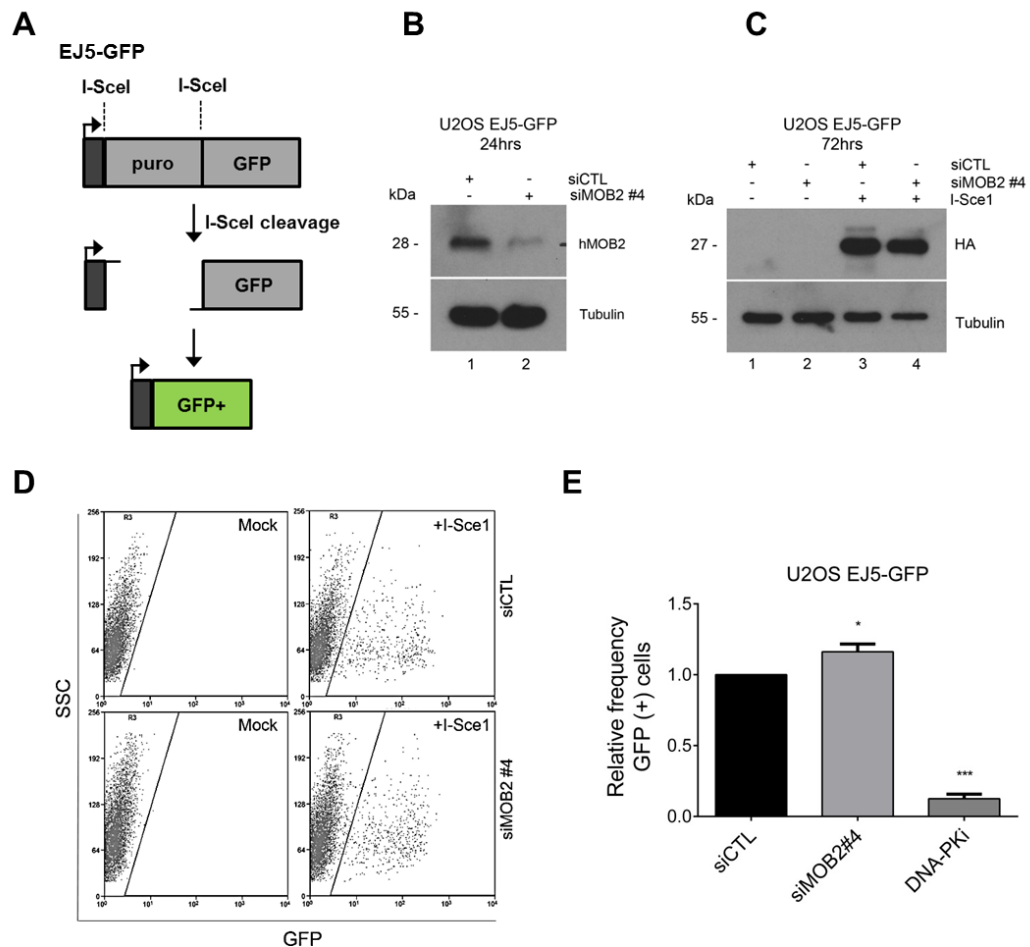


**Figure 4.5**

### **hMOB2 is dispensable for the DSB repair pathway NHEJ.**

(A) A schematic diagram of the NHEJ (EJ5-GFP) reporter assay. Modified from Gunn and Stark (2012). puro: puromycin (B) Immunoblotting with indicated antibodies of U2OS EJ5-GFP cell lysates from cells transiently transfected for 24 h with indicated siRNAs. (C) The cells prepared as in B were transiently transfected for 72 h with or without pCBASce1 (I-Sce1) and harvested for immunoblotting with indicated antibodies. (D) Representative FACS plots of the cells with GFP+ signals following 72 h of I-Sce1 transfection as outlined in C. (E) The cells prepared as in C were analysed after 72 h following I-Sce1 transfection. Cells which were untransfected or transfected with pEGFP (GFP) served as experimental negative and positive controls, respectively (data not shown). Cells transfected with pCBASce1 (I-Sce1) and treated with 10  $\mu$ M DNA-PK inhibitor (NU-7441) for 60 hours were used as an assay control. The bar graph displays the relative frequency of GFP+ cells normalised to control cells, calculated according to raw GFP% ( $n=3$ ,  $p$ -values are: siMOB2=0.048, DNA-PKi=6.8E-04 compared to siRNA control). Results

are presented as mean of replicates and error bars as mean  $\pm$  standard error of mean (SEM), statistical significance was calculated using the one-tailed unpaired Student's *t*-test.

**hMOB2-depleted cells display increased RPA foci formation.** The activities of MRN and ATM are essential in the early steps of HRR, where both facilitate the processing of DSB end resection to generate 3' ssDNA overhangs, which are significant for the initiation of HRR (Stracker and Petrini, 2011). We found that hMOB2 promotes (i) activated MRN and ATM recruitment to chromatin with DNA damage (Figure 4.2) and (ii) ATM signalling in response to DNA damage (Figure 4.3), hence, we also investigated whether the inefficient DSB repair by HRR in hMOB2-depleted cells was a consequence of defective ssDNA formation. As illustrated in Figure 4.6A, after the recognition step of a DSB by MRN, MRE11 together with the CtIP nuclease produces 3' ssDNA overhangs, which are then coated by the trimeric RPA complex (consisting of RPA-70, RPA-34, and RPA-14) (Buisson et al., 2010, Deans and West, 2011, Moynahan and Jasin, 2010). Therefore, we examined the efficiency of DNA end resection (ssDNA formation) judged by RPA foci formation in U2OS cells with or without hMOB2 manipulation (Figure 4.6B). Cells were treated with mitomycin C for 24 h, before being processed for immunofluorescence staining. We analysed only cells in S/G2 marked by the cell-cycle marker CENPF (centromere protein E, aka mitotin) (Figure 4.6C). As shown in Figure 4.6D, the immunodetection of RPA revealed a two-fold increase in the number of CENPF-positive cells with more than five RPA foci when hMOB2 was silenced. This finding suggests that ssDNA formation (the binding platform for RPA) is not decreased, but rather elevated, upon hMOB2 reduction. In line with this, we also found that RPA70 protein levels significantly increased upon hMOB2 knockdown (Figure 4.6A), suggesting a need for amplified RPA levels presumably due to persistent ssDNA formation upon hMOB2 depletion. Collectively, our data shown in Figure 4.6 propose that hMOB2 knockdown does not affect DSB end resection (ssDNA formation), indicating that the initiation of HRR is most likely intact in hMOB2-deficient cells.

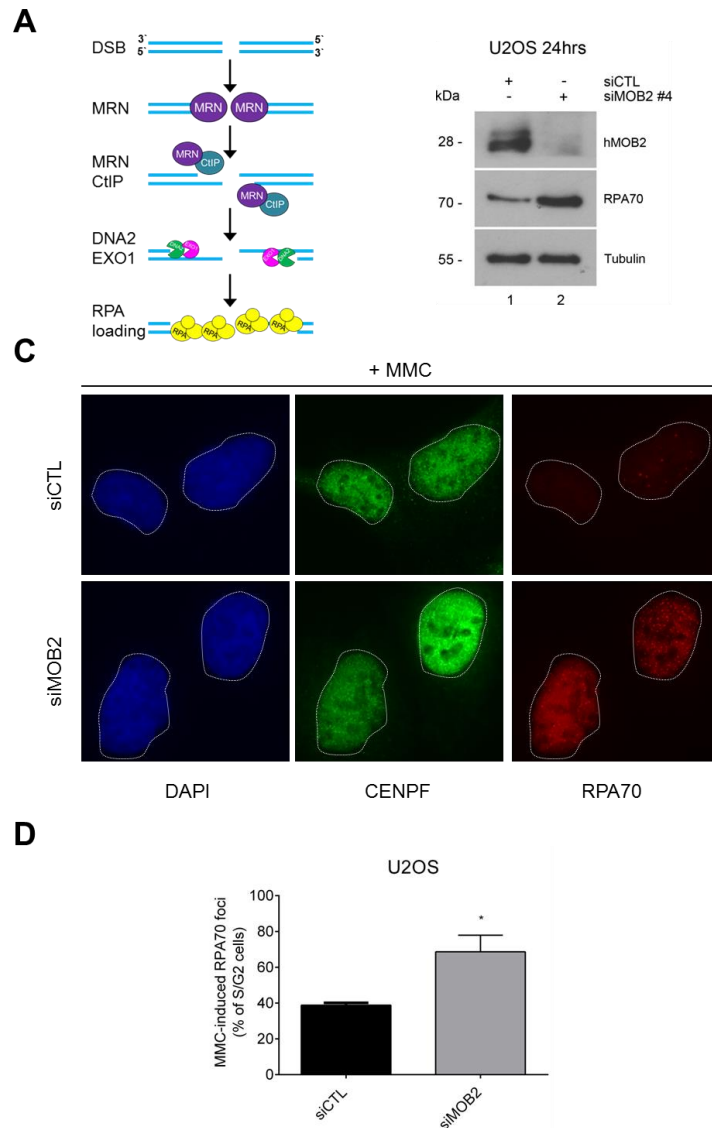


**Figure 4.6**

**hMOB2-deficient cells have increased RPA formation.**

(A) A schematic illustration of DNA end resection followed by RPA loading. Modified from Ferretti et al. (2013). (B) Immunoblotting of U2OS cells transiently transfected with indicated siRNAs (siCTL, siMOB2) for 24 h before analysis with indicated antibodies. (C) Representative images of immunodetection of RPA70 foci (red) and CENPF signals (green) in U2OS cells exposed to mitomycin C. DNA is stained blue. 24 h before mitomycin C treatment, U2OS cells were transiently transfected with indicated siRNAs (siCTL, siMOB2). The next day, cells were treated with 0.3  $\mu$ M mitomycin C for 24 h before processing for immunofluorescence. (D) Histogram showing percentages of mitomycin C-treated CENPF-positive U2OS cells with more than five RPA70 foci. >150 cells were scored per experiment ( $n=3$ ,  $p=0.041$ ). MMC: Mitomycin C. Results are presented as mean of replicates and error bars as mean  $\pm$  standard error of mean (SEM), statistical significance was calculated using the one-tailed unpaired Student's *t*-test.



**hMOB2 is required for RAD51 loading onto ssDNA.** Having observed that hMOB2-deficient cells display increased RPA foci formation (Figure 4.6), we were prompted to investigate the recruitment of RAD51 onto the resected chromatin to form ssDNA-RAD51 nucleoprotein filaments in hMOB2-knockdown cells. The RPA complex displays high binding activity for ssDNA tails, which inhibits RAD51 loading and thereby the HRR progression (Moynahan and Jasin, 2010). Hence, as illustrated in Figure 4.7A, the replacement of RPA by RAD51 requires a set of modifications of RAD51 by specific mediators (e.g. Yata et al. (2012) and Yata et al. (2014)). Here, we examined the efficiency of RAD51 focus formation in U2OS cells with or without hMOB2 manipulation (Figure 4.7B). As performed for the immunofluorescence of RPA, cells treated with mitomycin C for 24 h and only S/G2 cells (CENPF+) were scored (Figure 4.7C). As shown in Figure 4.7D, CENPF+ cells with hMOB2 knockdown showed a pronounced ablation in mitomycin C-induced RAD51 nucleofilament formation, which was not a result of diminished RAD51 protein levels (Figure 4.7B). Taken together, the data shown in Figures 4.6 and 4.7 collectively propose that hMOB2 deficiency results in impaired replacement of RPA by RAD51 polymers to form nucleoprotein filaments. Noteworthy, this notion is fully supported by our previous observation of compromised HRR efficiency upon hMOB2 knockdown (Figure 4.4).

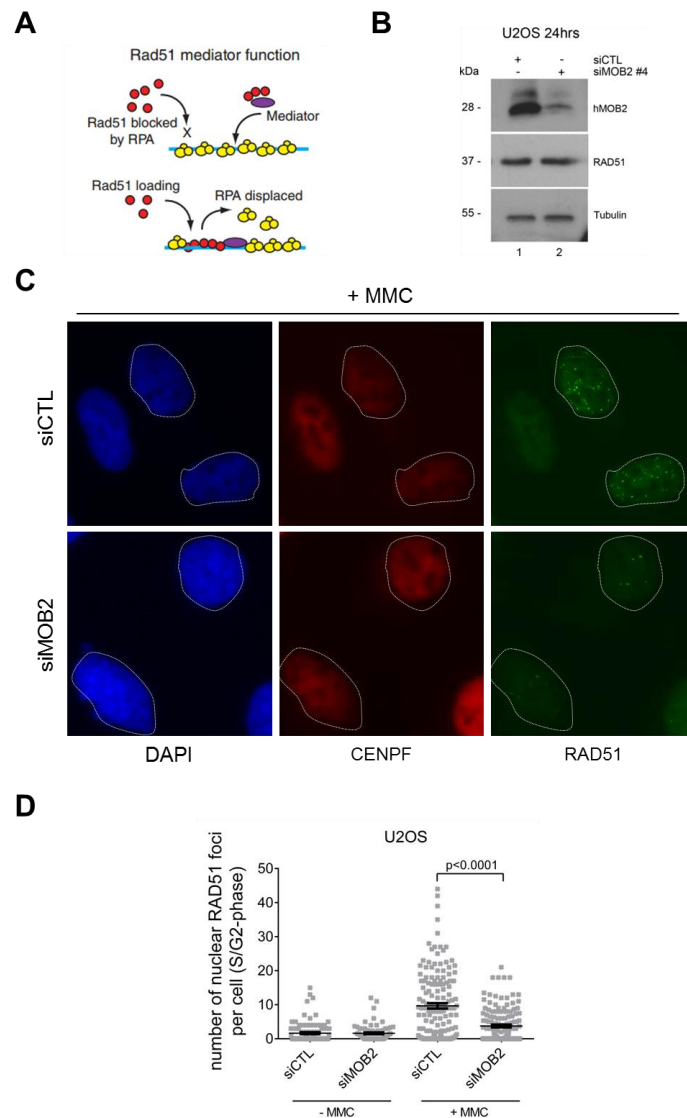


**Figure 4.7**

**hMOB2 promotes the damage-induced RAD51 focus formation.**

(A) A schematic illustration showing the replacement of RPA by RAD51 polymers to form ssDNA-RAD51 nucleoprotein filaments. Adapted from Holloman (2011). (B) Immunoblotting of U2OS cells transiently transfected with indicated siRNAs (siCTL, siMOB2) for 24 h before analysis with indicated antibodies. (C) Representative images of immunodetection of RAD51 foci (green) and CENPF signals (red) in U2OS cells exposed to mitomycin C. DNA is stained blue. 24 h before mitomycin C treatment, U2OS cells were transiently transfected with indicated siRNAs (siCTL, siMOB2). The next day, cells were treated with 0.3  $\mu$ M mitomycin C for 24 h before processing for immunofluorescence. (D) The dot blot graph presents quantification of nuclear RAD51 foci number in CENPF-positive U2OS cells treated with or without mitomycin C. >150 cells were scored per experiment ( $n=3$ ,  $p<0.0001$ ). MMC: Mitomycin C. Results are presented as mean of replicates and error bars as mean  $\pm$  standard error of mean (SEM), statistical significance was calculated using the Mann–Whitney test.

**hMOB2 supports PLK1-mediated RAD51 phosphorylation at Ser14.** The data presented in Figures 4.4 and 4.7 cumulatively suggest that hMOB2 silencing impairs DSB repair by HRR. Considering further that hMOB2-depleted cells displayed increased RPA foci formation combined with decreased RAD51 foci formation (Figures 4.6 and 4.7), we were tempted to speculate that the replacement of RPA by RAD51 was impaired upon hMOB2 depletion.

Considering that RAD51 phosphorylations by the PLK1 and CK2 kinases are essential for efficient RAD51 loading mediated by BRCA2 (Yata et al., 2014, Yata et al., 2012), we hypothesised that defective RAD51 loading upon hMOB2 knockdown is a consequence of altered phosphorylations of (i) BRCA2 at Ser3291 (Esashi et al., 2005, Yata et al., 2014), (ii) RAD51 at Ser14 (Yata et al., 2014, Yata et al., 2012), and/or (iii) RPA34 at Ser4/Ser8 (Liaw et al., 2011). Any alterations of these phosphorylation events could help to explain why RAD51 loading and HRR is diminished in hMOB2-depleted cells. Interestingly, the level of RAD51 Ser14 phosphorylation was significantly diminished in hMOB2-depleted cells after 24 h post-siRNA transfection without any effect on total RAD51 protein levels in the absence of any DNA damage inducing agent (Figure 4.8B-C).

RAD51 is phosphorylated at Ser14 in response to DNA damage induction (Yata et al., 2012), therefore, we tested next whether exogenously induced DNA damage successfully triggered Ser14 phosphorylation of RAD51 in hMOB2-depleted cells. We designed a time-course experiment using U2OS cells with or without hMOB2 depletion. 24 h post-siRNA transfection, cells were harvested (i) immediately, (ii) following treatment with mitomycin C for 12 h, (iii) after 24 h treatment with mitomycin C, or (iv) after 24 h mitomycin C treatment followed by 6 h incubation in drug-free medium. Strikingly, this revealed that Ser14 phosphorylation of RAD51 was severely compromised in hMOB2-deficient cells compared to controls (Figure 4.8D), highlighting that even in the presence of exogenous DNA damage Ser14 phosphorylation of RAD51 is impaired in hMOB2-knockdown cells. In contrast, the phosphorylations of BRCA2 at Ser3291 and RPA32/34 at Ser4/Ser8 were not altered upon hMOB2 depletion (Figure 4.8D).

To sum up, our results presented in this chapter suggest a novel function of hMOB2 in supporting the phosphorylation of RAD51 at Ser14, which is required for efficient RAD51 nucleofilament formation, which in turn is essential for efficient repair of DSBs by HRR.

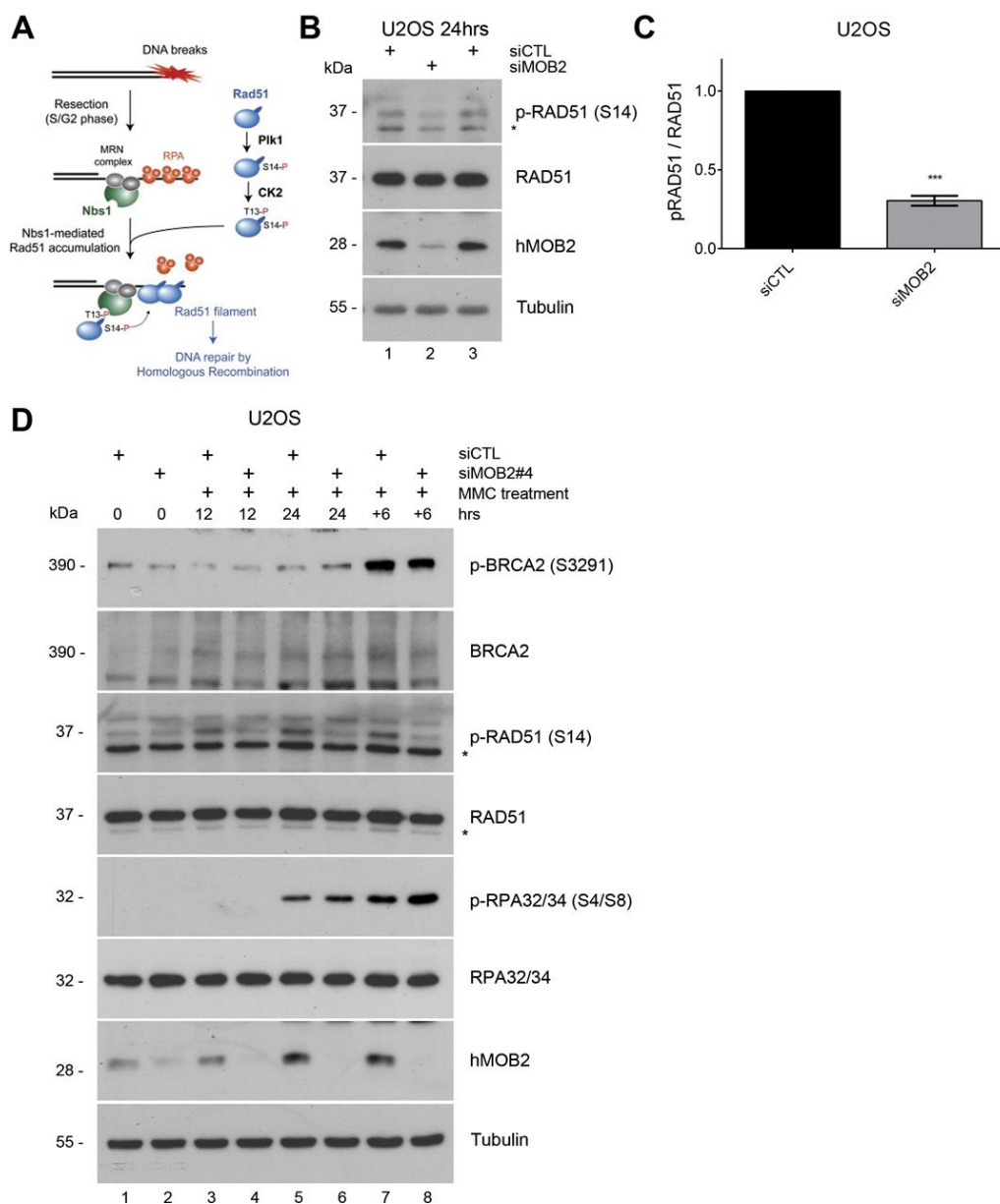


**Figure 4.8**

**hMOB2 is needed for efficient phosphorylation of RAD51.**

(A) A schematic diagram of the RAD51 nucleofilament stabilisation through the PLK1- and CK2-mediated phosphorylations. Adapted from Yata et al. (2012). (B) Immunoblotting with indicated antibodies of U2OS cell lysates from cells transiently transfected for 24 h with indicated siRNAs (siCTL, siMOB2). Blots represent three individual experiments. (C) Graphs showing RAD51 activation as judged by Ser14

phosphorylation obtained by densitometry quantification of Western blots shown in B (phosphorylated/total protein, siMOB2 was normalized to siCTL that was set to 1).  $n=3$ ,  $p$ -value= $9.9E-04$ . Results are presented as mean of replicates and error bars as mean  $\pm$  standard error of mean (SEM), statistical significance was calculated using the one-tailed unpaired Student's *t*-test. (D) Phosphorylation of BRCA2, RAD51, and RPA32/34 was analysed by immunoblotting with indicated antibodies of U2OS cell lysates from cells transiently transfected for 24 h with indicated siRNAs (siCTL, siMOB2). Following 24 h of transfection, cells were either harvested (0 h) or treated with 0.3  $\mu$ M mitomycin C for 12 h and 24 h and collected or further incubated in drug-free medium for 6 h and harvested before processing for immunoblotting. Asterisks (\*) mark an unspecific band in the RAD51 blots. Blots represent three individual experiments.

#### 4.4 Discussion

Here we show that hMOB2 can interact with the MRN component RAD50, and regulate MRN-mediated ATM signalling in the DDR. Even more importantly, we discovered that loss of hMOB2 compromises Ser14 phosphorylation of RAD51, which in turn impairs RAD51 loading onto ssDNA, and consequently diminishes repair of DSBs by HRR.

Like MRN deficient cells (Rupnik et al., 2010, Stracker and Petrini, 2011, Williams et al., 2010), hMOB2-depleted cells display impaired cell proliferation, defective cell cycle checkpoints, and suboptimal ATM activation as shown in chapter-3 on pages 135 and 143, and chapter-4 on page 169, respectively. Therefore, our data suggest that hMOB2 supports MRN functionality, which is crucial for DNA damage detection, DDR signalling, and cell cycle checkpoint activation, consequently promoting efficient DNA repair. Our results provide the first mechanistic insight into how hMOB2 can function in the DDR by suggesting that hMOB2 contributes to the DDR on distinct molecular levels. On one hand, hMOB2 contributes to MRN-mediated recruitment of activated ATM to damaged chromatin (Figure 4.2). On the other hand, hMOB2 seems to support MRN as an adaptor for ATM substrates such as SMC1, while hMOB2 is dispensable for IR-induced ATM-mediated phosphorylation of p53 and CHK2 (Figure 4.3). These findings suggest that hMOB2 is required to promote MRN-mediated signalling events, while hMOB2 is expendable for MRN-independent ATM signalling. This interpretation is in full agreement with published reports showing that SMC1 phosphorylation by ATM is MRN-dependent (Kim et al., 2002, Kitagawa et al., 2004, Yazdi et al., 2002) and defective ATM activation is quantitative, not absolute, in MRN mutant cells (Kitagawa et al., 2004, Waltes et al., 2009, Uziel et al., 2003, Theunissen et al., 2003), while MRN-mediated ATM activation is dispensable for CHK2 and p53 phosphorylation (Stracker et al., 2007, Lim et al., 2000).

Considering that hMOB2 deficiency results in spontaneous accumulation of DSBs, we also analysed the contribution of hMOB2 to DSB repair pathways. HRR and NHEJ are the two main repair pathways that deal with DSBs (Khanna and Jackson, 2001, Goodarzi and Jeggo, 2013, Jasin

and Rothstein, 2013, Chapman et al., 2012). Using GFP recombination reporter assays we discovered that loss of hMOB2 disrupts DSB repair by HRR (Figure 4.4), which can help to explain why DSBs accumulate spontaneously under normal conditions (Figure 3.10, in chapter-3 on page 150). Taken together, our data indicate that hMOB2 is an essential supporter of HRR, which led us to study the mechanism(s) through which hMOB2 can contribute to HRR.

The initial process of HRR is the formation of ssDNA overhangs on both sides of an DSB. The ssDNA tails are then coated by the RPA complex, which is subsequently replaced by RAD51 nucleofilaments. RAD51 nucleofilament formation is necessary for the subsequent steps of HRR including homology search and strand invasion (Buisson et al., 2010, Deans and West, 2011, Moynahan and Jasin, 2010). In this regard, the MRN component MRE11 together with the CtIP, EXO1 (exonuclease 1), and DNA2 nucleases are responsible for ssDNA formation (Sartori et al., 2007, Mimitou and Symington, 2009). Surprisingly, DNA end resection as judged by mitomycin C-induced RPA foci formation appears to be functional and persistent in hMOB2 depleted cells (Figure 4.6). This suggest that although hMOB2 deficiency limits MRN recruitment to damaged chromatin (Figure 4.2), the remaining recruitment of MRN is sufficient to initiate ssDNA formation in hMOB2-deficient cells. In this context, one needs to note that a recent study analysing the relative contribution of the MRE11, CtIP, EXO1, and DNA2 nucleases to the initial step of the HRR pathway revealed that CtIP and DNA2 are sufficient for accurate end resection to secure efficient DSB repair by HRR (Hoa et al., 2015). Collectively, our data together with other reports suggest that in spite of impaired MRN functionality upon hMOB2 knockdown the resection of DSBs is not effected, and hence the initiation steps of HRR are most likely fully functional in hMOB2-deficient cells.

Interestingly, in full support of our findings using GFP recombination reporter assays (Figure 4.4), we also discovered that hMOB2 silencing compromises mitomycin C-induced RAD51 loading to damaged chromatin (Figure 4.7). Since the efficient recruitment of RAD51 to ssDNA is required

for the continuation of HRR, we aimed to untangle how hMOB2 may support the replacement of RPA by RAD51 nucleofilaments. In this context, different mediators can regulate RAD51 loading onto RPA-coated ssDNA (Jasin and Rothstein, 2013). The interaction between BRCA2 and RAD51 supports RAD51-mediated HRR (Schlachter et al., 2011, Esashi et al., 2007, Davies and Pellegrini, 2007). Considerably, CDK-mediated phosphorylation of BRCA2 at Ser3291 is significant for RAD51 recruitment, since it negatively interferes with BRCA2/RAD51 complex formation (Esashi et al., 2005). Therefore, an increase of Ser3291 phosphorylation of BRCA2 upon hMOB2 knockdown would help us to understand why RAD51 recruitment and thereby HRR is impaired. However, we found that BRCA2 phosphorylation at Ser3291 seems unaffected in hMOB2 depleted cells (Figure 4.8D), suggesting that other mechanisms are responsible for the compromised RAD51 loading observed upon hMOB2 depletion. In this regard, it has been demonstrated by Murphy et al. (2014) that phosphorylated RPA34 promotes PALB2 recruitment to damaged chromatin, which in turn facilitates BRCA2 recruitment to RPA-coated ssDNA (Sy et al., 2009). Specifically, compromised Ser4/Ser8 hyperphosphorylation of RPA34 has been reported to impair RAD51 nucleofilament stability (Liaw et al., 2011). However, we observed that hMOB2 is very likely dispensable for the phosphorylation of RPA34 at Ser4/Ser8 sites (Figure 4.8D), thereby ruling out another possibility how hMOB2 deficiency may affect RAD51 recruitment to ssDNA.

Yata et al. (2012) demonstrated that PLK1-mediated phosphorylation of RAD51 at Ser14 is required to promote RAD51 accumulation at damaged chromatin via its phosphorylation-mediated interaction with NBS1 (Figure 4.8A) (Yata et al., 2012). Remarkably, we discovered that hMOB2 supports the phosphorylation of RAD51 at Ser14 in the absence or presence of exogenously induced DNA damage (Figure 4.8). This finding helps to explain why hMOB2-depleted cells show attenuated efficiency of HRR, since RAD51 phosphorylation at Ser14 can be essential for accurate HRR (Yata et al., 2012).

Here we report that the hMOB2 protein interacts with RAD50, a component of the MRN complex which supports cell cycle checkpoints and



ATM-mediated DDR signalling, which are crucial for the initiation and regulation of HRR (Helleday, 2010). Our study further shows that hMOB2 supports HRR by promoting RAD51 phosphorylation at Ser14, which stabilises RAD51 recruitment onto ssDNA coated by RPA (Yata et al., 2012). In line with this, our data suggest that hMOB2 deficiency impairs the replacement of RPA by RAD51 nucleoprotein filaments. Notably, these findings tempt us to speculate that hMOB2 plays a significant role in downstream of ssDNA formation in the HRR pathway. Taken together, a defective HRR upon hMOB2 depletion helps to explain why hMOB2 deficiency induces the spontaneous accumulation of DSBs, which in turn activates a p53/p21-dependent G1/S cell cycle checkpoint in untransformed proliferating human cells.

## **Acknowledgements**

I would like to Dr. Valenti Gomez for his contribution and help in this chapter. I would like to thank Miss. Angeliki Ditsiou, a Cancer MSc student whom I supervised in the laboratory (2015), for her contribution to generating Figures S4.3, S4.4, and S4.5 in the Supplementary section. I would further like to thank Dr. Jeremy Stark from Beckman Research Institute of the City of Hope (Duarte, USA) for generously providing U2OS DR-GFP and EJ5-GFP cells. I would also like to thank Dr. Fumiko Esashi from Sir William Dunn School of Pathology (Oxford, UK) for kindly providing phospho-BRCA2 (Ser3291) and phospho-RAD51 (Ser14) antibodies, and for her collaborative support of this project.

## 4.5 Supplementary information

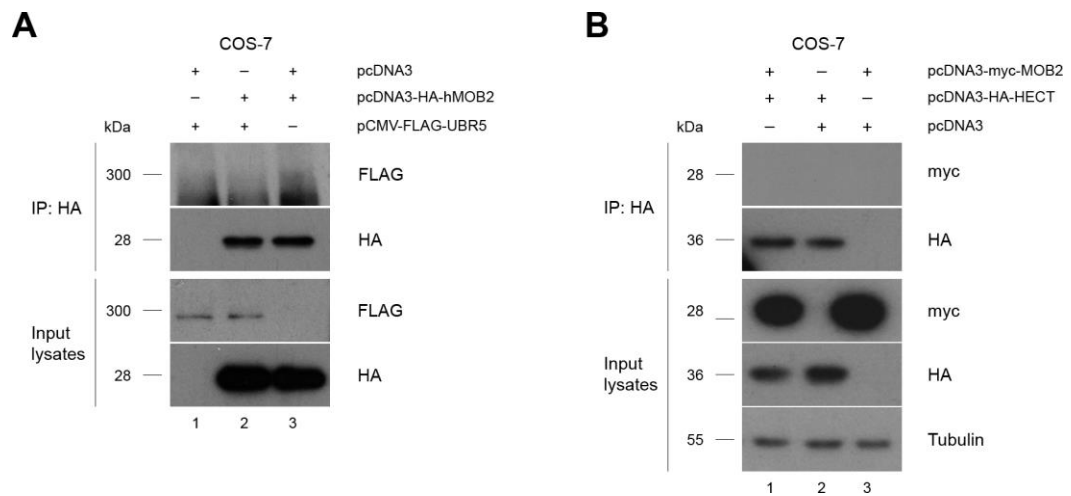


**Figure S4.1**

**hMOB2 neither interacts with full-length nor HECT domain only UBR5 (in support of Figure 4.1)**

(A) COS-7 lysates transiently expressing indicated combinations of FLAG-tagged UBR5 and HA-tagged hMOB2 were subjected to immunoprecipitation using an anti-HA 12CA5 antibody, before immunoblotting of immuno-complexes and input lysates. Blots represent more than one individual experiment. (B) COS-7 lysates transiently expressing indicated combinations of HA-tagged HECT domain of UBR5 and myc-tagged hMOB2 were subjected to immunoprecipitation using an anti-HA 12CA5 antibody, before immunoblotting of immuno-complexes and input lysates. The experiment was performed by Dr Valenti Gomez with my intellectual contribution. Blots represent more than one individual experiment.

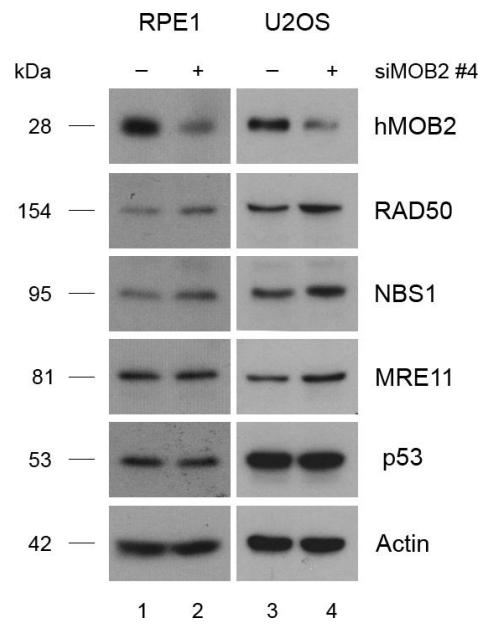


**Figure S4.2**

**Neither MRN was decreased, nor p53 levels were increased following 24 h of hMOB2 depletion (in support of Figure 4.2).**

Immunoblotting with indicated antibodies of RPE1 (left panel) or U2OS (right panel) cell lysates from cells transiently transfected for 24 h with indicated siRNAs. Blots represent more than one individual experiment.

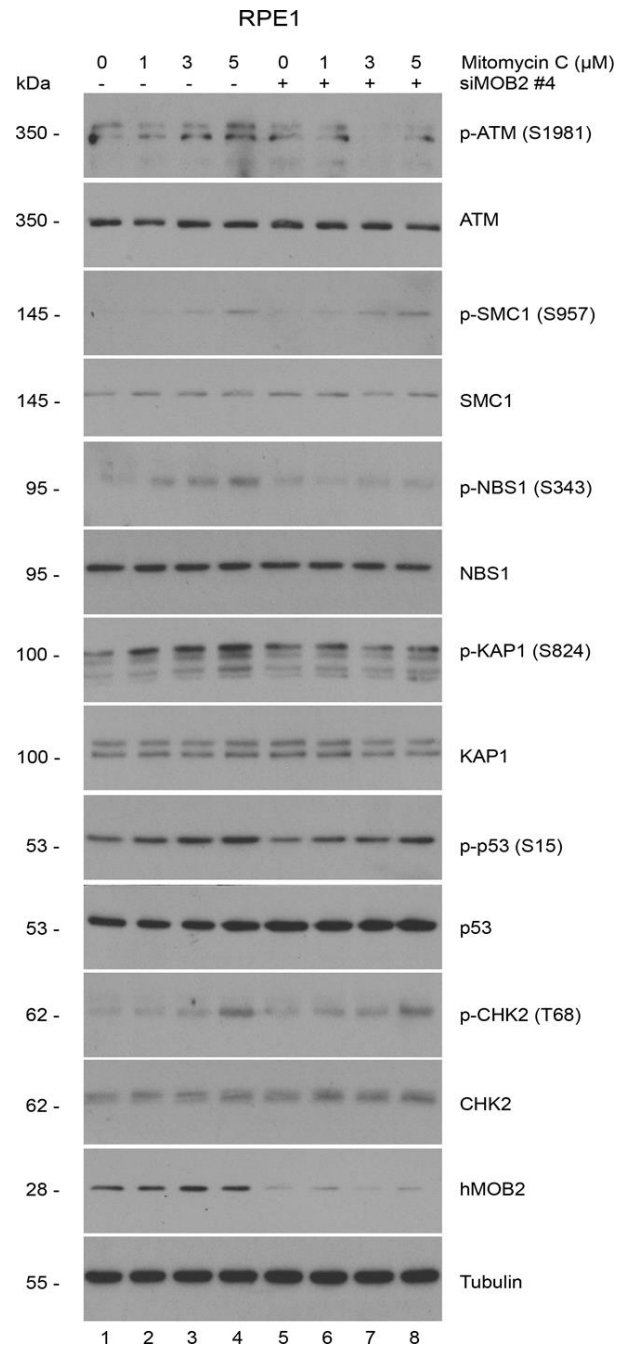


**Figure S4.3**

**hMOB2 supports mitomycin C-induced ATM signalling (in support of Figure 4.3).**

Phosphorylation of ATM and ATM substrates analysed by immunoblotting with indicated antibodies of RPE1 cell lysates from cells transiently transfected for 24 h with indicated siRNAs (–, siCTL; +, siMOB2). Cells were treated with indicated mitomycin C doses for 1 h, before processing for immunoblotting. The experiment was performed by me and Angeliki Ditsiou. Blots represent three individual experiments.

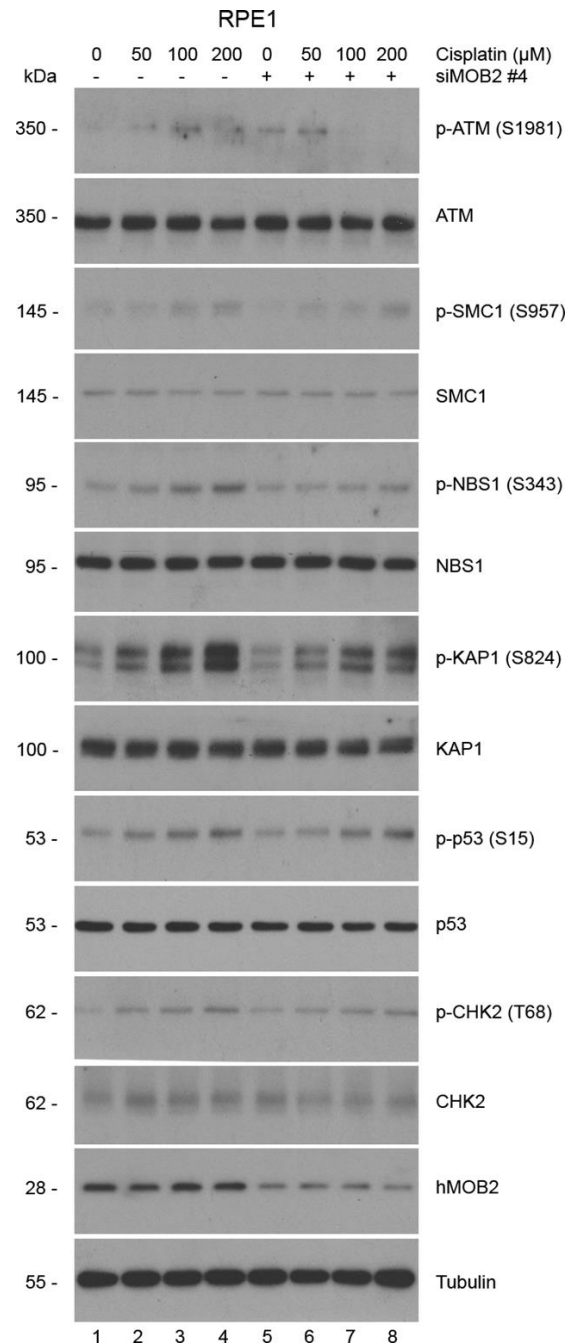


**Figure S4.4**

**hMOB2 supports cisplatin-induced ATM signalling (in support of Figure 4.3).** Phosphorylation of ATM and ATM substrates analysed by immunoblotting with indicated antibodies of RPE1 cell lysates from cells transiently transfected for 24 h with indicated siRNAs (-, siCTL; +, siMOB2). Cells were treated with indicated cisplatin doses for 1 h, before processing for immunoblotting. The experiment was performed by me and Angeliki Ditsiou. Blots represent three individual experiments.

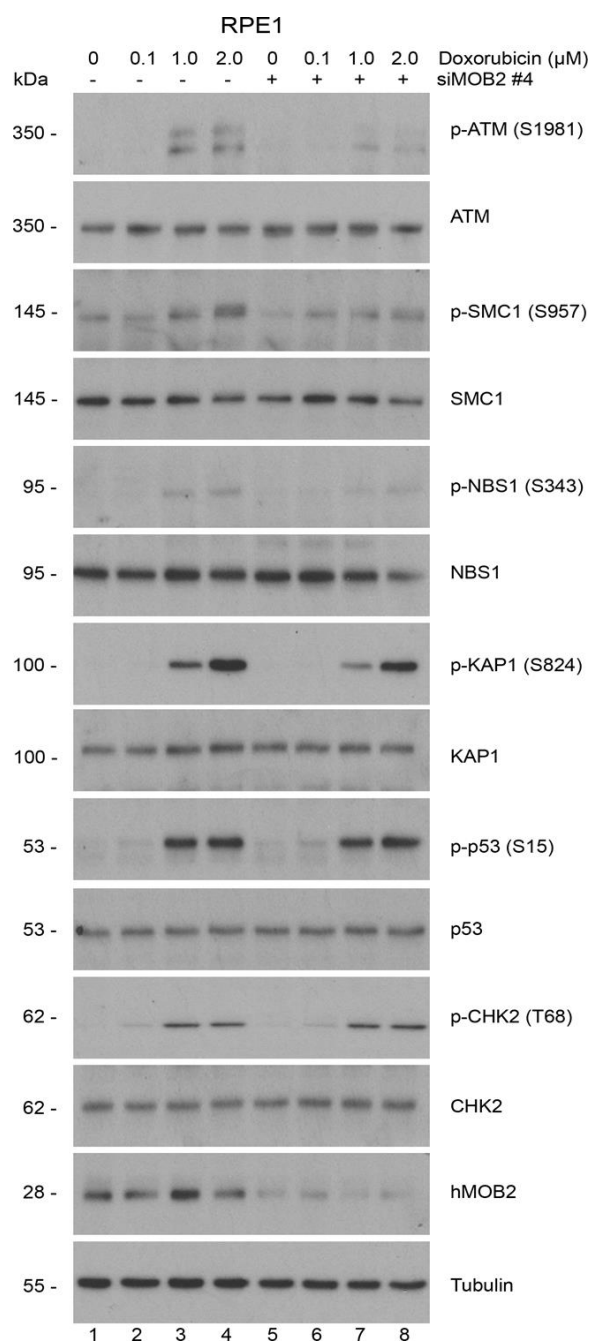


**Figure S4.5**

**hMOB2 supports doxorubicin-induced ATM signalling (in support of Figure 4.3).**

Phosphorylation of ATM and ATM substrates analysed by immunoblotting with indicated antibodies of RPE1 cell lysates from cells transiently transfected for 24 h with indicated siRNAs (–, siCTL; +, siMOB2). Cells were treated with indicated doxorubicin doses for 1 h, before processing for immunoblotting. The experiment was performed by me and Angeliki Ditsiou. Blots represent three individual experiments.

## Chapter 5      hMOB2 supports cancer cell survival upon ICL-inducing drugs and PARP inhibitors

Figures S5.1, S5.2C-D in the Supplementary section have been reprinted from Cellular Signalling, 27/2, Gomez, V., **Gundogdu, R.**, Gomez, M., Hoa, L., Panchal, N., O'Driscoll, M. and Hergovich, A., Regulation of DNA damage responses and cell cycle progression by hMOB2, 326–339., Copyright (2015), with permission from Elsevier (for details please see below).

License details provided by Elsevier and Copyright Clearance Center (RightsLink)	
License Number	3923230104627
License Date	Aug 06, 2016
Type of Use	reuse in a thesis/dissertation
Portion and Format	full article, both print and electronic



## 5.1 Introduction

Our data presented in the third and fourth chapters highlight the importance of hMOB2 as a novel DDR protein by showing that depletion of hMOB2 impairs (i) DNA damage cell cycle checkpoint activation, (ii) efficient MRN-ATM recruitment to damaged chromatin, (iii) ATM-mediated DDR signalling, (iv) RAD51 phosphorylation at Ser14 and thereby RAD51 loading onto ssDNA, and consequently (v) DSB repair by HRR. On the basis of these findings, we aimed to investigate whether loss of hMOB2 renders human cancer cells vulnerable to DNA-damaging agents, specifically to those generating lesions that are subjected to be repaired by the HRR mechanism (e.g. replication-associated DSBs) and whether hMOB2 offers any synthetic lethal interaction with other alternative DDR pathways.

Although clinical studies have repeatedly demonstrated that DNA-damaging treatments can be highly successful in treating cancer patients, our current understanding cannot explain the observed inconsistent responses at the molecular level (Helleday, 2010). Interestingly, the selective toxicity of DNA-damaging agents in a subtype of cancers has been suggested to be related to specific HRR defects (Helleday, 2010). For example, patients with primary ovarian cancers often respond well to platinum-based treatments such as cisplatin, which can be correlated with reduced expression of HRR proteins such as BRCA1 or FANCF (Taniguchi et al., 2003). Thus, it has become essential to identify key molecular DDR players that are determinants of cellular responses to anticancer treatments. Significantly, inhibition of alternative (compensatory) pathways may offer a targeted elimination of cancer cells by inducing selective cell death through synthetic lethality (Helleday, 2010, Curtin, 2012, Jackson and Helleday, 2016). For instance, HRR-defective cancer cells with BRCA1/2 inactivation can be selectively killed by PARP inhibitors (Bryant et al., 2005, Farmer et al., 2005). Considering the importance of BRCA1 and BRCA2 proteins in HRR, many other HRR proteins (e.g. MRE11, RAD50, NBS1, PALB2) have currently been investigated in numerous pre-clinical studies in the context of PARP inhibition (Walsh and Hodeib, 2016, Wang et al., 2016). Therefore, a significant fraction of cancer research aims to characterise novel biomarkers

that can be selectively targeted since they may offer a better therapeutic outcome for cancer patients with defective HRR in spite of wild-type *BRCA1/2* alleles.

## **5.2 Research aims**

Our results propose that hMOB2 through its involvement in HRR may represent a promising therapeutic benefit to predict cellular response to DNA-damaging anticancer treatments. Considering further that a genome-wide DDR screen proposes that hMOB2-depleted cells may have increased sensitivity to mitomycin C (Cotta-Ramusino et al., 2011), we aimed to investigate whether reduced hMOB2 expression makes cells more sensitive to:

- (i) ICL-inducing agents and other DNA-damaging treatments including radiotherapy,
- (ii) inactivation of compensatory DDR pathways such as NHEJ and BER.

### 5.3 Results

**hMOB2 depletion sensitises human cancer cells to ICL-inducing chemotherapeutics.** ICL-inducing agents (bifunctional alkylating chemicals) including mitomycin C and cisplatin can introduce DSBs by stalling replication forks at the intercross-link (Helleday, 2010). These types of replication-associated DSBs are selectively repaired by HRR, and therefore, decreased HRR functionality renders cells very sensitive to ICL-forming agents (Long et al., 2011, Kim and D'Andrea, 2012). For example, mitomycin C and cisplatin can selectively target tumour cells with HRR deficiency due to inactivation of *BRCA1/2* genes (Curtin, 2012). Considering these observations and that loss of hMOB2 impaired HRR functionality, we hypothesised that hMOB2-knockdown cells might display increased sensitivities to the ICL-inducing chemotherapeutics mitomycin C and cisplatin. To test this, we studied manipulations of U2OS cells as U2OS cells are routinely employed for clonogenic cell survival assays in regard to DNA damaging agents (Sartori et al., 2007). 24 h after siRNA transfection cells were subjected to acute (1 h) mitomycin C or cisplatin treatments (Figures 5.1A and Figure 5.2A, respectively). As anticipated, hMOB2-depleted cells were significantly sensitive to mitomycin C (Figure 5.1B-C) and cisplatin (Figure 5.2B-C), indicating that hMOB2 positively contributes to cell survival following exposure to ICL-inducing agents. These findings are fully consistent with the genome-wide DDR screen proposing that hMOB2 may contribute to mitomycin C sensitivity (Cotta-Ramusino et al., 2011). Additionally, we also analysed survival of hMOB2-deficient cells upon other DNA-damaging treatments including ionising radiation (IR) and topoisomerase inhibitors. We found that depletion of hMOB2 resulted in increased sensitivities to radiation and doxorubicin (see Figures S5.1 and S5.2B in the Supplementary section, pages 223- 224). In contrast, knockdown of hMOB2 did not sensitise cells to camptothecin or etoposide (see Figures S5.2A and S5.2C in the Supplementary section, page 224). These findings collectively propose that hMOB2 supports the repair of a specific subtype of DSBs (DNA lesions) by HRR.

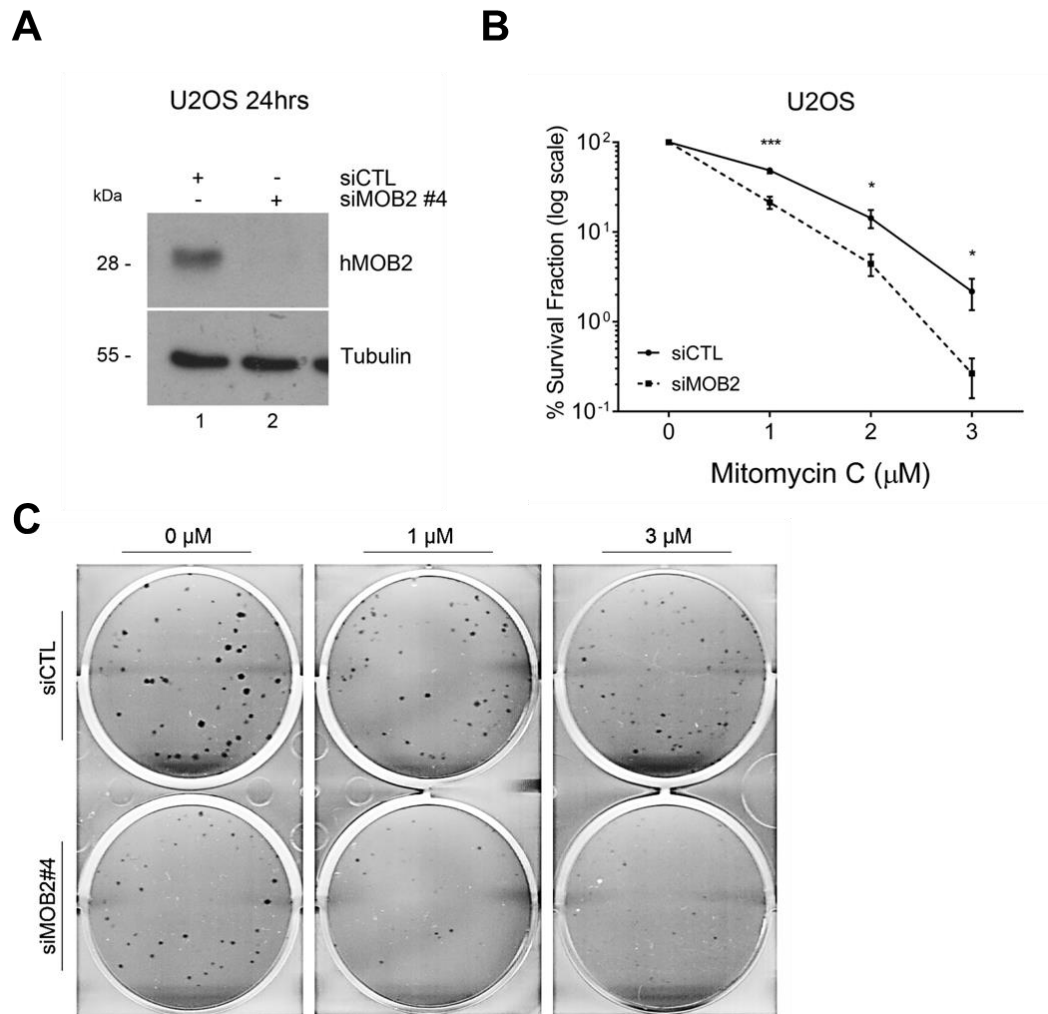


**Figure 5.1**

**hMOB2-depleted cells display significantly increased sensitivity to mitomycin C.**

(A) Immunoblotting with indicated antibodies of U2OS cell lysates from cells transiently transfected for 24 h with indicated siRNAs. (B) Clonogenic survival of U2OS cells upon hMOB2 knockdown (siMOB2#4) compared with controls (siCTL) in response to DMSO or mitomycin C treatment (1 h). Quantifications are shown as a percentage (in log scale) of colonies formed after treatment with indicated doses ( $n=4$ ). Results were corrected according to plating efficiencies of the corresponding untreated controls.  $p$ -values are: 1  $\mu$ M=8.3E-04, 2  $\mu$ M=0.025, 3  $\mu$ M=0.021. Results are presented as mean of replicates and error bars as mean  $\pm$  standard error of mean (SEM), statistical significance was calculated using the one-tailed unpaired Student's  $t$ -test. (C) Representative images of the clonogenic survival assays.

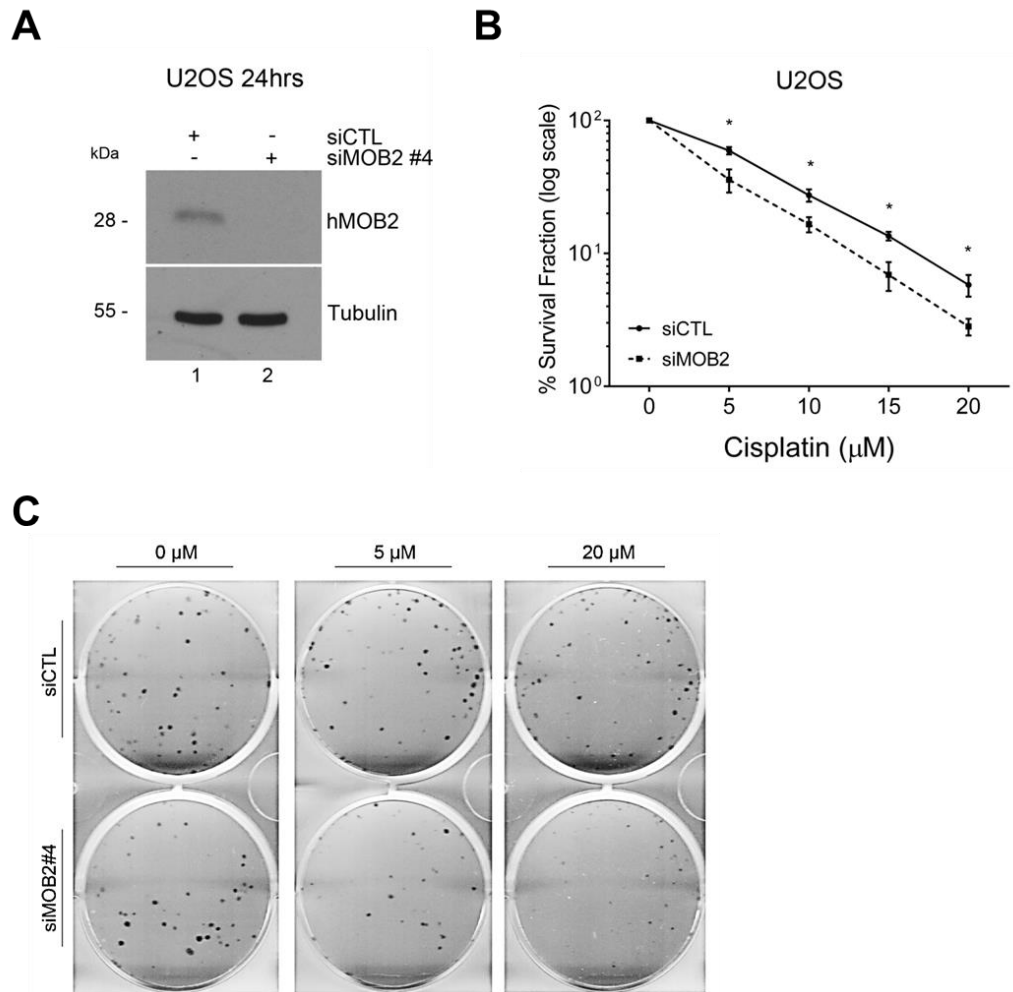


**Figure 5.2**

**hMOB2 deficiency significantly decreases survival of cancer cells upon cisplatin treatment.**

(A) Immunoblotting with indicated antibodies of U2OS cell lysates from cells transiently transfected for 24 h with indicated siRNAs. (B) Clonogenic survival of U2OS cells upon hMOB2 knockdown (siMOB2#4) compared with controls (siCTL) in response to cisplatin treatment (1 h). Quantifications are shown as a percentage (in log scale) of colonies formed after treatment with indicated doses (n=4). Results were corrected according to plating efficiencies of the corresponding untreated controls. *p*-values are: 5  $\mu$ M=0.018, 10  $\mu$ M=0.013, 15  $\mu$ M=0.01, 20  $\mu$ M=0.031. Results are presented as mean of replicates and error bars as mean  $\pm$  standard error of mean (SEM), statistical significance was calculated using the one-tailed unpaired Student's *t*-test. (C) Representative images of the clonogenic survival assays.

**ICLs are formed at comparable levels in hMOB2-proficient and -deficient cells.** To rule out that inconsistent formation of ICL adducts in

hMOB2-proficient vs. -deficient cells is the reason for the observed increased sensitivity to ICL agents, we compared the amount of ICL induction between control and hMOB2 knockdown cells (Figure 5.3A) using a modified alkaline Comet assay as explained in chapter-2, section 2.2.5.3, page 117 (Spanswick et al., 2010). As already reported (Spanswick et al., 2012, Wynne et al., 2007), cells displayed maximum ICL formation after 9 h post-cisplatin treatment. Notably, the ICL levels produced by cisplatin treatment in hMOB2-knockdown cells were comparable to control cells (Figure 5.3B). This suggests that the ICL-sensitivity of hMOB2-depleted cells was caused by compromised ICL repair and not an impairment of ICL adduct formation. Moreover, we observed that the unhooking kinetics of ICLs in hMOB2-deficient cells and control cells were similar during the time-course of our experiment (Figure 5.3B). This further suggests that the unhooking process of ICL lesions, which is mainly regulated by the canonical Fanconi anemia (FA) pathway (Collis et al., 2008), was not affected upon hMOB2 knockdown.

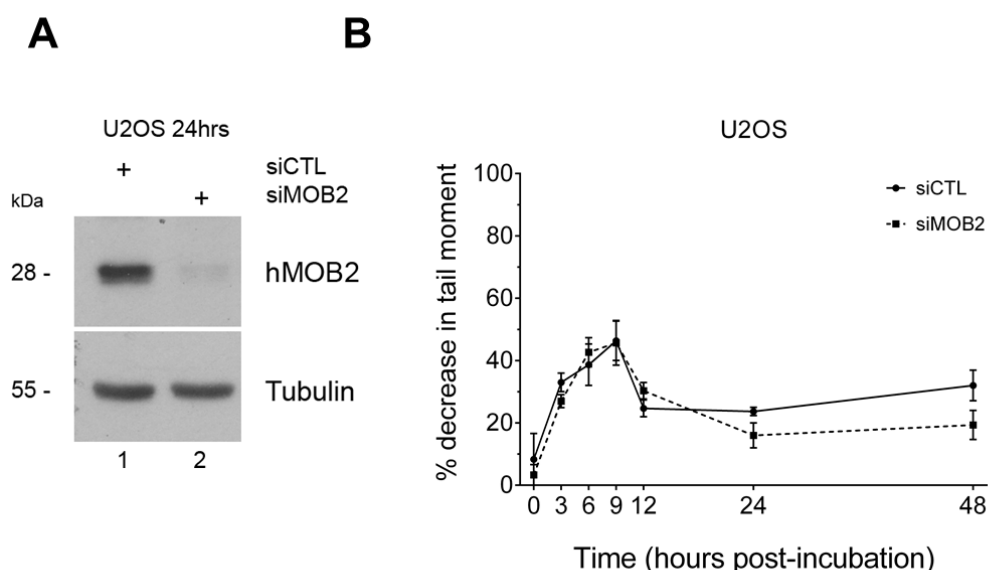


**Figure 5.3**

**Increased ICL-sensitivity of hMOB2-knockdown cells is not caused by inconsistent formation of ICL adducts.**

(A) Immunoblotting with indicated antibodies of U2OS cell lysates from cells transiently transfected for 24 h with indicated siRNAs. (B) Comet assay quantification of ICL formations produced by cisplatin in U2OS cells. 24 h after

siRNA transfection (siCTL, siMOB2#4) cells were treated for 1 h with 100  $\mu$ M cisplatin after which the drug was discarded and replenished with drug-free media. Cells were then incubated for indicated time points post-treatment to compare the amount of ICL formation between hMOB2-proficient and -deficient cells (n=3). Results are expressed as percentage decrease in tail moment mean for 50 cells counted at each point. *p*-values are: 0 h=0.31, 6 h=0.325, 9 h=0.473, 12 h=0.1, 48 h=0.067. Results are presented as mean of replicates and error bars as mean  $\pm$  standard error of mean (SEM), statistical significance was calculated using the one-tailed unpaired Student's *t*-test.

**Increased ICL-sensitivity of hMOB2-depleted cells is independent of the canonical FA pathway.** Depletion of hMOB2 rendered cells sensitive to ICL-inducing drugs (Figures 5.1 and 5.2). Following the initial FA pathway-coordinated ICL unhooking process, the remaining ICL lesions are subjected to be repaired by various pathways including HRR (Deans and West, 2011). The data presented in Figure 5.3B suggest that the FA pathway is fully operational to unhook ICLs in hMOB2-depleted cells. To directly establish that the involvement of hMOB2 in ICL resolution was independent of the FA pathway, we transiently co-depleted hMOB2 and FANCD2, a central component of the FA pathway (Deans and West, 2011, Williams et al., 2013) (Figure 5.4A) and subsequently analysed the mitomycin C-sensitivity by clonogenic survival assays. Single FANCD2-depleted cells were more sensitive to mitomycin C compared to hMOB2-depleted cells (Figure 5.4B-C). Even more significantly, cells with co-depletion of hMOB2 and FANCD2 exhibited even higher sensitivity to mitomycin C treatment (Figure 5.4B-C), suggesting a role for hMOB2 in ICL repair that is independent of the canonical FA pathway. Equally important, the survival of cells with co-depletion of hMOB2 and FANCD2 was even decreased compared to normal, hMOB2-deficient, or FANCD2-deficient cells in the absence of any exogenous DNA damage (Figure 5.4B-C). These findings cummulateively suggest a synthetic lethal interaction between the hMOB2- and FANCD2-regulated pathways. In this regard, we also observed that hMOB2 protein levels appear to be upregulated upon FANCD2 depletion (Figure 5.4A, lane 3), which suggests that potentially compensatory mechanisms are activated upon single FANCD2 knockdown.



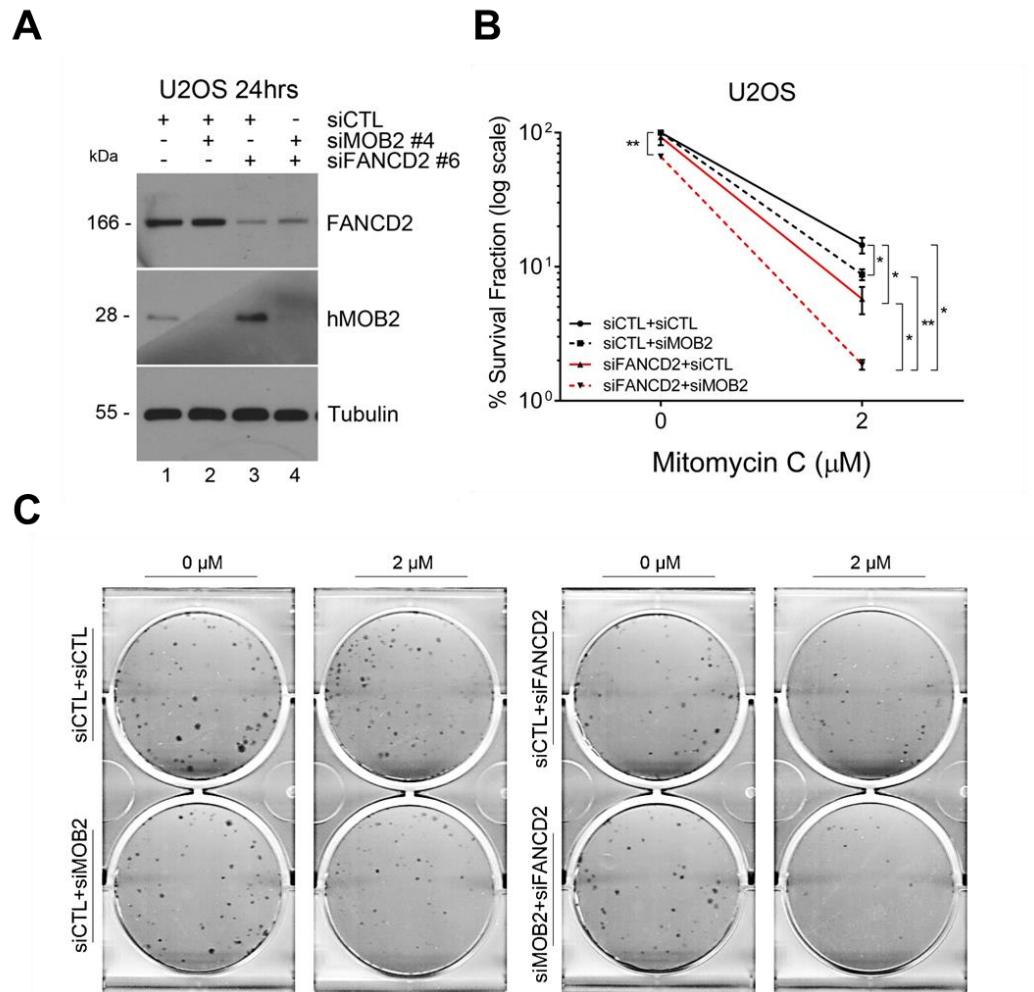


**Figure 5.4**

**hMOB2-knockdown cells show augmented sensitivity to ICL-inducing agents independent of the FA pathway.**

(A) Immunoblotting with indicated antibodies of U2OS cell lysates from cells transiently transfected for 24 h with indicated siRNAs. (B) Clonogenic survival of U2OS cells upon hMOB2 and/or FANCD2 knockdown (siMOB2#4, siFANCD2#6) compared with controls (siCTL) in response to DMSO or mitomycin C treatment (1 h). Quantifications are shown as a percentage (in log scale) of colonies formed after treatment with indicated doses ( $n=3$ ). Results were corrected according to plating efficiencies of the corresponding untreated controls.  $p$ -values are: 0  $\mu$ M, CTL-MOB2/FANCD2=0.003; 2  $\mu$ M, CTL-MOB2=0.04, CTL-FANCD2 =0.012, CTL-MOB2/FANCD2=0.011, MOB2-MOB2/FANCD2=5.7E-03, FANCD2-MOB2/FANCD2=0.048. Results are presented as mean of replicates and error bars as mean  $\pm$  standard error of mean (SEM), statistical significance was calculated using the one-tailed unpaired Student's  $t$ -test. (C) Representative images of the clonogenic survival assays.

**Blocking of classical NHEJ through DNA-PK inhibition lowers the survival of hMOB2-deficient cells.** A significant number of studies indicate that cancer cells deficient in DDR pathways gain a dependency on alternative (compensatory) pathways for their survival (Bryant et al., 2005, Farmer et al., 2005), which may explain the observed synthetic lethal interaction between the hMOB2- and FANCD2-regulated pathways (Figure 5.4). Given that hMOB2-deficient cells exhibited significantly attenuated HRR activity and increased NHEJ activity to repair DSBs (see Figures 4.4 and 4.5 in chapter-4 on pages 173-174), we investigated whether NHEJ inhibition may display a synthetic lethal interaction with hMOB2 knockdown.

The classical NHEJ mechanism is considered as the predominant DSB repair pathway that is functional throughout the entire cell cycle phases (Goodarzi and Jeggo, 2013). The DNA-PK enzyme functions critical roles in NHEJ, where it catalyses the re-ligation of DSBs by activating various downstream components of NHEJ (Goodarzi and Jeggo, 2013, Goldstein and Kastan, 2015). NU-7441 has been regularly used in pre-clinical studies as a highly potent and selective DNA-PK inhibitor (Davidson et al., 2013). Using our GFP-based reporter assays we confirmed that DNA-PK inhibition by NU-7441 blocks classical NHEJ (see Figure 4.5E in chapter-4 on page 174). Therefore, we examined next the effects of combined DNA-PK inhibition and hMOB2 knockdown. 24 h after siRNA transfection (Figure 5.5A) cells were treated with the DNA-PK inhibitor NU-7441 for 4 h. Interestingly, DNA-PK inhibition decreased the survival of hMOB2-deficient cells compared to controls (Figure 5.5B-C). This suggests that the observed increased in NHEJ activity upon hMOB2 depletion is likely to at least in part compensate for the decreased HRR activity in hMOB2-depleted cells.

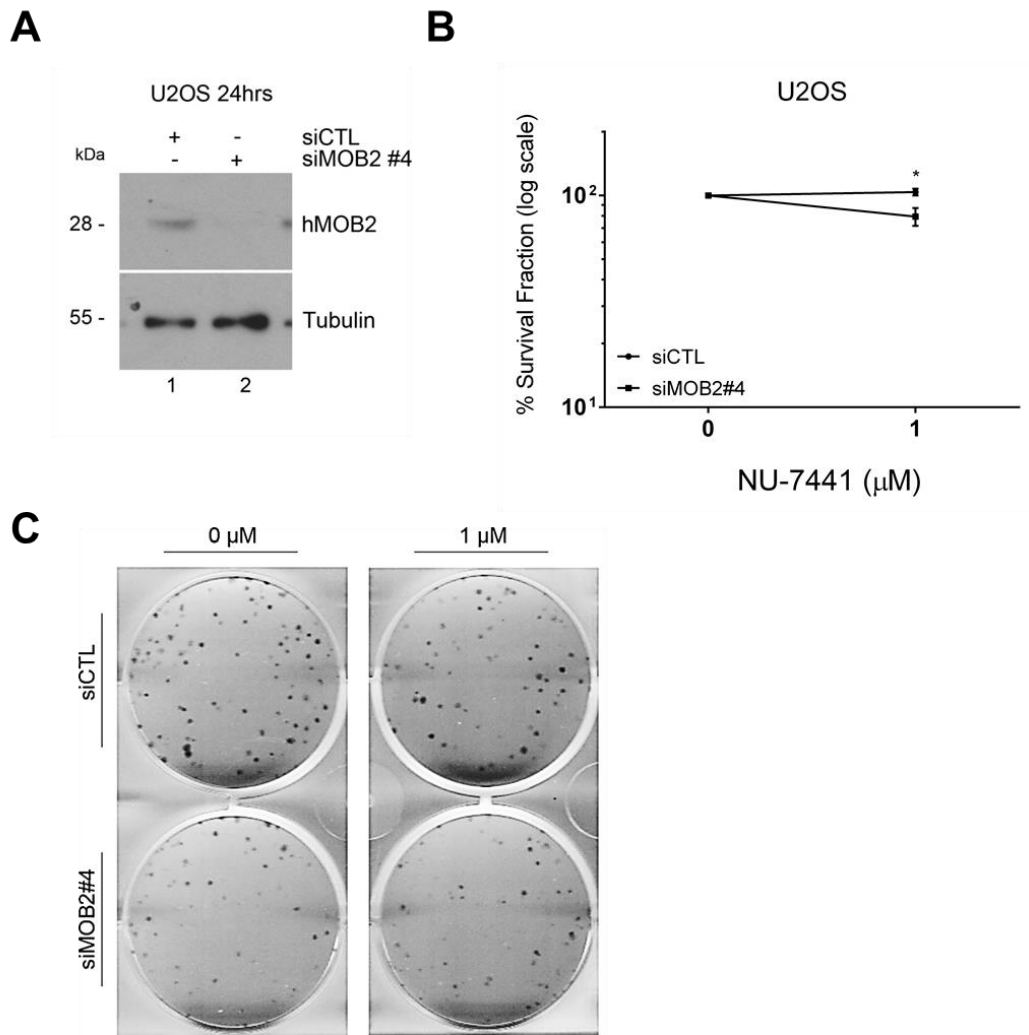


**Figure 5.5**

**hMOB2-depleted cells display reduced survival upon DNA-PK inhibition.**

(A) Immunoblotting with indicated antibodies of U2OS cell lysates from cells transiently transfected for 24 h with indicated siRNAs. (B) Clonogenic survival of U2OS cells upon hMOB2 knockdown (siMOB2#4) compared with controls (siCTL) in response to DMSO or DNA-PK inhibitor (NU-7441, 1  $\mu$ M or 10  $\mu$ M) treatment (4 h). Quantifications are shown as a percentage of colonies formed after treatment with indicated doses (log scale,  $n=4$ ). Results were corrected according to plating efficiencies of the corresponding untreated controls.  $p$ -values are: 1  $\mu$ M=0.021. Results are presented as mean of replicates and error bars as mean  $\pm$  standard error of mean (SEM), statistical significance was calculated using the one-tailed unpaired Student's  $t$ -test. (C) Representative images of the clonogenic survival assays.

**hMOB2 knockdown increases the radiosensitivity of NHEJ-deficient cells.** Given that NHEJ inactivation through DNA-PK inhibition reduced the survival of hMOB2-knockdown cells (Figure 5.5B-C), we next tested whether

the radiosensitivity of NHEJ-inhibited cells was elevated upon hMOB2 depletion. To do so, 24 h post-siRNA transfection (Figure 5.6A) cells were first pre-treated with the DNA-PK inhibitor NU-7441 for 1 h prior to IR that was followed by additional 16 h-incubation with NU-7441, as already defined in Zhao et al. (2006). Considerably, hMOB2 deficiency significantly potentiated the radiosensitivity of NHEJ-inhibited cells (Figure 5.6B-C). This finding highlights that the hMOB2- and DNA-PK-regulated pathways can display a synthetic lethal interaction upon exposure to radiation, which is likely a consequence of the elevated dependency of NHEJ-deficient cells on HRR upon exposure to higher levels of DNA damage.

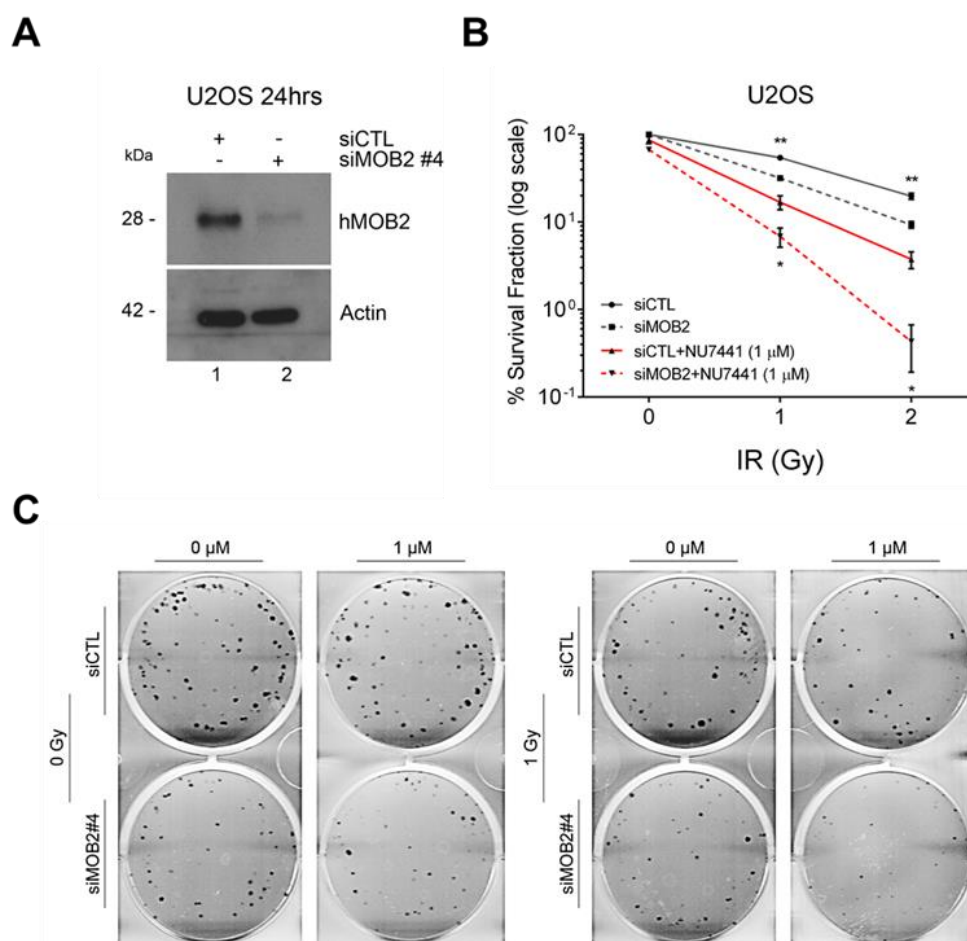


**Figure 5.6**

**hMOB2 deficiency elevates radiosensitivity of DNA-PK-inhibited cells.** (A) Immunoblotting with indicated antibodies of U2OS cell lysates from cells transiently transfected for 24 h with indicated siRNAs. (B) Clonogenic survival of U2OS cells upon hMOB2 knockdown (siMOB2#4) compared with controls (siCTL).

After 24 h of transfection, cells were pre-treated with DMSO or 1  $\mu$ M DNA-PK inhibitor (NU-7441) for 1 h and then treated with indicated doses of ionising radiation (IR) followed by 16 h-incubation with DMSO or NU-7441 (1  $\mu$ M). Quantifications are shown as a percentage (in log scale) of colonies formed after treatment with indicated doses (n=3). Results were corrected according to plating efficiencies of the corresponding untreated controls. *p*-values are: 1 Gy, MOB2=0.004, MOB2/DNA-PKi=0.029; 2 Gy, MOB2=0.005, MOB2/DNA-PKi =0.022. Results are presented as mean of replicates and error bars as mean  $\pm$  standard error of mean (SEM), statistical significance was calculated using the one-tailed unpaired Student's *t*-test. (C) Representative images of the clonogenic survival assays.

**hMOB2 knockdown neither sensitises nor radiosensitises cells to ATM inhibition.** Next, we employed the ATM inhibitor KU-55933 (Veuger and Curtin, 2014) to assess whether ATM inhibition may show a synthetic lethal interaction with hMOB2 knockdown. Importantly, ATM inhibition sensitises cells to mitomycin C and compromises HRR efficiency (Kirshner et al., 2009), as observed in hMOB2-depleted cells (Figure 5.1 and see Figure 4.4 in chapter-4 on page 173). 24 h after siRNA transfection (Figure 5.7A) cells were treated with the ATM inhibitor KU-55933 for 4 h. Not surprisingly, ATM inhibition did not sensitise hMOB2-deficient cells (Figure 5.7B-C). This confirmed our previous notions that hMOB2 and ATM act in the same pathway in repairing spontaneous DNA lesions. Notably, the FA pathway-deficient tumour cells are very sensitive to ATM inhibition (Kennedy et al., 2007), like we observed upon co-depletion of hMOB2 and FANCD2 (Figure 5.4), hence these data further strengthen our notion that hMOB2 functions together with ATM-regulated DNA repair, but independent of the FA pathway.

Next, considering that ATM inhibition by KU-55933 can sensitise cells to radiotherapy (Weber and Ryan, 2015), we examined whether hMOB2 knockdown might enhance the radiosensitivity to ATM inhibition. However, although we could confirm the reported radiosensitising effect of KU-55933 (Weber and Ryan, 2015), co-inactivation of hMOB2 and ATM did not show any additional impact on the cell survival upon IR treatment (see Figure S5.3 in the Supplementary section, page 225). In summary, these data indicate that hMOB2 depletion does not render cells more vulnerable to ATM inhibition, which presumably is a consequence of both hMOB2 and ATM acting in the same DDR pathway.

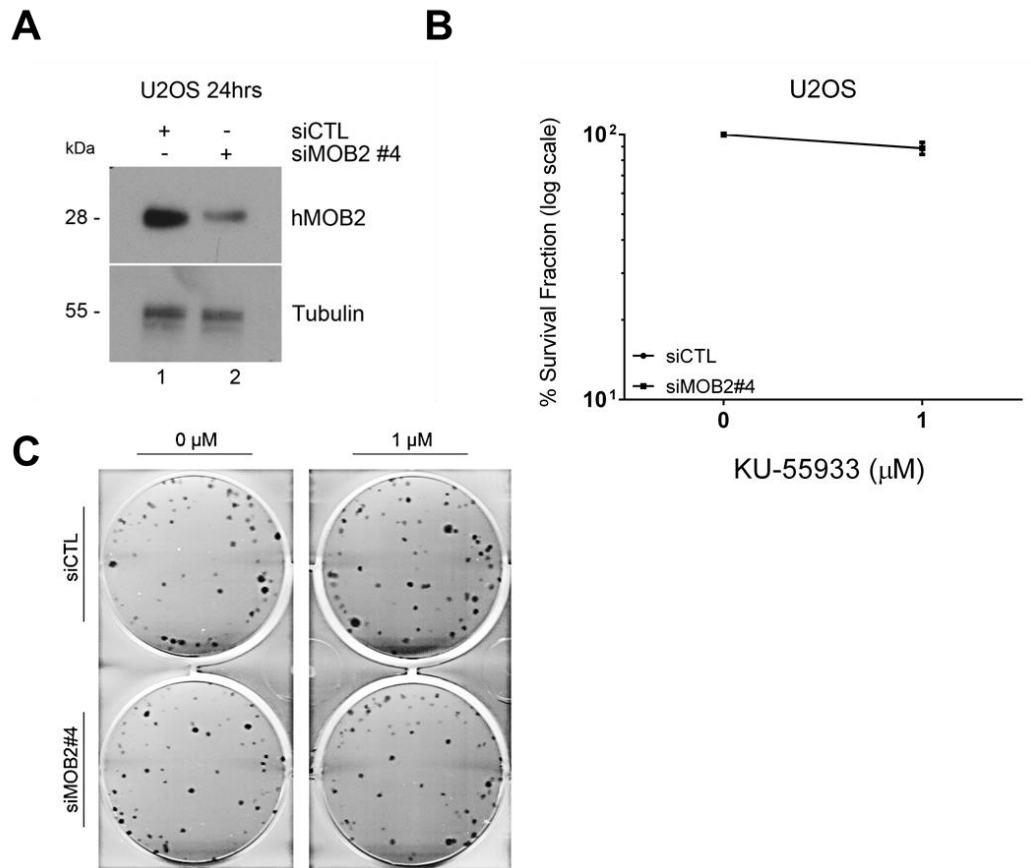


**Figure 5.7**

**ATM inhibition does not alter the survival of hMOB2-knockdown cells.**

(A) Immunoblotting with indicated antibodies of U2OS cell lysates from cells transiently transfected for 24 h with indicated siRNAs. (B) Clonogenic survival of U2OS cells upon hMOB2 knockdown (siMOB2#4) compared with controls (siCTL) in response to DMSO or ATM inhibitor (KU-55933, 1 μM) treatment (4 h). Quantifications are shown as a percentage of colonies formed after treatment with indicated doses (log scale, n=4). Results were corrected according to plating efficiencies of the corresponding untreated controls. Results are presented as mean of replicates and error bars as mean ± standard error of mean (SEM), statistical significance was calculated using the one-tailed unpaired Student's *t*-test. (C) Representative images of the clonogenic survival assays.

**hMOB2-deficient cells display increased sensitivity to PARP inhibition.**

So far, we found that hMOB2 deficiency impairs HRR (see Figure 4.4 in chapter-4 on page 173) and therefore sensitises cells to ICL-inducing agents mitomycin C and cisplatin (Figures 5.1 and 5.2). Moreover, our experiments revealed a synthetic lethal interaction between the hMOB2- and FANCD2 or NHEJ-regulated pathways (Figures 5.4 and 5.5). Several lines of evidence

strongly suggest that cancer cells with HRR deficiency (e.g. through *BRCA1/2* inactivation) show a significant hypersensitivity to PARP inhibition (Bryant et al., 2005, Farmer et al., 2005, Wang et al., 2016, Lord and Ashworth, 2016). Two types of PARP inhibition have been reported so far. First, PARP inhibition can impair SSB repair that is normally mediated by BER (base excision repair), leading to DSBs once replication forks are stalled and collapsed during DNA replication (Bryant et al., 2005, Farmer et al., 2005). Second, PARP inhibitors can trap PARP protein on DNA, ultimately causing DSBs (Murai et al., 2012). In this project we used three different PARP inhibitors: olaparib (AZD-2281, AstraZenaca), rucaparib (AG-014699, Clovic Oncology), and veliparib (ABT-888, AbbVie). It is worth to note that veliparib introduces less PARP-trapping compared to olaparib and rucaparib (Walsh and Hodeib, 2016, Benafif and Hall, 2015).

We hypothesised that hMOB2 depletion could sensitise cancer cells to these PARP inhibitors. Initially, we used olaparib, the first approved PARP inhibitor used in the clinic to treat patients with advanced and *BRCA1* or *BRCA2* mutant ovarian cancer (Wang et al., 2016). 24 h after siRNA transfection (Figure 5.8A), U2OS cells were treated with olaparib for 24 h in order to provide sufficient time for (i) the accumulation of PARP-inhibition-dependent SSBs and (ii) the conversion of SSBs into replication-associated DSBs. Remarkably, hMOB2 deficiency rendered U2OS cells highly sensitive to PARP inhibition (Figure 5.8B-C). This revealed that hMOB2- and PARP-regulated pathways can display a synthetic lethal interaction. Most likely, the HRR deficiency caused by hMOB2 knockdown renders cells more sensitive to PARP inhibition, as already observed for the other major regulators of HRR such as *BRCA1/2* (Bryant et al., 2005, Farmer et al., 2005), *MRE11* (Vilar et al., 2011), *RAD50* (Zhang et al., 2016), and *ATM* (Gilardini Montani et al., 2013).

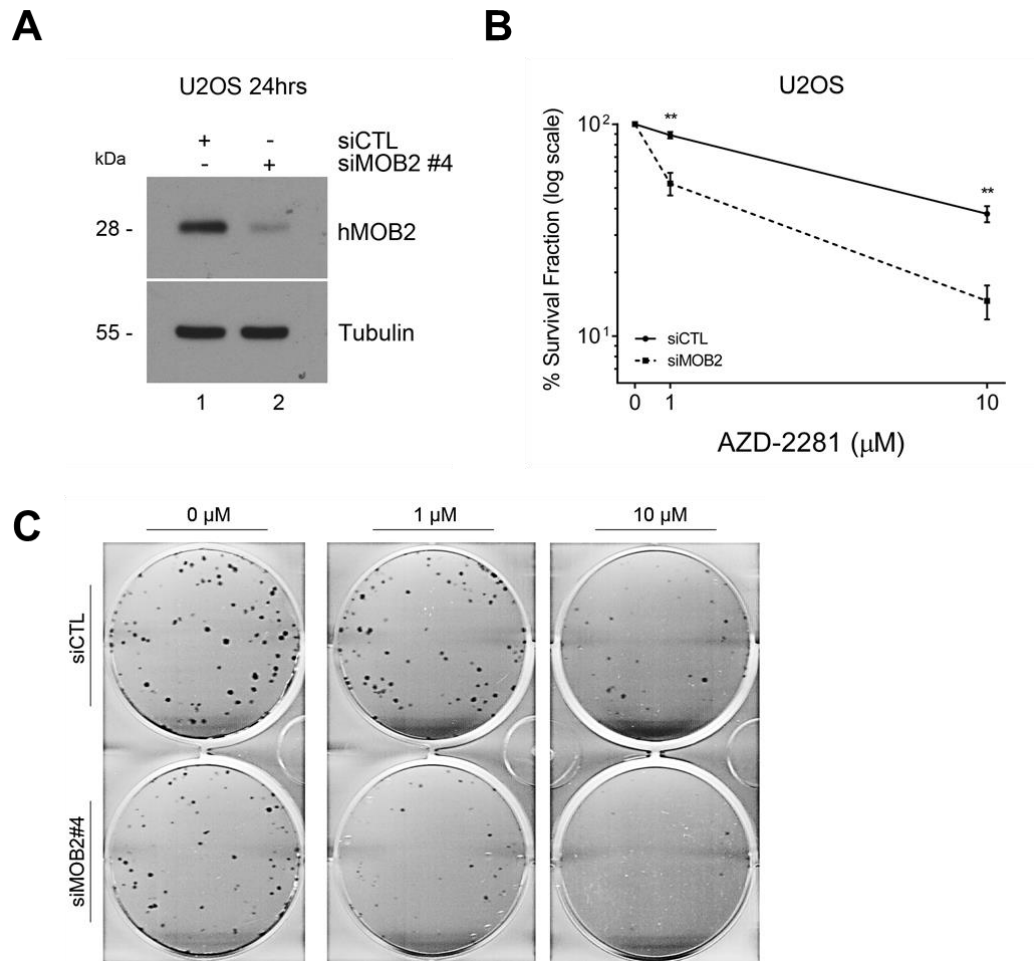


**Figure 5.8**

**hMOB2-depleted cells show increased sensitivity to PARP inhibition by olaparib.**

(A) Immunoblotting with indicated antibodies of U2OS cell lysates from cells transiently transfected for 24 h with indicated siRNAs. (B) Clonogenic survival of U2OS cells upon hMOB2 knockdown (siMOB2#4) compared with controls (siCTL) in response to DMSO or olaparib (AZD-2281, 1  $\mu$ M or 10  $\mu$ M) treatment (24 h). Quantifications are shown as a percentage (in log scale) of colonies formed after treatment with indicated doses (n=3). Results were corrected according to plating efficiencies of the corresponding untreated controls. *p*-values are: 1  $\mu$ M=0.008, 10  $\mu$ M=0.003. Results are presented as mean of replicates and error bars as mean  $\pm$  standard error of mean (SEM), statistical significance was calculated using the one-tailed unpaired Student's *t*-test. (C) Representative images of the clonogenic survival assays.

To consolidate our findings with U2OS cells (Figure 5.8), we studied additional human cancer cell lines. This revealed that siRNA-mediated depletion of hMOB2 also sensitised HCT116 colorectal cancer cells and



HOC7 ovarian cancer cells to olaparib (Figure 5.9). Next, we further extended our analysis by employing the PARP inhibitors rucaparib and veliparib. As observed with olaparib (Figure 5.8), treatments with rucaparib or veliparib also diminished the survival of hMOB2-depleted U2OS cells (Figure 5.10).

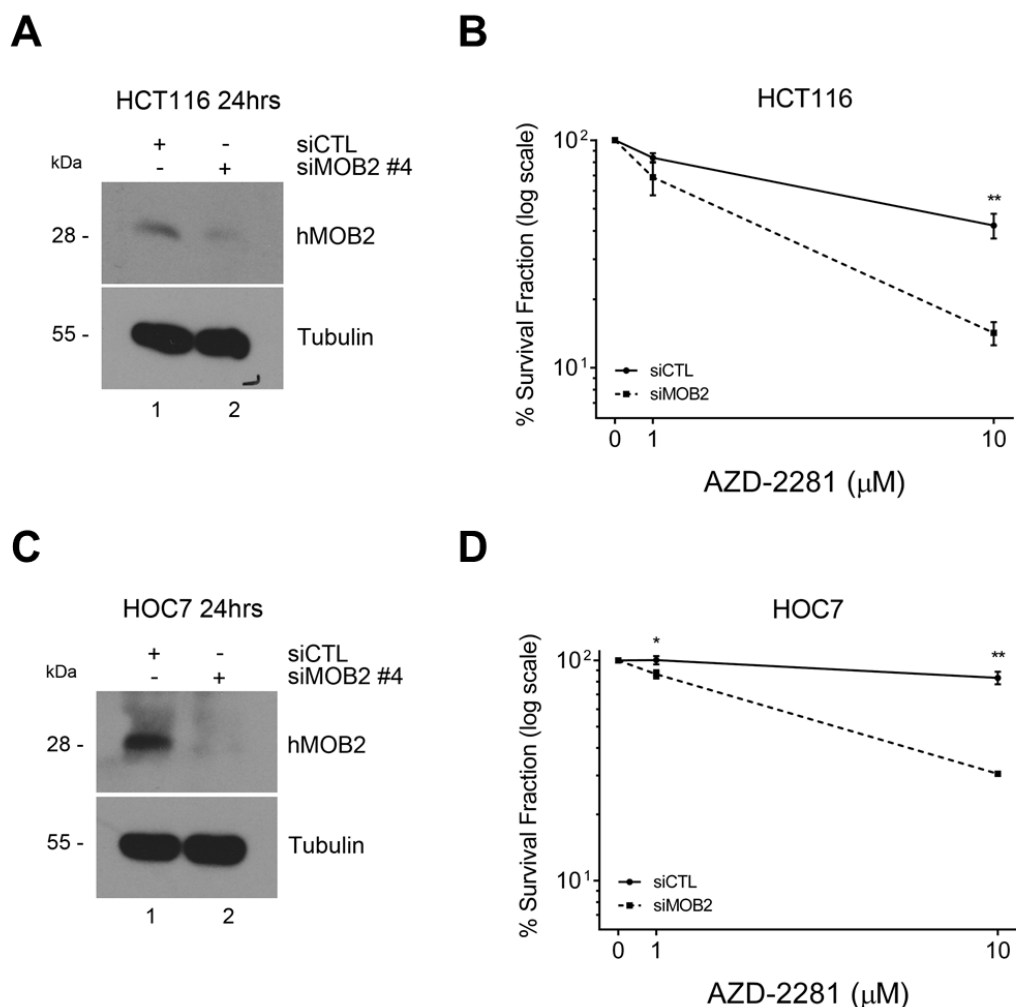


**Figure 5.9**

**PARP inhibition causes a significant reduction in the survival of the hMOB2-depleted human colorectal and ovarian cancer cells.**

(A) Immunoblotting with indicated antibodies of HCT116 cell lysates from cells transiently transfected for 24 h with indicated siRNAs. (B) Clonogenic survival of HCT116 cells upon hMOB2 knockdown (siMOB2#4) compared with controls (siCTL) in response to DMSO or olaparib (AZD-2281, 1  $\mu$ M or 10  $\mu$ M) treatment (24 h). Quantifications are shown as a percentage (in log scale) of colonies formed after treatment with indicated doses (n=4). Results were corrected according to plating efficiencies of the corresponding untreated controls. *p*-values are: 10  $\mu$ M=0.004. (C)

Immunoblotting of HOC7 cell lysates as explained in A. (D) Clonogenic survival of HOC7 cells as explained in B (n=3). *p*-values are: 1  $\mu$ M=0.04, 10  $\mu$ M=0.004. All results are presented as mean of replicates and error bars as mean  $\pm$  standard error of mean (SEM), statistical significance was calculated using the one-tailed unpaired Student's *t*-test.

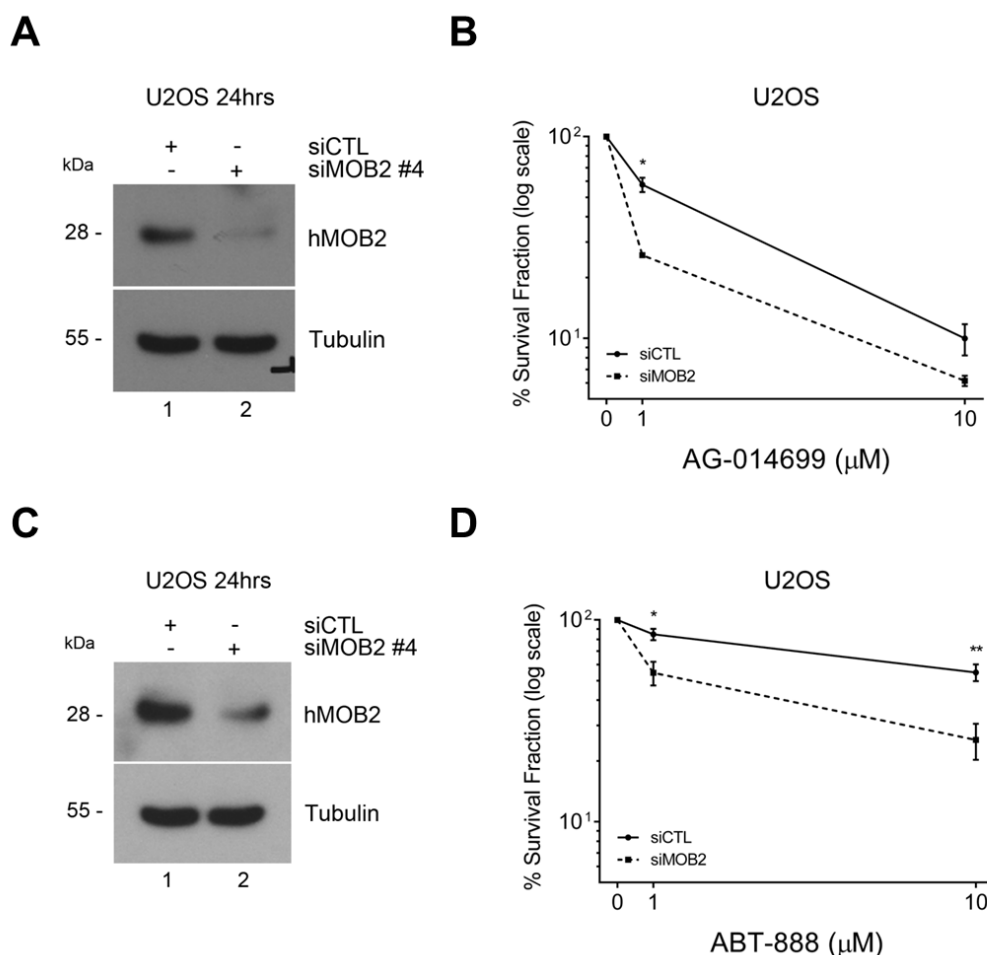


**Figure 5.10**

**hMOB2-depleted cells show elevated sensitivities to the PARP inhibitors rucaparib and veliparib.**

(A) Immunoblotting with indicated antibodies of U2OS cell lysates from cells transiently transfected for 24 h with indicated siRNAs. (B) Clonogenic survival of U2OS cells upon hMOB2 knockdown (siMOB2#4) compared with controls (siCTL) in response to DMSO or rucaparib (AG-014699, 1  $\mu$ M or 10  $\mu$ M) treatment (24 h). Quantifications are shown as a percentage (in log scale) of colonies formed after treatment with indicated doses (n=3). Results were corrected according to plating efficiencies of the corresponding untreated controls. *p*-values are: 1  $\mu$ M=0.01. (C) Immunoblotting of U2OS cell lysates as explained in A. (D) Clonogenic survival of U2OS cells treated with DMSO or veliparib (ABT-888) as explained in B (n=3). *p*-values are: 1  $\mu$ M=0.017, 10  $\mu$ M=0.008. All results are presented as mean of

replicates and error bars as mean  $\pm$  standard error of mean (SEM), statistical significance was calculated using the one-tailed unpaired Student's *t*-test.

Moreover, we analysed the expression levels of hMOB2 in a panel of human ovarian cancer cell lines and selected the cell lines with lowest and highest hMOB2 expression accompanied by wild-type *BRCA1/2* for further analysis (Figure 5.11A-B). The aim was to test whether there is a correlation between endogenous hMOB2 expression and PARP inhibitor sensitivity without any RNAi manipulations. We determined that the highest and the lowest expression levels of hMOB2 protein were detected in HOC7 and Ovca429 cells, respectively (Figure 5.11A, lanes 1 and 8, and Figure 5.11B). Noteworthy, both cell lines are *BRCA1/2* wild-type (Stordal et al., 2013), hence any difference between HOC7 and Ovca429 cells cannot be attributed to defective *BRCA1/2*. Consequently, we analysed the sensitivities of these cell lines to olaparib without any siRNA-manipulations. As shown in Figure 5.11C-D, sensitivity to olaparib was associated with hMOB2 protein levels in these two *BRCA1/2* wild-type ovarian cancer cell lines. Collectively, these results strongly support our notion that decreased hMOB2 levels significantly decrease cancer cell survival in response to olaparib treatment.

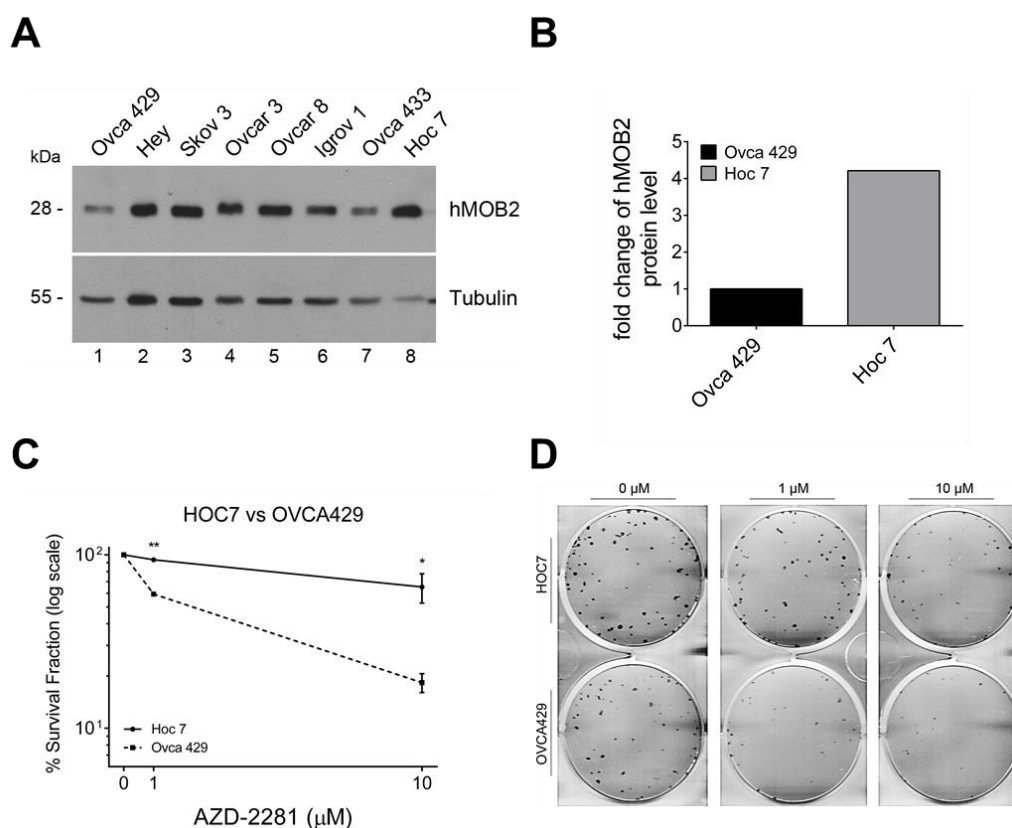


**Figure 5.11**

**The levels of hMOB2 protein correlate with the survival of ovarian cancer cells upon PARP inhibition.**

(A) A panel of ovarian cancer cells were processed for immunoblotting with indicated antibodies. (B) Histogram showing relative MOB2 protein levels of Ovca429 and HOC7 cells, obtained from densitometry quantification of Western blots shown in A. HOC7 was normalized to Ovca429 that was set to 1 (n=2) (C) Clonogenic survival of HOC7 and Ovca429 cells treated with DMSO or olaparib (AZD-2281, 1  $\mu$ M or 10  $\mu$ M) for 24 h. Quantifications are shown as a percentage (in log scale) of colonies formed after treatment with indicated doses (n=3). Results were corrected according to plating efficiencies of the corresponding untreated controls. *p*-values are: 1  $\mu$ M= 1.3E-03, 10  $\mu$ M=0.03. Results are presented as mean of replicates and error bars as mean  $\pm$  standard error of mean (SEM), statistical significance was calculated using the one-tailed unpaired Student's *t*-test. (D) Representative images of the clonogenic survival assays.

**Ectopic expression of RNAi-resistant hMOB2 abolishes the olaparib-sensitivity of hMOB2-depleted cells.** To further confirm that reduced levels of hMOB2 sensitises cancer cells to PARP inhibition, we conducted a phenotype RNAi rescue experiment. To do so, U2OS cells were stably transfected with an empty retroviral expression plasmid or a plasmid

encoding wild-type HA-hMOB2. Since Lys131 of MOB2 is to date the one and only known post-translational modification site of MOB2 (Wagner et al., 2012), we also generated cells stably expressing the HA-hMOB2 (K131R) mutant in order to decipher whether Lys131 of hMOB2 has a functional role. Next, we transiently reduced endogenous hMOB2 levels by an siRNA targeting the 3'UTR of hMOB2 (siMOB2#6, see section 2.1.7, page 91) in U2OS cells stably expressing exogenous RNAi-resistant hMOB2 wild-type or K131R variants (Figure 5.12A). 24 h post-siRNA transfection, cells were treated with olaparib for 24 h, as conducted previously (please see Figure 5.8). As expected, hMOB2 depletion in cells with empty vector expression decreased cell survival (Figure 5.12B) as observed in uninfected U2OS cells (Figure 5.8). In contrast, expression of exogenous RNAi-resistant hMOB2 (wt) in hMOB2-depleted cells restored cell survival upon olaparib treatment to levels observed in controls (Figure 5.12C). hMOB2 knockdown cells with expression of exogenous RNAi-resistant hMOB2 (K131R) also displayed cell survival levels that are comparable to controls (Figure 5.12D). Taken together, these RNAi rescue experiments establish that the decrease of hMOB2 protein levels is the cause of the observed olaparib sensitivity in our settings.

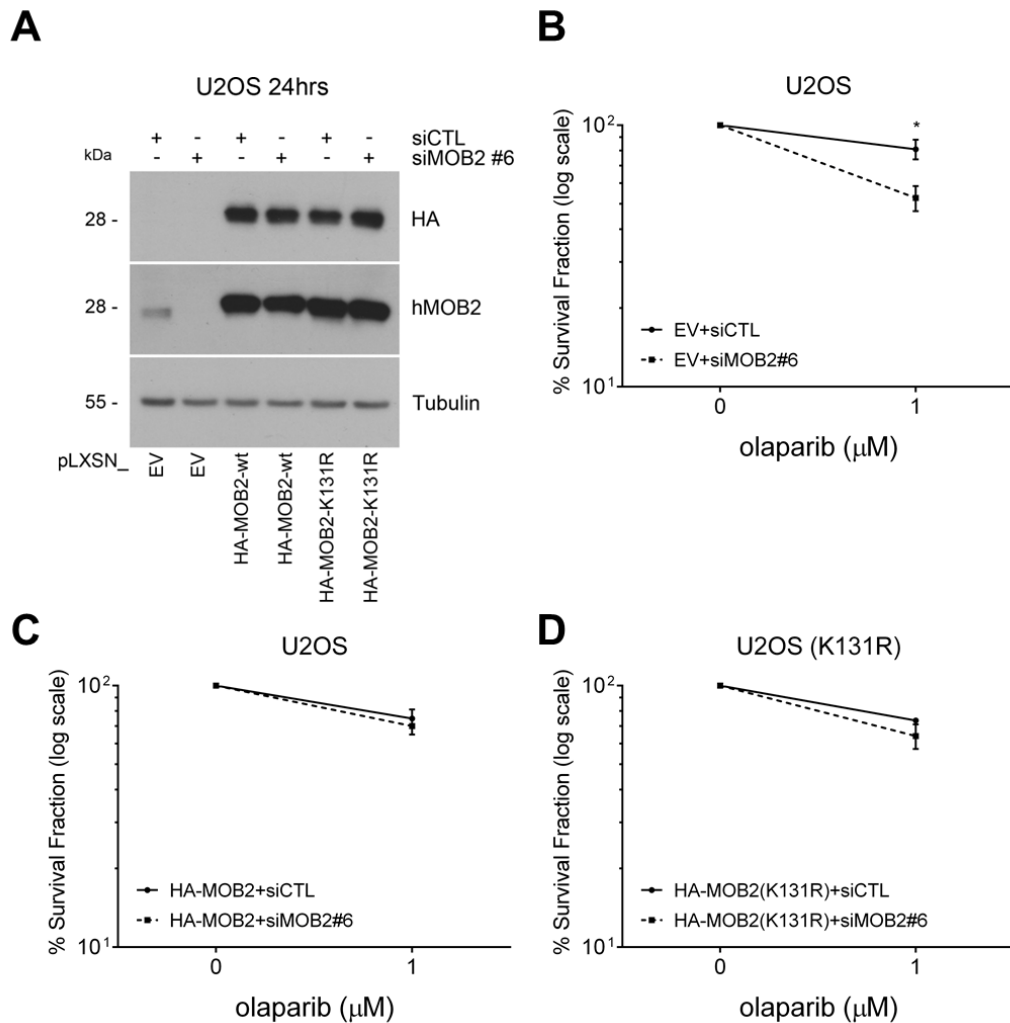


**Figure 5.12**

**hMOB2 supports cell survival in response to PARP inhibition.**

(A) U2OS cells stably expressing empty vector (EV), wild-type MOB2 (WT) or mutant MOB2 (K131R) were transiently transfected with indicated siRNAs (siCTL, siMOB2#6) and harvested 24 h later for immunoblotting. Expression of exogenous hMOB2 was assessed by both anti-HA and anti-hMOB2 antibodies. (B, C, D) Clonogenic survival of U2OS cells stably expressing empty vector (EV), wild-type MOB2 (WT) or mutant MOB2 (K131R) upon hMOB2 knockdown (siMOB2#6) compared with controls (siCTL). After 24 h of transfection, cells were treated with DMSO or olaparib (AZD-2281, 1  $\mu$ M) for 24 h. Quantifications are shown as a percentage of colonies formed after treatment with indicated doses (log scale, n=3). Results were corrected according to plating efficiencies of the corresponding untreated controls. *p*-value is: (EV) 1  $\mu$ M, MOB2= 0.018. All results are presented as mean of replicates and error bars as mean  $\pm$  standard error of mean (SEM), statistical significance was calculated using the one-tailed unpaired Student's *t*-test.

### **hMOB2 deficiency promotes radiosensitivity of PARP-inhibited cells.**

Our findings documented above suggest that hMOB2 knockdown is sufficient to render human cancer cells sensitive to PARP inhibitors. This prompted us to investigate further whether hMOB2 depletion can radiosensitise cancer cells upon olaparib treatment. In this regard, 24 h after siRNA transfection (Figure 5.13A), U2OS cells were initially pre-treated with olaparib for 1h before IR treatment that was followed by an additional 23 h incubation with olaparib. This experiment revealed that hMOB2 depletion combined with PARP inhibition markedly elevated the cytotoxicity of IR treatment (Figure 5.13B). Collectively, this final data set indicates that reduced hMOB2 levels can help to significantly radiosensitise human cancer cells when combined with PARP inhibition.

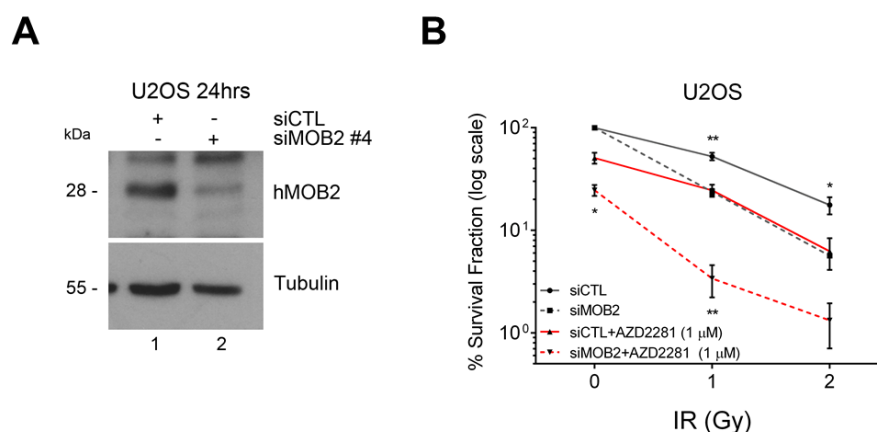


**Figure 5.13**

### **hMOB2 knockdown promotes radiosensitivity of PARP-inhibited cells.**

(A) Immunoblotting with indicated antibodies of U2OS cell lysates from cells transiently transfected for 24 h with indicated siRNAs. (B) Clonogenic survival of U2OS cells upon hMOB2 knockdown (siMOB2#4) compared with controls (siCTL). After 24 h of transfection, cells were pre-treated with DMSO or olaparib (AZD-2281, 1  $\mu$ M) for 1 h and then treated with indicated doses of ionising radiation (IR) followed by 23 h-incubation with DMSO or olaparib (AZD-2281, 1  $\mu$ M). Quantifications are shown as a percentage (in log scale) of colonies formed after treatment with indicated doses (n=3). Results were corrected according to plating efficiencies of the corresponding untreated controls. *p*-values are: 0Gy, MOB2/PARPi=0.017; 1 Gy, MOB2=0.007, MOB2/PARPi=0.007; 2 Gy, MOB2=0.035. Results are presented as mean of replicates and error bars as mean  $\pm$  standard error of mean (SEM), statistical significance was calculated using the one-tailed unpaired Student's *t*-test.

## 5.4 Discussion

Here we report data suggesting that HRR inactivation through hMOB2 depletion can significantly sensitise human cancer cells to ICL-inducing agents, radiation, doxorubicin, NHEJ inhibition and PARP inhibition. Most importantly, we found that the stratification of hMOB2 levels may offer a promising therapeutic benefit to specifically predict cellular response to PARP inhibitor treatments in the future.

Human cells are equipped to deal with ICL formations in the absence or presence of active DNA replication, where the latter is more deleterious to cells as repair of ICLs in S-phase generates toxic DSBs. Upon ICL recognition, ICL repair mechanisms, DDR signalling, and cell cycle checkpoints are triggered (Deans and West, 2011, Williams et al., 2013). We found that depletion of hMOB2 significantly sensitises human cancer cells to mitomycin C and cisplatin (Figures 5.1 and 5.2), two widely used ICL-generating chemotherapy drugs in the clinic. Considering that hMOB2-deficient cells have defective G1/S cell checkpoint activation upon DNA damage exposure (see Figure 3.7 in chapter-3 on page 144), it is possible that the majority of hMOB2-depleted cells treated with mitomycin C or cisplatin progress into S-phase and thereby promote the conversion of ICL lesions into replication-associated DSBs that are generally repaired by HRR (Deans and West, 2011, Kim and D'Andrea, 2012). This may help to explain why hMOB2-deficient cells display significantly enhanced sensitivity to mitomycin C or cisplatin (Figures 5.1 and 5.2).

In general, cells with HRR deficiency due to loss of essential HRR proteins such as BRCA2 or RAD51 are known to be highly sensitive to ICL-forming drugs (Moynahan et al., 2001, Kraakman-van der Zwet et al., 2002), as reported here upon hMOB2 knockdown. This notion is further supported by our finding indicating that hMOB2 is dispensable for NHEJ (see Figure 4.5 in chapter-4 on page 174) since NHEJ-deficient cells are not sensitive to ICL-inducing agents (Pace et al., 2010). Our theory that hMOB2-knockdown cells are HRR defective and hence are limited in DSB repair is further supported by the moderate sensitivity of hMOB2-deficient cells to IR (see Figure S5.1 in the Supplementary section, page 223), since IR typically induces direct DSBs



compared to ICL-forming agents (Helleday et al., 2008). NHEJ is the most dominant DSB repair mechanism, while the HRR pathway is actively employed to deal with more complex replication-associated DSBs in collaboration with other repair pathways (Helleday et al., 2008).

Notably, we also observed that hMOB2-depleted cells are sensitive to the topoisomerase II inhibitor doxorubicin, but not to etoposide or camptothecin (see Figure S5.2 in the Supplementary section, page 224). Topoisomerase I inhibitors such as camptothecin mostly induce SSBs and replication-associated DSBs (Wang, 2002, Helleday et al., 2008). However, since PARP1-deficient cells are hypersensitive to topoisomerase I inhibitors, it is most likely that the initial repair of camptothecin-induced DNA lesions is performed by the PARP-mediated BER pathway (Benafif and Hall, 2015). Therefore, it is not surprising that upon acute (1h) camptothecin treatment hMOB2-depleted cells survive normally (see Figure S5.2A-B in the Supplementary section, page 224). Nevertheless, we cannot exclude that hMOB2 deficiency may render cells sensitive to prolonged exposure to camptothecin that can cause replication fork collapse, and subsequently replication-associated DSBs (Pommier, 2006). In contrast to topoisomerase I inhibitors, topoisomerase II inhibitors such as doxorubicin or etoposide typically induce DSBs without any need for active DNA replication (Wang, 2002, Helleday et al., 2008). However, in contrast to etoposide, doxorubicin does not only block topoisomerase II activity but also causes other DNA lesions through DNA intercalation and ROS generation (Capranico et al., 1990, Pommier et al., 1991). Thus, it is not surprising that doxorubicin-induced DNA lesions are repaired slower than etoposide-induced DNA damage, suggesting that DSBs induced by doxorubicin are more cytotoxic than those induced by etoposide, since doxorubicin-induced DSBs most likely require intact HRR and NHEJ for repair (Schonn et al., 2011). In this regard, NHEJ restores DSBs faster than HRR and NHEJ routinely repairs the majority of DSBs (Iliakis et al., 1991, Goodarzi and Jeggo, 2013, Shibata et al., 2011), with the inhibition of DNA-PK-mediated NHEJ enhancing the cytotoxic effects of etoposide treatment in cancer cells (Zhao et al., 2006). Thus, etoposide-induced DSBs are very likely to be primarily corrected by

the NHEJ mechanism, which is not effected upon hMOB2 depletion (see Figure 4.5 in chapter-4 on page 174). Consequently, hMOB2-depleted cells are moderately sensitive to doxorubicin (see Figure S5.2C-D in the Supplementary section, page 224), but display not increased sensitivity to etoposide (see Figure S5.2E-F in the Supplementary section, page 224). A significant portion of DNA lesions induced by doxorubicin are very unlikely to be repaired in hMOB2-deficient cells, since HRR is predominantly employed to deal with doxorubicin-induced DNA damage (Spencer et al., 2008, Hawtin et al., 2010), and hMOB2-depleted cells are HRR-deficient (see Figure 4.4 in chapter-4 on page 173), hence hMOB2 knockdown cells struggle to tolerate doxorubicin-induced DNA damage.

Compared to the DNA-damaging treatments mentioned above, hMOB2-deficient cells exhibited higher sensitivity to ICL-inducing drugs (Figures 5.1 and 5.2). The FA pathway is specifically significant in replication-dependent ICL repair, therefore FA-deficient cells show hypersensitivity to ICL-forming drugs (Williams et al., 2013, Clauson et al., 2013). In this regard, after ICL recognition, unhooking of the ICL adduct is required for the remaining repair processing of DNA lesions by other DNA repair pathways such as HRR (Williams et al., 2013, Clauson et al., 2013). The data presented in Figure 5.3 show that hMOB2 deficiency does not affect the unhooking process of ICL-formations, since hMOB2-proficient and -deficient cells have comparable unhooking kinetics. Additionally, co-depletion of hMOB2 and FANCD2 reveals significantly higher cytotoxicity upon mitomycin C treatment compared to single depletion of each component (Figure 5.4). Notably, this synthetic lethal interaction between hMOB2- and FANCD2-regulated pathways was also observed upon co-depletion of hMOB2 and FANCD2 without any exogenous DNA damage (Figure 5.4B). These data collectively show that hMOB2 functions in ICL repair independent of the FA pathway, with hMOB2 most likely contributing to the repair of ICL-induced lesions by supporting HRR-mediated repair of replication-associated DSBs that form after ICL unhooking in S-phase (Deans and West, 2011, Williams et al., 2013, Kim and D'Andrea, 2012). However, in this regard, one should note that hMOB2 may contribute to ICL repair on an additional level. Yata et al.

(2014) recently showed that Ser14 phosphorylation of RAD51 stimulates the restart of DNA replication once the blockage is removed (Yata et al., 2014). Considering that hMOB2 supports Ser14 phosphorylation of RAD51 (see Figure 4.8 in chapter-4 on page 180), we are therefore tempted to speculate that once the ICL-adduct is detached from the replication fork by the FA pathway, hMOB2-deficient cells may then fail to promote the restart of DNA replication.

The synthetic lethality observed between hMOB2 and FANCD2 inspired us to test whether hMOB2 knockdown confers synthetic lethal interactions with other DDR pathways. This revealed that hMOB2-depleted cells are sensitive to NHEJ inhibition in the absence of exogenous DNA damage (Figure 5.5), suggesting that hMOB2-knockdown cells with deficient HRR can partly rely on NHEJ as a compensatory pathway to repair spontaneously induced DSBs. Moreover, increased cytotoxic radiosensitivity was observed when NHEJ is inhibited in hMOB2-knockdown cells (Figure 5.6). This revealed that hMOB2-depleted cells with defective HRR are hyperdependent on NHEJ upon exposure to intensive DNA damage.

In general, human cancer cells with HRR deficiency display remarkable hypersensitivity to PARP inhibition (Bryant et al., 2005, Farmer et al., 2005, Wang et al., 2016, Lord and Ashworth, 2016). Bryant and Helleday (2006) proposed already a decade ago that upon PARP inhibition cells accumulate unrepaired spontaneous SSBs, which are converted to DSBs during DNA replication owing to collapsed replication forks (Bryant and Helleday, 2006). Thus, PARP-inhibited cells rely on functional HRR to repair replication-associated DSBs in order to prevent the accumulation of unrepaired lethal DSBs (Veuger and Curtin, 2014, Helleday, 2010, Lord and Ashworth, 2016). In this regard, we discovered that hMOB2 deficiency significantly renders human cancer cells highly sensitive to the PARP inhibitors olaparib, rucaparib, and veliparib (Figures 5.8, 5.9, 5.10, and 5.12). Furthermore, hMOB2 protein levels seem to be negatively correlated with PARP inhibitor sensitivity in human ovarian cancer cell lines without any manipulations of endogenous hMOB2 (Figure 5.11). Considerably, hMOB2 knockdown also significantly increased the radiosensitivity of PARP-inhibited

cells (Figure 5.13). Taken together, our data presented in Figures 5.8 to 5.13 strongly suggest that hMOB2 protein levels can be of help to predict treatment responses to PARP inhibition.

It is noteworthy that hMOB2 knockdown impaired Ser14 phosphorylation of RAD51 (see Figure 4.8 in chapter-4 on page 180), which can help to explain the PARP-sensitivity of hMOB2-depleted cells. More specifically, Esashi and colleagues found that PLK1-dependent Ser14 phosphorylation of RAD51 promotes resistance to PARP inhibition by olaparib (Yata et al., 2012). In line with this report, Bartek and his team have recently identified TOPBP1 (topoisomerase IIb-binding protein 1) as a key determinant of PARP inhibitor sensitivity, with TOPBP1 directly interacting with PLK1 to promote PLK1-dependent Ser14 phosphorylation of RAD51 for RAD51 loading onto ssDNA (Moudry et al., 2016). However, additional investigations are now required to decipher how hMOB2 supports HRR to determine PARP inhibitor sensitivity through molecular processes involving PLK1-mediated Ser14 phosphorylation of RAD51.

In this regard, we cannot exclude the possibility that other aspects of the functions of hMOB2 may participate in HRR and PARP sensitivity, in addition to the regulation of RAD51 phosphorylation and loading. For example, we found that hMOB2 directly interacts with RAD50, a key component of the MRN DNA damage sensor complex (Rupnik et al., 2010), and can regulate MRN recruitment towards damaged chromatin (see Figures 4.1 and 4.2 in chapter-4 on pages 166 and 168). In this respect, MRN inactivation can render human breast cancer cells more sensitive to PARP inhibition (Oplustilova et al., 2012). Furthermore, a recent study showed that loss of RAD50 (either via RNAi or copy number deletion) significantly enhances PARP inhibitor-sensitivity of human ovarian cancer cells with wild-type *BRCA1/2* (Zhang et al., 2016), thereby indicating RAD50 as a predictive biomarker for a BRCAness phenotype and PARP inhibitor sensitivity. Consequently, the observed link between hMOB2 and RAD50 may be of functional relevance to understand how hMOB2 knockdown renders cancer cells hypersensitive to PARP inhibition.

We also discovered that hMOB2 depletion impairs ATM-mediated DDR signalling and recruitment of activated ATM onto damaged DNA (see Figures 4.2 and 4.3 in chapter-4 on pages 168 and 170). Intriguingly, ATM-deficient breast cancer cells are highly sensitive to olaparib (Gilardini Montani et al., 2013), and the olaparib-sensitivity of human gastric cancer cells negatively correlates with ATM protein levels (Kubota et al., 2014). Therefore, in addition to the role of hMOB2 in supporting RAD51 phosphorylation and loading, one also has to consider other possibilities to fully understand the hypersensitivity of hMOB2-depleted cells to PARP inhibitors. These possibilities include links between hMOB2, the MRN complex and the central DDR kinase ATM.

## **Acknowledgements**

I would like to thank Dr. Victoria Spanswick and Prof. John Hartley from the UCL Cancer Institute (London, UK) for their collaboration to perform Comet assays assessing ICL-formations (Figure 5.3). I would also like to thank Dr. Christina Gewinner from Eisai-UCL (London, UK) for providing a collection of ovarian cancer cell lines (Figure 5.11).

## 5.5 Supplementary information

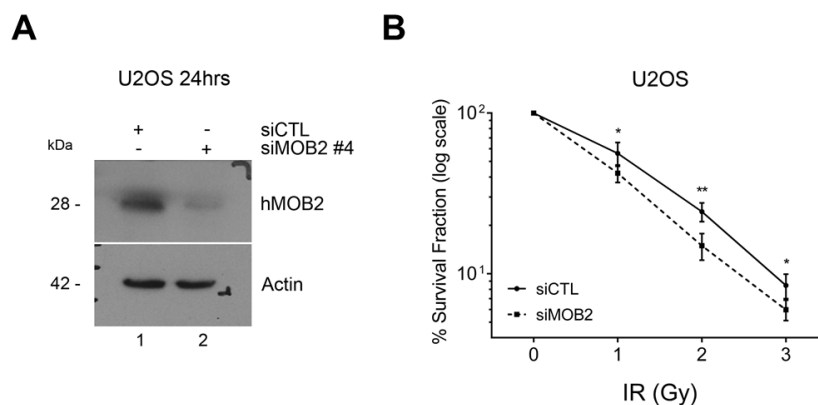


**Figure S5.1**

### **hMOB2 promotes cell survival response to IR-induced DNA damage.**

(A) Immunoblotting with indicated antibodies of U2OS cell lysates from cells transiently transfected for 24 h with indicated siRNAs. (B) Clonogenic survival of U2OS cells upon hMOB2 knockdown (siMOB2) compared with controls (siCTL) in response to ionising radiation (IR). Quantifications are shown as a percentage of colonies formed after treatment with indicated doses (n=4). Results were corrected according to plating efficiencies of the corresponding untreated controls. *p*-values are: 1 Gy = 0.039, 2 Gy = 0.005, 3 Gy = 0.035. Results are presented as mean of replicates and error bars as mean  $\pm$  standard error of mean (SEM), statistical significance was calculated using the one-tailed unpaired Student's *t*-test.

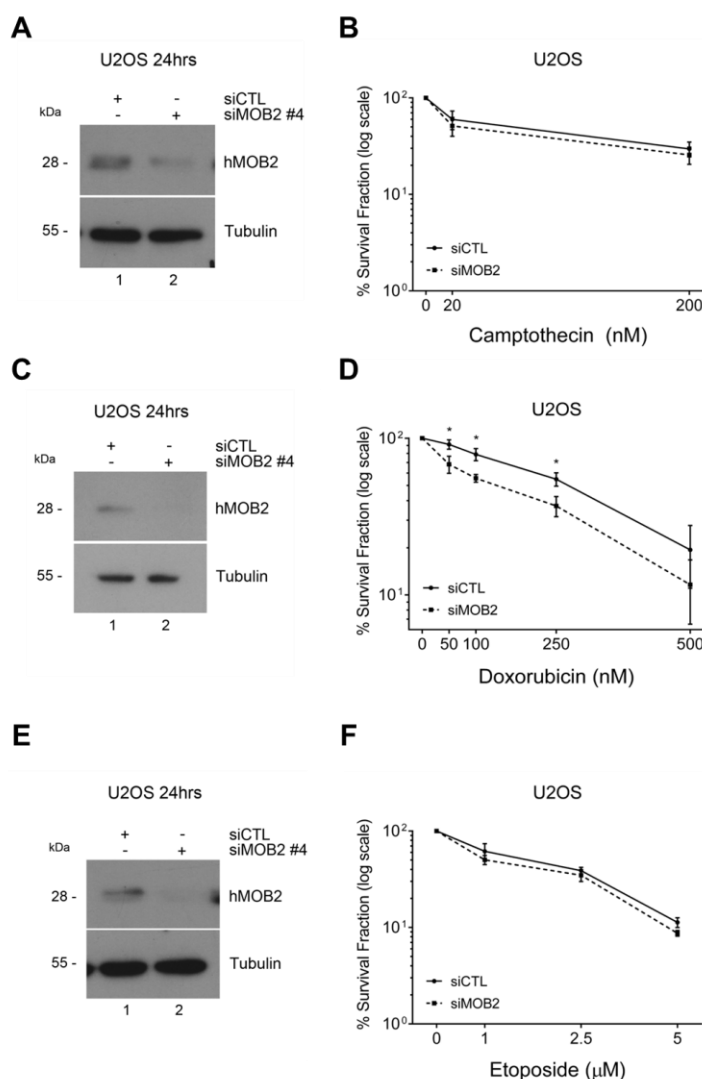


**Figure S5.2**

**hMOB2 deficiency shows different cellular response against DNA-damaging topoisomerase inhibitors.**

(A) Immunoblotting with indicated antibodies of U2OS cell lysates from cells transiently transfected for 24 h with indicated siRNAs. (B) Clonogenic survival of U2OS cells upon hMOB2 knockdown (siMOB2#4) compared with controls (siCTL) in response to DMSO or camptothecin treatment (1 h). Quantifications are shown as a percentage (in log scale) of colonies formed after treatment with indicated doses ( $n=3$ ). Results were corrected according to plating efficiencies of the corresponding untreated controls. (C) Immunoblotting of U2OS cell lysates as explained in A. (D) Clonogenic survival of U2OS cells treated with or without doxorubicin as explained in B ( $n=4$ ).  $p$ -values are: 50 nM=0.037, 100 nM=0.018, 250 nM=0.029, 500 nM=0.231. (E) Immunoblotting of U2OS cell lysates as explained in B. (F) Clonogenic survival of U2OS cells treated with DMSO or etoposide as explained in B ( $n=3$ ). All results are presented as mean of replicates and error bars as mean  $\pm$  standard error of mean (SEM), statistical significance was calculated using the one-tailed unpaired Student's  $t$ -test.



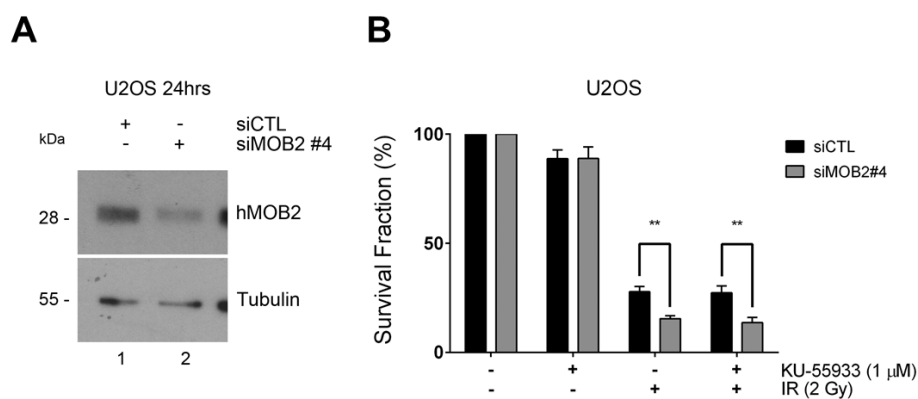


**Figure S5.3**

**hMOB2 knockdown does not enhance radiosensitivity of ATM-inhibited cells (in support of Figure 5.7).**

(A) Immunoblotting with indicated antibodies of U2OS cell lysates from cells transiently transfected for 24 h with indicated siRNAs. (B) Clonogenic survival of U2OS cells upon hMOB2 knockdown (siMOB2#4) compared with controls (siCTL). After 24 h of transfection, cells were pre-treated with DMSO or 1  $\mu$ M ATM inhibitor (KU-55933) followed by ionising radiation (IR, 2 Gy) treatment. Quantifications are shown as a percentage of colonies formed after treatment with indicated doses (n=3). Results were corrected according to plating efficiencies of the corresponding untreated controls. *p*-values are: 2 Gy, MOB2=0.003, MOB2/ATMi=0.006. Results are presented as mean of replicates and error bars as mean  $\pm$  standard error of mean (SEM), statistical significance was calculated using the one-tailed unpaired Student's *t*-test.

## Chapter 6      Final conclusions

The DNA damage response (DDR) is essential to maintain genomic integrity, and thereby to prevent tumorigenesis (Ciccia and Elledge, 2010). Upon inefficient DDR, persistence of unrepaired DNA damage can prompt cells to accumulate mutations that induce cell death, senescence, or cancer, with the gradual accumulation of double-strand breaks (DSBs) being primarily cytotoxic (Lindahl and Barnes, 2000, Khanna and Jackson, 2001, Vilenchik and Knudson, 2003). It is estimated that thousands of single-strand breaks (SSBs) and nearly 50 DSBs are generated endogenously per cell per day (Vilenchik and Knudson, 2003). As an essential DSB sensor, the MRN complex binds to and thereby stabilises broken DSB ends, and also stimulates the ATM signalling to control cell cycle checkpoints and DSB repair pathways (Rupnik et al., 2010, Shiloh and Ziv, 2013, Stracker et al., 2013, Lee and Paull, 2004, Lee and Paull, 2005a).

Homologous recombination repair (HRR) and non-homologous end joining (NHEJ) are the two main DSB repair pathways (Ciccia and Elledge, 2010, Jasin and Rothstein, 2013, Goodarzi and Jeggo, 2013). Specifically, HRR is employed during late S and G2 phases of the cell cycle using sister chromatids in order to repair damaged chromatin (Krejci et al., 2012, Jasin and Rothstein, 2013) while NHEJ functions throughout all cycle stages (Goodarzi and Jeggo, 2013). Cancer cells rely on a variety of non-oncogenic compensatory DDR pathways to ensure their survival (Ciccia and Elledge, 2010, Helleday et al., 2008, Helleday, 2010, Lord et al., 2015). In this regard, the concept of synthetic lethality is the targeting of non-oncogenic compensatory DDR pathways to achieve more selective and efficient cancer treatments (Lord et al., 2015, Veuger and Curtin, 2014). For example, poly (ADP-ribose) polymerase (PARP) inhibitors can inactivate SSB repair that is mainly mediated by PARP-dependent base excision repair (BER). Consequently, PARP inhibitions causes the accumulation of SSBs and ultimately the conversion of SSBs into DSBs in replicating cells (Ciccia and Elledge, 2010, Lord et al., 2015, Lord and Ashworth, 2016, Jackson and Helleday, 2016). HRR-proficient cells can repair such replication-associated

DSBs, while HRR-deficient cells fail to deal with DSBs, and therefore PARP inhibitors can selectively eliminate HRR-deficient cancer cells (Bryant et al., 2005, Farmer et al., 2005, Wang et al., 2016, Lord et al., 2015, Lord and Ashworth, 2016).

Significantly, a number of PARP inhibitors have been developed and are currently under clinical investigation for cancer treatment (Helleday et al., 2008, Wang et al., 2016). More specifically, olaparib (Lynparza, AstraZeneca) is the first FDA-approved PARP inhibitor for treatment of ovarian cancer patients with *BRCA1/2* mutations (Deeks, 2015, Wang et al., 2016). Additional phase III clinical trials in breast, pancreatic and gastric cancer are currently being conducted with olaparib (Deeks, 2015, Wang et al., 2016). Notably, considering that HRR-deficient cells with wild-type *BRCA1/2* are also reported to be sensitive to PARP inhibition (referred as a BRCAness phenotype) (Lord and Ashworth, 2016, Wang et al., 2016, Drew, 2015), the discovery and characterisation of novel HRR regulators is important to improve the future stratification of cancer patients for the suitability of treatments with PARP inhibitors.

Components of the Hippo pathway can function in collaboration with other signalling cascades in different cellular systems (Cottini et al., 2014, Levy et al., 2008, Strano and Blandino, 2007, Reuven et al., 2013). For instance, it has been showed that Hippo core components can play a major role in the induction of apoptosis upon DNA damage by stimulating the association of YAP with p73 (identified as a p53 family member). Through the activation of ATM-RASSF1A-MST2-LATS1 cascade, the YAP-p73 interaction can promote the transcriptional activation of pro-apoptotic genes such as *BAX* and *PUMA* in response to DNA damage (Hamilton et al., 2009, Strano et al., 2001), highlighting the importance of RASSF1A-mediated apoptotic response of the Hippo pathway in response DNA damage. Furthermore, LATS2 is phosphorylated at Ser408 by the CHK1 kinase upon replication stress and the activated LATS2 phosphorylates a key p53 regulator ASSP1 (apoptosis-stimulating protein of p53-1), causing ASSP1 translocation to the nucleus. The active LATS2/ASSP1/p53 complex binds to chromatin and promotes the transcriptional regulation of key apoptotic genes

(Sullivan and Lu, 2007, Pefani and O'Neill, 2016). Chiyoda et al. (2012) reported the LATS1-mediated G2/M transition upon DNA damage-induced inactivation of the PLK1 kinase. In response to DSB induction, the activated ATM/RASSF1A/LATS1 complex leads to phosphorylation of MYPT1 (mysin phosphatase target subunit 1) phosphatase, which regulates PLK1-dephosphorylation via PP1C (protein phosphatase 1 c). The dephosphorylated PLK1 kinase becomes inactivated and causes the G2/M checkpoint activation in order to restrict the mitotic entry upon DNA damage induction (Chiyoda et al., 2012). Additionally, Pefani et al. (2014) recently demonstrated that upon stalled fork progression, the ATR-RASSF1A-MST2-LATS1 cascade controls CDK activity and BRCA2 phosphorylation, thereby stabilising RAD51 nucleoprotein filaments to support HRR, which demonstrated that the Hippo pathway plays an important role in the maintenance of genome stability (Pefani et al., 2014). Taken together, diverse Hippo components can function in cellular responses to maintain genome stability or to eliminate damaged cells from the cell pool (Pefani and O'Neill, 2016), hence studies into expanding our understanding of DDR-related functions of Hippo members are warranted.

We describe herein novel functions of hMOB2 that supports DDR and DSB repair by HRR as illustrated in Figure 6.1. In chapter-3, we demonstrate that in proliferating untransformed human cells hMOB2 is required (i) to prevent spontaneous accumulation of unrepaired DSBs and (ii) to activate the G1/S cell cycle checkpoint in response to exogenous DNA damage. In chapter-4, we show that hMOB2 (i) directly interacts with RAD50, (ii) supports MRN-ATM recruitment to damaged chromatin, (iii) ATM-mediated DDR signalling, and (iv) RAD51 phosphorylation and thereby RAD51-mediated DSB repair by HRR. In chapter-5, we report that hMOB2 significantly supports cancer cell survival in response to (i) ICL-inducing agents and (ii) PARP inhibitors in human cancer cells.

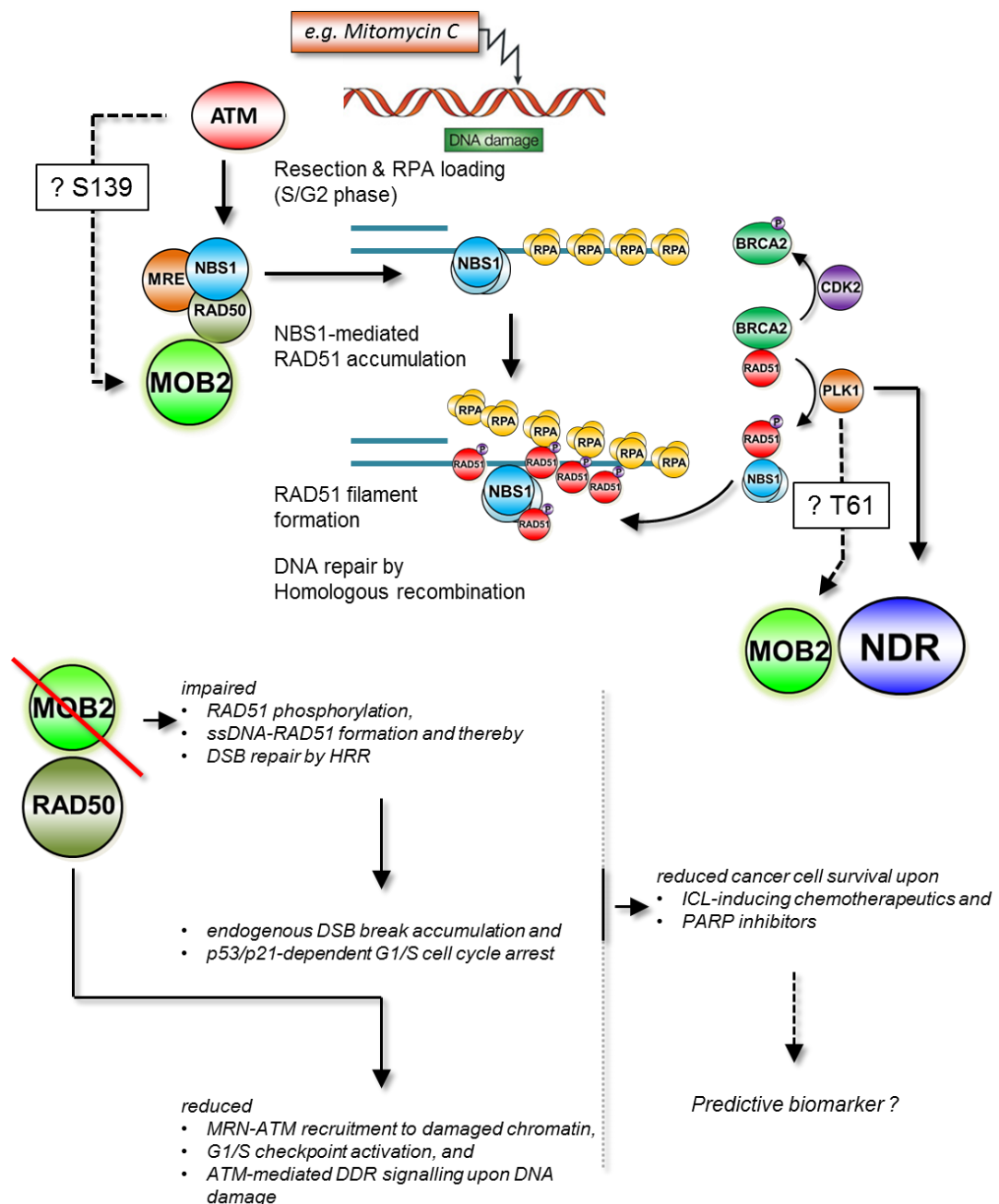


**Figure 6.1**

**The working model of regulation of DNA damage response and repair by hMOB2.**

We showed that hMOB2 interacts with the MRN component RAD50 and hMOB2-depletion impairs MRN recruitment to damaged DNA. The other MRN component NBS1 is reported to be significant in phospho-specific recruitment of RAD51 to resected ssDNA region, which initially depends on the PLK1-mediated RAD51 phosphorylation at Ser14. We also found that hMOB2 depletion compromises RAD51 phosphorylation at Ser14, which overall may explain the impaired HRR in hMOB2-deficient cells since RAD51 phosphorylation and recruitment to 3' ssDNA tails is essential in DSB repair by HRR.

In a nutshell, we discovered that hMOB2 is required to support distinct, but interlinked, events regulating cell cycle progression, DDR signalling and DSB repair. In the absence of exogenous DNA damage inducers, hMOB2-deficient cells accumulate unrepaired spontaneous DSBs, which trigger a p53/p21-dependent G1/S cell cycle arrest. The initial elicitor is likely the distorted recruitment of MRN to damaged chromatin, which consequently can impair efficient DNA repair. However, the remaining chromatin-bound MRN seems to be sufficient to trigger DDR signalling for a transient G1/S cell cycle arrest without exogenously induced DNA damage, although upon prolonged exposure to such DNA damage the G1/S checkpoint is defective upon hMOB2 knockdown. In addition to impaired MRN functionality, we also discovered that compromised RAD51 phosphorylation and RAD51 loading onto ssDNA can be observed in hMOB2-depleted cells. Thus, defective RAD51 functionality may also be a reason for the accumulation of unrepaired DSB in hMOB2-deficient cells. Therefore, more research is required to reveal the main source of DSB accumulation in untransformed human cells upon hMOB2 knockdown. A sheer volume of studies suggest that components of the HRR mechanism may also have a repair-independent regulatory function in nascent DNA protection during replication fork disruption (Schlacher et al., 2011). Considering that hMOB2 supports RAD51 recruitment to damaged chromatin and RAD51 is reported to have also repair-independent nascent DNA protection role in order to promote continues DNA synthesis (Schlacher et al., 2012, Hashimoto et al., 2010), hMOB2 may need to be investigated whether it promotes DNA end protection by supporting continues RAD51 loading to stalled replication forks in order to prevent replication fork collapse, thereby DSB induction. A combination of immunofluorescence and the DNA fibre experiments employing short hydroxyurea treatments (Pefani et al., 2014) that stalls replication fork progression would help us to understand the role of hMOB2 in the protection of nascent DNA. In summary, our findings suggest that hMOB2 knockdown triggers molecular alterations that allow the

accumulation of endogenous DNA damage, followed by a G1/S proliferation arrest. Therefore, future studies are warranted to decipher the initiation and progression of the accumulated DSBs in hMOB2-knockdown cells under normal physiological settings.

Upon exposure to high levels of exogenously induced DNA damage hMOB2 is needed for the activation of the G1/S and G2/M cell cycle checkpoints and ATM-mediated DDR signalling. We report here a defective G1/S checkpoint in hMOB2-depleted cells upon exposure to high DNA damage levels (Gomez et al., 2015), and Cotta-Ramusino et al. (2011) showed that hMOB2-depleted cells may have impaired activation of the IR-induced G2/M cell cycle checkpoint (Cotta-Ramusino et al., 2011). Most likely, these DDR cell cycle checkpoint defects and impaired ATM signalling are a consequence of impaired MRN functionality upon hMOB2 depletion, since hMOB2 is needed to support MRN functionality (Gomez et al., 2015) and MRN deficiencies can weaken the G1/S and G2/M cell cycle checkpoints (Rupnik et al., 2010, Stracker and Petrini, 2011, Williams et al., 2010). Moreover, hMOB2 is possibly also required for efficient ATM phosphorylation of other substrates, besides NBS1 and SMC1, since ATM has potentially more than 700 substrates (Shiloh and Ziv, 2013). Therefore, since MRN exists in diverse conformational and assembly states (Rupnik et al., 2010, Stracker and Petrini, 2011, Williams et al., 2010), future structural and biochemical studies are warranted to further dissect hMOB2 as facilitator of MRN recruitment to DNA damaged chromatin and as an adaptor for ATM substrates. Particular attention will be paid to dissecting the RAD50/hMOB2 interaction in the context of our Y2H mapping data (Gomez et al., 2015) and the unique architecture of RAD50, which is essential to support MRE11/RAD50 binding to DNA via MRE11's DNA binding motifs and RAD50's ABC domains, while DNA break tethering is achieved through RAD50's zinc hook domain supported by RAD50's coiled-coil structure (Rupnik et al., 2010, Stracker and Petrini, 2011, Williams et al., 2010).

We further discovered that hMOB2 depletion impairs phosphorylation of RAD51, which affected RAD51 loading onto ssDNA and ultimately DSB repair by RAD51-mediated HRR. Proteins such as BRCA2 and RAD51,

which are involved in the homology search and strand invasion/exchange steps of HRR, have been defined as the downstream regulators of HRR (Jasin and Rothstein, 2013). RAD51-mediated nucleofilament formation with ssDNA is an essential step of HRR (Jasin and Rothstein, 2013, Krejci et al., 2012). Significantly, *RAD51* gene disruption results in early embryonic lethality (Lim and Hasty, 1996, Tsuzuki et al., 1996), which is very likely due to compromised repair of replication-dependent DSBs in rapidly dividing embryonic cells, highlighting the indisputable importance of RAD51-regulated HRR for the repair of replication-associated DSBs. This notion is further supported by the observation that the sensitivity of HRR-deficient cells to ICL-inducing agents is mostly caused by replication-associated DSBs (Helleday et al., 2008, Helleday, 2010, Ciccio and Elledge, 2010). Collectively, impaired RAD51 function can cause genome instability, which highlights the importance of hMOB2 regarding PLK1-mediated RAD51 phosphorylation and subsequent nucleoprotein stabilisation.

PLK1 directly phosphorylates RAD51 at Ser14 site in a cell cycle and DNA damage dependent manner (Yata et al., 2012). The phosphorylation of RAD51 promotes RAD51 recruitment to damaged chromatin sites through its interaction with the FHA region of NBS1, which appears to be a crucial step for HRR (Yata et al., 2012) (Figure 6.1). We discovered that hMOB2 deficiency impairs PLK1-mediated RAD51 phosphorylation at Ser14, which can help to explain why hMOB2-deficient cell display compromised RAD51 loading onto ssDNA. However, future research is needed to reveal how hMOB2 supports PLK1-mediated RAD51 phosphorylation. In this regard, it was recently shown that CDK-elicited BRCA2 phosphorylation at Thr77 stimulates PLK1 binding to BRCA2, which in turn catalyses RAD51 phosphorylation at Ser14 (Yata et al., 2014). Therefore, it would be in particular interesting to test the status of Thr77 phosphorylation of BRCA2 in hMOB2-depleted cells.

In addition, PLK1-dependent phosphorylation of NDR1 was recently revealed as a switch to regulate hMOB1 vs. hMOB2-binding to NDR1 in the context of spindle orientation during mitosis (Yan et al., 2015). We initially reported that hMOB2 may function as a DDR protein independently of the



NDR1/2 kinase (Gomez et al., 2015). However, since the NDR1/2 kinases were recently linked to different aspects of the DDR (Park et al., 2015, Enomoto et al., 2013) and compensatory mechanisms were reported upon NDR1 or NDR2 loss-of-functions (Schmitz-Rohmer et al., 2015, Cornils et al., 2010), further research is warranted to dissect whether PLK1-regulated NDR signalling can contribute to DDR processes through hMOB2.

Noteworthy, we consistently observed that total hMOB2 protein levels are gradually increased in hMOB2-proficient cells in response to DNA damage (for example see Figure 4.8 in chapter-4 on page 180). In addition, we also detected that hMOB2 migrated at slower mobility in SDS-PAGE gels in response to DNA damage (for example see Figure 4.8 in chapter-4 on page 180). Thus, we are tempted to speculate that hMOB2 is post-translationally modified upon DNA damage, which may affect the half-life of hMOB2 proteins. Certainly, it will be important to understand the underlying mechanism(s) in order to fully understand the roles of hMOB2 in the management of cellular response to DNA damage. In this regard, we performed an online database search using Scansite (Obenauer et al., 2003) to identify possible post-translational modifications of hMOB2, in addition to the already described modification of Lys131 (Wagner et al., 2012). Significantly, this analysis predicts Ser139 and Thr61 of hMOB2 as potential phosphorylation sites by the ATM and PLK1 kinases, respectively. However, future research is now needed to decipher whether hMOB2 is subjected to any functionally relevant post-translational modification in response to DNA damage. We are confident that the RNAi rescue set up as developed in the context of olaparib sensitivity (please see Figure 5.12 in chapter-5 on page 214) will be of great help to define the possible importance of post-translational modifications of hMOB2 in the DRR.

Given that cell survival in response to DNA damage relies on proper cell cycle control, the cell cycle checkpoint interpretations mentioned above can also help to explain why hMOB2 contributes to cell survival upon exposure to DNA damage. Specifically, the survival in response to ICL-inducing agents and PARP inhibitors is of relevance in this context. Compared with controls, hMOB2-deficient cells challenged with ICL-inducing

drugs or PARP inhibitors very likely bypass the G1/S cell cycle checkpoint and therefore expose their DNA lesions to active DNA replication, which in turn can introduce deleterious replication-associated DSBs. We believe that this hypothesis is supported by the observed mitomycin C and cisplatin-sensitivities of hMOB2-depleted cells. More specifically, mitomycin C induces only minimal perturbations to the DNA structure while cisplatin is one of the most DNA-distorting ICL agents (Williams et al., 2013). Therefore, it is possible that the majority of hMOB2-knockdown cells treated with mitomycin C, compared to those treated with cisplatin, progress into S-phase and thereby promote the conversion of ICL lesions into replication-associated DSBs that are generally repaired by HRR (Ciccio and Elledge, 2010, Deans and West, 2011, Kim and D'Andrea, 2012, Williams et al., 2013). As a result, since hMOB2-knockdown cells have significantly decreased HRR efficiency, cells struggle to deal with these replication-induced DSBs and consequently undergo apoptosis. Nevertheless, we have only begun to understand how hMOB2 exactly supports cell survival through cell cycle checkpoint activation and HRR upon exposure to DNA damage. Thus, future studies are warranted to understand how hMOB2 regulates and wires cell cycle checkpoints and HRR activities.

Last, but not least, it is important to note that the human *MOB2* gene appears to display loss of heterozygosity (LOH) in more than 50% of testicular, bladder, cervical and ovarian carcinomas as illustrated in Table 6.1 below (Cerami et al., 2012), hence, hMOB2 might represent a novel tumour suppressor promoting the DDR response. For instance, approximately 50% of ovarian cancer cases are known to bear HRR-deficiency and display sensitivity to PARP inhibition (Drew, 2015). However, only a small portion of ovarian cancers are classified as *BRCA1* or *BRCA2* germline mutant (Venkitaraman, 2002, Walsh and Hodeib, 2016). Therefore, HRR-deficiency is very unlikely to be limited with germline *BRCA* mutations, underscoring the importance of discovering additional HRR components which may be utilised as therapeutic targets or as predictive markers for patient stratification. In this regard, future studies are therefore warranted to explore in yet to be developed animal models the consequences of MOB2 deficiency for tumour

formation and the response to DNA damaging treatments. Considering that at least 30% of cancer cell lines seem to display LOH of the *MOB2* gene (Cerami et al., 2012), tissue culture approaches may be able to complement these upcoming experiments. Although hMOB2 is unlikely to serve as good drug target, future studies are also needed to investigate whether hMOB2 expression may offer a means to stratify patients for ICL-forming drugs and PARP inhibitors, with the aim of potentially reducing the frequency of cancer therapy resistance (Holohan et al., 2013), in addition to further expanding our understanding of the role of hMOB2 in human cell biology and disease.

**Table 6-1: Copy number variations of the *MOB2* locus in human cancers as collated in cBioPortal (Cerami et al., 2012).**

Cancer	Heterozygous loss	Homozygous loss	Gain	Amplification
Testicular germ cell cancer	91/149 (61%)	0	11/149 (7.4%)	0
Ovarian serous cystadenocarcinoma	175/316 (55%)	2/316 (0.6%)	42/316 (13%)	0
Bladder urothelial carcinoma	67/127 (53%)	1/127 (1%)	11/127 (9%)	0
Bladder cancer	67/127 (52.8%)	0	11/127 (8.7%)	0
Uterine carcinosarcoma	27/56 (48%)	1/56 (2%)	6/56 (11%)	0
Esophageal carcinoma	42/92 (46%)	1/92 (1%)	8/92 (9%)	0
Melanoma	89/278 (32%)	0	29/278 (10%)	2/278 (0.7%)
Head and neck carcinoma	87/279 (31%)	2/279 (1%)	32/279 (11%)	0
Adrenocortical carcinoma	27/88 (31%)	1/88 (1%)	6/88 (7%)	0
Lung squamous cell carcinoma	53/177 (30%)	1/178 (0.6%)	15/178 (8%)	0
Breast invasive carcinoma	364/1456 (25%)	14/1456 (1%)	165/1456 (11%)	4/1456 (0.2%)

Pancreatic cancer	25/109 (23%)	4/109 (4%)	34/109 (31%)	15/109 (14%)
Sarcoma	45/207 (22%)	0	4/207 (2%)	2/207 (1%)
Glioblastoma	54/281 (19%)	3/281 (1%)	5/281 (2%)	0
Metastatic prostate cancer	28/150 (19%)	0	10/150 (7%)	0
Brain lower grade glioma	51/283 (18%)	11/283 (4%)	12/283 (4%)	2/283 (1%)
Stomach adenocarcinoma	47/287 (16%)	0	35/287 (12%)	2/287 (0.7%)
Kidney chromophobe	10/65 (15%)	0	15/65 (23%)	0
Access date: 30 August 2016				

## Chapter 7      Bibliography

- ADAMO, A., COLLIS, S. J., ADELMAN, C. A., SILVA, N., HOREJSI, Z., WARD, J. D., MARTINEZ-PEREZ, E., BOULTON, S. J. & LA VOLPE, A. 2010. Preventing Nonhomologous End Joining Suppresses DNA Repair Defects of Fanconi Anemia. *Molecular Cell*, 39, 25-35.
- ADAMS, D. J., WAHL, M. L., FLOWERS, J. L., SEN, B., COLVIN, M., DEWHIRST, M. W., MANIKUMAR, G. & WANI, M. C. 2006. Camptothecin analogs with enhanced activity against human breast cancer cells. II. Impact of the tumor pH gradient. *Cancer Chemother Pharmacol*, 57, 145-154.
- AGARWAL, M. L., TAYLOR, W. R., CHERNOV, M. V., CHERNOVA, O. B. & STARK, G. R. 1998. The p53 Network. *Journal of Biological Chemistry*, 273, 1-4.
- ALBERTS, B. 2008. *Molecular biology of the cell*, New York, Garland Science.
- ANDREASSEN, P. R. & REN, K. Q. 2009. Fanconi Anemia Proteins, DNA Interstrand Crosslink Repair Pathways, and Cancer Therapy. *Current Cancer Drug Targets*, 9, 101-117.
- BAIN, A. L., MASTROCOLA, A. S., TIBBETTS, R. S. & KHANNA, K. K. 2001. DNA Damage Response: From Tumourigenesis to Therapy. eLS. John Wiley & Sons, Ltd.
- BAKKENIST, C. J. & KASTAN, M. B. 2003. DNA damage activates ATM through intermolecular autophosphorylation and dimer dissociation. *Nature*, 421, 499-506.
- BAKKENIST, C. J. & KASTAN, M. B. 2004. Initiating cellular stress responses. *Cell*, 118, 9-17.
- BARTEK, J., BARTKOVA, J. & LUKAS, J. 2007. DNA damage signalling guards against activated oncogenes and tumour progression. *Oncogene*, 26, 7773-7779.
- BARTEK, J., FALCK, J. & LUKAS, J. 2001. CHK2 kinase--a busy messenger. *Nat Rev Mol Cell Biol*, 2, 877-86.
- BARTEK, J. & LUKAS, J. 2003. Chk1 and Chk2 kinases in checkpoint control and cancer. *Cancer Cell*, 3, 421-429.
- BARTEK, J. & LUKAS, J. 2007. DNA damage checkpoints: from initiation to recovery or adaptation. *Curr Opin Cell Biol*, 19, 238-45.
- BATCHELOR, E., LOEWER, A. & LAHAV, G. 2009. The ups and downs of p53: understanding protein dynamics in single cells. *Nat Rev Cancer*, 9, 371-7.
- BECKER, E., MEYER, V., MADAoui, H. & GUEROIS, R. 2006. Detection of a tandem BRCT in Nbs1 and Xrs2 with functional implications in the DNA damage response. *Bioinformatics*, 22, 1289-1292.
- BENAFIF, S. & HALL, M. 2015. An update on PARP inhibitors for the treatment of cancer. *Onco Targets Ther*, 8, 519-28.
- BICHSEL, S. J., TAMASKOVIC, R., STEGERT, M. R. & HEMMINGS, B. A. 2004. Mechanism of activation of NDR (nuclear Dbf2-related) protein kinase by the hMOB1 protein. *Journal of Biological Chemistry*, 279, 35228-35235.
- BIEGING, K. T., MELLO, S. S. & ATTARDI, L. D. 2014. Unravelling mechanisms of p53-mediated tumour suppression. *Nat Rev Cancer*, 14, 359-70.
- BODNAR, A. G., OUELLETTE, M., FROLKIS, M., HOLT, S. E., CHIU, C. P., MORIN, G. B., HARLEY, C. B., SHAY, J. W., LICHTSTEINER, S. & WRIGHT, W. E. 1998. Extension of life-span by introduction of telomerase into normal human cells. *Science*, 279, 349-352.

- BOTHOS, J., TUTTLE, R. L., OTTEY, M., LUCA, F. C. & HALAZONETIS, T. D. 2005. Human LATS1 is a mitotic exit network kinase. *Cancer Research*, 65, 6568-6575.
- BRADNER, W. T. 2001. Mitomycin C: a clinical update. *Cancer Treatment Reviews*, 27, 35-50.
- BROWN, J. S., KAYE, S. B. & YAP, T. A. 2016. PARP inhibitors: the race is on. *British Journal of Cancer*, 114, 713-715.
- BRUMMELKAMP, T. R., BERNARDS, R. & AGAMI, R. 2002. A system for stable expression of short interfering RNAs in mammalian cells. *Science*, 296, 550-3.
- BRYANT, H. E. & HELLEDAY, T. 2006. Inhibition of poly (ADP-ribose) polymerase activates ATM which is required for subsequent homologous recombination repair. *Nucleic Acids Research*, 34, 1685-1691.
- BRYANT, H. E., SCHULTZ, N., THOMAS, H. D., PARKER, K. M., FLOWER, D., LOPEZ, E., KYLE, S., MEUTH, M., CURTIN, N. J. & HELLEDAY, T. 2005. Specific killing of BRCA2-deficient tumours with inhibitors of poly(ADP-ribose) polymerase. *Nature*, 434, 913-917.
- BUISSON, R., DION-COTE, A. M., COULOMBE, Y., LAUNAY, H., CAI, H., STASIAK, A. Z., STASIAK, A., XIA, B. & MASSON, J. Y. 2010. Cooperation of breast cancer proteins PALB2 and piccolo BRCA2 in stimulating homologous recombination. *Nat Struct Mol Biol*, 17, 1247-54.
- BUNTING, S. F. & NUSSENZWEIG, A. 2013. End-joining, translocations and cancer. *Nat Rev Cancer*, 13, 443-54.
- BUNZ, F., DUTRIAUX, A., LENGAUER, C., WALDMAN, T., ZHOU, S., BROWN, J. P., SEDIVY, J. M., KINZLER, K. W. & VOGELSTEIN, B. 1998. Requirement for p53 and p21 to Sustain G2 Arrest After DNA Damage. *Science*, 282, 1497-1501.
- CAMPBELL, M. & GANETZKY, B. 2013. Identification of Mob2, a Novel Regulator of Larval Neuromuscular Junction Morphology, in Natural Populations of *Drosophila melanogaster*. *Genetics*, 195, 915-+.
- CAPRANICO, G., KOHN, K. W. & POMMIER, Y. 1990. Local sequence requirements for DNA cleavage by mammalian topoisomerase II in the presence of doxorubicin. *Nucleic Acids Res*, 18, 6611-9.
- CERAMI, E., GAO, J., DOGRUSOZ, U., GROSS, B. E., SUMER, S. O. & AKSOY, B. A. 2012. The cBio Cancer Genomics Portal: An Open Platform for Exploring Multidimensional Cancer Genomics Data (vol 2, pg 401, 2012). *Cancer Discovery*, 2, 960-960.
- CHALERMRUJINANANT, C., MICHOWSKI, W., SITTITHUMCHAREE, G., ESASHI, F. & JIRAWATNOTAI, S. 2016. Cyclin D1 promotes BRCA2-Rad51 interaction by restricting cyclin A/B-dependent BRCA2 phosphorylation. *Oncogene*, 35, 2815-2823.
- CHAMPOUX, J. J. 2001. DNA topoisomerases: Structure, function, and mechanism. *Annu Rev Biochem*, 70, 369-413.
- CHAN, E. H., NOUSIAINEN, M., CHALAMALASETTY, R. B., SCHAFER, A., NIGG, E. A. & SILLJE, H. H. W. 2005. The Ste20-like kinase Mst2 activates the human large tumor suppressor kinase Lats1. *Oncogene*, 24, 2076-2086.
- CHAPMAN, J. R., TAYLOR, M. R. G. & BOULTON, S. J. 2012. Playing the End Game: DNA Double-Strand Break Repair Pathway Choice. *Molecular Cell*, 47, 497-510.
- CHIYODA, T., SUGIYAMA, N., SHIMIZU, T., NAOE, H., KOBAYASHI, Y., ISHIZAWA, J., ARIMA, Y., TSUDA, H., ITO, M., KAIBUCHI, K., AOKI, D., ISHIHAMA, Y., SAYA, H. & KUNINAKA, S. 2012. LATS1/WARTS phosphorylates MYPT1 to counteract PLK1 and regulate mammalian mitotic progression. *Journal of Cell Biology*, 197, 625-641.

- CHRISTMANN, M., TOMICIC, M. T., ROOS, W. P. & KAINA, B. 2003. Mechanisms of human DNA repair: an update. *Toxicology*, 193, 3-34.
- CICCIA, A. & ELLEDGE, S. J. 2010. The DNA Damage Response: Making It Safe to Play with Knives. *Molecular Cell*, 40, 179-204.
- CIMPRICH, K. A. & CORTEZ, D. 2008. ATR: an essential regulator of genome integrity. *Nat Rev Mol Cell Biol*, 9, 616-27.
- CLAUSON, C., SCHARER, O. D. & NIEDERNHOFER, L. 2013. Advances in Understanding the Complex Mechanisms of DNA Interstrand Cross-Link Repair. *Cold Spring Harbor Perspectives in Biology*, 5.
- COLALUCA, I. N., TOSONI, D., NUCIFORO, P., SENIC-MATUGLIA, F., GALIMBERTI, V., VIALE, G., PECE, S. & DI FIORE, P. P. 2008. NUMB controls p53 tumour suppressor activity. *Nature*, 451, 76-U11.
- COLLIS, S. J., CICCIA, A., DEANS, A. J., HOREJSI, Z., MARTIN, J. S., MASLEN, S. L., SKEHEL, J. M., ELLEDGE, S. J., WEST, S. C. & BOULTON, S. J. 2008. FANCM and FAAP24 Function in ATR-Mediated Checkpoint Signaling Independently of the Fanconi Anemia Core Complex. *Molecular Cell*, 32, 313-324.
- COLMAN-LERNER, A., CHIN, T. E. & BRENT, R. 2001. Yeast Cbk1 and Mob2 activate daughter-specific genetic programs to induce asymmetric cell fates. *Cell*, 107, 739-50.
- COOK, D., HOA, L. Y., GOMEZ, V., GOMEZ, M. & HERGOVICH, A. 2014. Constitutively active NDR1-PIF kinase functions independent of MST1 and hMOB1 signalling. *Cell Signal*, 26, 1657-1667.
- CORNILS, H., KOHLER, R. S., HERGOVICH, A. & HEMMINGS, B. A. 2011a. Downstream of human NDR kinases: impacting on c-myc and p21 protein stability to control cell cycle progression. *Cell Cycle*, 10, 1897-904.
- CORNILS, H., KOHLER, R. S., HERGOVICH, A. & HEMMINGS, B. A. 2011b. Human NDR kinases control G(1)/S cell cycle transition by directly regulating p21 stability. *Mol Cell Biol*, 31, 1382-95.
- CORNILS, H., STEGERT, M. R., HERGOVICH, A., HYNX, D., SCHMITZ, D., DIRNHOFER, S. & HEMMINGS, B. A. 2010. Ablation of the kinase NDR1 predisposes mice to the development of T cell lymphoma. *Sci Signal*, 3, ra47.
- COSTANZO, V., ROBERTSON, K., BIBIKOVA, M., KIM, E., GRIECO, D., GOTTESMAN, M., CARROLL, D. & GAUTIER, J. 2001. Mre11 protein complex prevents double-strand break accumulation during chromosomal DNA replication. *Molecular Cell*, 8, 137-147.
- COTTA-RAMUSINO, C., MCDONALD, E. R., HUROV, K., SOWA, M. E., HARPER, J. W. & ELLEDGE, S. J. 2011. A DNA Damage Response Screen Identifies RHINO, a 9-1-1 and TopBP1 Interacting Protein Required for ATR Signaling. *Science*, 332, 1313-1317.
- COTTINI, F., HIDESHIMA, T., XU, C., SATTLER, M., DORI, M., AGNELLI, L., TEN HACKEN, E., BERTILACCIO, M. T., ANTONINI, E., NERI, A., PONZONI, M., MARCATTI, M., RICHARDSON, P. G., CARRASCO, R., KIMMELMAN, A. C., WONG, K. K., CALIGARIS-CAPPIO, F., BLANDINO, G., KUEHL, W. M., ANDERSON, K. C. & TONON, G. 2014. Rescue of Hippo coactivator YAP1 triggers DNA damage-induced apoptosis in hematological cancers. *Nat Med*, 20, 599-606.
- CRAIG, N. L. 2010. *Molecular biology : principles of genome function*, Oxford ; New York, Oxford University Press.
- CURTIN, N. J. 2012. DNA repair dysregulation from cancer driver to therapeutic target. *Nat Rev Cancer*, 12, 801-817.

- CZABOTAR, P. E., LESSENE, G., STRASSER, A. & ADAMS, J. M. 2014. Control of apoptosis by the BCL-2 protein family: implications for physiology and therapy. *Nature Reviews Molecular Cell Biology*, 15, 49-63.
- DALEY, J. M. & SUNG, P. 2013. RIF1 in DNA Break Repair Pathway Choice. *Molecular Cell*, 49, 840-841.
- DAVIDSON, D., AMREIN, L., PANASCI, L. & ALOYZ, R. 2013. Small molecules, inhibitors of DNA-PK, targeting DNA repair, and beyond. *Frontiers in Pharmacology*, 4.
- DAVIES, O. R. & PELLEGRINI, L. 2007. Interaction with the BRCA2 C terminus protects RAD51-DNA filaments from disassembly by BRC repeats. *Nat Struct Mol Biol*, 14, 475-83.
- DEANS, A. J. & WEST, S. C. 2011. DNA interstrand crosslink repair and cancer. *Nature Reviews Cancer*, 11, 467-480.
- DEBNATH, J., MUTHUSWAMY, S. K. & BRUGGE, J. S. 2003. Morphogenesis and oncogenesis of MCF-10A mammary epithelial acini grown in three-dimensional basement membrane cultures. *Methods*, 30, 256-268.
- DECKBAR, D., JEGGO, P. A. & LOBRICH, M. 2011. Understanding the limitations of radiation-induced cell cycle checkpoints. *Crit Rev Biochem Mol Biol*, 46, 271-83.
- DECKBAR, D., STIFF, T., KOCH, B., REIS, C., LOBRICH, M. & JEGGO, P. A. 2010. The limitations of the G1-S checkpoint. *Cancer Res*, 70, 4412-21.
- DEEKS, E. D. 2015. Olaparib: First Global Approval. *Drugs*, 75, 231-240.
- DENSHAM, R. M., GARVIN, A. J., STONE, H. R., STRACHAN, J., BALDOCK, R. A., DAZA-MARTIN, M., FLETCHER, A., BLAIR-REID, S., BEESLEY, J., JOHAL, B., PEARL, L. H., NEELY, R., KEEP, N. H., WATTS, F. Z. & MORRIS, J. R. 2016. Human BRCA1-BARD1 ubiquitin ligase activity counteracts chromatin barriers to DNA resection. *Nat Struct Mol Biol*, 23, 647-655.
- DEVROE, E., ERDJUMENT-BROMAGE, H., TEMPST, P. & SILVER, P. A. 2004. Human mob proteins regulate the NDR1 and NDR2 serine-threonine kinases. *Journal of Biological Chemistry*, 279, 24444-24451.
- DI LEONARDO, A., LINKE, S. P., CLARKIN, K. & WAHL, G. M. 1994. DNA damage triggers a prolonged p53-dependent G1 arrest and long-term induction of Cip1 in normal human fibroblasts. *Genes & Development*, 8, 2540-2551.
- DIETLEIN, F., THELEN, L. & REINHARDT, H. C. 2014. Cancer-specific defects in DNA repair pathways as targets for personalized therapeutic approaches. *Trends in Genetics*, 30, 326-339.
- DONG, J. X., FELDMANN, G., HUANG, J. B., WU, S., ZHANG, N. L., COMERFORD, S. A., GAYYED, M. F., ANDERS, R. A., MAITRA, A. & PAN, D. J. 2007. Elucidation of a universal size-control mechanism in *Drosophila* and mammals. *Cell*, 130, 1120-1133.
- DONZELLI, M. & DRAETTA, G. F. 2003. Regulating mammalian checkpoints through Cdc25 inactivation. *EMBO Reports*, 4, 671-677.
- DOWNS, J. A., NUSSENZWEIG, M. C. & NUSSENZWEIG, A. 2007. Chromatin dynamics and the preservation of genetic information. *Nature*, 447, 951-958.
- DREW, Y. 2015. The development of PARP inhibitors in ovarian cancer: from bench to bedside. *Br J Cancer*, 113 Suppl 1, S3-9.
- DYSON, N. 1998. The regulation of E2F by pRB-family proteins. *Genes & Development*, 12, 2245-2262.
- EL-DEIRY, W. S., HARPER, J. W., O'CONNOR, P. M., VELCULESCU, V. E., CANMAN, C. E., JACKMAN, J., PIETENPOL, J. A., BURRELL, M., HILL, D. E., WANG, Y. & ET AL. 1994. WAF1/CIP1 is induced in p53-mediated G1 arrest and apoptosis. *Cancer Res*, 54, 1169-74.



- EL-DEIRY, W. S., TOKINO, T., VELCULESCU, V. E., LEVY, D. B., PARSONS, R., TRENT, J. M., LIN, D., MERCER, W. E., KINZLER, K. W. & VOGELSTEIN, B. 1993. WAF1, a potential mediator of p53 tumor suppression. *Cell*, 75, 817-825.
- ENOMOTO, A., FUKASAWA, T., TAKAMATSU, N., ITO, M., MORITA, A., HOSOI, Y. & MIYAGAWA, K. 2013. The HSP90 inhibitor 17-allylamino-17-demethoxygeldanamycin modulates radiosensitivity by downregulating serine/threonine kinase 38 via Sp1 inhibition. *European Journal of Cancer*, 49, 3547-3558.
- ESASHI, F., CHRIST, N., GANNON, J., LIU, Y. L., HUNT, T., JASIN, M. & WEST, S. C. 2005. CDK-dependent phosphorylation of BRCA2 as a regulatory mechanism for recombinational repair. *Nature*, 434, 598-604.
- ESASHI, F., GALKIN, V. E., YU, X., EGELMAN, E. H. & WEST, S. C. 2007. Stabilization of RAD51 nucleoprotein filaments by the C-terminal region of BRCA2. *Nat Struct Mol Biol*, 14, 468-474.
- EVERS, B., HELLEDAY, T. & JONKERS, J. 2010. Targeting homologous recombination repair defects in cancer. *Trends Pharmacol Sci*, 31, 372-80.
- FALCK, J., COATES, J. & JACKSON, S. P. 2005. Conserved modes of recruitment of ATM, ATR and DNA-PKcs to sites of DNA damage. *Nature*, 434, 605-611.
- FALCK, J., MAILAND, N., SYLJUASEN, R. G., BARTEK, J. & LUKAS, J. 2001. The ATM-Chk2-Cdc25A checkpoint pathway guards against radioresistant DNA synthesis. *Nature*, 410, 842-847.
- FANG, K. M., LIU, Y. Y., LIN, C. H., FAN, S. S., TSAI, C. H. & TZENG, S. F. 2012. Mps one binder 2 gene upregulation in the stellation of astrocytes induced by cAMP-dependent pathway. *Journal of Cellular Biochemistry*, 113, 3019-3028.
- FARMER, H., MCCABE, N., LORD, C. J., TUTT, A. N. J., JOHNSON, D. A., RICHARDSON, T. B., SANTAROSA, M., DILLON, K. J., HICKSON, I., KNIGHTS, C., MARTIN, N. M. B., JACKSON, S. P., SMITH, G. C. M. & ASHWORTH, A. 2005. Targeting the DNA repair defect in BRCA mutant cells as a therapeutic strategy. *Nature*, 434, 917-921.
- FERRETTI, L. P., LAFRANCHI, L. & SARTORI, A. A. 2013. Controlling DNA-end resection: a new task for CDKs. *Frontiers in Genetics*, 4.
- FRANKEN, N. A. P., RODERMOND, H. M., STAP, J., HAVEMAN, J. & VAN BREE, C. 2006. Clonogenic assay of cells in vitro. *Nature Protocols*, 1, 2315-2319.
- FRIDMAN, J. S. & LOWE, S. W. 2003. Control of apoptosis by p53. *Oncogene*, 22, 9030-9040.
- FRITSCH, M., HAESSLER, C. & BRANDNER, G. 1993. Induction of nuclear accumulation of the tumor-suppressor protein p53 by DNA-damaging agents. *Oncogene*, 8, 307-18.
- FUKASAWA, T., ENOMOTO, A. & MIYAGAWA, K. 2015. Serine-Threonine Kinase 38 regulates CDC25A stability and the DNA damage-induced G2/M checkpoint. *Cell Signal*, 27, 1569-1575.
- GILARDINI MONTANI, M. S., PRODOSMO, A., STAGNI, V., MERLI, D., MONTEONOFRIO, L., GATTI, V., GENTILESCHI, M. P., BARILA, D. & SODDU, S. 2013. ATM-depletion in breast cancer cells confers sensitivity to PARP inhibition. *J Exp Clin Cancer Res*, 32, 95.
- GOLDSTEIN, M. & KASTAN, M. B. 2015. The DNA Damage Response: Implications for Tumor Responses to Radiation and Chemotherapy. *Annual Review of Medicine*, 66, 129-143.
- GOMEZ-MARTINEZ, M., SCHMITZ, D. & HERGOVICH, A. 2013. Generation of Stable Human Cell Lines with Tetracycline-inducible (Tet-on) shRNA or cDNA Expression. *Jove-Journal of Visualized Experiments*.

- GOMEZ, V., GUNDOGDU, R., GOMEZ, M., HOA, L., PANCHAL, N., O'DRISCOLL, M. & HERGOVICH, A. 2015. Regulation of DNA damage responses and cell cycle progression by hMOB2. *Cell Signal*, 27, 326-339.
- GOODARZI, A. A. & JEGGO, P. A. 2013. The Repair and Signaling Responses to DNA Double-Strand Breaks. *Advances in Genetics*, Vol 82, 82, 1-45.
- GOULOOZE, S. C., COHEN, A. F. & RISSMANN, R. 2016. Olaparib. *Br J Clin Pharmacol*, 81, 171-3.
- GRALLERT, B. & BOYE, E. 2008. The multiple facets of the intra-S checkpoint. *Cell Cycle*, 7, 2315-20.
- GREEN, D. R. & CHIPUK, J. E. 2006. p53 and metabolism: Inside the TIGAR. *Cell*, 126, 30-32.
- GUNN, A., BENNARDO, N., CHENG, A. & STARK, J. M. 2011. Correct End Use during End Joining of Multiple Chromosomal Double Strand Breaks Is Influenced by Repair Protein RAD50, DNA-dependent Protein Kinase DNA-PKcs, and Transcription Context. *Journal of Biological Chemistry*, 286, 42470-42482.
- GUNN, A. & STARK, J. M. 2012. I-SceI-based assays to examine distinct repair outcomes of mammalian chromosomal double strand breaks. *Amyloid Proteins: Methods and Protocols, Second Edition*, 920, 379-91.
- GURLEY, K. E. & KEMP, C. J. 2001. Synthetic lethality between mutation in Atm and DNA-PKcs during murine embryogenesis. *Current Biology*, 11, 191-194.
- HAMILTON, G., YEE, K. S., SCRACE, S. & O'NEILL, E. 2009. ATM regulates a RASSF1A-dependent DNA damage response. *Curr Biol*, 19, 2020-5.
- HANAHAH, D. & WEINBERG, R. A. 2000. The hallmarks of cancer. *Cell*, 100, 57-70.
- HANAHAH, D. & WEINBERG, R. A. 2011. Hallmarks of cancer: the next generation. *Cell*, 144, 646-74.
- HARRIS, S. L. & LEVINE, A. J. 2005. The p53 pathway: positive and negative feedback loops. *Oncogene*, 24, 2899-908.
- HARTLEY, J. M., SPANSWICK, V. J., GANDER, M., GIACOMINI, G., WHELAN, J., SOUHAMI, R. L. & HARTLEY, J. A. 1999. Measurement of DNA cross-linking in patients on ifosfamide therapy using the single cell gel electrophoresis (comet) assay. *Clinical Cancer Research*, 5, 507-512.
- HARVEY, K. F., ZHANG, X. M. & THOMAS, D. M. 2013. The Hippo pathway and human cancer. *Nature Reviews Cancer*, 13, 246-257.
- HASHIMOTO, Y., CHAUDHURI, A. R., LOPES, M. & COSTANZO, V. 2010. Rad51 protects nascent DNA from Mre11-dependent degradation and promotes continuous DNA synthesis. *Nature Structural & Molecular Biology*, 17, 1305-U268.
- HAWTIN, R. E., STOCKETT, D. E., WONG, O. K., LUNDIN, C., HELLEDAY, T. & FOX, J. A. 2010. Homologous recombination repair is essential for repair of vosaroxin-induced DNA double-strand breaks. *Oncotarget*, 1, 606-619.
- HE, Y., EMOTO, K., FANG, X., REN, N., TIAN, X., JAN, Y. N. & ADLER, P. N. 2005. Drosophila Mob family proteins interact with the related tricornered (Trc) and warts (Wts) kinases. *Mol Biol Cell*, 16, 4139-52.
- HELLEDAY, T. 2010. Homologous recombination in cancer development, treatment and development of drug resistance. *Ejc Supplements*, 8, 156-156.
- HELLEDAY, T., PETERMANN, E., LUNDIN, C., HODGSON, B. & SHARMA, R. A. 2008. DNA repair pathways as targets for cancer therapy. *Nat Rev Cancer*, 8, 193-204.
- HERGOVICH, A. 2011. MOB control: reviewing a conserved family of kinase regulators. *Cell Signal*, 23, 1433-40.
- HERGOVICH, A. 2012. Mammalian Hippo signalling: a kinase network regulated by protein-protein interactions. *Biochem Soc Trans*, 40, 124-8.

- HERGOVICH, A. 2013. Regulation and functions of mammalian LATS/NDR kinases: looking beyond canonical Hippo signalling. *Cell and Bioscience*, 3.
- HERGOVICH, A., BICHSEL, S. J. & HEMMING, B. A. 2005. Human NDR kinases are rapidly activated by MOB proteins through recruitment to the plasma membrane and phosphorylation. *Molecular and Cellular Biology*, 25, 8259-8272.
- HERGOVICH, A. & HEMMING, B. A. 2012. Hippo signalling in the G2/M cell cycle phase: Lessons learned from the yeast MEN and SIN pathways. *Seminars in Cell & Developmental Biology*, 23, 794-802.
- HERGOVICH, A., KOHLER, R. S., SCHMITZ, D., VICHALKOVSKI, A., CORNILS, H. & HEMMING, B. A. 2009. The MST1 and hMOB1 tumor suppressors control human centrosome duplication by regulating NDR kinase phosphorylation. *Curr Biol*, 19, 1692-702.
- HERGOVICH, A., LAMLA, S., NIGG, E. A. & HEMMING, B. A. 2007. Centrosome-associated NDR kinase regulates centrosome duplication. *Molecular Cell*, 25, 625-634.
- HERGOVICH, A., SCHMITZ, D. & HEMMING, B. A. 2006a. The human tumour suppressor LATS1 is activated by human MOB1 at the membrane. *Biochem Biophys Res Commun*, 345, 50-8.
- HERGOVICH, A., SCHMITZ, D. & HEMMING, B. A. 2006b. The human tumour suppressor LATS1 is activated by human MOB1 at the membrane. *Biochemical and Biophysical Research Communications*, 345, 50-58.
- HERGOVICH, A., STEGERT, M. R., SCHMITZ, D. & HEMMING, B. A. 2006c. NDR kinases regulate essential cell processes from yeast to humans. *Nat Rev Mol Cell Biol*, 7, 253-64.
- HEROLD, S., HOCK, A., HERKERT, B., BERNS, K., MULLENDERS, J., BEIJERSBERGEN, R., BERNARDS, R. & EILERS, M. 2008. Miz1 and HectH9 regulate the stability of the checkpoint protein, TopBP1. *Embo Journal*, 27, 2851-2861.
- HISATOMI, T., SUEOKA-ARAGANE, N., SATO, A., TOMIMASU, R., IDE, M., KURIMASA, A., OKAMOTO, K., KIMURA, S. & SUEOKA, E. 2011. NK314 potentiates antitumor activity with adult T-cell leukemia-lymphoma cells by inhibition of dual targets on topoisomerase II alpha and DNA-dependent protein kinase. *Blood*, 117, 3575-3584.
- HOA, L., KULABEROGLU, Y., GUNDOGDU, R., COOK, D., MAVIS, M., GOMEZ, M., GOMEZ, V. & HERGOVICH, A. 2016. The characterisation of LATS2 kinase regulation in Hippo-YAP signalling. *Cell Signal*, 28, 488-497.
- HOA, N. N., AKAGAWA, R., YAMASAKI, T., HIROTA, K., SASA, K., NATSUME, T., KOBAYASHI, J., SAKUMA, T., YAMAMOTO, T., KOMATSU, K., KANEMAKI, M. T., POMMIER, Y., TAKEDA, S. & SASANUMA, H. 2015. Relative contribution of four nucleases, CtIP, Dna2, Exo1 and Mre11, to the initial step of DNA double-strand break repair by homologous recombination in both the chicken DT40 and human TK6 cell lines. *Genes to Cells*, 20, 1059-1076.
- HOCHEGGER, H., TAKEDA, S. & HUNT, T. 2008. Cyclin-dependent kinases and cell-cycle transitions: does one fit all? *Nat Rev Mol Cell Biol*, 9, 910-6.
- HOEIJMAKERS, J. H. 2009. DNA damage, aging, and cancer. *N Engl J Med*, 361, 1475-85.
- HOGLUND, A., STROMVALL, K., LI, Y., FORSHELL, L. P. & NILSSON, J. A. 2011. Chk2 deficiency in Myc overexpressing lymphoma cells elicits a synergistic lethal response in combination with PARP inhibition. *Cell Cycle*, 10, 3598-607.
- HOLLANDER, M. C. & FORNACE, A. J., JR. 2002. Genomic instability, centrosome amplification, cell cycle checkpoints and Gadd45a. *Oncogene*, 21, 6228-33.

- HOLLOMAN, W. K. 2011. Unraveling the mechanism of BRCA2 in homologous recombination. *Nat Struct Mol Biol*, 18, 748-754.
- HOLOHAN, C., VAN SCHAEYBROECK, S., LONGLEY, D. B. & JOHNSTON, P. G. 2013. Cancer drug resistance: an evolving paradigm. *Nature Reviews Cancer*, 13, 714-726.
- HOPFNER, K. P., CRAIG, L., MONCALIAN, G., ZINKEL, R. A., USUI, T., OWEN, B. A. L., KARCHER, A., HENDERSON, B., BODMER, J. L., MCMURRAY, C. T., CARNEY, J. P., PETRINI, J. H. J. & TAINER, J. A. 2002. The Rad50 zinc-hook is a structure joining Mre11 complexes in DNA recombination and repair. *Nature*, 418, 562-566.
- HOPFNER, K. P., KARCHER, A., CRAIG, L., WOO, T. T., CARNEY, J. P. & TAINER, J. A. 2001. Structural biochemistry and interaction architecture of the DNA double-strand break repair Mre11 nuclease and Rad50-ATPase. *Cell*, 105, 473-485.
- HOU, M. C., GUERTIN, D. A. & MCCOLLUM, D. 2004. Initiation of cytokinesis is controlled through multiple modes of regulation of the Sid2p-Mob1p kinase complex. *Mol Cell Biol*, 24, 3262-76.
- HOU, M. C., WILEY, D. J., VERDE, F. & MCCOLLUM, D. 2003. Mob2p interacts with the protein kinase Orb6p to promote coordination of cell polarity with cell cycle progression. *J Cell Sci*, 116, 125-35.
- HUANG, Y. L. & LI, L. 2013. DNA crosslinking damage and cancer - a tale of friend and foe. *Translational Cancer Research*, 2, 144-154.
- ILIAKIS, G. E., METZGER, L., DENKO, N. & STAMATO, T. D. 1991. Detection of DNA Double-Strand Breaks in Synchronous Cultures of Cho Cells by Means of Asymmetric Field Inversion Gel-Electrophoresis. *International Journal of Radiation Biology*, 59, 321-341.
- IYAMA, T. & WILSON, D. M., 3RD 2013. DNA repair mechanisms in dividing and non-dividing cells. *DNA Repair (Amst)*, 12, 620-36.
- JACKSON, S. P. & BARTEK, J. 2009. The DNA-damage response in human biology and disease. *Nature*, 461, 1071-1078.
- JACKSON, S. P. & HELLEDAY, T. 2016. DNA REPAIR. Drugging DNA repair. *Science*, 352, 1178-9.
- JANSEN, J. M., BARRY, M. F., YOO, C. K. & WEISS, E. L. 2006. Phosphoregulation of Cbk1 is critical for RAM network control of transcription and morphogenesis. *J Cell Biol*, 175, 755-66.
- JASIN, M. & ROTHSTEIN, R. 2013. Repair of Strand Breaks by Homologous Recombination. *Cold Spring Harbor Perspectives in Biology*, 5.
- JIANG, H., REINHARDT, H. C., BARTKOVA, J., TOMMISKA, J., BLOMQVIST, C., NEVANLINNA, H., BARTEK, J., YAFFE, M. B. & HEMANN, M. T. 2009. The combined status of ATM and p53 link tumor development with therapeutic response. *Genes & Development*, 23, 1895-1909.
- JIRICNY, J. 2006. The multifaceted mismatch-repair system. *Nat Rev Mol Cell Biol*, 7, 335-46.
- KANAI, M., KUME, K., MIYAHARA, K., SAKAI, K., NAKAMURA, K., LEONHARD, K., WILEY, D. J., VERDE, F., TODA, T. & HIRATA, D. 2005. Fission yeast MO25 protein is localized at SPB and septum and is essential for cell morphogenesis. *Embo Journal*, 24, 3012-25.
- KASTAN, M. B. & BARTEK, J. 2004. Cell-cycle checkpoints and cancer. *Nature*, 432, 316-323.
- KASTAN, M. B. & LIM, D. S. 2000. The many substrates and functions of ATM. *Nature Reviews Molecular Cell Biology*, 1, 179-186.
- KASTAN, M. B., ONYEKWERE, O., SIDRANSKY, D., VOGELSTEIN, B. & CRAIG, R. W. 1991. Participation of p53 Protein in the Cellular Response to DNA Damage. *Cancer Research*, 51, 6304-6311.

- KASTAN, M. B., ZHAN, Q., EL-DEIRY, W. S., CARRIER, F., JACKS, T., WALSH, W. V., PLUNKETT, B. S., VOGELSTEIN, B. & FORNACE JR, A. J. 1992. A mammalian cell cycle checkpoint pathway utilizing p53 and GADD45 is defective in ataxia-telangiectasia. *Cell*, 71, 587-597.
- KELLEY, M. R., LOGSDON, D. & FISHEL, M. L. 2014. Targeting DNA repair pathways for cancer treatment: what's new? *Future Oncology*, 10, 1215-1237.
- KENNEDY, R. D., CHEN, C. C., STUCKERT, P., ARCHILA, E. M., DE LA VEGA, M. A., MOREAU, L. A., SHIMAMURA, A. & D'ANDREA, A. D. 2007. Fanconi anemia pathway-deficient tumor cells are hypersensitive to inhibition of ataxia telangiectasia mutated. *Journal of Clinical Investigation*, 117, 1440-1449.
- KENNEDY, R. D. & D'ANDREA, A. D. 2006. DNA repair pathways in clinical practice: Lessons from pediatric cancer susceptibility syndromes. *Journal of Clinical Oncology*, 24, 3799-3808.
- KERZENDORFER, C. & O'DRISCOLL, M. 2009. Human DNA damage response and repair deficiency syndromes: linking genomic instability and cell cycle checkpoint proficiency. *DNA Repair (Amst)*, 8, 1139-52.
- KHANNA, K. K. & JACKSON, S. P. 2001. DNA double-strand breaks: signaling, repair and the cancer connection. *Nat Genet*, 27, 247-54.
- KIM, H. & D'ANDREA, A. D. 2012. Regulation of DNA cross-link repair by the Fanconi anemia/BRCA pathway. *Genes & Development*, 26, 1393-1408.
- KIM, J. S., LEE, C., BONIFANT, C. L., RESSOM, H. & WALDMAN, T. 2007. Activation of p53-dependent growth suppression in human cells by mutations in PTEN or PIK3CA. *Mol Cell Biol*, 27, 662-77.
- KIM, S. T., XU, B. & KASTAN, M. B. 2002. Involvement of the cohesin protein, Smc1, in Atm-dependent and independent responses to DNA damage. *Genes & Development*, 16, 560-570.
- KIM, Y. J. & WILSON, D. M., 3RD 2012. Overview of base excision repair biochemistry. *Curr Mol Pharmacol*, 5, 3-13.
- KIRSHNER, M., RATHAVS, M., NIZAN, A., ESSERS, J., KANAAR, R., SHILOH, Y. & BARZILAI, A. 2009. Analysis of the relationships between ATM and the Rad54 paralogs involved in homologous recombination repair. *DNA Repair (Amst)*, 8, 253-61.
- KITAGAWA, R., BAKKENIST, C. J., MCKINNON, P. J. & KASTAN, M. B. 2004. Phosphorylation of SMC1 is a critical downstream event in the ATM-NBS1-BRCA1 pathway. *Genes & Development*, 18, 1423-1438.
- KLAUSNER, R. D. 2002. The fabric of cancer cell biology-Weaving together the strands. *Cancer Cell*, 1, 3-10.
- KLEINER, R. E., VERMA, P., MOLLOY, K. R., CHAIT, B. T. & KAPOOR, T. M. 2015. Chemical proteomics reveals a gammaH2AX-53BP1 interaction in the DNA damage response. *Nat Chem Biol*, 11, 807-14.
- KOBAYASHI, J., TAUCHI, H., SAKAMOTO, S., NAKAMURA, A., MORISHIMA, K., MATSUURA, S., KOBAYASHI, T., TAMAI, K., TANIMOTO, K. & KOMATSU, K. 2002. NBS1 localizes to gamma-H2AX foci through interaction with the FHA/BRCT domain. *Current Biology*, 12, 1846-1851.
- KOHLER, R. S., SCHMITZ, D., CORNILS, H., HEMMINGS, B. A. & HERGOVICH, A. 2010. Differential NDR/LATS Interactions with the Human MOB Family Reveal a Negative Role for Human MOB2 in the Regulation of Human NDR Kinases. *Molecular and Cellular Biology*, 30, 4507-4520.
- KRAAKMAN-VAN DER ZWET, M., OVERKAMP, W. J. I., VAN LANGE, R. E. E., ESSERS, J., VAN DUIJN-GOEDHART, A., WIGGERS, I., SWAMINATHAN, S., VAN BUUL, P. P. W., ERRAMI, A., TAN, R. T. L., JASPERS, N. G. J., SHARAN, S. K., KANAAR, R. & ZDZIENICKA, M. Z. 2002. Brca2 (XRCC11)

- deficiency results in radioresistant DNA synthesis and a higher frequency of spontaneous deletions. *Molecular and Cellular Biology*, 22, 669-679.
- KREJCI, L., ALTMANNOVA, V., SPIREK, M. & ZHAO, X. L. 2012. Homologous recombination and its regulation. *Nucleic Acids Research*, 40, 5795-5818.
- KROKAN, H. E. & BJORAS, M. 2013. Base Excision Repair. *Cold Spring Harbor Perspectives in Biology*, 5.
- KRUSE, J. P. & GU, W. 2009. Modes of p53 Regulation. *Cell*, 137, 609-622.
- KUBOTA, E., WILLIAMSON, C. T., YE, R., ELEGBEDE, A., PETERSON, L., LEES-MILLER, S. P. & BEBB, D. G. 2014. Low ATM protein expression and depletion of p53 correlates with olaparib sensitivity in gastric cancer cell lines. *Cell Cycle*, 13, 2129-37.
- LAI, Z. C., WEI, X. M., SHIMIZU, T., RAMOS, E., ROHRBAUGH, M., NIKOLAIDIS, N., HO, L. L. & LI, Y. 2005. Control of cell proliferation and apoptosis by Mob as tumor suppressor, Mats. *Cell*, 120, 675-685.
- LAVIN, M. F. & SHILOH, Y. 1997. The genetic defect in ataxia-telangiectasia. *Annual review of immunology*, 15, 177-202.
- LEE, J. H. & PAULL, T. T. 2004. Direct activation of the ATM protein kinase by the Mre11/Rad50/Nbs1 complex. *Science*, 304, 93-6.
- LEE, J. H. & PAULL, T. T. 2005a. ATM activation by DNA double-strand breaks through the Mre11-Rad50-Nbs1 complex. *Science*, 308, 551-554.
- LEE, J. H. & PAULL, T. T. 2005b. ATM activation by DNA double-strand breaks through the Mre11-Rad50-Nbs1 complex (vol 308, pg 551, 2005). *Science*, 308, 1870-1870.
- LEVY, D., ADAMOVICH, Y., REUVEN, N. & SHAUL, Y. 2008. Yap1 phosphorylation by c-Abl is a critical step in selective activation of proapoptotic genes in response to DNA damage. *Mol Cell*, 29, 350-61.
- LIAW, H., LEE, D. & MYUNG, K. 2011. DNA-PK-Dependent RPA2 Hyperphosphorylation Facilitates DNA Repair and Suppresses Sister Chromatid Exchange. *Plos One*, 6.
- LIEBER, M. R., MA, Y. M., PANNICKE, U. & SCHWARZ, K. 2003. Mechanism and regulation of human non-homologous DNA end-joining. *Nature Reviews Molecular Cell Biology*, 4, 712-720.
- LIM, D. S. & HASTY, P. 1996. A mutation in mouse rad51 results in an early embryonic lethal that is suppressed by a mutation in p53. *Molecular and Cellular Biology*, 16, 7133-7143.
- LIM, D. S., KIM, S. T., XU, B., MASER, R. S., LIN, J. Y., PETRINI, J. H. J. & KASTAN, M. B. 2000. ATM phosphorylates p95/nbs1 in an S-phase checkpoint pathway. *Nature*, 404, 613-+.
- LIN, C. H., HSIEH, M. L. & FAN, S. S. 2011. The promotion of neurite formation in Neuro2A cells by mouse Mob2 protein. *FEBS Letters*, 585, 523-530.
- LINDAHL, T. 1993. Instability and Decay of the Primary Structure of DNA. *Nature*, 362, 709-715.
- LINDAHL, T. & BARNES, D. E. 2000. Repair of endogenous DNA damage. *Cold Spring Harb Symp Quant Biol*, 65, 127-33.
- LINDAHL, T. & NYBERG, B. 1972. Rate of depurination of native deoxyribonucleic acid. *Biochemistry*, 11, 3610-8.
- LINDAHL, T. & WOOD, R. D. 1999. Quality control by DNA repair. *Science*, 286, 1897-1905.
- LINDQVIST, A., RODRIGUEZ-BRAVO, V. & MEDEMA, R. H. 2009. The decision to enter mitosis: feedback and redundancy in the mitotic entry network. *J Cell Biol*, 185, 193-202.
- LING, S. & LIN, W. C. 2011. EDD inhibits ATM-mediated phosphorylation of p53. *J Biol Chem*, 286, 14972-82.

- LIU, L. Y., LIN, C. H. & FAN, S. S. 2009. Function of *Drosophila* mob2 in photoreceptor morphogenesis. *Cell and Tissue Research*, 338, 377-389.
- LIVAK, K. J. & SCHMITTGEN, T. D. 2001. Analysis of relative gene expression data using real-time quantitative PCR and the 2(-Delta Delta C(T)) Method. *Methods*, 25, 402-8.
- LOEB, L. A. & HARRIS, C. C. 2008. Advances in chemical carcinogenesis: a historical review and prospective. *Cancer Res*, 68, 6863-72.
- LOEWER, A., BATCHELOR, E., GAGLIA, G. & LAHAV, G. 2010. Basal dynamics of p53 reveal transcriptionally attenuated pulses in cycling cells. *Cell*, 142, 89-100.
- LONG, D. T., RASCHLE, M., JOUKOV, V. & WALTER, J. C. 2011. Mechanism of RAD51-Dependent DNA Interstrand Cross-Link Repair. *Science*, 333, 84-87.
- LOPEZ-CONTRERAS, A. J. A. F.-C., O. 2012. Signalling DNA Damage. *Protein Phosphorylation in Human Health*.
- LORD, C. J. & ASHWORTH, A. 2016. BRCAness revisited. *Nat Rev Cancer*, 16, 110-20.
- LORD, C. J., TUTT, A. N. J. & ASHWORTH, A. 2015. Synthetic Lethality and Cancer Therapy: Lessons Learned from the Development of PARP Inhibitors. *Annual Review of Medicine*, Vol 66, 66, 455-470.
- LOWE, S. W., SCHMITT, E. M., SMITH, S. W., OSBORNE, B. A. & JACKS, T. 1993. P53 Is Required for Radiation-Induced Apoptosis in Mouse Thymocytes. *Nature*, 362, 847-849.
- LUCA, F. C. & WINEY, M. 1998. MOB1, an essential yeast gene required for completion of mitosis and maintenance of ploidy. *Mol Biol Cell*, 9, 29-46.
- MA, H. T. & POON, R. Y. 2011a. How protein kinases co-ordinate mitosis in animal cells. *The Biochemical journal*, 435, 17-31.
- MA, H. T. & POON, R. Y. C. 2011b. How protein kinases co-ordinate mitosis in animal cells. *Biochemical Journal*, 435, 17-31.
- MALTZMAN, W. & CZYZYK, L. 1984. UV irradiation stimulates levels of p53 cellular tumor antigen in nontransformed mouse cells. *Molecular and Cellular Biology*, 4, 1689-1694.
- MALUMBRES, M., HARLOW, E., HUNT, T., HUNTER, T., LAHTI, J. M., MANNING, G., MORGAN, D. O., TSAI, L. H. & WOLGEMUTH, D. J. 2009. Cyclin-dependent kinases: a family portrait. *Nat Cell Biol*, 11, 1275-6.
- MAO, Z. Y., BOZZELLA, M., SELUANOV, A. & GORBUNOVA, V. 2008. DNA repair by nonhomologous end joining and homologous recombination during cell cycle in human cells. *Cell Cycle*, 7, 2902-2906.
- MATEO, J., CARREIRA, S., SANDHU, S., MIRANDA, S., MOSSOP, H., PEREZ-LOPEZ, R., NAVA RODRIGUES, D., ROBINSON, D., OMLIN, A., TUNARIU, N., BOYSEN, G., PORTA, N., FLOHR, P., GILLMAN, A., FIGUEIREDO, I., PAULDING, C., SEED, G., JAIN, S., RALPH, C., PROTHEROE, A., HUSSAIN, S., JONES, R., ELLIOTT, T., MCGOVERN, U., BIANCHINI, D., GOODALL, J., ZAFEIRIOU, Z., WILLIAMSON, C. T., FERRALDESCHI, R., RIISNAES, R., EBBS, B., FOWLER, G., RODA, D., YUAN, W., WU, Y. M., CAO, X., BROUGH, R., PEMBERTON, H., A'HERN, R., SWAIN, A., KUNJU, L. P., EELES, R., ATTARD, G., LORD, C. J., ASHWORTH, A., RUBIN, M. A., KNUDSEN, K. E., FENG, F. Y., CHINNAIYAN, A. M., HALL, E. & DE BONO, J. S. 2015. DNA-Repair Defects and Olaparib in Metastatic Prostate Cancer. *N Engl J Med*, 373, 1697-708.
- MATOKA, S., KANG, J. G., PATINO, W. D., WRAGG, A., BOEHM, M., GAVRILOVA, O., HURLEY, P. J., BUNZ, F. & HWANG, P. M. 2006. p53 regulates mitochondrial respiration. *Cardiovascular Drugs and Therapy*, 20, 415-415.

- MATSUOKA, S., BALLIF, B. A., SMOGORZEWSKA, A., MCDONALD, E. R., HUROV, K. E., LUO, J., BAKALARSKI, C. E., ZHAO, Z. M., SOLIMINI, N., LERENTHAL, Y., SHILOH, Y., GYGI, S. P. & ELLEDGE, S. J. 2007. ATM and ATR substrate analysis reveals extensive protein networks responsive to DNA damage. *Science*, 316, 1160-1166.
- MENENDEZ, D., INGA, A. & RESNICK, M. A. 2009. The expanding universe of p53 targets. *Nat Rev Cancer*, 9, 724-737.
- MENG, Z., MOROISHI, T. & GUAN, K. L. 2016. Mechanisms of Hippo pathway regulation. *Genes Dev*, 30, 1-17.
- MENG, Z. P., MOROISHI, T., MOTTIER-PAVIE, V., PLOUFFE, S. W., HANSEN, C. G., HONG, A. W., PARK, H. W., MO, J. S., LU, W. Q., LU, S. C., FLORES, F., YU, F. X., HALDER, G. & GUAN, K. L. 2015. MAP4K family kinases act in parallel to MST1/2 to activate LATS1/2 in the Hippo pathway. *Nature Communications*, 6.
- MEYN, M. S. 1995. Ataxia-Telangiectasia and Cellular Responses to DNA Damage. *Cancer Research*, 55, 5991-6001.
- MIMITOU, E. P. & SYMINGTON, L. S. 2009. Nucleases and helicases take center stage in homologous recombination. *Trends in Biochemical Sciences*, 34, 264-72.
- MITTNACHT, S. 1998. Control of pRB phosphorylation. *Current Opinion in Genetics & Development*, 8, 21-27.
- MORENO-HERRERO, F., DE JAGER, M., DEKKER, N. H., KANAAR, R., WYMAN, C. & DEKKER, C. 2005. Mesoscale conformational changes in the DNA-repair complex Rad50/Mre11/Nbs1 upon binding DNA. *Nature*, 437, 440-443.
- MOUDRY, P., WATANABE, K., WOLANIN, K. M., BARTKOVA, J., WASSING, I. E., WATANABE, S., STRAUSS, R., PEDERSEN, R. T., OESTERGAARD, V. H., LISBY, M., ANDUJAR-SANCHEZ, M., MAYA-MENDOZA, A., ESASHI, F., LUKAS, J. & BARTEK, J. 2016. TOPBP1 regulates RAD51 phosphorylation and chromatin loading and determines PARP inhibitor sensitivity. *Journal of Cell Biology*, 212, 281-288.
- MOYNAHAN, M. E. & JASIN, M. 2010. Mitotic homologous recombination maintains genomic stability and suppresses tumorigenesis. *Nature Reviews Molecular Cell Biology*, 11, 196-207.
- MOYNAHAN, M. E., PIERCE, A. J. & JASIN, M. 2001. BRCA2 is required for homology-directed repair of chromosomal breaks. *Molecular Cell*, 7, 263-272.
- MUNRO, S., CARR, S. M. & LA THANGUE, N. B. 2012. Diversity within the pRb pathway: is there a code of conduct? *Oncogene*, 31, 4343-4352.
- MURAI, J., HUANG, S. Y. N., DAS, B. B., RENAUD, A., ZHANG, Y. P., DOROSHOW, J. H., JI, J. P., TAKEDA, S. & POMMIER, Y. 2012. Trapping of PARP1 and PARP2 by Clinical PARP Inhibitors. *Cancer Research*, 72, 5588-5599.
- MURPHY, A. K., FITZGERALD, M., RO, T., KIM, J. H., RABINOWITSCH, A. I., CHOWDHURY, D., SCHILDKRAUT, C. L. & BOROWIEC, J. A. 2014. Phosphorylated RPA recruits PALB2 to stalled DNA replication forks to facilitate fork recovery. *Journal of Cell Biology*, 206, 493-507.
- NEGRINI, S., GORGOLIS, V. G. & HALAZONETIS, T. D. 2010. Genomic instability - an evolving hallmark of cancer. *Nature Reviews Molecular Cell Biology*, 11, 220-228.
- NELSON, B., KURISCHKO, C., HORECKA, J., MODY, M., NAIR, P., PRATT, L., ZOUGMAN, A., MCBROOM, L. D., HUGHES, T. R., BOONE, C. & LUCA, F. C. 2003. RAM: a conserved signaling network that regulates Ace2p



- transcriptional activity and polarized morphogenesis. *Mol Biol Cell*, 14, 3782-803.
- NISHIO, M., HAMADA, K., KAWAHARA, K., SASAKI, M., NOGUCHI, F., CHIBA, S., MIZUNO, K., SUZUKI, S. O., DONG, Y. Y., TOKUDA, M., MORIKAWA, T., HIKASA, H., EGGENSCHWILER, J., YABUTA, N., NOJIMA, H., NAKAGAWA, K., HATA, Y., NISHINA, H., MIMORI, K., MORI, M., SASAKI, T., MAK, T. W., NAKANO, T., ITAMI, S. & SUZUKI, A. 2012. Cancer susceptibility and embryonic lethality in Mob1a/1b double-mutant mice. *Journal of Clinical Investigation*, 122, 4505-4518.
- NISHIO, M., SUGIMACHI, K., GOTO, H., WANG, J., MORIKAWA, T., MIYACHI, Y., TAKANO, Y., HIKASA, H., ITOH, T., SUZUKI, S. O., KURIHARA, H., AISHIMA, S., LEASK, A., SASAKI, T., NAKANO, T., NISHINA, H., NISHIKAWA, Y., SEKIDO, Y., NAKAO, K., SHIN-YA, K., MIMORI, K. & SUZUKI, A. 2016. Dysregulated YAP1/TAZ and TGF-beta signaling mediate hepatocarcinogenesis in Mob1a/1b-deficient mice. *Proceedings of the National Academy of Sciences of the United States of America*, 113, E71-E80.
- NITISS, J. L. 2009. Targeting DNA topoisomerase II in cancer chemotherapy. *Nat Rev Cancer*, 9, 338-50.
- NOLL, D. M., MASON, T. M. & MILLER, P. S. 2006. Formation and repair of interstrand cross-links in DNA. *Chemical Reviews*, 106, 277-301.
- O'DRISCOLL, M. & JEGGO, P. A. 2006. The role of double-strand break repair [mdash] insights from human genetics. *Nat Rev Genet*, 7, 45-54.
- OBENAUER, J. C., CANTLEY, L. C. & YAFFE, M. B. 2003. Scansite 2.0: proteome-wide prediction of cell signaling interactions using short sequence motifs. *Nucleic Acids Research*, 31, 3635-3641.
- ODA, E., OHKI, R., MURASAWA, H., NEMOTO, J., SHIBUE, T., YAMASHITA, T., TOKINO, T., TANIGUCHI, T. & TANAKA, N. 2000. Noxa, a BH3-only member of the Bcl-2 family and candidate mediator of p53-induced apoptosis. *Science*, 288, 1053-8.
- OKAMOTO, K. & SAGATA, N. 2007. Mechanism for inactivation of the mitotic inhibitory kinase Wee1 at M phase. *Proceedings of the National Academy of Sciences of the United States of America*, 104, 3753-3758.
- OPLUSTILOVA, L., WOLANIN, K., MISTRIK, M., KORINKOVA, G., SIMKOVA, D., BOUCHAL, J., LENOBEL, R., BARTKOVA, J., LAU, A., O'CONNOR, M. J., LUKAS, J. & BARTEK, J. 2012. Evaluation of candidate biomarkers to predict cancer cell sensitivity or resistance to PARP-1 inhibitor treatment. *Cell Cycle*, 11, 3837-3850.
- PACE, P., MOSEDALE, G., HODSKINSON, M. R., ROSADO, I. V., SIVASUBRAMANIAM, M. & PATEL, K. J. 2010. Ku70 Corrupts DNA Repair in the Absence of the Fanconi Anemia Pathway. *Science*, 329, 219-223.
- PANIER, S. & DUROCHER, D. 2009. Regulatory ubiquitylation in response to DNA double-strand breaks. *DNA Repair*, 8, 436-443.
- PANIER, S. & DUROCHER, D. 2013. Push back to respond better: regulatory inhibition of the DNA double-strand break response. *Nature Reviews Molecular Cell Biology*, 14, 661-672.
- PARK, J. M., CHOI, J. Y., YI, J. M., CHUNG, J. W., LEEM, S. H., KOH, S. S. & KANG, T. H. 2015. NDR1 modulates the UV-induced DNA-damage checkpoint and nucleotide excision repair. *Biochemical and Biophysical Research Communications*, 461, 543-548.
- PAULL, T. T. 2016. Available: <http://www.hhmi.org/research/biochemical-analysis-dna-damage-and-oxidative-stress-responses>.
- PAULL, T. T. & GELLERT, M. 1998. The 3' to 5' exonuclease activity of Mre11 facilitates repair of DNA double-strand breaks. *Molecular Cell*, 1, 969-979.

- PEFANI, D. E., LATUSEK, R., PIRES, I., GRAWENDA, A. M., YEE, K. S., HAMILTON, G., VAN DER WEYDEN, L., ESASHI, F., HAMMOND, E. M. & O'NEILL, E. 2014. RASSF1A-LATS1 signalling stabilizes replication forks by restricting CDK2-mediated phosphorylation of BRCA2. *Nature Cell Biology*, 16, 962-971.
- PEFANI, D. E. & O'NEILL, E. 2016. Hippo pathway and protection of genome stability in response to DNA damage. *Febs Journal*, 283, 1392-1403.
- PETERMANN, E., ORTA, M. L., ISSAEVA, N., SCHULTZ, N. & HELLEDAY, T. 2010. Hydroxyurea-Stalled Replication Forks Become Progressively Inactivated and Require Two Different RAD51-Mediated Pathways for Restart and Repair. *Molecular Cell*, 37, 492-502.
- PETITJEAN, A., MATHE, E., KATO, S., ISHIOKA, C., TAVTIGIAN, S. V., HAINAUT, P. & OLIVIER, M. 2007. Impact of mutant p53 functional properties on TP53 mutation patterns and tumor phenotype: lessons from recent developments in the IARC TP53 database. *Human Mutation*, 28, 622-629.
- PIERCE, A. J., JOHNSON, R. D., THOMPSON, L. H. & JASIN, M. 1999. XRCC3 promotes homology-directed repair of DNA damage in mammalian cells. *Genes Dev*, 13, 2633-8.
- PLONER, C., KOFLER, R. & VILLUNGER, A. 2008. Noxa: at the tip of the balance between life and death. *Oncogene*, 27, S84-S92.
- POLO, S. E. & JACKSON, S. P. 2011. Dynamics of DNA damage response proteins at DNA breaks: a focus on protein modifications. *Genes & Development*, 25, 409-433.
- POMMIER, Y. 2006. Topoisomerase I inhibitors: camptothecins and beyond. *Nature Reviews Cancer*, 6, 789-802.
- POMMIER, Y., CAPRANICO, G., ORR, A. & KOHN, K. W. 1991. Local base sequence preferences for DNA cleavage by mammalian topoisomerase II in the presence of amsacrine or teniposide. *Nucleic Acids Res*, 19, 5973-80.
- POMMIER, Y., LEO, E., ZHANG, H. L. & MARCHAND, C. 2010. DNA Topoisomerases and Their Poisoning by Anticancer and Antibacterial Drugs. *Chem Biol*, 17, 421-433.
- PONCHON, L., DUMAS, C., KAJAVA, A. V., FESQUET, D. & PADILLA, A. 2004. NMR solution structure of Mob1, a mitotic exit network protein and its interaction with an NDR kinase peptide. *Journal of Molecular Biology*, 337, 167-182.
- PRAKASH, R., ZHANG, Y., FENG, W. & JASIN, M. 2015. Homologous recombination and human health: the roles of BRCA1, BRCA2, and associated proteins. *Cold Spring Harb Perspect Biol*, 7, a016600.
- PRASKOVA, M., XIA, F. & AVRUCH, J. 2008. MOBKL1A/MOBKL1B phosphorylation by MST1 and MST2 inhibits cell proliferation. *Current Biology*, 18, 311-321.
- PURVIS, J. E., KARHOHS, K. W., MOCK, C., BATCHELOR, E., LOEWER, A. & LAHAV, G. 2012. p53 dynamics control cell fate. *Science*, 336, 1440-4.
- QU, Y., HAN, B. C., YU, Y., YAO, W. W., BOSE, S., KARLAN, B. Y., GIULIANO, A. E. & CUI, X. J. 2015. Evaluation of MCF10A as a Reliable Model for Normal Human Mammary Epithelial Cells. *Plos One*, 10.
- RABENAU, K. & HOFSTATTER, E. 2016. DNA Damage Repair and the Emerging Role of Poly(ADP-ribose) Polymerase Inhibition in Cancer Therapeutics. *Clinical Therapeutics*, 38, 1577-1588.
- REINHARDT, H. C. & YAFFE, M. B. 2009. Kinases that control the cell cycle in response to DNA damage: Chk1, Chk2, and MK2. *Curr Opin Cell Biol*, 21, 245-255.

- REINHARDT, H. C. & YAFFE, M. B. 2013. Phospho-Ser/Thr-binding domains: navigating the cell cycle and DNA damage response. *Nature Reviews Molecular Cell Biology*, 14, 563-580.
- REUVEN, N., ADLER, J., MELTSE, V. & SHAUL, Y. 2013. The Hippo pathway kinase Lats2 prevents DNA damage-induced apoptosis through inhibition of the tyrosine kinase c-Abl. *Cell Death Differ*, 20, 1330-40.
- RILEY, T., SONTAG, E., CHEN, P. & LEVINE, A. 2008. Transcriptional control of human p53-regulated genes. *Nat Rev Mol Cell Biol*, 9, 402-412.
- ROOSSINK, F., WIERINGA, H. W., NOORDHUIS, M. G., TEN HOOR, K. A., KOK, M., SLAGTER-MENKEMA, L., HOLLEMA, H., DE BOCK, G. H., PRAS, E., DE VRIES, E. G. E., DE JONG, S., VAN DER ZEE, A. G. J., SCHUURING, E., WISMAN, G. B. A. & VAN VUGT, M. A. T. M. 2012. The role of ATM and 53BP1 as predictive markers in cervical cancer. *International Journal of Cancer*, 131, 2056-2066.
- RUPNIK, A., LOWNDES, N. F. & GRENON, M. 2010. MRN and the race to the break. *Chromosoma*, 119, 115-135.
- SAN FILIPPO, J., SUNG, P. & KLEIN, H. 2008. Mechanism of eukaryotic homologous recombination. *Annu Rev Biochem*, 77, 229-57.
- SANTIVASI, W. L. & XIA, F. 2014. Ionizing Radiation-Induced DNA Damage, Response, and Repair. *Antioxid Redox Signal*, 21, 251-259.
- SARTORI, A. A., LUKAS, C., COATES, J., MISTRIK, M., FU, S., BARTEK, J., BAER, R., LUKAS, J. & JACKSON, S. P. 2007. Human CtIP promotes DNA end resection. *Nature*, 450, 509-514.
- SAVITSKY, K., BARSHIRA, A., GILAD, S., ROTMAN, G., ZIV, Y., VANAGAITE, L., TAGLE, D. A., SMITH, S., UZIEL, T., SFEZ, S., ASHKENAZI, M., PECKER, I., FRYDMAN, M., HARNIK, R., PATANJALI, S. R., SIMMONS, A., CLINES, G. A., SARTIEL, A., GATTI, R. A., CHESSA, L., SANAL, O., LAVIN, M. F., JASPERS, N. G. J., MALCOLM, A., TAYLOR, R., ARLETT, C. F., MIKI, T., WEISSMAN, S. M., LOVETT, M., COLLINS, F. S. & SHILOH, Y. 1995. A Single Ataxia-Telangiectasia Gene with a Product Similar to Pi-3 Kinase. *Science*, 268, 1749-1753.
- SCHLACHER, K., CHRIST, N., SIAUD, N., EGASHIRA, A., WU, H. & JASIN, M. 2011. Double-strand break repair-independent role for BRCA2 in blocking stalled replication fork degradation by MRE11. *Cell*, 145, 529-42.
- SCHLACHER, K., WU, H. & JASIN, M. 2012. A Distinct Replication Fork Protection Pathway Connects Fanconi Anemia Tumor Suppressors to RAD51-BRCA1/2. *Cancer Cell*, 22, 106-116.
- SCHMITZ-ROHMER, D., PROBST, S., YANG, Z. Z., LAURENT, F., STADLER, M. B., ZUNIGA, A., ZELLER, R., HYNX, D., HEMMINGS, B. A. & HERGOVICH, A. 2015. NDR Kinases Are Essential for Somitogenesis and Cardiac Looping during Mouse Embryonic Development. *Plos One*, 10, e0136566.
- SCHONN, I., HENNESEN, J. & DARTSCH, D. C. 2011. Ku70 and Rad51 vary in their importance for the repair of doxorubicin- versus etoposide-induced DNA damage. *Apoptosis*, 16, 359-369.
- SELIMOGLU, R. B., A.; JOFFRE, C.; MEUNIER, B.; PARRINI, M.C.; FESQUET, D.; FORMSTECHE, E.; CASONE, I.; HERGOVICH, A.; CAMONIS, J. 2014. RalA GTPase and MAP4K4 function through NDR1 activation in stress response and apoptotic signaling. *HSOA Journal of Cell Biology and Cell Metabolism*, 1.
- SHAHEEN, M., ALLEN, C., NICKOLOFF, J. A. & HROMAS, R. 2011. Synthetic lethality: exploiting the addiction of cancer to DNA repair. *Blood*, 117, 6074-6082.
- SHEPHERD, G. M. 2003. Hypersensitivity reactions to chemotherapeutic drugs. *Clinical Reviews in Allergy & Immunology*, 24, 253-262.

- SHERR, C. J. & ROBERTS, J. M. 1999. CDK inhibitors: positive and negative regulators of G1-phase progression. *Genes Dev*, 13, 1501-12.
- SHIBATA, A., CONRAD, S., BIRRAUX, J., GEUTING, V., BARTON, O., ISMAIL, A., KAKAROUGKAS, A., MEEK, K., TAUCHER-SCHOLZ, G., LOBRICH, M. & JEGGO, P. A. 2011. Factors determining DNA double-strand break repair pathway choice in G2 phase. *Embo Journal*, 30, 1079-1092.
- SHIBUE, T., SUZUKI, S., OKAMOTO, H., YOSHIDA, H., OHBA, Y., TAKAOKA, A. & TANIGUCHI, T. 2006. Differential contribution of Puma and Noxa in dual regulation of p53-mediated apoptotic pathways. *Embo Journal*, 25, 4952-4962.
- SHILOH, Y. 2003. ATM and related protein kinases: safeguarding genome integrity. *Nat Rev Cancer*, 3, 155-68.
- SHILOH, Y. & ZIV, Y. 2013. The ATM protein kinase: regulating the cellular response to genotoxic stress, and more. *Nature Reviews Molecular Cell Biology*, 14, 197-210.
- SHRIVASTAV, M., DE HARO, L. P. & NICKOLOFF, J. A. 2008. Regulation of DNA double-strand break repair pathway choice. *Cell Res*, 18, 134-47.
- SONNENBLICK, A., DE AZAMBUJA, E., AZIM, H. A., JR. & PICCART, M. 2015. An update on PARP inhibitors--moving to the adjuvant setting. *Nat Rev Clin Oncol*, 12, 27-41.
- SORENSEN, C. S., SYLJUASEN, R. G., FALCK, J., SCHROEDER, T., RONNSTRAND, L., KHANNA, K. K., ZHOU, B. B., BARTEK, J. & LUKAS, J. 2003. Chk1 regulates the S phase checkpoint by coupling the physiological turnover and ionizing radiation-induced accelerated proteolysis of Cdc25A. *Cancer cell*, 3, 247-58.
- SPANSWICK, V. J., HARTLEY, J. M. & HARTLEY, J. A. 2010. Measurement of DNA interstrand crosslinking in individual cells using the Single Cell Gel Electrophoresis (Comet) assay. *Amyloid Proteins: Methods and Protocols, Second Edition*, 613, 267-82.
- SPANSWICK, V. J., LOWE, H. L., NEWTON, C., BINGHAM, J. P., BAGNOBIANCHI, A., KIAKOS, K., CRADDOCK, C., LEDERMANN, J. A., HOCHHAUSER, D. & HARTLEY, J. A. 2012. Evidence for different mechanisms of 'unhooking' for melphalan and cisplatin-induced DNA interstrand cross-links in vitro and in clinical acquired resistant tumour samples. *Bmc Cancer*, 12.
- SPEIDEL, D. 2015. The role of DNA damage responses in p53 biology. *Arch Toxicol*, 89, 501-17.
- SPENCER, D. M. S., BILARDI, R. A., KOCH, T. H., POST, G. C., NAFIE, J. W., KIMURA, K., CUTTS, S. M. & PHILLIPS, D. R. 2008. DNA repair in response to anthracycline-DNA adducts: A role for both homologous recombination and nucleotide excision repair. *Mutation Research-Fundamental and Molecular Mechanisms of Mutagenesis*, 638, 110-121.
- STAVRIDIS, E. S., HARRIS, K. G., HUYEN, Y., BOTHOS, J., VERWOERD, P. M., STAYROOK, S. E., PAVLETICH, N. P., JEFFREY, P. D. & LUCA, F. C. 2003. Crystal structure of a human Mob1 protein: Toward understanding mob-regulated cell cycle pathways. *Structure*, 11, 1163-1170.
- STEWART, G. S., MASER, R. S., STANKOVIC, T., BRESSAN, D. A., KAPLAN, M. I., JASPERS, N. G. J., RAAMS, A., BYRD, P. J., PETRINI, J. H. J. & TAYLOR, A. M. R. 1999. The DNA double-strand break repair gene hMRE11 is mutated in individuals with an ataxia-telangiectasia-like disorder. *Cell*, 99, 577-587.
- STEWART, N., HICKS, G. G., PARASKEVAS, F. & MOWAT, M. 1995. Evidence for a second cell cycle block at G2/M by p53. *Oncogene*, 10, 109-15.

- STORDAL, B., TIMMS, K., FARRELLY, A., GALLAGHER, D., BUSSCHOTS, S., RENAUD, M., THERY, J., WILLIAMS, D., POTTER, J., TRAN, T., KORPANTY, G., CREMONA, M., CAREY, M., LI, J., LI, Y., ASLAN, O., O'LEARY, J. J., MILLS, G. B. & HENNESSY, B. T. 2013. BRCA1/2 mutation analysis in 41 ovarian cell lines reveals only one functionally deleterious BRCA1 mutation. *Mol Oncol*, 7, 567-79.
- STRACKER, T. H., MORALES, M., COUTO, S. S., HUSSEIN, H. & PETRINI, J. H. J. 2007. The carboxy terminus of NBS1 is required for induction of apoptosis by the MRE11 complex. *Nature*, 447, 218-U7.
- STRACKER, T. H. & PETRINI, J. H. J. 2011. The MRE11 complex: starting from the ends. *Nature Reviews Molecular Cell Biology*, 12, 90-103.
- STRACKER, T. H., ROIG, I., KNOBEL, P. A. & MARJANOVIC, M. 2013. The ATM signaling network in development and disease. *Frontiers in Genetics*, 4.
- STRANO, S. & BLANDINO, G. 2007. YAP1 meets tumor suppression. *Mol Cell*, 27, 863-4.
- STRANO, S., MUNARRIZ, E., ROSSI, M., CASTAGNOLI, L., SHAUL, Y., SACCHI, A., OREN, M., SUDOL, M., CESARENI, G. & BLANDINO, G. 2001. Physical interaction with Yes-associated protein enhances p73 transcriptional activity. *Journal of Biological Chemistry*, 276, 15164-15173.
- STRATTON, M. R., CAMPBELL, P. J. & FUTREAL, P. A. 2009. The cancer genome. *Nature*, 458, 719-724.
- STUMPF, C. R., MORENO, M. V., OLSHEN, A. B., TAYLOR, B. S. & RUGGERO, D. 2013. The Translational Landscape of the Mammalian Cell Cycle. *Molecular Cell*, 52, 574-582.
- SUGRUE, M. M., SHIN, D. Y., LEE, S. W. & AARONSON, S. A. 1997. Wild-type p53 triggers a rapid senescence program in human tumor cells lacking functional p53. *Proc Natl Acad Sci U S A*, 94, 9648-53.
- SULLI, G., DI MICCO, R. & DI FAGAGNA, F. D. 2012. Crosstalk between chromatin state and DNA damage response in cellular senescence and cancer. *Nature Reviews Cancer*, 12.
- SULLIVAN, A. & LU, X. 2007. ASPP: a new family of oncogenes and tumour suppressor genes. *British Journal of Cancer*, 96, 196-200.
- SULTANA, R., MCNEILL, D. R., ABBOTTS, R., MOHAMMED, M. Z., ZDZIENICKA, M. Z., QUTOB, H., SEEDHOUSE, C., LAUGHTON, C. A., FISCHER, P. M., PATEL, P. M., WILSON, D. M. & MADHUSUDAN, S. 2012. Synthetic lethal targeting of DNA double-strand break repair deficient cells by human apurinic/apyrimidinic endonuclease inhibitors. *International Journal of Cancer*, 131, 2433-2444.
- SY, S. M. H., HUEN, M. S. Y., CHEN, J. & LIVINGSTON, D. M. 2009. PALB2 Is an Integral Component of the BRCA Complex Required for Homologous Recombination Repair. *Proceedings of the National Academy of Sciences of the United States of America*, 106, 7155-7160.
- SYMINGTON, L. S. & GAUTIER, J. 2011. Double-Strand Break End Resection and Repair Pathway Choice. *Annual Review Genetics*, Vol 45, 45, 247-271.
- TACAR, O., SRIAMORNSAK, P. & DASS, C. R. 2013. Doxorubicin: an update on anticancer molecular action, toxicity and novel drug delivery systems. *Journal of Pharmacy and Pharmacology*, 65, 157-170.
- TAKIMOTO, C. H., WRIGHT, J. & ARBUCK, S. G. 1998. Clinical applications of the camptothecins. *Biochim Biophys Acta*, 1400, 107-19.
- TANG, F. Y., GILL, J., FICHT, X., BARTHLOTT, T., CORNILS, H., SCHMITZ-ROHMER, D., HYNX, D., ZHOU, D. W., ZHANG, L., XUE, G. D., GRZMIL, M., YANG, Z. Z., HERGOVICH, A., HOLLAENDER, G. A., STEIN, J. V., HEMMINGS, B. A. & MATTHIAS, P. 2015. The kinases NDR1/2 act

- downstream of the Hippo homolog MST1 to mediate both egress of thymocytes from the thymus and lymphocyte motility. *Sci Signal*, 8.
- TANG, F. Y., ZHANG, L., XUE, G. D., HYNX, D., WANG, Y. H., CRON, P. D., HUNDSRUCKER, C., HERGOVICH, A., FRANK, S., HEMMINGS, B. A. & SCHMITZ-ROHMER, D. 2014. hMOB3 Modulates MST1 Apoptotic Signaling and Supports Tumor Growth in Glioblastoma Multiforme. *Cancer Research*, 74, 3779-3789.
- TANIGUCHI, T., TISCHKOWITZ, M., AMEZIANE, N., HODGSON, S. V., MATHEW, C. G., JOENJE, H., MOK, S. C. & D'ANDREA, A. D. 2003. Disruption of the Fanconi anemia-BRCA pathway in cisplatin-sensitive ovarian tumors. *Nat Med*, 9, 568-574.
- TAYLOR, W. R., DEPRIMO, S. E., AGARWAL, A., AGARWAL, M. L., SCHONTHAL, A. H., KATULA, K. S. & STARK, G. R. 1999. Mechanisms of G2 arrest in response to overexpression of p53. *Mol Biol Cell*, 10, 3607-22.
- TAYLOR, W. R. & STARK, G. R. 2001. Regulation of the G2/M transition by p53. *Oncogene*, 20, 1803-15.
- THEUNISSEN, J. W., KAPLAN, M. I., HUNT, P. A., WILLIAMS, B. R., FERGUSON, D. O., ALT, F. W. & PETRINI, J. H. 2003. Checkpoint failure and chromosomal instability without lymphomagenesis in Mre11(ATLD1/ATLD1) mice. *Mol Cell*, 12, 1511-23.
- THOMPSON, L. H. 2012. Recognition, signaling, and repair of DNA double-strand breaks produced by ionizing radiation in mammalian cells: The molecular choreography. *Mutation Research-Reviews in Mutation Research*, 751, 158-246.
- TICHY, E. D., PILLAI, R., DENG, L., LIANG, L., TISCHFIELD, J., SCHWEMBERGER, S. J., BABCOCK, G. F. & STAMBROOK, P. J. 2010. Mouse Embryonic Stem Cells, but Not Somatic Cells, Predominantly Use Homologous Recombination to Repair Double-Strand DNA Breaks. *Stem Cells and Development*, 19, 1699-1711.
- TRENZ, K., SMITH, E., SMITH, S. & COSTANZO, V. 2006. ATM and ATR promote Mre11 dependent restart of collapsed replication forks and prevent accumulation of DNA breaks. *Embo Journal*, 25, 1764-1774.
- TSUZUKI, T., FUJII, Y., SAKUMI, K., TOMINAGA, Y., NAKAO, K., SEKIGUCHI, M., MATSUSHIRO, A., YOSHIMURA, Y. & MORITA, T. 1996. Targeted disruption of the Rad51 gene leads to lethality in embryonic mice. *Proceedings of the National Academy of Sciences of the United States of America*, 93, 6236-6240.
- ULTANIR, S. K., HERTZ, N. T., LI, G. N., GE, W. P., BURLINGAME, A. L., PLEASURE, S. J., SHOKAT, K. M., JAN, L. Y. & JAN, Y. N. 2012. Chemical Genetic Identification of NDR1/2 Kinase Substrates AAK1 and Rabin8 Uncovers Their Roles in Dendrite Arborization and Spine Development. *Neuron*, 73, 1127-1142.
- ULUKAN, H. & SWAAN, P. W. 2002. Camptothecins - A review of their chemotherapeutic potential. *Drugs*, 62, 2039-2057.
- UZIEL, T., LERENTHAL, Y., MOYAL, L., ANDEGEKO, Y., MITTELMAN, L. & SHILOH, Y. 2003. Requirement of the MRN complex for ATM activation by DNA damage. *Embo Journal*, 22, 5612-5621.
- VARON, R., VISSINGA, C., PLATZER, M., CEROSALETTO, K. M., CHRZANOWSKA, K. H., SAAR, K., BECKMANN, G., SEEMANOVA, E., COOPER, P. R., NOWAK, N. J., STUMM, M., WEEMAES, C. M. R., GATTI, R. A., WILSON, R. K., DIGWEED, M., ROSENTHAL, A., SPERLING, K., CONCANNON, P. & REIS, A. 1998. Nibrin, a novel DNA double-strand break repair protein, is mutated in Nijmegen breakage syndrome. *Cell*, 93, 467-476.

- VENKITARAMAN, A. R. 2002. Cancer susceptibility and the functions of BRCA1 and BRCA2. *Cell*, 108, 171-82.
- VERMEULEN, K., VAN BOCKSTAELE, D. R. & BERNEMAN, Z. N. 2003. The cell cycle: a review of regulation, deregulation and therapeutic targets in cancer. *Cell Prolif*, 36, 131-49.
- VEUGER, S. & CURTIN, N. J. 2014. Chapter 8 - Inhibition of DNA Repair as a Therapeutic Target. In: NEIDLE, S. (ed.) *Cancer Drug Design and Discovery (Second Edition)*. San Diego: Academic Press.
- VICHALKOVSKI, A., GRESKO, E., CORNILS, H., HERGOVICH, A., SCHMITZ, D. & HEMMING, B. A. 2008. NDR kinase is activated by RASSF1A/MST1 in response to Fas receptor stimulation and promotes apoptosis. *Curr Biol*, 18, 1889-95.
- VILAR, E., BARTNIK, C. M., STENZEL, S. L., RASKIN, L., AHN, J., MORENO, V., MUKHERJEE, B., INIESTA, M. D., MORGAN, M. A., RENNERT, G. & GRUBER, S. B. 2011. MRE11 Deficiency Increases Sensitivity to Poly(ADP-ribose) Polymerase Inhibition in Microsatellite Unstable Colorectal Cancers. *Cancer Research*, 71, 2632-2642.
- VILENCHIK, M. M. & KNUDSON, A. G. 2003. Endogenous DNA double-strand breaks: Production, fidelity of repair, and induction of cancer. *Proceedings of the National Academy of Sciences of the United States of America*, 100, 12871-12876.
- VOGELSTEIN, B., LANE, D. & LEVINE, A. J. 2000. Surfing the p53 network. *Nature*, 408, 307-310.
- VOUSDEN, K. H. 2006. Outcomes of p53 activation--spoilt for choice. *J Cell Sci*, 119, 5015-20.
- VOUSDEN, K. H. & LANE, D. P. 2007. p53 in health and disease. *Nat Rev Mol Cell Biol*, 8, 275-283.
- VOUSDEN, K. H. & LU, X. 2002. Live or let die: the cell's response to p53. *Nat Rev Cancer*, 2, 594-604.
- VOUSDEN, K. H. & PRIVES, C. 2009. Blinded by the Light: The Growing Complexity of p53. *Cell*, 137, 413-431.
- WAGNER, S. A., BELI, P., WEINERT, B. T., SCHOLZ, C., KELSTRUP, C. D., YOUNG, C., NIELSEN, M. L., OLSEN, J. V., BRAKEBUSCH, C. & CHOUDHARY, C. 2012. Proteomic analyses reveal divergent ubiquitylation site patterns in murine tissues. *Mol Cell Proteomics*, 11, 1578-85.
- WAHL, G. M. & CARR, A. M. 2001. The evolution of diverse biological responses to DNA damage: insights from yeast and p53. *Nature cell biology*, 3, E277-86.
- WAHL, G. M., LINKE, S. P., PAULSON, T. G. & HUANG, L. C. 1997. Maintaining genetic stability through TP53 mediated checkpoint control. *Cancer Surveys*, 29, 183-219.
- WALSH, C. S. & HODEIB, M. 2016. Leveraging DNA repair deficiency in gynecologic oncology. *Curr Opin Obstet Gynecol*, 28, 24-31.
- WALTES, R., KALB, R., GATEI, M., KIJAS, A. W., STUMM, M., SOBECK, A., WIELAND, B., VARON, R., LERENTHAL, Y., LAVIN, M. F., SCHINDLER, D. & DORK, T. 2009. Human RAD50 Deficiency in a Nijmegen Breakage Syndrome-like Disorder. *Am J Hum Genet*, 84, 605-616.
- WANG, J. C. 2002. Cellular roles of DNA topoisomerases: A molecular perspective. *Nature Reviews Molecular Cell Biology*, 3, 430-440.
- WANG, L. C. & GAUTIER, J. 2010. The Fanconi anemia pathway and ICL repair: implications for cancer therapy. *Crit Rev Biochem Mol Biol*, 45, 424-439.
- WANG, Y. Q., WANG, P. Y., WANG, Y. T., YANG, G. F., ZHANG, A. & MIAO, Z. H. 2016. An Update on Poly(ADP-ribose)polymerase-1 (PARP-1) Inhibitors: Opportunities and Challenges in Cancer Therapy. *J Med Chem*.

- WANG, Z. X., WANG, H. Y. & WU, M. C. 2001. Identification and characterization of a novel human hepatocellular carcinoma-associated gene. *British Journal of Cancer*, 85, 1162-1167.
- WEBER, A. M. & RYAN, A. J. 2015. ATM and ATR as therapeutic targets in cancer. *Pharmacol Ther*, 149, 124-138.
- WEISS, E. L., KURISCHKO, C., ZHANG, C., SHOKAT, K., DRUBIN, D. G. & LUCA, F. C. 2002. The *Saccharomyces cerevisiae* Mob2p-Cbk1p kinase complex promotes polarized growth and acts with the mitotic exit network to facilitate daughter cell-specific localization of Ace2p transcription factor. *J Cell Biol*, 158, 885-900.
- WILLIAMS, G. J., LEES-MILLER, S. P. & TAINER, J. A. 2010. Mre11-Rad50-Nbs1 conformations and the control of sensing, signaling, and effector responses at DNA double-strand breaks. *DNA Repair*, 9, 1299-1306.
- WILLIAMS, H. L., GOTTESMAN, M. E. & GAUTIER, J. 2013. The differences between ICL repair during and outside of S phase. *Trends in Biochemical Sciences*, 38, 386-393.
- WILLIAMS, R. S., DODSON, G. E., LIMBO, O., YAMADA, Y., WILLIAMS, J. S., GUENTHER, G., CLASSEN, S., GLOVER, J. N. M., IWASAKI, H., RUSSELL, P. & TAINER, J. A. 2009. Nbs1 Flexibly Tethers Ctp1 and Mre11-Rad50 to Coordinate DNA Double-Strand Break Processing and Repair. *Cell*, 139, 87-99.
- WILLIAMS, R. S., MONCALIAN, G., WILLIAMS, J. S., YAMADA, Y., LIMBO, O., SHIN, D. S., GROOCCOCK, L. M., CAHILL, D., HITOMI, C., GUENTHER, G., MOIANI, D., CARNEY, J. P., RUSSELL, P. & TAINER, J. A. 2008. Mre11 dimers coordinate DNA end bridging and nuclease processing in double-strand-break repair. *Cell*, 135, 97-109.
- WYNNE, P., NEWTON, C., LEDERMANN, J., OLAITAN, A., MOULD, T. A. & HARTLEY, J. A. 2007. Enhanced repair of DNA interstrand crosslinking in ovarian cancer cells from patients following treatment with platinum-based chemotherapy. *British Journal of Cancer*, 97, 927-933.
- XIA, B., SHENG, Q., NAKANISHI, K., OHASHI, A., WU, J., CHRIST, N., LIU, X., JASIN, M., COUCH, F. J. & LIVINGSTON, D. M. 2006. Control of BRCA2 cellular and clinical functions by a nuclear partner, PALB2. *Mol Cell*, 22, 719-29.
- YABUTA, N., OKADA, N., ITO, A., HOSOMI, T., NISHIHARA, S., SASAYAMA, Y., FUJIMORI, A., OKUZAKI, D., ZHAO, H., IKAWA, M., OKABE, M. & NOJIMA, H. 2007. Lats2 is an essential mitotic regulator required for the coordination of cell division. *Journal of Biological Chemistry*, 282, 19259-19271.
- YAN, M., CHU, L., QIN, B., WANG, Z., LIU, X., JIN, C., ZHANG, G., GOMEZ, M., HERGOVICH, A., CHEN, Z., HE, P., GAO, X. & YAO, X. 2015. Regulation of NDR1 activity by PLK1 ensures proper spindle orientation in mitosis. *Sci Rep*, 5, 10449.
- YATA, K., BLEUYARD, J. Y., NAKATO, R., RALF, C., KATOU, Y., SCHWAB, R. A., NIEDZWIEDZ, W., SHIRAHIGE, K. & ESASHI, F. 2014. BRCA2 Coordinates the Activities of Cell-Cycle Kinases to Promote Genome Stability. *Cell Reports*, 7, 1547-1559.
- YATA, K., LLOYD, J., MASLEN, S., BLEUYARD, J. Y., SKEHEL, M., SMERDON, S. J. & ESASHI, F. 2012. Plk1 and CK2 Act in Concert to Regulate Rad51 during DNA Double Strand Break Repair. *Molecular Cell*, 45, 371-383.
- YAZDI, P. T., WANG, Y., ZHAO, S., PATEL, N., LEE, E. Y. H. P. & QIN, J. 2002. SMC1 is a downstream effector in the ATM/NBS1 branch of the human S-phase checkpoint. *Genes & Development*, 16, 571-582.
- YU, F. X. & GUAN, K. L. 2013. The Hippo pathway: regulators and regulations. *Genes Dev*, 27, 355-71.



- YU, F. X., ZHAO, B. & GUAN, K. L. 2015. Hippo Pathway in Organ Size Control, Tissue Homeostasis, and Cancer. *Cell*, 163, 811-28.
- YU, J. & ZHANG, L. 2009. PUMA, a potent killer with or without p53. *Oncogene*, 27, S71-S83.
- ZHANG, K., RODRIGUEZ-AZNAR, E., YABUTA, N., OWEN, R. J., MINGOT, J. M., NOJIMA, H., NIETO, M. A. & LONGMORE, G. D. 2012. Lats2 kinase potentiates Snail1 activity by promoting nuclear retention upon phosphorylation. *Embo Journal*, 31, 29-43.
- ZHANG, L., TANG, F. Y., TERRACCIANO, L., HYNX, D., KOHLER, R., BICHET, S., HESS, D., CRON, P., HEMMINGS, B. A., HERGOVICH, A. & SCHMITZ-ROHMER, D. 2015. NDR Functions as a Physiological YAP1 Kinase in the Intestinal Epithelium. *Current Biology*, 25, 296-305.
- ZHANG, M., LIU, G. Y., XUE, F. X., EDWARDS, R., SOOD, A. K., ZHANG, W. & YANG, D. 2016. Copy number deletion of RAD50 as predictive marker of BRCAness and PARP inhibitor response in BRCA wild type ovarian cancer. *Gynecologic Oncology*, 141, 57-64.
- ZHAO, B., WEI, X., LI, W., UDAN, R. S., YANG, Q., KIM, J., XIE, J., IKENOUE, T., YU, J., LI, L., ZHENG, P., YE, K., CHINNAIYAN, A., HALDER, G., LAI, Z. C. & GUAN, K. L. 2007. Inactivation of YAP oncoprotein by the Hippo pathway is involved in cell contact inhibition and tissue growth control. *Genes & Development*, 21, 2747-2761.
- ZHAO, Y., THOMAS, H. D., BATEY, M. A., COWELL, I. G., RICHARDSON, C. J., GRIFFIN, R. J., CALVERT, A. H., NEWELL, D. R., SMITH, G. C. M. & CURTIN, N. J. 2006. Preclinical evaluation of a potent novel DNA-dependent protein kinase inhibitor NU7441. *Cancer Research*, 66, 5354-5362.
- ZHENG, Y. G., WANG, W., LIU, B., DENG, H., USTER, E. & PAN, D. J. 2015. Identification of Happyhour/MAP4K as Alternative Hpo/Mst-like Kinases in the Hippo Kinase Cascade. *Dev Cell*, 34, 642-655.
- ZHOU, D. W., CONRAD, C., XIA, F., PARK, J. S., PAYER, B., YIN, Y., LAUWERS, G. Y., THASLER, W., LEE, J. T., AVRUCH, J. & BARDEESY, N. 2009. Mst1 and Mst2 Maintain Hepatocyte Quiescence and Suppress Hepatocellular Carcinoma Development through Inactivation of the Yap1 Oncogene. *Cancer Cell*, 16, 425-438.
- ZOU, L. & ELLEDGE, S. J. 2003. Sensing DNA damage through ATRIP recognition of RPA-ssDNA complexes. *Science*, 300, 1542-1548.